Biochemical investigations of *Plasmodium falciparum* erythrocyte invasion pathways using recombinant merozoite surface proteins produced in a mammalian expression system

Madushi Wanaguru

Downing College, University of Cambridge

A dissertation submitted for the degree of

Doctor of Philosophy

September 2012

For Amma

Declaration

This dissertation is the result of my own work and includes nothing which is the outcome of work done in collaboration except where specifically indicated in the text. This dissertation does not exceed the word limit set by the Biology Degree Committee.

Summary

The invasion of erythrocytes by *Plasmodium falciparum* merozoites is mediated by low-affinity, extracellular interactions between surface proteins on the host and parasite cells. Identification of these interactions *in vitro* is technically challenging; not only are *P. falciparum* proteins hard to express recombinantly in heterologous systems, but detecting their transient interactions with erythrocyte receptors is difficult using traditional biochemical methods. Two significant advances in this area of research have recently been made in our laboratory. Firstly, a strategy has been optimised for the production of soluble full-length ectodomains of *P. falciparum* merozoite surface proteins, in a mammalian expression system. Secondly, an ELISA-based method, AVEXIS (avidity-based extracellular interaction screening) has been developed which enables low-affinity interactions between proteins to be identified in a high-throughput manner. The AVEXIS assay is, however, limited for use with soluble proteins and as such cannot be used for the analysis of multi-pass membrane proteins. In my PhD, I developed a flow-cytometry based, high-throughput assay for identifying low-affinity interactions between recombinant *P. falciparum* proteins and receptors displayed on the surface of cells. I used this assay in combination with other biochemical and biophysical methods such as AVEXIS and surface plasmon resonance to investigate selected aspects/interactions of erythrocyte invasion in three projects.

P. falciparum EBA175 is the known ligand of the erythrocyte receptor Glycophorin A, which carries the antigenic determinants of the human MN blood group system. In my first project, I showed that the mammalian-expressed, full-length ectodomain of EBA175 (*Pf*EBA175 FL) is functionally similar to native EBA175 isolated from parasite cultures and that it binds MN Glycophorin A with a slightly higher affinity than the MM form. I also found that *Pf*EBA175

RII, a truncated derivative containing only the extracellular region known to be essential for interacting with erythrocytes, binds to native Glycophorin A with a one order of magnitude lower affinity than *Pf*EBA175 FL, suggesting some role played by regions outside of RII to facilitate binding.

The closest relatives of *P. falciparum* are found amongst the *Laverania* family of great ape parasites, which appear to be strictly host-specific in their natural environments. In my second project, I investigated the potential contributions of EBA175-Glycophorin A and another parasite ligand-host receptor interaction, RH5-Basigin (BSG), towards the determination of host-specificity in *Laverania.* I only observed a relatively small difference in the affinities for native human Glycophorin A, between *Pf*EBA175 and orthologues of EBA175 from two chimpanzee parasites *P. reichenowi* and *P. billcollinsi*, which suggests that this interaction may not play a significant role in the determination of host-specificity in *Laverania*. On the other hand, I saw clear host-selectivity in the recognition of BSG orthologues from human, chimpanzee and gorilla, by *P. falciparum* RH5 and identified residues that confer this specificity by generating and testing site-directed mutants of the BSG orthologues.

Although multi-pass receptors are fairly abundant on the erythrocyte surface, no such receptor has yet been conclusively identified to play a role in erythrocyte invasion by *P. falciparum*. To potentially identify such a novel interaction, I screened a library of mammalian-expressed *P. falciparum* proteins against a panel of recombinant erythrocyte multi-pass receptors, in my third project. I also tested the library of merozoite proteins for binding to human erythrocytes and to a large panel of synthetic carbohydrates. A number of putative interactions were identified in the screens and are awaiting characterisation.

Acknowledgements

I am most indebted to Gavin Wright, for the opportunity to work in his lab and for the thorough and patient mentorship throughout the course of my PhD. I am also very grateful to Julian Rayner for his advice and encouragement.

I wish to thank Cecile Crosnier and Josefin Bartholdoson for their kind help and advice, Zenon Zenonos for the anti-Basigin monoclonals and Leyla Bustamante for the human erythrocytes. I am also grateful to Bee Ng and William Cheng for flow cytometry training and Gareth Powell for confocal microscopy training. I'm lucky to have worked with my colleagues in Team 30, everyone of whom have helped me in one way or another.

I'm very obliged to my friends for standing by me through the ups and downs of PhD life, in particular Jenn and Laure, who were pillars of emotional support. Nothing of course would ever have been possible without my family; my brothers, Chamitha and Miraj and most of all my father, Bandula.

Table of Contents

Chapter 1

General Introduction

1.1 Malaria is a global health problem.

Malaria has posed a serious threat to the human race from antiquity and around 40% of the world's population live in areas at risk of malaria transmission today (Snow *et al*., 2005; Winzeler, 2008). Caused by the apicomplexan parasite, *Plasmodium*, malaria accounted for at least 216 million clinical cases globally in 2010, with 655,000 to 1.2 million deaths (WHO, 2011; Murray *et al*., 2012). The mortality rates were highest in sub-Saharan Africa and 85- 90% of the malaria-related deaths occurred amongst children under the age of five and pregnant women.

Long neglected as a disease of poverty that primarily affects the developing world, investment for prevention and treatment of malaria has seen a rapid surge within the last decade (Snow *et al*., 2008; Geels *et al*., 2011; Greenwood & Targett, 2011). Funding from a number of agencies including the Global Fund, the World Bank and the US President's Malaria Initiative has enabled the scaling up of control measures for malaria, such as treatment with artemisinin-combination therapy and the use of insecticide-treated bed nets (Snow *et al*., 2008; Geels *et al*., 2011; Greenwood & Targett, 2011). Widespread implementation of these tools has led to a significant decrease in the incidence of malaria in endemic countries, with a 31% reduction in global malaria deaths from 2004 to 2010 (Murray *et al*., 2012). However, the current *status quo* is threatened by the potential spread of artemisinin-resistance parasite strains from south-east Asia and the propagation of insecticide-resistance in the mosquito vector populations (Greenwood & Targett, 2011; Geels *et al*., 2011).

An efficacious vaccine that provides sufficient protective immunity against malaria is clearly imperative for challenging this disease on a global scale (Crompton *et al*., 2010). However, numerous attempts at developing such a vaccine have yielded only limited success so far, mainly

due to inadequate understanding of the complex biology of *Plasmodium* and its mechanisms of immune evasion (Greenwood& Targett, 2011; Geels *et al*., 2011).

1.2 Five different species of *Plasmodium* can cause malaria in humans.

Until very recently only four species of *Plasmodium*, namely *P. falciparum*, *P. vivax*, *P. ovale* and *P. malariae* were believed to infect humans, with *P. vivax* being the most geographically widespread and *P. falciparum* the most lethal (Mendis *et al*., 2001). The discovery of naturally-acquired *P. knowlesi* infections amongst human populations in Southeast Asia has, however, changed this perception (Singh *et al*., 2004; Lee *et al*., 2011). *P. knowlesi*, a simian parasite found primarily in macaques, is thought to be transmitted to humans zoonotically, with no evidence (yet) of the parasite having undergone an adaptive host-switch from monkey to human (Lee *et al*., 2011).

The work described in this thesis was focused mainly on *P. falciparum*, the malaria parasite associated with the most severe clinical symptoms and the majority of malaria-related fatalities. (Snow *et al*., 2005).

1.3 The closest relatives of *P. falciparum* are great ape parasites of the *Laverania* family.

Interestingly, *P. falciparum* is only distantly related to the other human malaria parasites and is generally believed to have undergone a host switch after an ancient zoonotic transfer event from a non-human primate host (Prugnolle *et al*., 2011a; Rayner *et al.*, 2011; Duval and Ariey, 2012). However, the identity of the immediate predecessor of *P. falciparum* is a matter of some contention (Liu *et al*., 2010; Prugnolle *et al.*, 2011b). The chimpanzee parasite, *P. reichenowi*, first identified in the early 1920s, was the only known close relative of *P. falciparum* for many decades and widely believed to be its predecessor (Rayner *et al*., 2011). This paradigm was

challenged in 2009, by the discovery of another, closely-related *Plasmodium* species, *P. gaboni*, in two pet chimpanzees in Gabon (Ollomo *et al*., 2009). This study was followed by four others which reported the identification of *P. falciparum*-like parasites in African apes (Rich *et al*., 2009; Krief *et al.*, 2010; Prugnolle *et al*., 2010; Rayner *et al*., 2011). No definite conclusions, however, could be drawn from these studies with respect to the number and natural host-preferences of the parasite species, due to only a relatively few samples being analysed, most of them derived from captive apes. African apes are highly endangered, so invasive studies of wild-living populations are not a possibility (Rayner *et al*., 2011). In a large scale study conducted by Liu *et al*. (2010), this hurdle was circumvented by collecting and analysing more than 3000 fecal samples from forest-dwelling apes in Africa. Sequence analysis of *Plasmodium* mitochondrial, apicoplast and nuclear DNA recovered from these samples led to the identification of six distinct clades of *P. falciparum*-related parasites, collectively referred to as the *Laverania* family, found at high prevalence rates in great apes. The six clades were observed to be strictly host-specific with *P. reichenowi* (C1), *P. gaboni* (C2) and *P. billcollinsi* (C3) found only in chimpanzees and *P. praefalciparum* (G1), *P. adleri* (G2) and *P. blacklocki* (G3) restricted to gorillas (Figure 1). Furthermore, *P. praefalciparum* was identified as a likely direct predecessor of *P. falciparum*.

This postulated gorilla-origin of *P. falciparum* has since been brought into question by Prugnolle *et al*. (2011b). In their study, Prugnolle and colleagues analysed more than 300 blood samples from ten different species of African monkeys and discovered the presence of *P. falciparum*-like sequences in one sample (out of 29 tested) from one species, the old world monkey, *Cercopithecus nictitans* (greater spot-nosed monkey). Although the possibility of *P. falciparum*

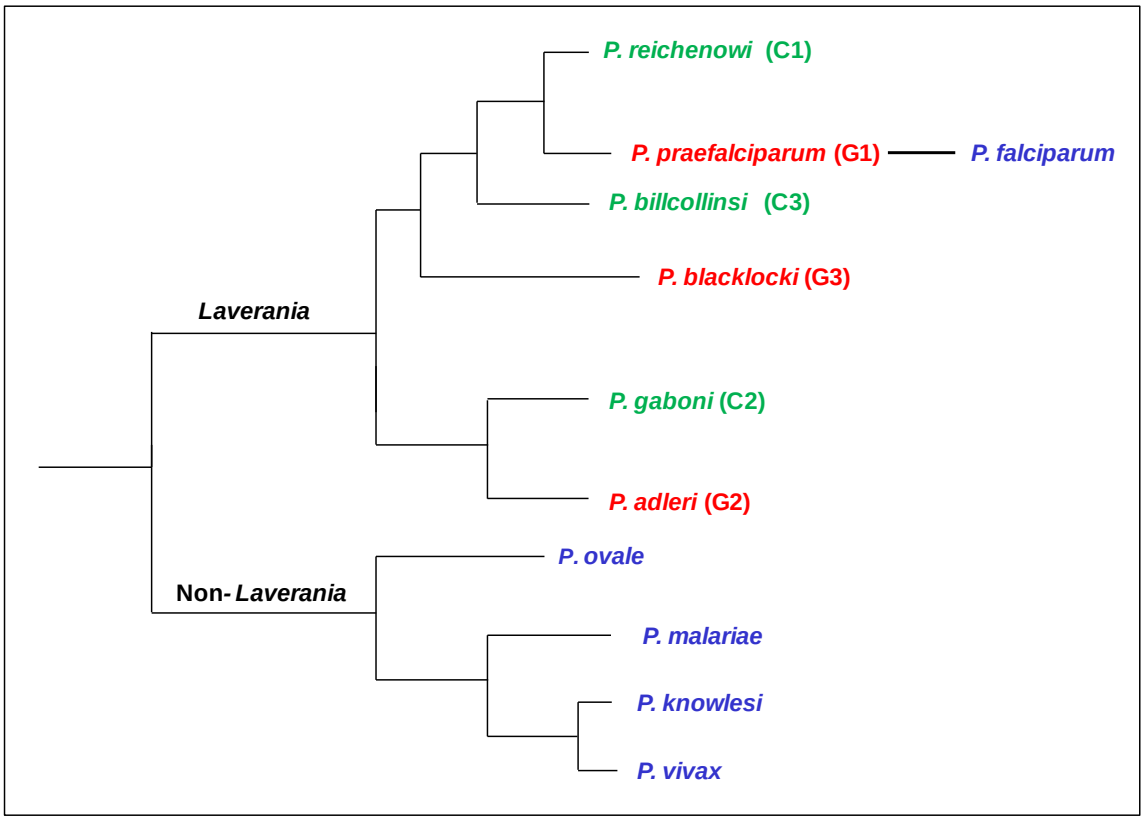

Figure 1. Simplified diagram of the phylogenetic relationships between human and great ape *Plasmodium* species. The two main lineages of *Plasmodium* are indicated with the parasites colour coded according to the primary host infected in the natural environment. Blue-human, red- gorilla, green-chimpanzee.

originating in monkeys rather than in gorillas was raised on the strength of this observation, it is yet to be validated by more substantial evidence (Prugnolle *et al*., 2011b). In fact, a very recent survey of wild-living *C. nictitans*, found no *P. falciparum*-like parasites in any individual (out of 300 tested), leading to the proposal that the original sample detected in a pet monkey may be a rare case of human to primate transmission (Ayouba *et al*., 2012).

1.4 *P. falciparum* has a complex life cycle.

The life cycle of *P. falciparum*, which comprises multiple morphologically distinct states, involves two stages of asexual multiplication in the human host and a period of sexual reproduction in the mosquito vector (Figure 2) (Winzeler, 2008; Kappe *et al*., 2010). Upon being injected into the peripheral circulation of a human host by the infectious bite of a female *Anopheles* mosquito, *P. falciparum* sporozoites migrate to the liver where they divide and differentiate in hepatocytes to form schizonts. After an incubation period of about 10 days, these schizonts rupture to release merozoites which in turn invade erythrocytes and multiply in progressive 48-hour cycles. In this stage, the number of merozoites can increase by 10^3-10^9 fold and some of the parasites leave the cycle to differentiate into male and female gametocytes. Upon ingestion by a mosquito, these gametocytes undergo fertilisation and maturation in the midgut to generate infective ookinetes which migrate through the midgut wall developing into oocysts. The oocysts harbour sporozoites which, when released, accumulate in the salivary glands of the mosquito, ready for transmission to other human hosts.

The erythrocytic stage of the parasite, obligatory for maintaining a sustained infection in the human host, is also responsible for the numerous clinical symptoms associated with malaria (Miller *et al*., 2002; Evans & Wellems, 2002). The release of merozoites into the blood stream following the rupture of host erythrocytes, at the end of each 48-hour development cycle, is

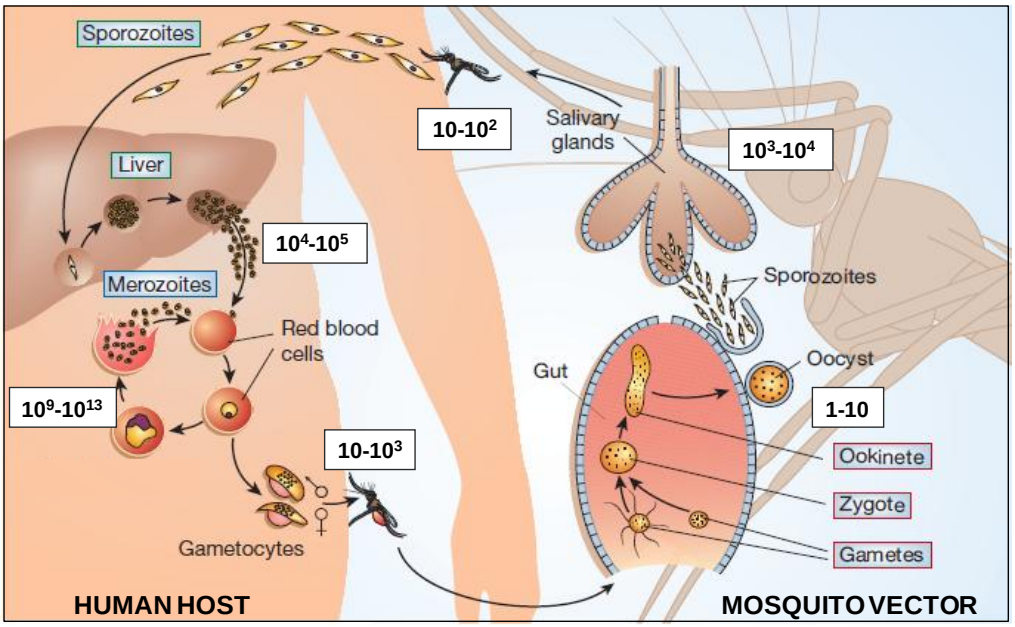

Figure 2. The life cycle of *Plasmodium falciparum* in the human host and the *Anopheles gambiae* mosquito vector. Sporozoites injected into the human host by the *Plasmodium*-infected mosquito first migrate to the liver, where they invade hepatocytes and develop into merozoites. Upon release into the blood stream, these merozoites infect erythrocytes, within which they grow and multiply to generate daughter merozoites that continue onto invade other erythrocytes, once discharged. All the clinical symptoms of malaria are caused by the erythrocytic stage of the parasite. Some intra-erythrocytic stage parasites develop into gametocytes, which are taken up by the mosquito vector during feeding. Gametes fuse to form zygotes which develop into ookinetes that infect the mosquito midgut. The resulting oocysts produce sporozoites which accumulate in the salivary glands of the mosquito ready for transmission to the next human host. The numbers shown indicate parasite population sizes at different stages of the life cycle. (The schematic was adapted from Ménard, 2005).

associated with the periodic fever, paroxysms and sweats characteristic of malaria. The sequestration of *P. falciparum*-infected erythrocytes in microcapillaries perfusing critical organs such as the brain and lung can cause serious life-threatening conditions including severe anemia, coma and pulmonary edema.

Understanding the molecular basis of the machinery that mediates the invasion of erythrocytes by *P. falciparum* merozoites is hence crucial to the development of new anti-malaria therapeutics (Bannister & Mitchell, 2003; Cowman & Crabb, 2006).

1.5 The invasion of human erythrocytes by *P. falciparum* merozoites is a multi-step process mediated by interactions between cell-surface proteins.

P. falciparum merozoites are ~1.2 μm in length and ellipsoidal with a polar structural organisation (Figure 3 A) (Garcia *et al*., 2008). Three sets of secretory organelles, the rhoptries, micronemes and dense granules are located at the apical end together with three cytoskeletal rings (polar rings) that provide structural support. The organelles which carry the genetic information and metabolic machinery necessary for parasite growth and development, the nucleus, mitochondrion and apicoplast, lie at the wider posterior end (Bannister & Mitchell, 2003; Garcia *et al*., 2008). Each merozoite also has a double membrane structure called the inner membrane complex (IMC), located immediately beneath the plasma membrane (except for a small gap at the apex) and connected to it by numerous actin filaments (Farrow *et al*., 2011). The cytosolic side of the IMC is coupled to two or three microtubules, which extend in parallel from the third polar ring to the posterior and play a role in the targeting of apical organelles during merozoite assembly, in addition to their mechanical role (Garcia *et al*., 2008). The outer surface of the merozoite is covered by a 15 nm thick, adhesive coat comprising clumps of narrow, protruding bristles (Garcia *et al.*, 2008).

Invasion of erythrocytes by *P. falciparum* merozoites is driven by a series of specific molecular recognition events between surface proteins on the host and parasite cells (Figure 3 B) (Bannister & Mitchell, 2003; Cowman & Crabb, 2006; Garcia *et al*., 2008; Harvey *et al*., 2012). Although the process of erythrocyte invasion is fairly well understood at the gross ultrastructural level (Aikawa *et al*., 1978), the precise timing and nature of the molecular events are still in the process of being elucidated. The initial tethering of a merozoite to a target erythrocyte is reversible and can occur at any point on the parasite surface. This is presumed to be mediated by proteins which constitute the outer coat of the parasite via relatively long-range (20-30 nm) interactions with their erythrocyte receptors (Cowman & Crabb, 2006; Garcia *et al*., 2008). The merozoite then undergoes re-orientation so that the apical end of the parasite is brought into juxtaposition with the host surface membrane allowing a much closer interaction (Aikawa *et al*., 1978; Gilson & Crabb, 2009). The re-orientation process appears to involve the partial wrapping of the erythrocyte surface around the merozoite and enables proteins secreted from the micronemes and the rhoptries to form an irreversible "tight junction" between the parasite and the host (Aikawa *et al*., 1978; Bannister *et al*., 1975). The movement of the ring-like tight junction from the apical to the posterior end of the merozoite is driven by an acto-myosin motor coupled to the IMC and leads to the internalisation of the merozoite within a parasitophorous vacuole inside the erythrocyte (Keeley & Soldati, 2004; Baum *et al*., 2006). The surface coat of the parasite is removed at the moving junction by the calcium sensitive serine protease, SUB2, a micronemal protein that translocates across the parasite surface (Harris *et al*., 2005; Withers-Martinez *et al*., 2012). Once the posterior end of the parasite is reached, the adhesive proteins that mediate the tight junction are also removed. This is proposed to involve serine proteases of the rhomboid family, ROM1-4, which cleave the proteins from within the phospholipid bilayer,

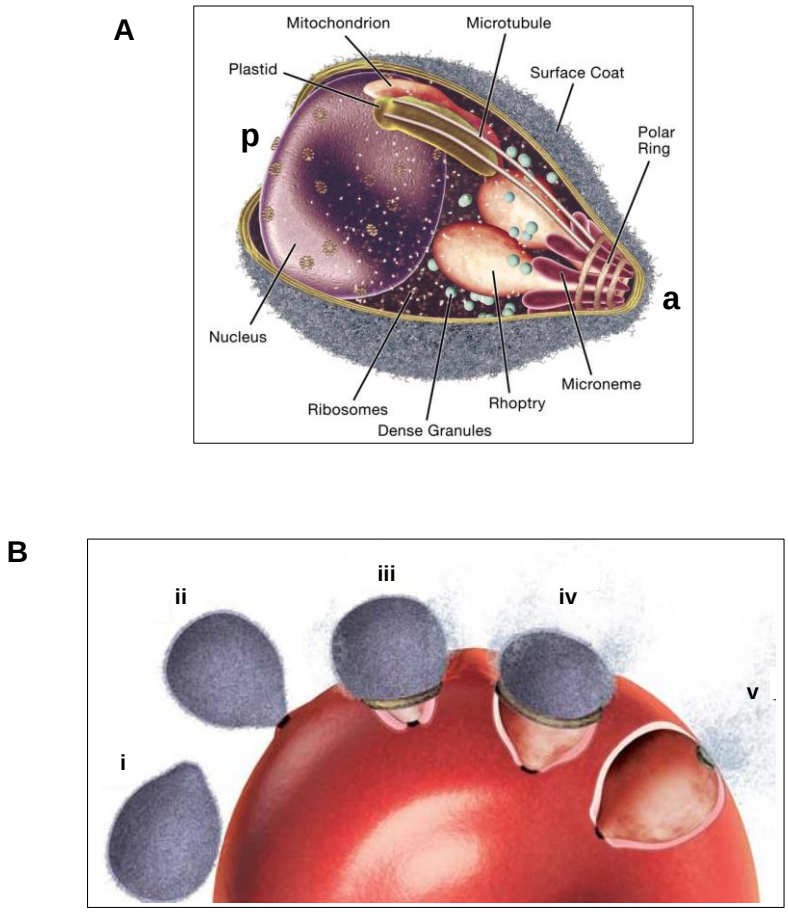

Figure 3. Invasion of erythrocytes by *Plasmodium falciparum* merozoites. A) The merozoite has a polarised structural morphology, a-apical end, p-posterior end. The secretory organelles at the apical end, the rhoptries, micronemes and dense granules, release their contents during erythrocyte invasion, whereas the bristly, adhesive coat which covers the entire outer surface of the cell plays an important role in initiating contact with erythrocytes. **B)** The multiple stages of erythrocyte invasion. i) Initial reversible tethering of the merozoite is mediated by 'long-distance' interactions between proteins constituting the outer coat of the parasite and erythrocyte receptors. ii) Re-orientation of the merozoite brings the apical end in contact with the erythrocyte, allowing proteins secreted from the apical organelles to form a tight junction by interacting with their erythrocyte receptors. iii) and iv) Movement of the tight junction from the apical to the posterior end of the parasite is powered by the actin-myosin motor. The surface coat of the parasite is removed at the moving junction by a serine protease. v) Adhesins forming the tight junction are proteolytically removed upon reaching the posterior end and the parasite is sealed within the parasitophorous vacuole. (The schematics were adapted from Cowman & Crabb, 2006).

facilitating the resealing of the membrane (O'Donnell *et al*., 2006; Garcia *et al*., 2008).

The release of micronemal and rhoptry proteins during invasion is proposed to be a sequential, two-step process, occurring in response to distinct external signals (Singh *et al*., 2010). Exposure of *P. falciparum* merozoites to the low K^+ concentrations found in the blood plasma, leads to a rise in its cytosolic Ca^{2+} levels, which triggers the secretion of micronemal proteins to the apical surface. The subsequent interactions of the micronemal proteins with their erythrocyte receptors restore cytosolic Ca^{2+} to basal levels, triggering the release of rhoptry proteins.

1.6 Primary contact with erythrocytes is proposed to be mediated by proteins that constitute the outer coat of *P. falciparum* merozoites.

More than 30 proteins have been identified by genomic analysis to comprise the outer coat of *P. falciparum* merozoites and these are likely to be important for the initial recognition and reversible binding of erythrocytes by the parasite (Cowman & Crabb, 2006; Garcia *et al*., 2008). The glycosylphosphatidylinositol (GPI)-anchored ligands of the surface coat are in general essential for normal erythrocyte-stage development and are mostly clustered within detergent-resistant membrane domains with their associated peripheral proteins (Sanders *et al*., 2005; Cowman & Crabb, 2006). MSP1, the most abundant of the GPI-anchored ligands is synthesised as a 195 kDa precursor and subsequently processed to generate a complex of four fragments held together non-covalently on the surface of merozoites until erythrocyte invasion (Bentley, 2006; Garcia *et al.*, 2008). The GPI-anchored fragment, $MSP1_{42}$, is again proteolytically cleaved by SUB2 just distally to two tandem EGF (epidermal growth factor) domains, during invasion, to generate a 19 kDa fragment, $MSP1_{19}$, which is held on the merozoite as it enters the erythrocyte (Blackman *et al*., 1991; Harris *et al*., 2005). Prevention of this second processing step has been shown to preclude invasion (Blackman *et al*., 1994; Bentley, 2006). Although a definitive

function for MSP1 in invasion is yet to be identified, there is some evidence to suggest that it may be a ligand for the multi-pass protein band 3, the second most abundant protein on human erythrocytes (Goel *et al*., 2003). The other GPI-anchored proteins on the merozoite surface include Pf12 and Pf38 which carry dual 6-cys domains and are predicted to be putative ligands for erythrocyte receptors, based on structural similarity to SAG proteins of *Toxoplasma gondii* (Gerloff *et al*., 2005; Cowman & Crabb 2006).

Peripheral proteins are secreted into the parasitophorous vacuole and attach to the surface of developing merozoites, via interaction with GPI-anchored ligands (Cowman & Crabb, 2006; Garcia *et al*., 2008). Such proteins identified to date include members of MSP3, MSP7 and SERA families and Pf41, another 6-cys ligand (Sanders *et al*., 2005; Cowman & Crabb, 2006; Garcia *et al*., 2008). MSP6 (MSP3.2) and MSP7 (MSP7.1) are known to form a non-covalent complex with the fragments of MSP1 on the merozoite surface and peptides derived from these have been demonstrated to bind to erythrocytes; however, the biological implications of these interactions are still poorly understood (Burgess *et al.*, 2005; Kadekoppala & Holder, 2010; Kadekoppala *et al.*, 2008). The SERA family of surface proteins carry a central protease domain with an active site cysteine or serine (Hodder *et al.*, 2009). The most abundant member of this family, SERA5, has been shown to be essential for parasite survival in the blood stage, but its recent crystal structure has cast doubt on its ability to function as a protease (Hodder *et al.*, 2009).

1.7 Merozoite proteins of the EBL and RH families play a critical role during erythrocyte invasion.

The erythrocyte-binding-like proteins (EBLs) and the reticulocyte-binding-like-homolog proteins (RHs) are two broad families of merozoite surface proteins secreted from the apical organelles. They are known to interact directly with erythrocyte receptors and are proposed to facilitate a step of the invasion pathway downstream from the initial contact with the erythrocyte, such as apical re-orientation or formation of the tight junction (Harvey *et al.,* 2012; Riglar *et al.,* 2011). In *P. falciparum* the EBL family includes EBA175 (MAL7P1.176), EBA140 (MAL13P1.60), EBA181 (PFA0125c) and EBL-1, all of which are type I transmembrane proteins with two cysteine-rich regions, Region II (RII) and Region VI (RVI), in the extracellular domain (Adams *et al*., 2001; Cowman & Crabb, 2006; Tham *et al*., 2012). The amino-terminal RII mediates erythrocyte binding and comprises two tandem Duffy-binding-like (DBL) domains, F1 and F2, which are homologous to the single DBL domain of the *P. vivax* Duffy-binding-protein (DBP) (Sim *et al*., 1994). RVI is proposed to play a role in the trafficking of the EBAs to the micronemes (Gilberger *et al*., 2003; Withers-Martinez *et al*., 2008). A gene, *eba165* has been identified that could potentially code for a fifth member of the EBA family, however, this gene carries a number of misssense mutations and a functional protein has not yet been identified in any *P. falciparum* strain (Triglia *et al.*, 2001 Tham *et al*., 2012).

The *P. falciparum* RH proteins are homologous to rhoptry proteins in *P. yoelii* (rodent parasite) and *P. vivax* (Rayner *et al*., 2000). This family consists of RH1 (PFD0110w), RH2a (PF13_0198), RH2b (MAL13P1.176), RH4 (PFD1150c) and RH5 (PFD1145c), of which only RH5 lacks a transmembrane region (Rayner *et al*., 2000; Rayner *et al*., 2001; Triglia *et al*., 2001; Taylor *et al*., 2001; Rodriguez *et al*., 2008). RH2a and RH2b are identical apart from a region

close to the carboxyl terminus indicating a possible gene duplication event followed by evolutionary drift (Rayner *et al*., 2000). Similar to *eba165*, the sixth *rh* paralog, *rh3* also has missense mutations and is a transcribed pseudogene (Taylor *et al*., 2001). All *ebl* and *rh* genes can be disrupted, with the exception of *rh5* suggesting that their encoded proteins perform functionally redundant roles (Duraisingh *et al*., 2003; Baum *et al*., 2009; Lopaticki *et al*., 2011). However, a minimal complement of these proteins appears to be necessary for merozoites to bind erythrocytes with sufficient affinity to activate the downstream processes that commit the parasite for invasion (Duraisingh *et al.*, 2003).

To date an erythrocyte receptor has been identified for three of the EBAs and two of the Rhs. EBA175, EBL-1 and EBA140 interact with the Glycophorins A, B and C respectively in a sialic acid-dependent manner (Camus and Hadely, 1985; Sim, 1995; Maier *et al*., 2002; Mayer *et al*., 2009), whereas RH4 and RH5 do not require sialic acid for the recognition of their respective receptors, CR1 and Basigin (BSG) (Crosnier *et al.*, 2011; Spadafora *et al.*, 2010). RH2a and RH2b have also been shown to bind to erythrocytes in a sialic acid independent manner, but their receptors have not yet been identified (Gaur & Chitnis, 2011). Interestingly only the RH5-BSG interaction has been shown to be essential for invasion, supporting the hypothesis that the other EBAs and RHs are functionally redundant (Crosnier *et al*., 2011; Tham *et al*., 2012). Having an array of ligands that can bind erythrocytes via different receptors probably enables the parasite to counter the highly polymorphic nature of the erythrocyte receptors, whilst reinforcing its ability to evade the human immune response using phenotypic variation (Harvey *et al*., 2012; Tham *et al*., 2012).

RH5 has also been shown to interact with another essential parasite protein, RIPR (RH5 interacting protein), which also lacks a transmembrane region (Chen *et al*., 2011). RIPR is a

micronemal protein that complexes with RH5 after secretion onto the merozoite surface, however, unlike RH5 it does not appear to interact directly with erythrocytes (Chen *et al*., 2011).

1.8 The micronemal protein AMA 1 is essential for tight junction formation.

AMA1 is a micronemal protein that is highly conserved across the *Apicomplexa* and in *P. falciparum* merozoites it is known to be essential for erythrocyte invasion (Triglia *et al*., 2000; Cowman & Crabb, 2006). AMA1 is not required for the initial attachment to erythrocytes or for apical re-orientation of the parasite (Mitchell *et al*., 2004; Treeck et al., 2009; Harvey *et al*., 2012), it is instead proposed to play a central role in tight junction formation via its interaction with the RON (rhoptry neck) complex, which occurs after the translocation of the latter to the erythrocyte surface (Riglar *et al.*, 2011). RON2, a membrane-spanning protein, has been identified as the immediate interacting partner of AMA1 within the RON complex and its binding site has been mapped to the hydrophobic groove on PAN (plasminogen, apple, nematode) domain I of AMA1 (Vulliez-Le Normand *et al.*, 2012; Bai *et al.*, 2005; Pizarro *et al.*, 2005).

1.9 Adhesins may be coupled to the molecular motor by MTRAP to allow movement of the tight junction.

In *P. falciparum* sporozoites, extracellular adhesins are coupled to the actin-myosin motor by the TRAP protein, which itself is linked to the parasite cytoskeleton via aldolase (Buscaglia *et al*., 2003). A similar membrane-spanning, thrombospondin type I repeats (TSR) domain-containing protein, MTRAP, is proposed to play the same role in merozoites (Baum *et al*., 2006). MTRAP is essential for the erythrocyte stage development of *P. falciparum* and its cytoplasmic tail has been shown to bind to aldolase *in vitro* (Baum *et al*., 2006; Morahan *et al*., 2009). Whereas, the

TSR-domain containing extracellular region of MTRAP has recently been demonstrated to bind erythrocytes via interaction with a putative receptor, Semaphorin 7A (Uchime *et al*., 2012; Bartholdoson *et al*., unpublished data). Other TSR domain containing proteins expressed at the merozoite stage include PTRAMP, SPATR and TLP, but the functional role of these proteins are not yet known (Baum *et al*., 2006; Heiss *et al*., 2008; Morahan *et al*., 2009).

1.10 *P. falciparum* merozoite surface proteins are important candidates for a blood-stage vaccine.

Clinical immunity to malaria develops slowly in response to a number of repeated exposures and is primarily associated with the presence of protective antibodies which act against blood-stage parasites (Cohen *et al.,* 1961; Geels *et al.,* 2011). The goal of an effective blood-stage vaccine is to mimic this natural immunity by inducing an immune response capable of inhibiting the erythrocytic development of the parasite (Greenwood & Targett, 2011). Merozoite surface proteins are the most likely candidates for such a blood stage vaccine as they are exposed to the immune system (albeit briefly) at each replication cycle (Section 1.3).

The blood-stage vaccine candidates that have so far been evaluated in epidemiological studies and clinical trials are limited in number and were almost all known before the completion of the *P. falciparum* genome sequence in 2002 (Conway *et al.,* 2000; Fowkes *et al.,* 2010; Osier *et al.,* 2008). To date, only seven merozoite surface proteins have been approved for clinical testing as vaccine candidates; MSP1, MSP2, MSP3, AMA1, EBA175, GLURP and SERA5 (Schwartz *et al.,* 2012). The most advanced of these, MSP1 and AMA1, did not afford significant protection from *P. falciparum* infection in recent phase II trials (Geels et al., 2011; Schwartz *et al.,* 2012). This has mainly been attributed to the highly polymorphic nature of these proteins resulting in antibodies raised against one haplotype failing to recognise others and has led to the usefulness

of MSP1 and AMA1 as vaccine candidates to be questioned (Geels et al., 2011; Hill, 2011; Schwartz *et al.,* 2012).

To increase the chance of developing an effective blood-stage vaccine, resources must be channelled towards identifying new candidates (Hill, 2011). Even though the sequencing of the *P. falciparum* genome has revealed a large number of merozoite surface proteins (Gardner *et al.,* 2002), determining which of these should be prioritised as vaccine candidates is a difficult task as a functional role in erythrocyte invasion is not known for the vast majority. Not only are these *P. falciparum* surface proteins hard to express recombinantly but identifying their extracellular interactions with erythrocyte receptors is difficult and beyond the scope of conventional biochemical methods for systematically identifying protein-protein interactions on a genome wide scale, such as yeast-2-hybrid screening and tandem affinity purification-mass spectrometry (TAP-MS) (Bei & Duraisingh, 2012).

1.11 Many prokaryotic and eukaryotic expression systems have been tested for the production of *P. falciparum* proteins in recombinant form.

Bioinformatic tools are often useful for identifying certain properties of selected proteins and for predicting their possible biological roles. However, such inferences are not possible in some cases (e.g. when the protein to be characterised has little sequence homology to any protein of known function) and in-depth structural and functional characterisation of any protein always requires experimentation with molecular biology techniques (Birkholtz *et al.*, 2008). Production of *P. falciparum* proteins in a recombinant form is a necessity as it is very difficult to isolate them in sufficient quantities from the parasite for *in vitro* experiments. A variety of heterologous and cell-free systems have been tested for expression of *P. falciparum* surface proteins with modest success (Birkholtz *et al.*, 2008). The difficulty in expressing *P. falciparum* proteins in

recombinant form is mainly attributed to the very high A+T content of the genes and the prevalence of repetitive amino acid sequences (Tsuboi *et al.,* 2008). Integral membrane proteins are in particular challenging to express in a biochemically-amenable manner due to their hydrophobic membrane-spanning domains and efforts have therefore been focused on the production of their soluble, truncated ectodomains.

The most widely used expression host for *P. falciparum* proteins is still *Escherichia coli* (Birkholtz *et al.,* 2008). Although cost effective, fast and easy to use, recombinant proteins expressed in these cells are often insoluble and sequestered in inclusion bodies. Such aggregated proteins can be solubilised and refolded to their native conformation (Pandey *et al*., 2002; Bai *et al*., 2005). However, protein refolding is a complicated process that requires several steps of optimisation and conditions which are suitable for one protein may not necessarily be appropriate for another, therefore its use in large scale, high throughput production of proteins is limited (Birkholtz *et al.,* 2008).

Two species of yeast, *Saccharomyces cerevisiae* and *Pichia pastoris* are also commonly used for production of *P. falciparum* proteins (Birkholtz *et al.,* 2008). Fragments of a number of merozoite surface proteins, including current vaccine candidates EBA175, AMA1, MSP1 and MSP3 have been successfully expressed in yeast in active, soluble form (Zang & Pan, 2005; Tolia *et al*., 2005; El Sahly *et al*., 2010). A major advantage of yeast over *E. coli* as an expression host is the secretion of recombinant proteins fused to yeast hormones into the growth media. Not only does this bypass the problem of over-expressed proteins aggregating in insoluble inclusion bodies, it also simplifies downstream protein purification. Recombinant proteins expressed in yeast are furthermore subjected to eukaryotic post-translational modifications, some such as disulphide-bond formation facilitate the correct folding of *P.*

falciparum surface proteins but others such as N- and O-glycosylation are potentially disadvantageous as plasmodial proteins are not glycosylated in the parasite (Gowda & Davidson, 1999). Additionally as yeast recognises some A+T containing codons as termination signals *P. falciparum* coding sequences need to be codon optimised for expression in these systems (Birkholtz *et al.*, 2008).

Other heterologous systems used for the production of *P. falciparum* proteins include expression from baculoviral vectors in insect cells (Birkholtz *et al.*, 2008). As the host cells recognise eukaryotic targeting signals and perform most post-translational modifications this system has been used successfully to produce immunologically active fragments of some *P. falciparum* proteins including EBA175 and AMA1 (Narum *et al*., 1993; Ockenhouse *et al*., 2001).

In vitro translation in cell-free systems has been used with some success for a number of *P. falciparum* surface proteins (Tsuboi *et al.*, 2008; Crompton *et al.*, 2010; Trieu *et al.*, 2011). Such systems can be easily manipulated for the production of correctly folded proteins and post-translational modifications can be facilitated by the use of eukaryotic cell extracts. They are also amenable to automation and hence high-throughput screening strategies. However, these systems have high-running costs and the availability of cell-free extracts is restricted as their preparation in laboratories is generally impractical (Farrokhi *et al*., 2009).

1.12 Studying extracellular interactions between *P. falciparum* merozoites and human erythrocytes using *in vitro* biochemical techniques is challenging.

Extracellular binding events between cell surface proteins are generally of very low affinity (equilibrium dissociation constants (K_D) in the μM to mM range) and the interactions between *P. falciparum* merozoite surface proteins and their erythrocyte receptors are no exception (Wright, 2009; Bei and Duraisingh, 2012). The highly transient nature of such interactions, with half lives

of less than 0.5 sec when measured in the monomeric state, limits the use of traditional biochemical assays based on affinity purification strategies, for their detection and characterisation (Bei and Duraisingh, 2012; Wright, 2009).

On the surface of cells, membrane proteins are locally concentrated in the context of the lipid bilayer and essentially displayed as multimeric arrays, which allows their interactions to occur with high avidity (Wright, 2009). Cell-based assays are therefore suitable for the identification of individually weak protein-protein interactions and have been used widely for investigating the binding of *P. falciparum* proteins to erythrocytic receptors.

Over the millennia, *P. falciparum* has exerted considerable selection pressure in the shaping of the human genome and a number of naturally occurring polymorphisms in erythrocyte proteins have been found to be associated with reduced risk of malaria (Evans and Wellems, 2002; Bei and Duraisingh, 2012). *In vitro* studies using polymorphic erythrocytes have facilitated the identification and/or verification of specific surface proteins as host receptors utilised by *P. falciparum* during invasion (Crosnier *et al*., 2011; Maier *et al.*, 2002; Mayer *et al*., 2009; Spadafora *et al*., 2010). The five known erythrocyte receptors of *P. falciparum* are all polymorphic blood group antigens (Bei and Duraisingh, 2012).

Interactions between erythrocyte receptors and their parasite ligands have also been biochemically characterised by pre-treatment of erythrocytes with specific enzymes, prior to performing the binding assays (Bei and Duraisingh, 2012). The requirement of some of the known interactions for sialic acid for example was identified by treatment of erythrocytes with the enzyme neuraminidase (Camus and Hadely, 1985; Thompson *et al*., 2001; Maier *et al*., 2002; Mayer *et al*., 2009). Treatment with the proteases trypsin and chymotrypsin has also been used

widely for classifying the different receptors used for invasion (Camus and Hadely, 1985; Thompson *et al*., 2001; Baum *et al*., 2009).

1.13 Work in this laboratory: expression of a library of *P. falciparum* merozoite surface proteins and avidity-based extracellular interaction screening (AVEXIS).

Mammalian expression systems are well-characterised, can aid the correct folding *P. falciparum* proteins in their secretory compartments and impart necessary post-translational modifications (Birkholtz *et al.,* 2008) . Despite these advantages, they have not been used for the preparative expression of *P. falciparum* surface proteins in the past, mainly due to the low yields of recombinant proteins obtained from traditional mammalian cell lines grown in adherent culture (Birkholtz *et al.,* 2008). However, many mammalian cell lines have now been adapted for growth at high densities in liquid culture and are routinely used in the research community for expressing various recombinant proteins in milligram to gram quantities (Tom *et al*., 2008). The suspension-adapted human embryonic kidney cell line stably expressing the Epstein-Barr virus nuclear antigen 1, HEK293E, is the most commonly used cell line for large-scale production of recombinant proteins (Tom *et al.*, 2008).

Our laboratory recently used HEK293E as the expression host for successfully producing the entire ectodomains of 50 *P. falciparum* merozoite surface proteins in soluble form (Table 1, Figure 4 A) (Cecile Wright-Crosnier, unpublished data). The majority of these proteins had previously not been expressed in an active form or produced as only small soluble fragments using heterologous and cell free systems. Successful expression of the *P. falciparum* proteins in HEK293E was achieved by codon optimisation of the native coding sequences for mammalian expression, replacement of the endogenous signal peptides with one from mouse to promote secretion and systematic removal of potential N-linked glycosylation sites. The proteins were

also expressed with the immunoglobulin-like domains 3 and 4 of rat Cd4 as a fusion partner. Cd4 was selected on the basis of its high levels of expression in mammalian systems, its well characterized structure and the availability of conformationally-sensitive anti-Cd4 monoclonal antibodies which can be used for quantitation and purification of the fusion proteins (Brown and Barclay, 1994).

The library of *P. falciparum* merozoite proteins was tested against a panel of 40 full-length ectodomains of single-pass erythrocyte receptors using AVEXIS (avidity-based extracellular interaction screening), an ELISA-based high-throughput screening platform developed in our laboratory (Cecile Crosnier, unpublished data). This screen identified the erythrocyte receptors for two *P. falciparum* proteins, RH5 and MTRAP, discussed previously (Crosnier *et al*., 2011; Bartholdoson *et al*., unpublished data). The detection of low affinity interactions is facilitated in the AVEXIS assay, as both 'bait' and 'prey' proteins are used in multimeric forms to enable potential binding events to occur with high avidity (Figure 4 B). The bait proteins, expressed with biotin tags, are multimerised by immobilisation on streptavidin-coated plates, whereas the prey proteins are produced as pentamers by fusion with the pentamerisation domain of the rat cartilaginous oligomeric matrix protein (COMP) (Bushell *et al.*, 2008).

1.14 Work described in this thesis

The three studies that were undertaken for this thesis are briefly described below. In all three, a number of different biochemical approaches were used to investigate the low-affinity interactions between *Plasmodium* surface proteins, produced recombinantly using the mammalian expression system optimised in our laboratory, and native and recombinant human erythrocyte receptors.

Sub-cellular location	Official nomenclature	Synonym/s	Accession Number	Region expressed	Len. (aa)
SURFACE (GPI-ANCHORED)	MSP1		PFI1475w	V20-S1701	1682
	MSP2		PFB0300c	I20-N246	227
	MSP4		PFB0310c	Y29-S253	225
	MSP5		PFB0305c	N22-S251	230
	MSP10		PFF0995c	H27-S503	477
	Pf12	P12	PFF0615c	H26-S323	298
	P12p		PFF0620c	Y21-T349	329
	Pf38	P38	PFE0395c	Q22-S328	307
	Pf92		PF13_0338	A26-S770	745
	Pf113		PF14_0201	Y23-K942	920
	PF3D7_1136200		PF11_0373	L19-G656	638
	PF3D7_1431400*		PF14_0293	N25-S968	944
SURFACE (PERIPHERAL)	MSP3	MSP3.1, SPAM	PF10_0345	K26-H354	328
	MSP6	MSP3.2	PF10_0346	Y17-N371	355
	H101	MSP3.3	PF10_0347	Q23-N424	402
	MSP11	H103, MSP3.7	PF10_0352	K27-Y405	379
	MSP3.4		PF10_0350	N26-K697	672
	MSP3.8		PF10_0355	Y23-N762	740
	MSP7	MSP7.1	PF13_0197	T28-M351	324
	MSRP1	MSP7.2	PF13_0196	Y22-T379	358
	MSRP2	MSP7.3	MAL13P1.174	K24-T280	257
	MSRP3	MSP7.4	PF13_0193	Q24-S298	275
	Pf41	P41	PFD0240c	K21-S378	358
	MSP9	p101, ABRA	PFL1385c	N24-S742	719
MICRONEME	AMA1	Pf83, RMA1	PF11_0344	Q25-T541	517
	EBA140	BAEBL	MAL13P1.60	I26-P1135	1110
	EBA175		MAL7P1.176	A21-P1424	1404
	EBA181	JESEBL	PFA0125c	I27-S1488	1462
	EBL1*		PF13_0115	K22-N2584	2563
	ASP		PFD0295c	A20-S708	689
	MTRAP		PF10_0281	I23-K432	410
	PTRAMP*	TRAMP, TSP-3	PFL0870w	N25-S306	282
	GAMA	PSOP9	PF08_0008	L22-P710	689
RHOPTRY	RH5		PFD1145c	F25-Q526	502
	RAP1*		PF14_0102	I23-D782	760
	RAP2*		PFE0080c	D22-L398	387
	RAP3*		PFE0075c	N23-K400	378
	CLAG3.2*	RhopH1(3.2)	PFC0110w	K21-H1416	1396
	RhopH2*		PFI1445w	L20-S1378	1359
	RhopH3		PFI0265c	K25-L897	873
	SPATR		PFB0570w	E22-C250	229
	AARP		PFD1105w	K18-P191	174
	Pf34	PV2	PFD0955w	N25-S306	282
	RON3*		PFL2505c	N22-N249	228
	RON6		PFB0680w	F16-T949	934
	RAMA		MAL7P1.208	Y17-K838	821
OTHER	TLP	TRAP2	PFF0800w	E24-P1306	1283
	PTEX150	Pf112	PF14_0344	A20-N993	974
	ETRAMP10.2	PfJ323	PF10_0323	R25-R52	28
	PF3D7_0606800		PFF0335c	V23-K299	277

Table 1. Members of the *P. falciparum* merozoite surface protein library. The 50 proteins are grouped and colour-coded according to their known/predicted sub-cellular localisation. Light blue-GPI-anchored surface proteins, dark blue- peripheral surface proteins, green-micronemal proteins, red-rhoptry proteins, orange-other proteins (no information about sub-cellular location). In the case of each protein, the full-length ectodomain was expressed, as indicated by the N-and C-terminal residues and their locations. Nine of the proteins from the library were expressed at very low levels and are indicated by *.

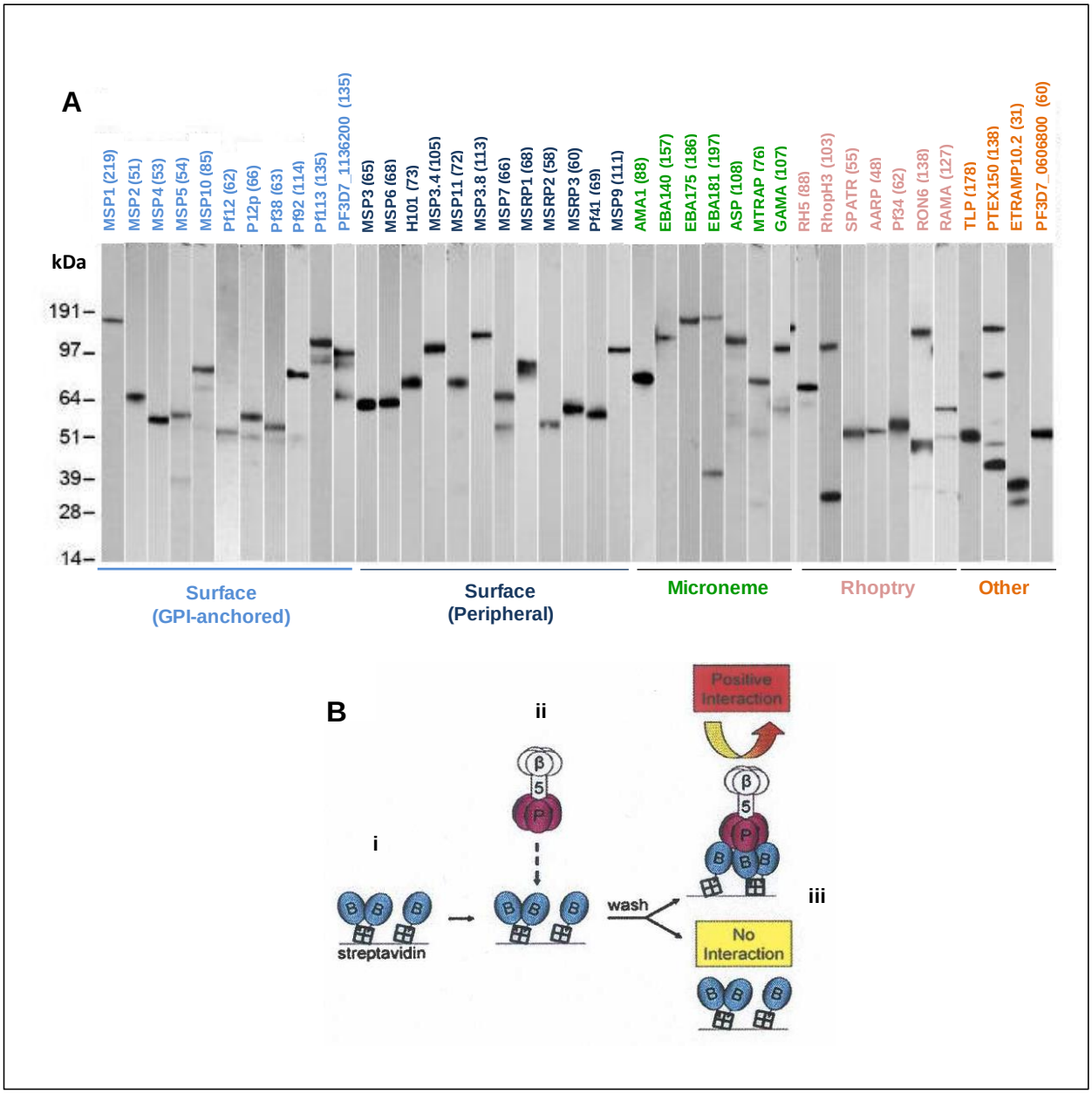
A
MSP1 (219)
MSP2 (51)
MSP4 (53)
MSP5 (54)
MSP10 (85)
Pf12 (62)
P12p (66)
Pf38 (63)
Pf92 (114)
Pf113 (135)
PF3D7_1136200 (135)
MSP3 (65)
MSP6 (68)
H101 (73)
MSP3.4 (105)
MSP11 (72)
MSP3.8 (113)
MSP7 (66)
MSRP1 (68)
MSRP2 (58)
MSRP3 (60)
Pf41 (69)
MSP9 (111)
AMA1 (88)
EBA140 (157)
EBA175 (186)
EBA181 (197)
ASP (108)
MTRAP (76)
GAMA (107)
RH5 (88)
RhopH3 (103)
SPATR (55)
AARP (48)
Pf34 (62)
RON6 (138)
RAMA (127)
TLP (178)
PTEX150 (138)
ETRAMP10.2 (31)
PF3D7_0606800 (60)
kDa
191
97
64
51
39
28
14
Surface (GPI-anchored)
Surface (Peripheral)
Microneme
Rhoptry
Other
B
i
ii
iii
streptavidin
wash
Positive Interaction
No Interaction

Figure 4. Previous work in this laboratory: a library of *P. falciparum* merozoite surface proteins was expressed and tested against a panel of erythrocyte receptor ectodomains by AVEXIS (avidity-based extracellular interaction screening). A) The full-length ectodomains of 50 *P. falciparum* surface proteins were expressed in soluble form using the mammalian HEK293E expression system. Only 41 of the proteins, expressed with a C-terminal Cd4 (25 kDa) tag, could be detected by western blotting (Cecile Crosnier, unpublished data). **B)** A simplified schematic representing the main steps of the AVEXIS assay, designed for detecting low affinity interactions between the soluble extracellular domains of membrane proteins expressed as mono-biotinylated 'baits' and pentameric β-lactamase-tagged 'preys'. i) Immobilisation of biotinylated 'bait' proteins on a streptavidin-coated plate. ii) Incubation of the immobilised 'baits' with the pentameric β-lactamase-tagged 'prey' proteins. iii) Detection of putative 'bait-prey' interactions by adding a colorimetric β-lactamase substrate after removal of non-bound 'preys' by stringent washing. (The schematic was adapted from Bushell *et al*., 2008).

Project A (Chapter 3): Functional validation of a mammalian-expressed EBA175 antigen and comparative analysis of its binding to MM and MN forms of human Glycophorin A.

P. falciparum EBA175 is the known ligand of the erythrocyte receptor Glycophorin A, which carries the antigenic determinants of the human MN blood group system. The goal of this study was to apply a range of biochemical and biophysical tools to investigate the EBA175-Glycophorin A interaction at a molecular level. The recombinant full-length ectodomain of EBA175 (*Pf*EBA175 FL), produced using the mammalian expression system optimised in our laboratory, was firstly confirmed to be functionally similar to native EBA175 isolated from parasite cultures by demonstrating its binding to human erythrocytes in a sialic acid- and Glycophorin A-dependent manner. The protein was then tested for direct binding to both native human Glycophorin A purified from erythrocytes and to the recombinantly-expressed full-length ectodomain of human Glycophorin A. Binding of *Pf*EBA175 FL was observed only to native Glycophorin A. The attempts to enhance the sialylation of recombinant Glycophorin A by co-expression with sialyl transferases and a sialic acid transporter were partially successful, but did not confer detectable binding of *Pf*EBA175 FL. Kinetic analysis of the interaction of *Pf*EBA175 FL with native Glycophorin A, by surface plasmon resonance (SPR), revealed the K_D to be ~ 0.24 µM. SPR analysis further revealed a slightly higher (x 1.3) affinity of *Pf*EBA175 FL for Glycophorin A from MN erythrocytes in comparison to that from MM erythrocytes. *Pf*EBA175 RII, a truncated derivative containing only the region known to be essential for interacting with erythrocytes, was observed to bind to native Glycophorin A with a ~10-fold lower affinity than *Pf*EBA175 FL, suggesting some role played by regions outside of RII to facilitate binding.

Project B (Chapter 4): Investigating the host-specificity of *Plasmodium* merozoite: primate erythrocyte interactions in the *Laverania* family.

The *Laverania* family of great ape parasites are stringently host-specific in their natural environment, with clades C1-C3 found only in chimpanzees and clades G1-G3 restricted to gorillas. *P. falciparum* falls within the G1 clade, and is hypothesized to have adapted to humans after a single cross-species transmission event from gorilla. The goal of this study was to investigate whether two known parasite ligand-host receptor interactions, EBA175-Glycophorin A and RH5-Basigin (BSG), could contribute towards the determination of host-specificity in *Laverania*. Both interactions studied are known to be important for the invasion of human erythrocytes by *P. falciparum*. EBA175 orthologues from three *Laverania* species, namely the human parasite *P. falciparum* and the chimpanzee parasites *P. reichenowi* and *P. billcollinsi* were all observed to bind to human erythrocytes in a sialic-acid dependent manner. SPR analysis of the binding of these EBA175 orthologues to native human Glycophorin A revealed only a ~2-fold lower affinity of the chimpanzee parasite proteins for the human erythrocyte receptor in comparison to the human parasite protein, suggesting that the EBA175-Glycophorin A interaction may not be a significant determinant of *Laverania* host-specificity. Investigating the binding of the *P. falciparum* and *P. reichenowi* RH5 proteins to human, chimpanzee (*Pan troglodytes*) and gorilla (*Gorilla gorilla*) Basigin on the other hand, revealed no binding of *P. reichenowi* RH5 to BSG. *P. falciparum* RH5 also did not recognise gorilla BSG and bound to chimpanzee BSG with a 15-fold lower affinity than to human BSG. Residues that confer host-specificity were then identified by generating site-directed mutants of the BSG orthologues and analysing their interactions with *P. falciparum* RH5.

Project C (Chapter 5): Development of high-throughput assays for characterising a library of *P. falciparum* merozoite surface proteins.

More than 250 *P. falciparum* merozoite proteins are now known but the vast majority of these have no identified function. To determine which of the novel *P. falciparum* antigens should be prioritised as potential vaccine candidates, their functional characterisation with the use of high-throughput strategies is a necessity. Traditional methods such as tandem affinity purification-mass spectrometry, used for identifying protein-protein interactions on a global scale, are not suitable for the detection of low affinity, extracellular interactions between merozoite surface proteins and their receptors on the erythrocyte surface. The ELISA-based, high-throughput screening platform, AVEXIS, developed in our laboratory is optimised for the identification of such interactions between recombinantly-expressed proteins, but cannot be used with multi-pass receptors, which are difficult to produce as correctly-folded soluble fragments. In this study, a library of 33 *P. falciparum* surface proteins was screened against erythrocytes and a panel of 41 erythrocytic multi-pass receptors, using a novel, flow-cytometry based, high-throughput approach. The *P. falciparum* proteins were multimerised by immobilisation on fluorescent beads for this purpose and each of the erythrocytic multi-pass receptors was expressed recombinantly on the surface of HEK293E cells. 13 putative interactions, between *P. falciparum* ligands and erythrocyte multi-pass receptors, were identified in the screen. Of these, the binding of the *P. falciparum* proteins, AARP and MSP11, to the erythrocyte proteins, Fatty acid transporter 4 and Plasma membrane $Ca2^{+}$ transporting ATPase 4, respectively, were the most significant. Nine of the *P. falciparum* proteins that showed binding to cells, were subsequently tested against a panel of 55 synthetic carbohydrate probes, using an ELISA-based approach, to identify whether their binding was glycan-dependent.

1.15 BIBLIOGRAPHY

Adams, J. H., Blair, P. L., Kaneko, O., & Peterson, D. S. (2001). An expanding ebl family of *Plasmodium falciparum*. *Trends in Parasitology*, *17*(6), 297-9.

Aikawa, M., Miller, L. H., Johnson, J., & Rabbege, J. (1978). Erythrocyte entry by malarial parasites. A moving junction between erythrocyte and parasite. *The Journal of Cell Biology*, *77*(1), 72-82.

Ayouba, A., Mouacha, F., Learn, G. H., Mpoudi-Ngole, E., Rayner, J. C., Sharp, P. M., Hahn, B. H., *et al*. (2012). Ubiquitous Hepatocystis infections, but no evidence of *Plasmodium falciparum*-like malaria parasites in wild greater spot-nosed monkeys (Cercopithecus nictitans). *International Journal for Parasitology*, *42*(8), 709-13.

Bai, T., Becker, M., Gupta, A., Strike, P., Murphy, V. J., Anders, R. F., & Batchelor, A. H. (2005). Structure of AMA1 from *Plasmodium falciparum* reveals a clustering of polymorphisms that surround a conserved hydrophobic pocket. *Proceedings of the National Academy of Sciences of the United States of America*, *102*(36), 12736-41.

Bannister, L H, Butcher, G. a, Dennis, E. D., & Mitchell, G. H. (1975). Structure and invasive behaviour of *Plasmodium knowlesi* merozoites *in vitro*. *Parasitology*, *71*(3), 483-91.

Bannister, L., & Mitchell, G. (2003). The ins, outs and roundabouts of malaria. *Trends in Parasitology*, *19*(5), 209-213.

Baum, J., Chen, L., Healer, J., Lopaticki, S., Boyle, M., Triglia, T., Ehlgen, F., *et al*. (2009). Reticulocyte-binding protein homologue 5 - an essential adhesin involved in invasion of human erythrocytes by *Plasmodium falciparum*. *International Journal for Parasitology*, *39*(3), 371-80.

Baum, J., Maier, A. G., Good, R. T., Simpson, K. M., & Cowman, A. F. (2005). Invasion by *P. falciparum* merozoites suggests a hierarchy of molecular interactions. *PLoS Pathogens*, *1*(4), e37.

Baum, J., Richard, D., Healer, J., Rug, M., Krnajski, Z., Gilberger, T.-W., Green, J. L., Holder, A. A., & Cowman, A. F. (2006). A conserved molecular motor drives cell invasion and gliding motility across malaria life cycle stages and other apicomplexan parasites. *The Journal of Biological Chemistry*, *281*(8), 5197-208.

Bei, A. K., & Duraisingh, M. T. (2012). Functional analysis of erythrocyte determinants of *Plasmodium* infection. *International Journal for Parasitology*, *42*(6), 575-582.

Bentley, G. A. (2006). Functional and immunological insights from the three-dimensional structures of *Plasmodium* surface proteins. *Current Opinion in Microbiology*, *9*(4), 395-400.

Birkholtz, L.-M., Blatch, G., Coetzer, T. L., Hoppe, H. C., Human, E., Morris, E. J., Ngcete, Z., *et al*. (2008). Heterologous expression of plasmodial proteins for structural studies and functional annotation. *Malaria Journal, 7*, 197.

Blackman, B. M. J., Scott-finnigan, T. J., Shai, S., & Holder, A. A. (1994). Antibodies inhibit the protease-mediated processing of a malaria merozoite surface protein. *The Journal of Experimental Medicine, 180*(1), 389-93.

Blackman, M. J., Ling, I. I., Nicholls, S. C., & Holder, A. A. (1991). Proteolytic processing of the *Plasmodium falciparum* merozoite surface protein-1 produces a membrane-bound fragment containing two epidermal growth factor-like domains. *Molecular and Biochemical Parasitology, 49*(1), 29-33.

Brown, M. H., & Barclay, A. N. (1994). Expression of immunoglobulin and scavenger receptor superfamily domains as chimeric *p*roteins with domains 3 and 4 of CD4 for ligand analysis. *Protein Engineering, 7*(4), 515-21.

Burgess, B. R., Schuck, P., & Garboczi, D. N. (2005). Dissection of merozoite surface protein 3, a representative of a family of *Plasmodium falciparum* surface proteins, reveals an oligomeric and highly elongated molecule. *The Journal of Biological Chemistry, 280*(44), 37236-45.

Buscaglia, C. A., Coppens, I., Hol, W. G., & Nussenzweig, V. (2003). Sites of interaction between aldolase and thrombospondin-related anonymous protein in *Plasmodium*. *Molecular Biology of the Cell, 14*(12), 4947-4957.

Bushell, K. M., Söllner, C., Schuster-Boeckler, B., Bateman, A., & Wright, G. J. (2008). Large-scale screening for novel low-affinity extracellular protein interactions. *Genome Research, 18*(4), 622-30.

Camus, D., & Hadley, T. J. (1985). A *Plasmodium falciparum* antigen that binds to host erythrocytes and merozoites. *Science, 230*(4725), 553-556.

Chen, L., Lopaticki, S., Riglar, D. T., Dekiwadia, C., Uboldi, A. D., Tham, W.-H., O'Neill, M. T., *et al*. (2011). An EGF-like protein forms a complex with PfRh5 and is required for invasion of human erythrocytes by *Plasmodium falciparum*. *PLoS Pathogens, 7*(9), e1002199.

Cohen, S., Mcgregor, A., & Carrington, S. (1961). Gamma-globulin and acquired immunity to human malaria. *Nature, 192*(4804), 733-737.

Conway, D., Cavanagh, D., Tanabe, K., & Roper, C. (2000). A principal target of human immunity to malaria identified by molecular population genetic and immunological analyses. *Nature Medicine, 6*(6), 689-692.

Cowman, A. F., & Crabb, B. S. (2006). Invasion of red blood cells by malaria parasites. *Cell*, *124*(4), 755-66.

Crompton, P. D., Kayala, M. A., Traore, B., Kayentao, K., Ongoiba, A., Weiss, G. E., Molina, D. M., *et al*. (2010). A prospective analysis of the Ab response to *Plasmodium falciparum* before and after a malaria season by protein microarray. *Proceedings of the National Academy of Sciences of the United States of America*, *107*(15), 6958-63.

Crompton, P., & Pierce, S. (2010). Advances and challenges in malaria vaccine development. *The Journal of Clinical Investigation*, *120*(12), 4168-4178.

Crosnier, C., Bustamante, L. Y., Bartholdson, S. J., Bei, A. K., Theron, M., Uchikawa, M., Mboup, S., *et al*. (2011). Basigin is a receptor essential for erythrocyte invasion by *Plasmodium falciparum*. *Nature*, *480*(7378), 534-7.

Duraisingh, M. T., Triglia, T., Ralph, S. a, Rayner, J. C., Barnwell, J. W., McFadden, G. I., & Cowman, A. F. (2003). Phenotypic variation of *Plasmodium falciparum* merozoite proteins directs receptor targeting for invasion of human erythrocytes. *The EMBO Journal*, *22*(5), 1047-57.

Duval, L., & Ariey, F. (2012). Ape *Plasmodium* parasites as a source of human outbreaks. *Clinical Microbiology and Infection*, *18*(6), 528-32.

El Sahly, H. M., Patel, S. M., Atmar, R. L., Lanford, T. a, Dube, T., Thompson, D., Sim, B. K. L., *et al*. (2010). Safety and immunogenicity of a recombinant nonglycosylated erythrocyte binding antigen 175 Region II malaria vaccine in healthy adults living in an area where malaria is not endemic. *Clinical and Vaccine Immunology*, *17*(10), 1552-9.

Evans, A. G., & Wellems, T. E. (2002). Coevolutionary genetics of *Plasmodium* malaria parasites and their human hosts. *Integrative and Comparative Biology*, *42*(2), 401-7.

Farrokhi, N., Hrmova, M., Burton, R. A., & Fincher, G. B. (2009). Heterologous and cell free protein expression systems. *Methods in Molecular Biology*, *513*, 175-98.

Farrow, R. E., Green, J., Katsimitsoulia, Z., Taylor, W. R., Holder, A. A., & Molloy, J. E. (2011). The mechanism of erythrocyte invasion by the malarial parasite, *Plasmodium falciparum*. *Seminars in Cell & Developmental Biology*, *22*(9), 953-60.

Fowkes, F. J. I., Richards, J. S., Simpson, J. A, & Beeson, J. G. (2010). The relationship between anti-merozoite antibodies and incidence of *Plasmodium falciparum* malaria: A systematic review and meta-analysis. *PLoS Medicine*, *7*(1), e1000218.

Garcia, C. R. S., Azevedo, M. F. D., Wunderlich, G., Budu, A., Young, J. A., & Bannister, L. (2008). *Plasmodium* in the Postgenomic Era: New Insights into the Molecular Cell Biology of Malaria Parasites. *Cell*, *266*(7), 85-156.

Gardner, M. J., Hall, N., Fung, E., White, O., Berriman, M., Hyman, R. W., Carlton, J. M., *et al*. (2002). Genome sequence of the human malaria parasite *Plasmodium falciparum*. *Nature*, *419*(6906), 498-511.

Gaur, D., & Chitnis, C. E. (2011). Molecular interactions and signaling mechanisms during erythrocyte invasion by malaria parasites. *Current Opinion in Microbiology*, *14*(4), 422-8.

Geels, M. J., Imoukhuede, E. B., Imbault, N., van Schooten, H., McWade, T., Troye-Blomberg, M., Dobbelaer, R., *et al*. (2011). European Vaccine Initiative: lessons from developing malaria vaccines. *Expert Review of Vaccines*, *10*(12), 1697-708.

Gerloff, D. L., Creasey, A., Maslau, S., & Carter, R. (2005). Structural models for the protein family characterized by gamete surface protein Pfs230 of *Plasmodium falciparum*. *Proceedings of the National Academy of Sciences of the United States of America*, *102*(38), 13598-603.

Gilberger, T.-W., Thompson, J. K., Reed, M. B., Good, R. T., & Cowman, A. F. (2003). The cytoplasmic domain of the *Plasmodium falciparum* ligand EBA-175 is essential for invasion but not protein trafficking. *The Journal of Cell Biology*, *162*(2), 317-27.

Gilson, P. R., & Crabb, B. S. (2009). Morphology and kinetics of the three distinct phases of red blood cell invasion by *Plasmodium falciparum* merozoites. *International Journal for Parasitology*, *39*(1), 91-6.

Goel, V. K., Li, X., Chen, H., Liu, S.-C., Chishti, A. H., & Oh, S. S. (2003). Band 3 is a host receptor binding merozoite surface protein 1 during the *Plasmodium falciparum* invasion of erythrocytes. *Proceedings of the National Academy of Sciences of the United States of America*, *100*(9), 5164-9.

Gowda, D. C., & Davidson, E. A. (1999). Protein glycosylation in the malaria parasite. *Parasitology Today*, *15*(4), 147-52.

Greenwood, B. M., & Targett, G. A. T. (2011). Malaria vaccines and the new malaria agenda. *Clinical Microbiology and Infection,17*(11), 1600-7.

Harris, P. K., Yeoh, S., Dluzewski, A. R., Donnell, R. A. O., Withers-martinez, C., Hackett, F., Bannister, L. H., *et al*. (2005). Molecular Identification of a Malaria Merozoite Surface Sheddase. *PLoS Pathogens*, *1*(3), 241-51.

Harvey, K. L., Gilson, P. R., & Crabb, B. S. (2012). A model for the progression of receptor–ligand interactions during erythrocyte invasion by *Plasmodium falciparum*. *International Journal for Parasitology*, *42*(6), 567-573.

Heiss, K., Nie, H., Kumar, S., Daly, T. M., Bergman, L. W., & Matuschewski, K. (2008). Functional characterization of a redundant *Plasmodium* TRAP family invasin, TRAP-like

protein, by aldolase binding and a genetic complementation test. *Eukaryotic Cell*, *7*(6), 1062-70.

Hill, A. V. S. (2011). Vaccines against malaria. *Philosophical transactions of the Royal Society of London. Series B, Biological sciences*, *366*(1579), 2806-14.

Hodder, A. N., Malby, R. L., Clarke, O. B., Fairlie, W. D., Colman, P. M., Crabb, B. S., & Smith, B. J. (2009). Structural insights into the protease-like antigen *Plasmodium falciparum* SERA5 and its noncanonical active-site serine. *Journal of Molecular Biology*, *392*(1), 154-65.

Kadekoppala, M., & Holder, A. A. (2010). Merozoite surface proteins of the malaria parasite: the MSP1 complex and the MSP7 family. *International Journal for Parasitology*, *40*(10), 1155-61.

Kadekoppala, M., O'Donnell, R. A., Grainger, M., Crabb, B. S., & Holder, A. A. (2008). Deletion of the *Plasmodium falciparum* merozoite surface protein 7 gene impairs parasite invasion of erythrocytes. *Eukaryotic Cell*, *7*(12), 2123-32.

Kappe, S. H. I., Vaughan, A. M., Boddey, J. a, & Cowman, A. F. (2010). That was then but this is now: malaria research in the time of an eradication agenda. *Science*, *328*(5980), 862-6.

Keeley, A., & Soldati, D. (2004). The glideosome: a molecular machine powering motility and host-cell invasion by Apicomplexa. *Trends in Cell Biology*, *14*(10), 528-532.

Krief, S., Escalante, A. A., Pacheco, M. A., Mugisha, L., André, C., Halbwax, M., Fischer, A., *et al*. (2010). On the diversity of malaria parasites in African apes and the origin of *Plasmodium falciparum* from Bonobos. *PLoS Pathogens*, *6*(2), e1000765.

Lee, K.-S., Divis, P. C. S., Zakaria, S. K., Matusop, A., Julin, R. A., Conway, D. J., Cox-Singh, J., *et al*. (2011). *Plasmodium knowlesi*: reservoir hosts and tracking the emergence in humans and macaques. *PLoS Pathogens*, *7*(4), e1002015.

Liu, W, Li, Y., Learn, G., Rudicell, R., & Robertson, J. (2010). Origin of the human malaria parasite *Plasmodium falciparum* in gorillas. *Nature*, *467*(7314), 420-425.

Lopaticki, S., Maier, A. G., Thompson, J., Wilson, D. W., Tham, W.-H., Triglia, T., Gout, A., *et al*. (2011). Reticulocyte and erythrocyte binding-like proteins function cooperatively in invasion of human erythrocytes by malaria parasites. *Infection and Immunity*, *79*(3), 1107-17.

Maier, A. G., Duraisingh, M. T., Reeder, J. C., Patel, S. S., Kazura, J. W., Zimmerman, P. A., & Cowman, A. F. (2002). *Plasmodium falciparum* erythrocyte invasion through glycophorin C and selection for Gerbich negativity in human populations. *Nature Medicine*, *9*(1), 87-92.

Mayer, D. C. G., Cofie, J., Jiang, L., Hartl, D. L., Tracy, E., Kabat, J., Mendoza, L. H., *et al*. (2009). Glycophorin B is the erythrocyte receptor of *Plasmodium falciparum* erythrocyte-binding ligand, EBL-1. *Proceedings of the National Academy of Sciences of the United States of America*, *106*(13), 5348-52.

Mendis, K., Sina, B. J., Marchesini, P., & Carter, R. (2001). The neglected burden of *Plasmodium vivax* malaria. *The American Journal of Tropical Medicine and Hygiene*, *64*(1-2 Suppl), 97-106.

Miller, L. H., Baruch, D. I., Marsh, K., & Doumbo, O. K. (2002). The pathogenic basis of malaria. *Nature*, *415*(6872), 673-9.

Mitchell, G H, Thomas, A. W., Margos, G., Dluzewski, A. R., & Bannister, L. H. (2004). Apical membrane antigen 1, a major malaria vaccine candidate , mediates the close attachment of invasive merozoites to host red blood cells. *Infection and Immunity*, *72*(1), 154-8.

Morahan, B. J., Wang, L., & Coppel, R. L. (2009). No TRAP, no invasion. *Trends in Parasitology*, *25*(2), 77-84.

Murray, C. J. L., Rosenfeld, L. C., Lim, S. S., Andrews, K. G., Foreman, K. J., Haring, D., Fullman, N., *et al*. (2012). Global malaria mortality between 1980 and 2010: a systematic analysis. *Lancet*, *379*(9814), 413-31.

Ménard, R. (2005). Knockout malaria vaccine? *Nature*, *433*(1), 6-7.

Narum, D L, Welling, G. W., & Thomas, A. W. (1993). Ion-exchange-immunoaffinity purification of a recombinant baculovirus *Plasmodium falciparum* apical membrane antigen, PF83/AMA-1. *Journal of Chromatography. A*, *657*(2), 357-63.

Ockenhouse, C. F., Barbosa, A., Blackall, D. P., Murphy, C. I., Kashala, O., Dutta, S., Lanar, D. E., *et al*. (2001). Sialic acid-dependent binding of baculovirus-expressed recombinant antigens from *Plasmodium falciparum* EBA-175 to Glycophorin A. *Molecular and Biochemical Parasitology*, *113*(1), 9-21.

O'Donnell, R. A., Hackett, F., Howell, S. A., Treeck, M., Struck, N., Krnajski, Z., Withers-Martinez, C., *et al*. (2006). Intramembrane proteolysis mediates shedding of a key adhesin during erythrocyte invasion by the malaria parasite. *The Journal of Cell Biology*, *174*(7), 1023-33.

Ollomo, B., Durand, P., Prugnolle, F., Douzery, E., Arnathau, C., Nkoghe, D., Leroy, E., *et al*. (2009). A new malaria agent in African hominids. *PLoS Pathogens*, *5*(5), e1000446.

Osier, F. H. A., Fegan, G., Polley, S. D., Murungi, L., Verra, F., Tetteh, K. K. A., Lowe, B., *et al.* (2008). Breadth and magnitude of antibody responses to multiple *Plasmodium*

falciparum merozoite antigens are associated with protection from clinical malaria. *Infection and Immunity, 76*(5), 2240-8.

Pandey, K. C., Singh, S., Pattnaik, P., Pillai, C. R., Pillai, U., Lynn, A., Jain, S. K., *et al*. (2002). Bacterially expressed and refolded receptor binding domain of *Plasmodium falciparum* EBA-175 elicits invasion inhibitory antibodies. *Molecular and Biochemical Parasitology, 123*(1), 23-33.

Pizarro, J. C., Vulliez-Le Normand, B., Chesne-Seck, M.-L., Collins, C. R., Withers-Martinez, C., Hackett, F., Blackman, M. J., *et al*. (2005). Crystal structure of the malaria vaccine candidate apical membrane antigen 1. *Science, 308*(5720), 408-11.

Prugnolle, F., Durand, P., Neel, C., Ollomo, B., Ayala, F. J., Arnathau, C., Etienne, L., *et al*. (2010). African great apes are natural hosts of multiple related malaria species, including *Plasmodium falciparum*. *Proceedings of the National Academy of Sciences of the United States of America, 107*(4), 1458-63.

Prugnolle, F., Durand, P., Ollomo, B., Duval, L., Ariey, F., Arnathau, C., Gonzalez, J.-P., *et al*. (2011a). A fresh look at the origin of *Plasmodium falciparum*, the most malignant malaria agent. *PLoS Pathogens, 7*(2), e1001283.

Prugnolle, F., Ollomo, B., Durand, P., Yalcindag, E., Arnathau, C., & Elguero, E. (2011b). African monkeys are infected by *Plasmodium falciparum* nonhuman primate-specific strains. *Proceedings of the National Academy of Sciences of the United States of America, 108*(29), 11948-53.

Rayner, J. C., Galinski, M. R., Ingravallo, P., & Barnwell, J. W. (2000). Two *Plasmodium falciparum* genes express merozoite proteins that are related to *Plasmodium vivax* and *Plasmodium yoelii* adhesive proteins involved in host cell selection and invasion. *Proceedings of the National Academy of Sciences of the United States of America, 97*(17), 9648-53.

Rayner, J. C., Vargas-Serrato, E., Huber, C. S., Galinski, M. R., & Barnwell, J. W. (2001). A *Plasmodium falciparum* homologue of *Plasmodium vivax* reticulocyte binding protein (PvRBP1) defines a trypsin-resistant erythrocyte invasion pathway. *The Journal of Experimental Medicine, 194*(11), 1571-81.

Rayner, J. C., Liu, W., Peeters, M., Sharp, P. M., & Hahn, B. H. (2011, May). A plethora of Plasmodium species in wild apes: a source of human infection? *Trends in Parasitology,27*(5), 222-9.

Rich, S. M., Leendertz, F. H., Xu, G., LeBreton, M., Djoko, C. F., Aminake, M. N., Takang, E. E., *et al*. (2009). The origin of malignant malaria. *Proceedings of the National Academy of Sciences of the United States of America, 106*(35), 14902-7.

Riglar, D. T., Richard, D., Wilson, D. W., Boyle, M. J., Dekiwadia, C., Turnbull, L., Angrisano, F., *et al*. (2011). Super-resolution dissection of coordinated events during malaria parasite invasion of the human erythrocyte. *Cell Host & Microbe, 9*(1), 9-20.

Rodriguez, M., Lustigman, S., Montero, E., Oksov, Y., & Lobo, C. A. (2008). PfRH5: a novel reticulocyte-binding family homolog of *Plasmodium falciparum* that binds to the erythrocyte, and an investigation of its receptor. *PloS One*, *3*(10), e3300.

Sanders, P. R., Gilson, P. R., Cantin, G. T., Greenbaum, D. C., Nebl, T., Carucci, D. J., McConville, M. J., *et al*. (2005). Distinct protein classes including novel merozoite surface antigens in Raft-like membranes of *Plasmodium falciparum*. *The Journal of Biological Chemistry*, *280*(48), 40169-76.

Schwartz, L., Brown, G. V., Genton, B., & Moorthy, V. S. (2012). A review of malaria vaccine clinical projects based on the WHO rainbow table. *Malaria Journal, 11*(1), 11.

Sim, B. K. (1995). EBA-175: an erythrocyte-binding ligand of *Plasmodium falciparum*. *Parasitology Today (Personal ed.), 11*(6), 213-7.

Singh, B., Kim Sung, L., Matusop, A., Radhakrishnan, A., Shamsul, S. S. G., Cox-Singh, J., Thomas, A., et al. (2004). A large focus of naturally acquired *Plasmodium knowlesi* infections in human beings. *Lancet, 363*(9414), 1017-24.

Singh, S., Alam, M. M., Pal-Bhowmick, I., Brzostowski, J. A., & Chitnis, C. E. (2010). Distinct external signals trigger sequential release of apical organelles during erythrocyte invasion by malaria parasites. *PLoS Pathogens*, *6*(2), e1000746.

Snow, R. W., Guerra, C. A., Mutheu, J. J., & Hay, S. I. (2008). International funding for malaria control in relation to populations at risk of stable *Plasmodium falciparum* transmission. *PLoS Medicine, 5*(7), e142.

Snow, R. W., Guerra, C. A., Noor, A. M., Myint, H. Y., & Hay, S. I. (2005). The global distribution of clinical episodes of *Plasmodium falciparum* malaria. *Nature*, *434*(7030), 214-217.

Spadafora, C., Awandare, G. A., Kopydlowski, K. M., Czege, J., Moch, J. K., Finberg, R. W., Tsokos, G. C., *et al*. (2010). Complement receptor 1 is a sialic acid-independent erythrocyte receptor of *Plasmodium falciparum*. *PLoS Pathogens*, *6*(6), e1000968.

Taylor, H. M., Grainger, M., & Holder, A. A. (2002). Variation in the expression of a *Plasmodium falciparum* protein family implicated in erythrocyte invasion variation in the expression of a *Plasmodium falciparum* protein family implicated in erythrocyte invasion. *Infection and Immunity, 70*(10), 5779-89.

Taylor, H. M., Triglia, T., Thompson, J., Fowler, R., Wickham, M. E., Cowman, A. F., Holder, A. A., *et al*. (2001). *Plasmodium falciparum* homologue of the genes for *Plasmodium vivax* and *Plasmodium yoelii* adhesive proteins, which is transcribed but not translated. *Infection and Immunity*, *69*(6), 3635-45.

Tham, W.-H., Healer, J., & Cowman, A. F. (2012). Erythrocyte and reticulocyte binding-like proteins of *Plasmodium falciparum*. *Trends in Parasitology*, *28*(1), 23-30.

Thompson, J K, Triglia, T., Reed, M. B., & Cowman, A. F. (2001). A novel ligand from *Plasmodium falciparum* that binds to a sialic acid-containing receptor on the surface of human erythrocytes. *Molecular Microbiology*, *41*(1), 47-58.

Tolia, N. H., Enemark, E. J., Sim, B. K. L., & Joshua-Tor, L. (2005). Structural basis for the EBA-175 erythrocyte invasion pathway of the malaria parasite *Plasmodium falciparum*. *Cell*, *122*(2), 183-93.

Tom, R., Bisson, L., & Durocher, Y. (2008). Culture of HEK293-EBNA1 Cells for Production of Recombinant Proteins. *Cold Spring Harbor Protocols*, *2008*(4), pdb.prot4976.

Treeck, M., Zacherl, S., Herrmann, S., Cabrera, A., Kono, M., Struck, N. S., Engelberg, K., *et al*. (2009). Functional analysis of the leading malaria vaccine candidate AMA-1 reveals an essential role for the cytoplasmic domain in the invasion process. *PLoS Pathogens*, *5*(3), e1000322.

Trieu, A., Kayala, M. A., Burk, C., Molina, D. M., Freilich, D. A., Richie, T. L., Baldi, P., *et al*. (2011). Sterile protective immunity to malaria is associated with a panel of novel *P. falciparum* antigens. *Molecular & Cellular Proteomics*, *10*(9), M111.007948.

Triglia, T, Healer, J., Caruana, S. R., Hodder, A. N., Anders, R. F., Crabb, B. S., & Cowman, A. F. (2000). Apical membrane antigen 1 plays a central role in erythrocyte invasion by *Plasmodium* species. *Molecular Microbiology*, *38*(4), 706-18.

Triglia, T., Thompson, J. K., & Cowman, A. F. (2001). An EBA175 homologue which is transcribed but not translated in erythrocytic stages of *Plasmodium falciparum*. *Molecular and Biochemical Parasitology*, *116*(1), 55-63.

Triglia, T., Thompson, J., Caruana, S. R., Speed, T., Cowman, A. F., & Delorenzi, M. (2001). Identification of proteins from *Plasmodium falciparum* that are homologous to reticulocyte binding proteins in *Plasmodium vivax*. *Infection and Immunity*, *69*(2), 1084-92

Tsuboi, T., Takeo, S., Iriko, H., Jin, L., Tsuchimochi, M., Matsuda, S., Han, E.-T., *et al.* (2008). Wheat germ cell-free system-based production of malaria proteins for discovery of novel vaccine candidates. *Infection and Immunity*, *76*(4), 1702-8.

Uchime, O., Herrera, R., Reiter, K., Kotova, S., Shimp, R. L., Miura, K., Jones, D., *et al*. (2012). Analysis of the conformation and function of the *Plasmodium falciparum* merozoite proteins MTRAP and PTRAMP. *Eukaryotic Cell*, 615-625.

Vulliez-Le Normand, B., Tonkin, M. L., Lamarque, M. H., Langer, S., Hoos, S., Roques, M., Saul, F. A., *et al*. (2012). Structural and functional insights into the malaria parasite moving junction complex. *PLoS Pathogens, 8*(6), e1002755.

WHO (2011). World Malaria Report 2011.World Health Organisation, Geneva, Switzerland.

Winzeler, E. A. (2008). Malaria research in the post-genomic era. *Nature, 455*(7214), 751-6.

Withers-Martinez, C., Haire, L. F., Hackett, F., Walker, P. A., Howell, S. A., Smerdon, S. J., Dodson, G. G., *et al*. (2008). Malarial EBA-175 region VI crystallographic structure reveals a KIX-like binding interface. *Journal of Molecular Biology, 375*(3), 773-81.

Withers-Martinez, C., Suarez, C., Fulle, S., Kher, S., Penzo, M., Ebejer, J.-P., Koussis, K., *et al.* (2012). *Plasmodium* subtilisin-like protease 1 (SUB1): Insights into the active-site structure, specificity and function of a pan-malaria drug target. *International Journal for Parasitology, 42*(6), 597-612.

Wright, G. J. (2009). Signal initiation in biological systems: the properties and detection of transient extracellular protein interactions. *Molecular BioSystems, 5*, 1405-1412.

Zhang, D., & Pan, W. (2005). Evaluation of three *Pichia pastoris*-expressed *Plasmodium falciparum* merozoite proteins as a combination vaccine against infection with blood-stage parasites. *Infection and Immunity, 73*(10), 6530-36.

Chapter 2

Materials and methods

2.1 Production of recombinant membrane protein ectodomains

The full-length ectodomains of membrane proteins were produced in soluble, recombinant form using an established system based on transient transfection of the HEK293E human cell line (Durocher *et al.,* 2002). The cells, adapted for suspension culture, were maintained in Freestyle media (*Invitrogen*) supplemented with 1% fetal bovine serum, 50 µg/ml of geneticin (*Sigma*), 100 units/ml penicillin (*Invitrogen*) and 100 µg/ml streptomycin (*Invitrogen*), incubated at 37°C, 5% CO_2 and 70% humidity with orbital shaking at 120 r. p. m.

2.1.1 Design and construction of expression plasmids

All expression plasmids used for the production of membrane protein ectodomains are listed in Table 3. The sequences encoding the full-length ectodomains were codon optimised for expression in mammalian cells, using the *GeneART* gene synthesis service (*Invitrogen).* The optimised sequences were then cloned into pTT3-based expression vectors (Durocher *et al.,* 2002) containing a region coding for the immunoglobulin-like domains 3 and 4 rat Cd4 (Brown and Barclay, 1994) together with either

i. A 17-amino acid peptide substrate for the *Escherichia coli* biotin ligase BirA (Brown *et al.,* 1998; Bushell *et al.,* 2008) or
ii. The pentamerisation domain of the rat cartilaginous oligomeric matrix protein (COMP) (Tomschy *et al.*, 1996) with an ampicillin resistance protein (TEM) β-lactamase (Bushell *et al*., 2008) or
iii. A hexa-His tag as represented in Figure 5.

Endogenous signal peptides were included for erythrocyte membrane proteins, however those of *Plasmodium* proteins were replaced by the leader sequence of the mouse variable κ light chain 7-

33 (Crosnier *et al.*, 2010) during gene synthesis. The potential N-linked glycosylation sites (N-X-S/T) of *Plasmodium* proteins were also systematically removed by substituting alanine for serine/threonine at these sites.

Flanking unique NotI (5') and AscI (3') restriction endonuclease recognition sites were introduced to all sequences encoding the membrane protein ectodomains during gene assembly and were used for cloning into the expression vectors. Briefly, after digestion with NotI (*New England BioLabs, NEB*) and AscI (*NEB*) overnight at 37°C both the vectors and inserts were resolved by agarose gel electrophoresis (Section 2.1.1.2) and purified using the QIAquick Gel Extraction kit (*QIAGEN*) as per manufacturer's instructions. Ligations were performed overnight at 16°C with T4 DNA Ligase (*Roche*) using 20 ng of vector and 50 ng of insert DNA per reaction in ligation buffer (50 mM Tris-HCl, 10 mM MgCl*2*, 1 mM ATP, 10 mM dithiothreitol, pH 7.5). Chemically-competent *E.coli* TOP10 cells (*Sigma*) were transformed with the ligation products and positive clones were selected on LB-agar plates containing 100 µg/ml of ampicillin. The presence of an insert of the correct size was confirmed by colony PCR using vector-specific primers flanking the insert site, A and B (Table 2) as described below (Section 2.1.1.1). Plasmids were then purified using the QIAprep Miniprep Spin kit (*QIAGEN*) according to the manufacturer's instructions, tested again for the correct insert via NotI and AscI digestion and sequenced with primers A and B. Sequence-verified expression plasmids were used to transform TOP10 cells. Single positive clones were then inoculated into 100 ml cultures of LB broth supplemented with 100 µg/ml of ampicillin and grown overnight at 37°C with shaking at 200 r. p. m. Plasmids were purified from these cultures using the PureLink^{TM} HiPure Plasmid Maxiprep kit (*Invitrogen*). The purified plasmid DNA was assessed for quantity and quality by measuring the absorbances at 260 nm (A_{260}) and 280 nm (A_{280}) using a spectrophotometer. In terms of

purity, A_{260}/A_{280} ratios between 1.8-1.95 were considered to be acceptable. All plasmid DNA preparations were diluted to 1 mg/ml in buffer TE for use in transfections.

To express fragments of ectodomains, appropriate segments of coding sequence were PCR-amplified from the expression constructs of the full-length ectodomains, using flanking primers (Table 2) containing NotI (forward primer) and AscI (reverse primer) restriction sites, and cloned into expression vectors as described before.

2.1.1.1 PCR

All PCR reactions were performed with the KOD Hot Start DNA polymerase (*Novagen*) in the thermophilic buffer provided by the manufacturer supplemented with 1 mM of $MgSO_4$ and dNTPs (0.2 mM each). 1 U of the polymerase and 0.3 µM of each primer were used per reaction. When the template was a purified plasmid (at 10 ng per reaction), the cycling parameters used were:

Step	Temperature (°C)	Time (min)
1	94	4
2	94	1
3	58	0.5
4	72	0.33/kbp
5	Go to step 2, repeat for 25 cycles	
6	72	7

When colony PCR was performed for testing bacterial transformants, the Step 1 above was extended to 15 min, but the other cycling parameters were kept the same.

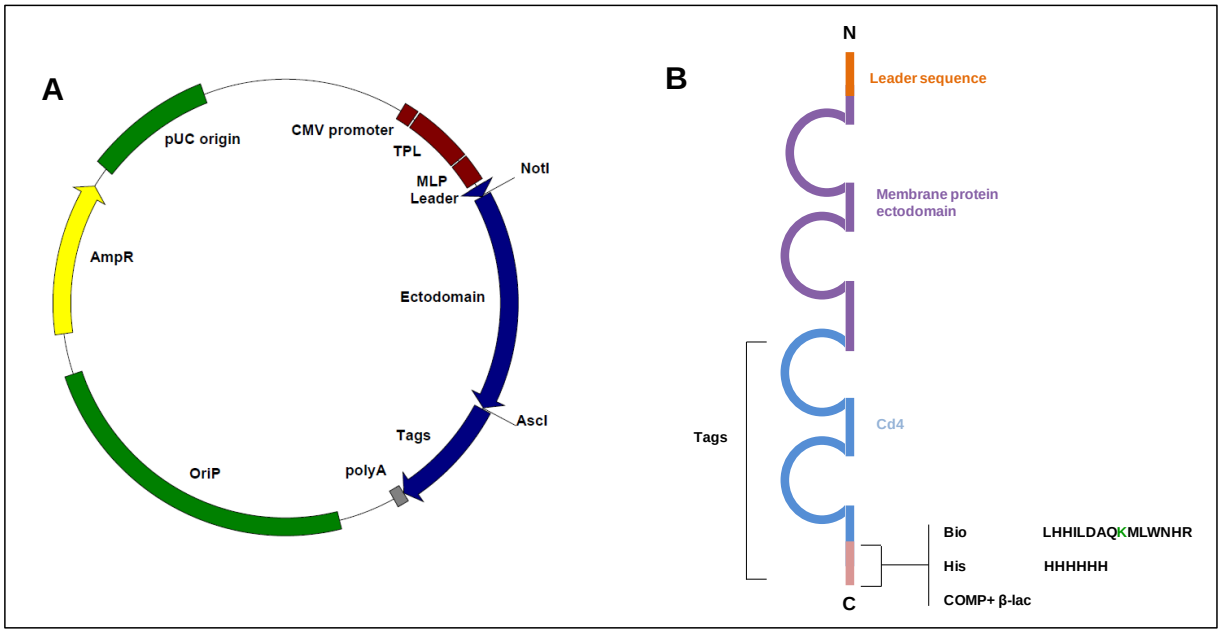

Figure 5. Design of recombinant membrane protein ectodomains. A) Genetic map of expression plasmids used for the production of membrane protein ectodomains (schematic diagram drawn-to-scale). CMV promoter – cytomegalovirus promoter, TPL –tripartite leader sequence, MLP – adenovirus major late promoter enhancer, Leader- leader sequence of the mouse variable κ light chain (included only in expression plasmids of *Plasmodium* proteins), NotI – NotI restriction enzyme recognition site, Ectodomain – sequence encoding the membrane protein extracellular domain, AscI –AscI restriction enzyme recognition site, Tags – sequences coding for domains 3+4 of rat Cd4 and one of the following i) a biotinylatable peptide tag, ii) pentamerisation domain of the rat COMP protein and ampicillin resistance protein β-lactamase or iii) hexa-histidine tag, polyA – SV40 polyadenylation sequence, OriP – Epstein-Barr virus origin of replication, AmpR – β-lactamase gene, pUC origin – bacterial origin of replication. **B)** A simplified schematic of a recombinant *Plasmodium* membrane protein ectodomain with the N-terminal leader sequence derived from a mouse antibody and C-terminal fusion tags. The sequences are given only for the short peptide tags. Cd4: domains 3 and 4 of rat Cd4. Bio: peptide substrate for the biotin ligase BirA. The biotinylatable lysine residue is indicated in green. His: hexa-His. COMP+ β-lac: the pentamerisation domain of the rat COMP protein and the ampicillin resistance protein β-lactamase.

2.1.1.2 Agarose gel electrophoresis

DNA samples diluted in loading buffer (30% glycerol, 0.25% bromophenol blue, 0.25% xylene cyanol FF) were loaded onto 1% agarose, TAE-buffered (40 mM tris, 20 mM acetic acid, 1 mM EDTA) gels containing 0.1 µg/ml ethidium bromide. After electrophoresis at a constant voltage of 120V, DNA was visualised using a UV transilluminator (*BIORAD*).

2.1.2 Transient transfection of expression plasmids

Expression plasmids for recombinant membrane protein ectodomains were transiently transfected into HEK293E primarily using the cationic reagent polyethylenimine (PEI) (Tom *et al.,* 2008a). Cells were split into 50 ml of fresh media at a density of $2.5x10^5$ cells/ml and allowed to recover for 24 hours prior to transfection. Each culture was then inoculated with the transfection mix: 25 µl of the expression plasmid (at 1 mg/ml) and 50 µl of linear PEI (at 1 mg/ml) in 2 ml of non-supplemented Freestyle media that had been incubated together for 10 mins at room temperature. Six days after transfection cells and cell debris were removed by centrifugation at 3220*g* for 5 min, supernatants were then filtered (0.2-µm filter) and stored at 4°C until use. When producing biotinylated proteins, the culture media was supplemented with 100 µM D-biotin and 2.5 µl of a plasmid (at 1 mg/ml) coding for a secreted form of BirA (Bushell *et al.*, 2008) was included in the transfection mix. After harvesting, filtered culture supernatants containing biotinylated proteins were dialysed against 5 L of HBS (0.14 M NaCl, 5 mM KCl, 2 mM CaCl2, 1 mM MgCl2, 10 mM HEPES) over 2 days (7 changes of buffer) in Snakeskin dialysis tubing (10 kDa MWCO, *Thermo Scientific*) to remove excess D-biotin.

2.2 Qualitative and quantitative assessment of recombinant membrane protein ectodomains

2.2.1 SDS-polyacrylamide gel electrophoresis (SDS-PAGE)

Proteins were analysed by SDS-PAGE using Novex NuPage 4-12% Bis-Tris pre-cast gels (*Invitrogen*), as per manufacturer's instructions. Electrophoresis was performed at a constant voltage of 200 V for about 1 hour and proteins were visualized using either the SilverXpress silver staining kit (*Invitrogen*) or a Coomassie brilliant blue (G250) staining solution (*Thermo Scientific*) according to the manufacturers' protocols. The Pierce glycoprotein staining kit (*Thermo Scientific*) was used for specifically detecting glycosylated proteins

2.2.2 Western blotting

Western blotting was used to confirm the size of biotinylated proteins. After separation by SDS-PAGE, proteins were transferred to PVDF membranes using a XCell II blotting module (*Novex*), at a constant voltage of 30 V for 1 hour at room temperature in NuPage transfer buffer (25 mM Bicine, 25 mM Bis-Tris, 1 mM EDTA, 0.05 mM Chlorobutanol) (*Invitrogen*) supplemented with 10% methanol. The blots were incubated overnight in HBS and 2% BSA to block non-specific binding sites. They were then probed with horseradish peroxidase (HRP)-conjugated Extravidin (1:1000 dilution; *Sigma*), which was detected by chemiluminescence with Hyperfilm (*GE Healthcare*) exposure. Extravidin is a neutral, deglycosylated form of Avidin with higher specificity.

2.2.3 Enzyme-linked-immunosorbent assays (ELISAs) of biotinylated membrane protein ectodomains

ELISAs were performed as previously described in Bushell *et al.* (2008). Biotinylated proteins were immobilised on streptavidin-coated 96-well plates (*Nunc*) for 1 h before incubation with the primary antibody (diluted to 10 µg/ml in HBS and 1% BSA (HBS-BSA), unless stated otherwise) for another hour. The plates were then washed in HBS and 0.1% Tween-20 (HBST) before incubation with a suitable secondary antibody conjugated to alkaline phosphatase (*Sigma*) for 30-45 mins. Plates were then washed three times in HBST and once in HBS before the addition of *p*-nitrophenyl phosphate (Substrate 104; *Sigma*) at 1 mg/ml (100 µl/well). Absorbance was measured at 405 nm on a PHERAstar plus *(BMG Labtech)* plate reader after 10-15 mins. All the steps in the procedure were carried out at room temperature. In addition to quantifying biotinylated proteins, ELISAs were used for testing the conformational state of ligands by means of specific antibodies that recognise non-linear, heat-labile epitopes. For the latter analysis, proteins were heat-treated for 10 min at 80°C and then incubated on ice for a further 10 min, prior to use in ELISAs with untreated controls.

2.2.4 Normalisation of β-lactamase tagged membrane protein ectodomains

Beta-lactamase tagged pentameric proteins were normalised as described in Bushell *et al.* (2008) by monitoring their enzymatic activity in a nitrocefin (*Calbiochem*) turnover assay. 20 µl of 2-fold serial dilutions of harvested culture supernatants were incubated with 60 µl of nitrocefin (at 125 µg/ml) for a period of 10 mins at room temperature, during which nitrocefin turnover was quantified by monitoring the absorbance at 485 nm on a PHERAstar plus *(BMG Labtech)* plate reader. Normalisation of proteins was achieved either by concentrating with 20 kDa MWCO spin concentrators or diluting as required.

2.2.5 Purification of His-tagged membrane protein ectodomains

His-tagged proteins were purified from harvested culture supernatants on nickel-charged sepharose columns (HisTrap HP 1 ml; *GE Healthcare*) using the ÄKTAxpress purification system (*GE Healthcare*). In each instance, the column was pre-equilibrated with binding buffer (20 mM sodium phosphate, 40 mM imidazole, 0.5 M NaCl, pH 7.4) at a flow rate of 1 ml/min. The harvested supernatant (> 150 ml) was supplemented with imidazole (10 mM) and NaCl (100 mM), then passed over the column at 1 ml/min. When loading was complete, the column was washed with 15 column volumes (15 CV) of binding buffer to remove non-specific adherents and with 10 CV of elution buffer (20 mM sodium phosphate, 0.4 M imidazole, 0.5 M NaCl, pH 7.4) to recover specifically-bound protein. The eluant was monitored at 280 nm in real-time and collected in 0.5 ml fractions. The two/three fractions with the highest concentration of purified protein (as estimated by measuring the absorbance at 280 nm) were analysed by SDS-PAGE and pooled for downstream applications.

His-tagged proteins recovered from nickel column purification were further purified by gel filtration prior to use in surface plasmon resonance experiments. This step was necessary for removing protein aggregates. The gel filtration column (Superdex Tricorn 200 10/600 GL, *GE Healthcare*) connected to ÄKTAxpress was pre-equilibrated with 2 CV of the running buffer, HBS-EP (10 mM HEPES, 150 mM NaCl, 30 mM EDTA, 0.05% polyoxyethylenesorbitan 20, pH 7.4) before injecting each protein sample (< 1.5 % of column volume). This was followed by further washing with the running buffer at a flow rate of 1 ml/min. 1 ml fractions were collected once 22 ml of running buffer (equivalent to the void volume of the column) had passed through the column. Absorbance at 280 nm and *in silico* predicted extension coefficients were used to estimate the concentrations of peak fractions. The actual sizes of proteins and their

conformational states (i.e. monomer, dimer or oligomer) were deduced from the elution volumes of the peak fractions, by comparison against a standard curve generated using well-defined protein standards from the low molecular weight and high molecular weight gel filtration calibration kits (*GE Healthcare*).

2.3 *In vitro* biotinylation of native Glycophorin A

Native Glycophorin A purified from human erythrocytes (*Sigma*) was re-suspended in HBS and biotinylated *in vitro* using a 20-fold molar excess of EZ-link sulfo-NHS-biotin (*Thermo Scientific*) for 30 mins at room temperature. The biotinylated protein preparations were then dialysed against 5 L HBS overnight (3 changes of buffer) in Slide-A-Lyzer dialysis cassettes (3.5 kDa MWCO, *Thermo Scientific*) to remove free, unconjugated biotin. The biotinylation of Glycophorin A was confirmed by ELISA on streptavidin-coated plates as described in section 2.2.3 for recombinant membrane protein ectodomains.

2.4 Expression and analysis of erythrocyte multi-pass membrane proteins

Erythrocyte multi-pass membrane proteins were transiently expressed with their endogenous signal sequences and C-terminal Myc/DDK tags on the surface of HEK293E cells using TrueORF plasmids commercially available from *OriGene* (Figure 6). To obtain sufficient quantities of DNA for transfection, the TrueORF expression plasmids were propagated in *E. coli* TOP10 cells (*Sigma*) and purified using the PureLink^{TM} HiPure Plasmid Maxiprep kit (*Invitrogen*). All TrueORF clones used were verified by DNA sequencing.

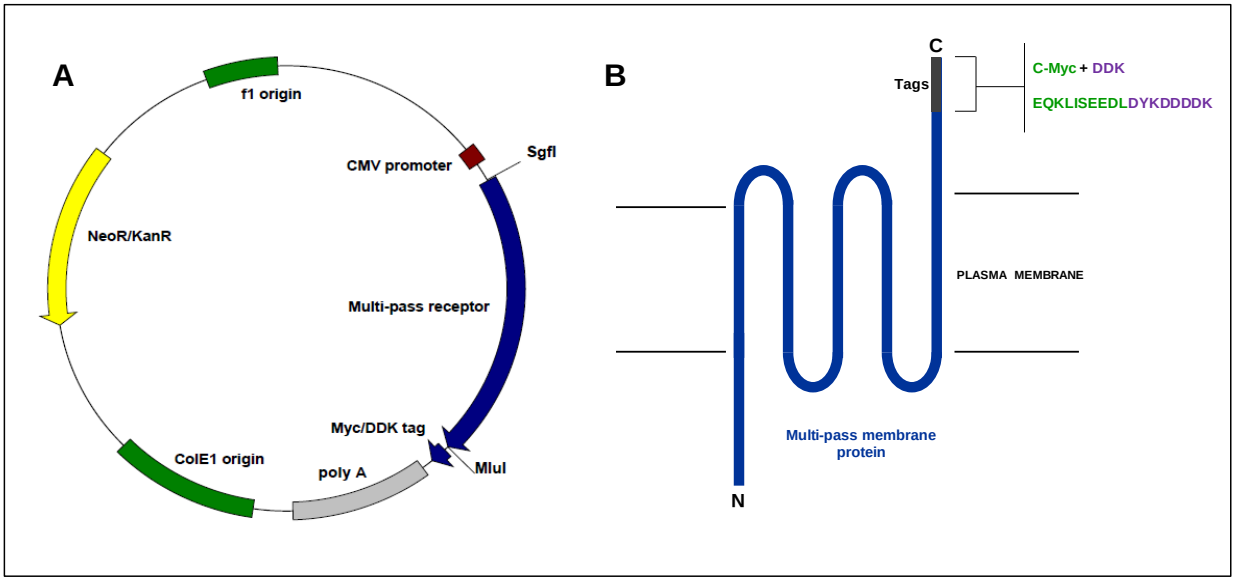

Figure 6. Design of recombinant multi-pass membrane proteins. A) Genetic map of TrueORF plasmids used for the transient expression of erythrocyte multi-pass receptors on the surface of HEK293E cells (schematic diagram drawn-to-scale). CMV promoter – cytomegalovirus promoter, SgfI – SgfI restriction enzyme recognition site, Multi-pass receptor – sequence encoding the multi-pass receptor, MluI –MluI restriction enzyme recognition site, Myc/DDK tag –, polyA – SV40 polyadenylation sequence, ColE1 origin- bacterial origin of replication, NeoR/KanR –neomycin phosphotransferase gene, f1 origin – phage origin of replication. The vector sequence is available at the *OriGene* website http://www.origene.com/destination_vector/PS100001.aspx. **B)** A simplified schematic of a recombinant multi-pass receptor. The peptide sequences of the C-terminal Myc and DDK tags are indicated in green and purple respectively.

2.4.1 Transient transfection of TrueORF plasmids

293Fectin (*Invitrogen*) (Tom *et al.*, 2008b) was primarily used as the reagent for transfecting HEK293E with these plasmids. Each transfection was performed with $2.5x10^7$ cells in 25 ml of media (passaged at half the density a day before), 25 µl of the expression plasmid (at 1 mg/ml), 50 µl of 293Fectin and 2 ml of the OPTI-MEM I media (*Invitrogen*). 293Fectin and DNA were each pre-incubated with 1 ml of OPTI-MEM I for about 5 mins at room temperature prior to being mixed together and then incubated for a further 20 mins at room temperature before addition to cells. The cells were harvested 48 hours after transfection by gentle centrifugation at 199 *g* for 4 mins.

2.4.2 Monitoring expression of multi-pass membrane proteins by flow cytometry

Expression of the recombinant multi-pass membrane proteins was investigated by staining non-permeabilised HEK293E cells, with an appropriate primary antibody (at 0.5 µg/million cells) for 1 h at room temperature with shaking, followed by three washes in HBS-BSA and incubation with a FITC-conjugated secondary antibody for a further 30 mins at room temperature. After being washed thrice in HBS-BSA to remove non-bound antibody, cells were monitored on a BD LSRII cytometer (*BD Biosciences*) using the BD FACS Diva software. Forward scatter (FSC) and side scatter (SSC) voltages of 275 V and 260 V respectively and a threshold of 26,100 on FSC were applied to select the cell population. FITC was excited by a blue laser and detected with a 530/30 filter. The results were analysed using Flow Jo v7.5.3 software (*Tree Star, Inc*).

2.4.3 Confirming expression of multi-pass membrane proteins by confocal microscopy

Expression of the recombinant multi-pass membrane proteins at the surface of HEK293E cells was also confirmed by confocal microscopy. Briefly, cells stained with the appropriate antibodies as described before (section 2.4.2), were counter stained with Slow-Fade Gold-DAPI (*Invitrogen*) on a poly-L-lysine coated microscope slide for a minimum of 10 min at room temperature. Images were captured on a Leica TCS SP5/DM6000 confocal microscope.

2.5 Identifying and characterising low-affinity protein-protein interactions

The highly transient nature ($t_{1/2}$ < 0.1 sec) of low-affinity protein-protein interactions is a major impediment to their identification and characterisation. In the first two methods described below, multimeric reagents were used to increase the avidity of the interactions, thereby prolonging them and enabling their detection. The third method allows molecular interactions to be monitored as they happen in real-time.

2.5.1 Cell-based binding assays with 'prey' protein arrays immobilised on beads

The protocol from Brown (2002) was adapted for detecting binding of recombinant *Plasmodium* membrane protein ectodomains (the 'preys') to receptors on the surface of erythrocytes and HEK293E cells. The mono-biotinylated *Plasmodium* proteins were multimerised by immobilisation on streptavidin-coated Nile red fluorescent 0.4-0.6 µm microbeads (*Spherotech Inc*) by incubation for 1 h at 4°C, followed by sonication for 20 min at a frequency of 35-45 kHz to disrupt aggregates. The multimeric arrays were then presented to cells that had been aliquoted on flat-bottomed 96-well microtitre plates at a density of approximately 3 x 10^5 cells/well (the ratio of cells: beads used was 1:200). After incubation for 1 h at 4°C with the protein arrays, the

cells were washed twice in HBS-BSA and analysed by flow cytometry. The data was acquired on a BD LSRII cytometer (*BD Biosciences*) using the BD FACS Diva software. Nile Red was excited by a blue laser and detected with a 575/26 filter. FSC and SSC voltages of 430 V and SSC 300 V respectively and a threshold of 26,100 on FSC were applied when analysing erythrocytes. HEK293E cells were detected with FSC and SSC voltages of 275 V and 260 V respectively and a FSC threshold of 26,100. The flow cytometry results were analysed using Flow Jo v7.5.3 software (*Tree Star, Inc*). Specificity of detected interactions was confirmed by pre-treatment of cells with the enzymes trypsin, chymotrypsin and neuraminidase and by pre-incubation with monoclonal antibodies.

2.5.1.1 Pre-treatment of cells

All pre-treatments of HEK293E cells and erythrocytes were carried out in non-supplemented Freestyle (*Invitrogen*) and RPMI 1640 (*Invitrogen*) respectively.

A. Trypsin/chymotrypsin treatment of cells

5 x 10^7 cells were incubated with 50 µl of 0.25, 0.5 or 1 mg/ml of tosyl-sulfonyl phenylalanyl chloromethyl ketone (TPCK)-treated trypsin from bovine pancreas (*Sigma*) or with 50 µl of 0.25, 0.5 or 1 mg/ml of tosyl lysyl chloromethyl ketone (TLCK)-treated chymotrypsin from bovine pancreas (*Sigma*), for 1 h at 37°C with periodic shaking. The cells were then washed once and treated with 0.5 mg/ml of Soybean trypsin-chymotrypsin inhibitor (*Sigma*) for 10 min on a rotating wheel at room temperature. The cells were finally washed twice before use in binding assays.

B. Neuraminidase treatment

5 x 10^7 cells were incubated with 50 µl of 100 mU/ml *of Vibrio cholera* neuraminidase (*Sigma*) for 1 h at 37°C with periodic shaking, after which they were washed twice prior to binding assays.

C. Pre-incubation with monoclonal antibodies

5 x 10^7 cells were incubated with 25 µg of the monoclonal antibodies for 1 h at room temperature with shaking. The cells were then washed twice before performing binding assays.

2.5.2 Avidity-based extracellular interactions screen (AVEXIS)

The protocol was adapted from Bushell *et al.* (2008). Biotinylated proteins (the baits) were immobilised on streptavidin-coated 96-well plates (*NUNC*) at concentrations sufficient for complete saturation of the available binding surface/well (as determined by ELISA). The plates were then washed twice in HBST and blocked with HBS-BSA (100 µl per well) for 30 mins at room temperature before addition of normalised β-lactamase tagged pentameric proteins (the preys) and incubation for 2 h. The plates were then washed three times in HBST and once in HBS. Nitrocefin (125 µg/ml; 60 µl per well) was added and developed for the stated lengths of time, after which absorbance was measured at 485 nm on a PHERAstar plus *(BMG Labtech)* plate reader. All steps were performed at room temperature.

2.5.3 Surface plasmon resonance (SPR)

Surface plasmon resonance was used to determine kinetic parameters for protein-protein interactions. All SPR experiments were performed on a Biacore T100 instrument using HBS-EP as the running buffer at 37°C.

Non-biotinylated bait proteins were immobilised on CM5 sensor chips (*GE Healthcare*) via amine groups using an amine coupling kit (*GE Healthcare*). In order to determine suitable coupling conditions, electrostatic pre-concentration of the baits on the sensor surfaces was tested at different pHs by injecting the baits (at 50 µg/ml) in 10 mM sodium acetate (pH 6.0-4.0) at a flow rate of 10 µl/min. Each 2 min pulse of ligand was followed by a 1 min injection of 1 M ethanolamine-HCl (pH 8.5) to remove electrostatically-bound ligand. When immobilising the baits covalently, the sensor surfaces were first activated with a 7 min injection of 0.2 M 1-ethyl-3-(3-dimethylaminopropyl)-carbodiimide (EDC) and 0.05 M N-hydroxysuccinimide (NHS) at a flow rate of 10 µl/min prior to injecting the baits.

When biotinylated proteins were used as baits they were directly immobilised on streptavidin-coated sensor chips (Series S Sensor Chip SA; *GE Healthcare*). Prior to bait immobilisation, the sensor surfaces were activated with three 1 min injections of 1 M NaCl and 50 mM NaOH at a flow rate of 30 µl/min. Biotinylated rat Cd4, the negative control bait, was immobilised in the reference flow cell (flow cell 1) of each chip and each 'query' bait protein was immobilised at a molar equivalent amount to Cd4 in a different flow cell. Flow rates of 30 µl/min and 10 µl/min were used respectively for immobilising recombinant membrane protein ectodomains and native Glycophorin A. To monitor protein-protein interactions, increasing concentrations of purified analyte proteins were injected across the immobilised baits on sensor surfaces at the indicated flow rates. At the end of each injection cycle the surface was 'regenerated' with a pulse of 5 M NaCl. Duplicate injections of the same analyte concentration were performed in each experiment and were superimposable indicating no loss of ligand activity after surface regeneration. Both kinetic and equilibrium binding parameters were derived from the data using the Biacore T100

evaluation software (*GE Healthcare*). Each SPR experiment was performed at least twice using independent preparations of both ligand and analyte proteins.

2.6 Studying protein-glycan interactions

Two ELISA-based assays were used for studying interactions between glycan-binding proteins and sugar moieties.

2.6.1 Lectin binding assay

Biotinylated lectins (*Vector Labs*) were immobilised on streptavidin-coated 96-well plates (*Nunc*) at 10 µg/ml (100 µl/well) for 1 h. The plates were then washed twice in HBST and blocked with HBS-BSA (100 µl per well) for 30 mins. The immobilised lectins were then incubated either with putatively glycosylated β-lactamase-tagged pentamers of recombinant membrane protein ectodomains (100 µl/well) or with purified native Glycophorin (0.02 mg/ml, 100 µl/well) for 2 h. The plates were then washed three times in HBST and once in HBS. The pentameric 'preys' were then detected with nitrocefin as described for the AVEXIS assay in section 2.5.2. To detect native Glycophorin A, the plates were incubated with an anti-Glycophorin A mouse monoclonal, BRIC 256 (diluted to 10 µg/ml in HBS-BSA, 100 µl/well) (*Abcam*) for 1 h and an alkaline-phosphatase conjugated anti-mouse secondary (diluted 1:5000 in HBS-BSA, 100 µl/well) (*Sigma*) for 30 mins before the addition of the alkaline phosphatase substrate, *p*-nitrophenyl phosphate (Substrate 104; *Sigma*) at 1 mg/ml (100 µl/well) and measuring the absorbance at 405 nm on a PHERAstar plus *(BMG Labtech)* plate reader. All steps were performed at room temperature.

2.6.2 High-throughput screen for identifying glycan binding specificities of *P. falciparum* membrane proteins

Mono-biotinylated synthetic carbohydrate probes (*GlycoTech*) were immobilised at 50 µg/ml (100 µl/well) or at the stated concentrations on streptavidin-coated 96-well plates (*Nunc*) for 1 h at room temperature. The plates were then washed twice in HBST and blocked with HBS-BSA (100 µl per well) for 30 mins before addition of normalised β-lactamase tagged pentameric proteins (the preys) and incubation for 2 h at room temperature. The plates were then washed three times in HBST and once in HBS before detection of the prey proteins using nitrocefin as described before in section 2.5.2.

2.7 TABLES

Table 2. Primers used in PCR reactions. The NotI and AscI restriction sites are indicated in purple and red respectively.

Primer name	Sequence (5'⟶ 3')
A	CCACTTTGCCTTTCTCTCCA
B	ATGTCCTTCCGAGTGAGAGA
EBA175 RII-F	GTAGAAAAAAGCGGCCGCCATCAACAACGGCCGGAACACCGCCA
***Pf*EBA175 RII_R**	GTAGAAAAAAGGCGCGCCGACGGCTTCCTGGCTGGTCTGCTCG
***Pr*EBA175RII_R**	GTAGAAAAAAGGCGCGCCCTTCTGTTCCTCGGTGTCGGCCTCG

Table 3. Expression plasmids used for the work described in this thesis.

Species	Protein name (accession number)	Fusion tags	Source of expression plasmid
Rat	Domains 3 and 4 of Cd4 (Cd4 tag) (NP_036837.1)	Biotin	Gavin Wright
		COMP+ β-lactamase	
	Full-length ectodomains of Cd200 and Cd200R	Biotin	
		Transmembrane domain of Cd200R + EGFP	
	α-2,6-sialyltransferase 1 (NP_001106815.1)		Cecile Crosnier
***P. falciparum* (3D7)**	Full-length ectodomains of merozoite surface proteins (Table 1)	Cd4+ Biotin	*GeneART*
		Cd4+ COMP+ β-lactamase	Cecile Crosnier
	Full-length ectodomain of RH5 (PFD1145c)	Cd4+His	
	Full-length ectodomain of EBA175 (MAL7P1.176)		Madushi Wanaguru
	RII of the ectodomain of EBA175 (MAL7P1.176)	Cd4+ Biotin	
		Cd4+ COMP+ β-lactamase	
		Cd4+His	
P. reichenowi	Full-length ectodomain of EBA175	Cd4+ Biotin	*GeneART*
	RII of the ectodomain of EBA175	Cd4+ Biotin	Madushi Wanaguru

		Cd4+ COMP+ β-lactamase	
		Cd4+His	
	Full-length ectodomain of RH5	Cd4+Biotin	*GeneART*
		Cd4+ COMP+ β-lactamase	Madushi Wanaguru
		Cd4+His	
P. billcollinsi	RII of the ectodomain of EBA175	Cd4+ Biotin	*GeneART*
		Cd4+ COMP+ β-lactamase	Madushi Wanaguru
		Cd4+His	
Human	Full-length ectodomains of Glycophorin A (NP_002090.4) and Glycophorin B (NP_002091.3)	Cd4+ COMP+ β-lactamase	*GeneART*
		Cd4+ Biotin	Cecile Crosnier
		Cd4+His	
	Full-length ectodomain of Basigin (NP_940991.1)	Cd4+ COMP+ β-lactamase	
		Cd4+ Biotin	
		Cd4+His	Josefin Bartholdson
	Domain 1 of Basigin (NP_940991.1)	Cd4+ Biotin	
	Domain 2 of Basigin (NP_940991.1)		
	Site-directed mutants of Basigin (Table 6)	Cd4+ Biotin	*GeneART*
	α-2,3-sialyltransferase 1 (NP_003024.1)		*OriGene* (TrueClones)
	CMP-sialic acid transporter (NP_006407.1)		

	Multi-pass membrane proteins (Table 7)	c-Myc+ DDK	*OriGene* (TrueORF clones)
Chimpanzee	Full-length ectodomain of Basigin	Cd4+ Biotin	*GeneART*
		Cd4+ COMP+ β-lactamase	Madushi Wanaguru
		Cd4+His	
	Site-directed mutants of Basigin (Table 6)	Cd4+ Biotin	*GeneART*
Gorilla	Full-length ectodomain of Basigin	Cd4+ Biotin	*GeneART*
		Cd4+ COMP+ β-lactamase	Madushi Wanaguru
		Cd4+His	

Table 4. Antibodies used for the work described in this thesis.

Antibody	Source/reference
Anti-Glycophorin A mouse monoclonals (BRIC 256 and 11E4B7)	*Abcam*
Anti-human BSG mouse monoclonals (MEM-M6/1, MEM-M6/2 and MEM-M6/6)	
Anti-Duffy goat polyclonal	
FITC-conjugated donkey anti-goat secondary	
Anti-c-Myc mouse monoclonal	

Anti- *P. falciparum* Rh5 rabbit polyclonals	Cecile Crosnier
Anti- *P. falciparum* EBA175 RII mouse monoclonals (R217 and R218)	David Narum (Sim *et al*., 2011)
Alkaline phosphatase conjugated goat anti-rabbit secondary	*Jackson ImmunoResearch Laboratories*
Anti- *P. falciparum* EBA175 RVI mouse monoclonal	Mike Blackman (O'Donnell *et al*., 2006)
Anti- *P. falciparum* Rh5 mouse monoclonals	Sandy Douglas
Anti-Cd4 mouse monoclonal (OX68)	*Serotec*
W6/32 mouse monoclonal	
Alkaline phosphatase conjugated goat anti-mouse secondary	*Sigma*
FITC-conjugated goat anti-mouse secondary	
Anti-CD200R mouse monoclonal (OX102)	(Wright *et al*., 2000)
Anti-human BSG mouse monoclonals (MEM-M6/4, MEM-M6/8, MEM-M6/10 and MEM-M6/11)	Zenon Zenonos (Koch *et a*l., 1999)

2.8 BIBLIOGRAPHY

Brown, M.H., Boles, K., van der Merwe, P.A., Kumar, V., Mathew, P.A. and Barclay, A.N. (1998) 2B4, the natural killer and T cell immunoglobulin superfamily surface protein, is a ligand for CD48. *Journal of Experimental Medicine, 188* (11), 2083-2090.

Brown, M.H. (2002) Detection of low-affinity ligand-receptor interactions at the cell surface with fluorescent microspheres. *Current Protocols in Immunology*, Chapter 18: Unit 18.2

Brown, M. H., & Barclay, A. N. (1994). Expression of immunoglobulin and scavenger receptor superfamily domains as chimeric *p*roteins with domains 3 and 4 of CD4 for ligand analysis. *Protein Engineering, 7*(4), 515-21.

Bushell, K. M., Söllner, C., Schuster-Boeckler, B., Bateman, A., & Wright, G. J. (2008). Large-scale screening for novel low-affinity extracellular protein interactions. *Genome Research, 18*(4), 622-30.

Crosnier, C., Staudt, N., & Wright, G. J. (2010). A rapid and scalable method for selecting recombinant mouse monoclonal antibodies. *BMC Biology, 8*, 76.

Durocher, Y., Perret, S., & Kamen, A. (2002). High-level and high-throughput recombinant protein production by transient transfection of suspension-growing human 293-EBNA1 cells. *Nucleic Acids Research, 30*(2), E9.

Koch, C., Staffler, G., Hüttinger, R., Hilgert, I., Prager, E., Cerný, J., Steinlein, P., *et al*. (1999). T cell activation-associated epitopes of CD147 in regulation of the T cell response, and their definition by antibody affinity and antigen density. *International Immunology, 11*(5), 777-86.

O'Donnell, R. A., Hackett, F., Howell, S. A., Treeck, M., Struck, N., Krnajski, Z., Withers-Martinez, C., *et al*. (2006). Intramembrane proteolysis mediates shedding of a key adhesin during erythrocyte invasion by the malaria parasite. *The Journal of Cell Biology, 174*(7), 1023-33.

Tom, R., Bisson, L., & Durocher, Y. (2008a). Transfection of HEK293-EBNA1 Cells in Suspension with Linear PEI for Production of Recombinant Proteins. *Cold Spring Harbor Protocols, 2008*(4), pdb.prot4977-pdb.prot4977.

Tom, R., Bisson, L., & Durocher, Y. (2008b). Transfection of HEK293-EBNA1 Cells in Suspension with 293fectin for Production of Recombinant Proteins. *Cold Spring Harbor Protocols, 2008*(4), pdb.prot4979-pdb.prot4979.

Tomschy, A., Fauser, C., Landwehr, R., & Engel, J. (1996). Homophilic adhesion of E-cadherin occurs by a co-operative two-step interaction of N-terminal domains. *The EMBO Journal*, *15*(14), 3507-14.

Wright, G J, Puklavec, M. J., Willis, A. C., Hoek, R. M., Sedgwick, J. D., Brown, M. H., & Barclay, A. N. (2000). Lymphoid/neuronal cell surface OX2 glycoprotein recognizes a novel receptor on macrophages implicated in the control of their function. *Immunity*, *13*(2), 233-42.

Chapter 3

Functional validation of a mammalian-expressed EBA175 antigen and comparative analysis of its binding to MM and MN forms of human Glycophorin A

3.1 INTRODUCTION

3.1.1 Identification and characterisation of *P. falciparum* EBA175 (*Pf*EBA175).

EBA175 was first identified on the basis of its ability to bind human erythrocytes, which seemed to correlate with invasion efficiency (Camus and Hadley, 1985). *Pf*EBA175 is synthesised as a 190 kDa membrane-spanning protein which is later proteolytically cleaved during erythrocyte invasion to release the 175 kDa extracellular domain, hence its name (Orlandi *et al*., 1990). Much of the earliest characterisation of *Pf*EBA175 was carried out using this soluble 175 kDa fragment of the native protein isolated from parasite culture supernatants.

*Pf*EBA175 is one of the four members of the EBL family known to be expressed at the merozoite stage of the *P. falciparum* life cycle (Section 1.7). The members of the EBL family share a strikingly similar gene structure, and this homology has been used to define six regions, RI-RVI, on their ectodomains (Figure 7 A) (Adams *et al*., 1992). Two of these regions, RII and RVI, both contain conserved cysteine and aromatic amino acid residues (Adams *et al*., 1992). RII was initially identified to mediate erythrocyte binding when truncated segments of the *Pf*EBA175 ectodomain were recombinantly expressed on the surface of monkey COS cells and tested for rosetting of erythrocytes (Sim *et al*., 1994). The structure of *Pf*EBA175 RII, which comprises two DBL domains in tandem (F1 and F2), was elucidated by X-ray crystallography to be dimeric, with the constituent monomers interacting in a parallel, handshake arrangement (Figure 7 B) (Tolia *et al*., 2005). The carboxyl-terminal RVI of the *Pf*EBA175 ectodomain is proposed to mediate the trafficking of the protein to micronemes, via interactions with components of the parasite protein-sorting machinery (Gilberger *et al*., 2003). The X-ray crystal structure of this region has revealed the presence of a disulphide-bridged four-helix bundle

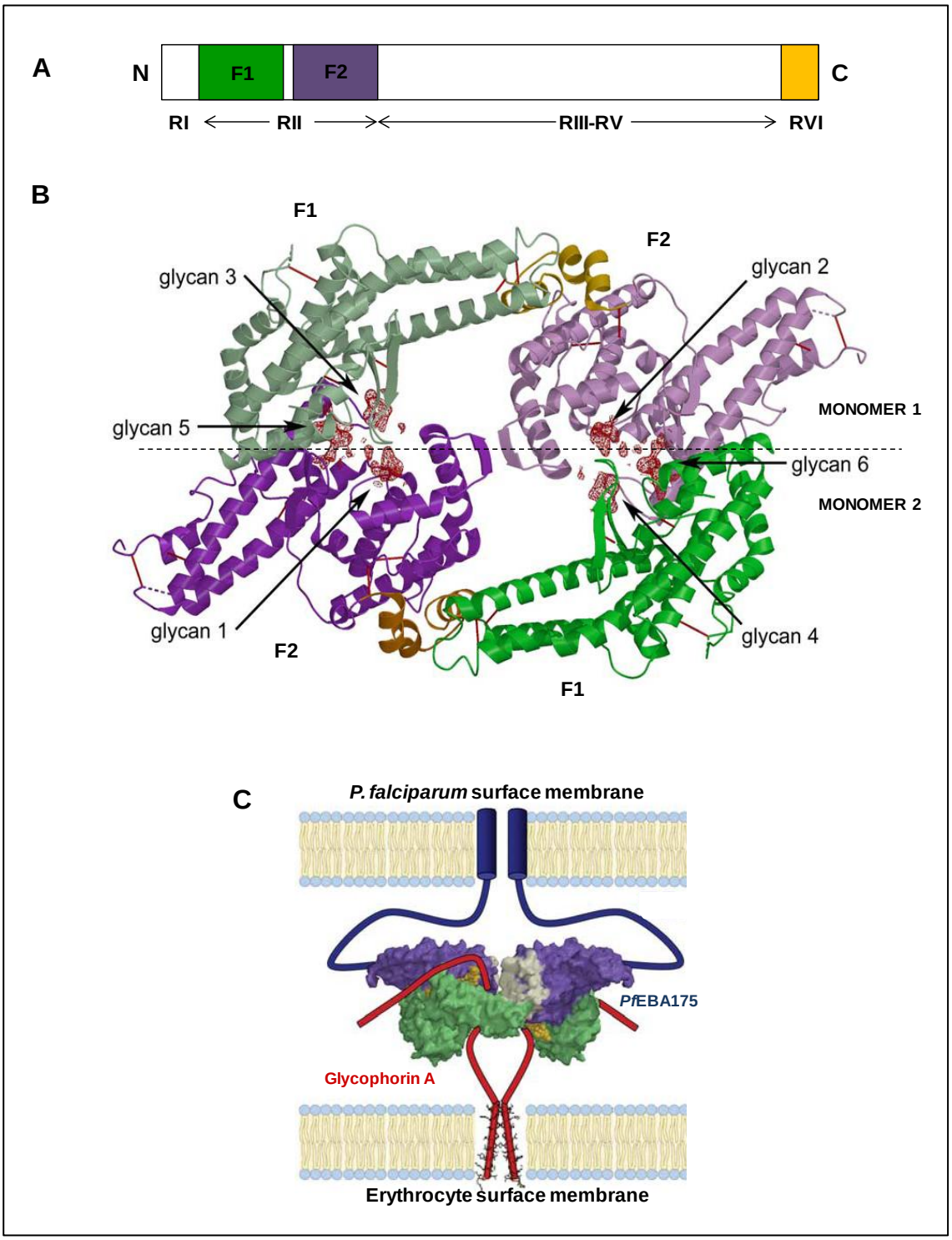
A
N
F1
F2
C
RI
RII
RIII-RV
RVI
B
F1
F2
glycan 3
glycan 2
glycan 5
MONOMER 1
glycan 6
MONOMER 2
glycan 1
F2
glycan 4
F1
C
P. falciparum surface membrane
PfEBA175
Glycophorin A
Erythrocyte surface membrane

Figure 7. *Pf*EBA175 RII: **structure and mode of binding. A)** Schematic of the extracellular domain of *Pf*EBA175 with the six regions of homology (RI-RVI) indicated. The N-terminal RII, which binds to erythrocytes, is rich in cysteine and contains two tandem DBP domains, F1 and F2. **B)** A ribbon representation of the *Pf*EBA175 RII dimer after co-crystallisation with the substrate analogue, α-2, 3-sialyllactose. In the dimer, the two *Pf*EBA175 RII monomers interact in a parallel, handshake arrangement with the F1 domain of one interacting with the F2 domain of the other and *vice versa*. The two monomers are shaded in different intensities in the schematic. The F1 domains are indicated in green and the F2 domains in purple. There are six putative glycan binding sites in the dimer, all located at the interface between the two monomers. Four of the sites are contained within two channels that span the dimer and the other two are found in a deep groove with restricted access from the top surface of the dimer. **C)** Schematic representing the 'ligand-induced dimerisation' model for the *Pf*EBA175-Glycophorin A interaction. This model proposes that free *Pf*EBA175 is predominantly monomeric and that dimerisation occurs upon receptor engagement. (Schematics **B** and **C** were adapted from Tolia *et al.*, 2005).

related to the KIX domain of the CREB-binding protein, which may be involved in such interactions (Withers-Martinez *et al*., 2008).

3.1.2 Interaction of *Pf*EBA175 with the erythrocyte receptor, Glycophorin A.

The *Pf*EBA175 receptor, Glycophorin A, is the most abundant integral membrane protein on the human erythrocyte surface with about 8 x 10^5 copies per cell (Auffray, 2001). It is a type I transmembrane protein which forms homodimers via reversible associations between the hydrophobic membrane-spanning domains (Mackenzie *et al*., 1997). The 70-amino acid extracellular domain of the protein contains the M and N blood group antigens, with the M phenotype characterised by Ser-1 and Gly-5 and the N phenotype by Leu-1 and Glu-5 (Figure 8 A) (Chasis & Mohandas, 1992). The M and N alleles are co-dominant, therefore, heterozygous individuals who carry both alleles, express the M as well as the N form of Glycophorin A, giving rise to the MN blood type. Homozygous individuals who express either the M or the N form of this erythrocyte receptor are of the MM or the NN blood type, respectively. This domain is also heavily sialylated, with 15 O-linked oligosaccharides and 1 N-linked glycan carrying terminal sialic acid (also called N-acetyl neuraminic acid, Neu5Ac) residues (Figure 8) (Tomita & Marchesi, 1975). The Neu5Ac (α-2,3) Gal sequence of the O-linked oligosaccharides has been shown to be essential for the recognition of Glycophorin A by *Pf*EBA175 (Figure 8 B) (Orlandi *et al*., 1992). Co-crystallisation of *Pf*EBA175RII with a structural analogue of this oligosaccharide, α-2,3-sialyllactose, has revealed six putative glycan binding sites at the dimer interface of the parasite protein, with four of the sites located within two channels that span the dimer and another two in a deep groove accessible only through a cavity at the top of the dimer (Figure 7 B) (Tolia *et al*., 2005). Interestingly, the F2 domains of the monomers contributed 75%

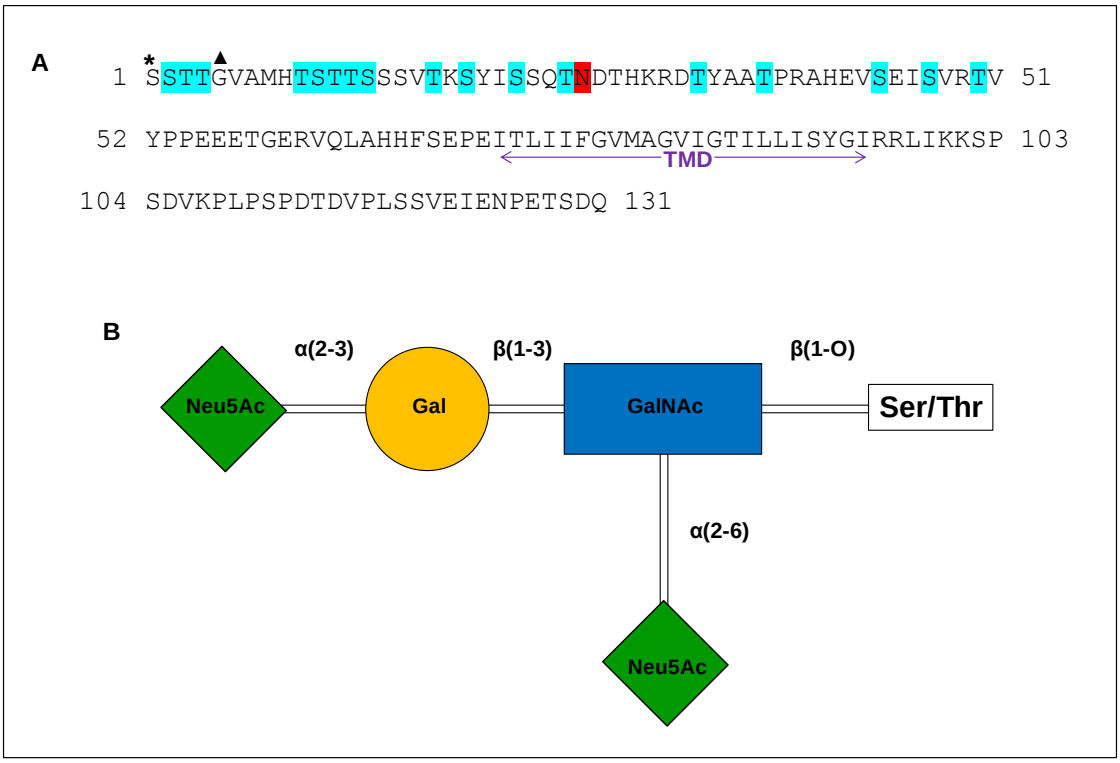

Figure 8. Human Glycophorin A: primary sequence with annotated features. A) Amino acid sequence of mature Glycophorin A (UniProtKB/Swiss-Prot Accession number: P02724), with the potential O-glycosylation sites in the extracellular domain shaded in blue and the N-glycosylation site in red. The given sequence is that of the M antigen. The N antigen of Glycophorin A contains a leucine at position 1 (*) and a glutamate at position 5 (▲). **B)** A schematic diagram of the predominant form of the O-linked tetrasaccharides on Glycophorin A. Neu5Ac-N-acetyl neuraminic acid, Gal-galactose, GalNAc-N-acetylgalactosamine. The glycosidic linkages of the sugar moieties are also indicated.

of the residues in contact with the glycans in the crystal structure, supporting the previous observation of F2 binding to erythrocytes in the absence of F1 (Sim *et al*., 1994; Tolia *et al*., 2005).

Based on the locations of the glycan binding sites in the *Pf*EBA175 RII crystal structure and the predominance of the monomeric form of *Pf*EBA175 RII in solution, Tolia *et al.* (2005) have proposed a ligand-induced dimerisation model for the erythrocyte binding of EBA175, with monomeric EBA175 assembling into a dimer around the dimeric extracellular region of Glycophorin A during invasion (Figure 7 C). This model is also consistent with recent structural studies investigating the mode of binding of the *P. vivax* orthologue DBP RII to its sulfotyrosine-carrying receptor, DARC (Batchelor *et al*., 2012).

3.1.3 *Pf*EBA 175 is an important vaccine candidate.

Some strains of *P. falciparum* such as FVO, Dd2 and MCamp are dependent on the presence of sialic acid on erythrocytes for invasion, whereas others including 3D7, HB3 and 7G8 are capable of invading neuraminidase-treated (i.e. sialic acid-depleted) erythrocytes with relatively high efficiency *in vitro* (Jiang *et al*., 2011). The differential requirement for sialic acid is proposed to reflect the usage of alternative merozoite ligand-erythrocyte receptor pairs for invasion by the various *P. falciparum* strains (Jiang *et al*., 2011; Narum *et al*., 2000; Zhang & Pan, 2005).

Although the interaction between *Pf*EBA175 and Glycophorin A is dependent on the erythrocyte receptor being sialylated, antibodies raised against *Pf*EBA175 RII have been shown to inhibit erythrocyte invasion by both sialic acid-dependent and independent strains of *P. falciparum in vitro* (Narum *et al*., 2000), presumably because *Pf*EBA175 is still functional in both types of strains. This hypothesis is supported by genetic data, where deletion of *Pf*EBA175 in 3D7, a sialic acid-independent stain, results in a shift in the invasion pathways (Duraisingh *et al*., 2003).

Anti-*Pf*EBA175 RII antibodies block the binding of native *Pf*EBA175 from different strains of *P. falciparum* to Glycophorin A, which is probably how they inhibit invasion (Jiang *et al.*, 2011). Interestingly, antibodies raised against RIII-V of the *Pf*EBA175 extracellular domain can also inhibit invasion, leading to the suggestion that these regions may also play a role in a sialic acid-dependent and/or independent invasion pathway (Lopaticki *et al*., 2011; Narum *et al*., 2000).

Based on the observed inhibition of *P. falciparum* blood-stage growth by antibodies directed against *Pf*EBA175 *in vitro* and the detection of anti-*Pf*EBA175 antibodies in malaria-immune individuals, *Pf*EBA175 is currently in consideration as a potential vaccine candidate against severe malaria (El Sahly *et al.,* 2010). The large size of the extracellular domain of *Pf*EBA175 is a technical hurdle for its successful expression as a recombinant protein in heterologous systems, hence, most *in vitro* studies for characterising this protein and assessing its suitability as a vaccine candidate have been conducted with RII, as a substitute. *Pf*EBA175 RII aggregates in insoluble inclusion bodies when over-expressed in *E. coli*, but is soluble and functionally active when produced in insect cells from baculoviral vectors or in the yeast, *Pichia pastoris* (El Sahly *et al*., 2010; Pandey *et al*., 2002; Ockenhouse *et al*., 2001). Antibodies raised against such recombinantly expressed-*Pf*EBA175 RII from one strain of *P. falciparum* have been shown to inhibit invasion by multiple other strains (Jiang *et al*., 2011). However, the level of inhibition observed is at most ~ 60%, suggesting that *Pf*EBA175 RII might not be very efficacious as a vaccine on its own (Narum *et al*., 2000).

3.1.4 Work described in the chapter

Native *Pf*EBA175 is released into *P. falciparum* culture supernatants as the 175 kDa full-length ectodomain fragment. Biochemical investigations of the *Pf*EBA175-Glycophorin A interaction, however, have mainly been performed using the much shorter *Pf*EBA175 RII fragment, as the

production of the full-length ectodomain (*Pf*EBA175 FL) in soluble recombinant form was not feasible in the traditional heterologous expression systems. There is a possibility of extracellular regions of *Pf*EBA175 outside of RII playing a yet unidentified role in erythrocyte invasion. *Pf*EBA175 FL is therefore potentially a better vaccine candidate than *Pf*EBA175 RII on its own. In this study, a soluble *Pf*EBA175 FL antigen, produced using a codon-optimised expression construct in mammalian cells, was extensively characterised using biochemical methods to confirm functional similarity to native *Pf*EBA175 isolated from parasite cultures and to gain mechanistic insight into its interaction with Glycophorin A. The binding of recombinant *Pf*EBA175 FL to human erythrocytes, native human Glycophorin A (purified from MM and MN erythrocytes) and a recombinantly-expressed full-length ectodomain of human Glycophorin A, was analysed.

3.2 RESULTS

3.2.1 *Pf*EBA175 FL was expressed as a soluble fusion protein and immunologically characterised.

The coding sequence of the full-length ectodomain of *Pf*EBA175 was derived from the 3D7 isolate of *P. falciparum* (MAL7P1.176) and codon optimised by gene synthesis for expression in the suspension culture-adapted human cell line, HEK293E (Section 2.1.1). As *P. falciparum* proteins are not known to be glycosylated (Gowda & Davidson, 1999), the potential N-linked glycosylation sites on *Pf*EBA175 were systematically removed during gene synthesis to prevent inappropriate addition of glycans in the human secretory pathway. The full-length ectodomain of *Pf*EBA175 (*Pf*EBA175 FL) was produced as a fusion protein with a mouse signal peptide to ensure secretion into the cell culture medium and with two carboxyl-terminal fusion partners: Cd4 and an enzymatically biotinylatable peptide tag (Section 2.1.1 and Figure 5). Expression of

biotinylated *Pf*EBA175 FL at the expected size of 185.7 kDa was confirmed by western blotting (Figure 9 A). Biotinylated Cd4, of 25 kDa, was used as a positive control in the blot.

*Pf*EBA175 FL was quantified relative to the highly expressed protein Cd4 (typical yield > 1 mg/ml) by ELISA as described in section 2.2.3. The ELISA results shown indicate an approximately 16-fold lower expression of *Pf*EBA175 FL (Figure 9 B). However, the levels of expression of both Cd4 and *Pf*EBA175 FL were observed to vary quite significantly from one batch of transfections to another (data not shown), most likely due to differences in transfection efficiency.

To determine whether the recombinant *Pf*EBA175 FL was correctly folded, its recognition by two mouse monoclonal antibodies, R217 and R218 were tested. R217 and R218, raised against a *Pf*EBA175 RII antigen produced using a baculovirus expression system, are known to bind to non-linear, heat-labile epitopes within EBA175 RII (Sim *et al*., 2011). *Pf*EBA175 FL was recognised by both R217 and R218 and heat-treatment of *Pf*EBA175 FL was observed to significantly reduce this immuno-reactivity, suggesting that the R217 and R218 epitopes are correctly folded in the mammalian-expressed full-length ectodomain. No significant binding of R217 and R218 to Cd4, the negative control, was observed (Figure 9 C).

Another mouse monoclonal antibody, raised against a yeast-derived *Pf*EBA175 RVI antigen (O'Donnell *et al.*, 2006) was also tested against *Pf*EBA175 FL by ELISA as described previously (Figure 9 D). This antibody showed similar binding to both untreated and heat-treated samples of *Pf*EBA175 FL, suggesting that it recognises a non-heat labile, linear epitope within EBA175 RVI. No binding of this antibody was seen to Cd4, the negative control.

All available anti-EBA175 monoclonals that recognise heat-labile epitopes therefore indicate that *Pf*EBA175 FL is correctly folded.

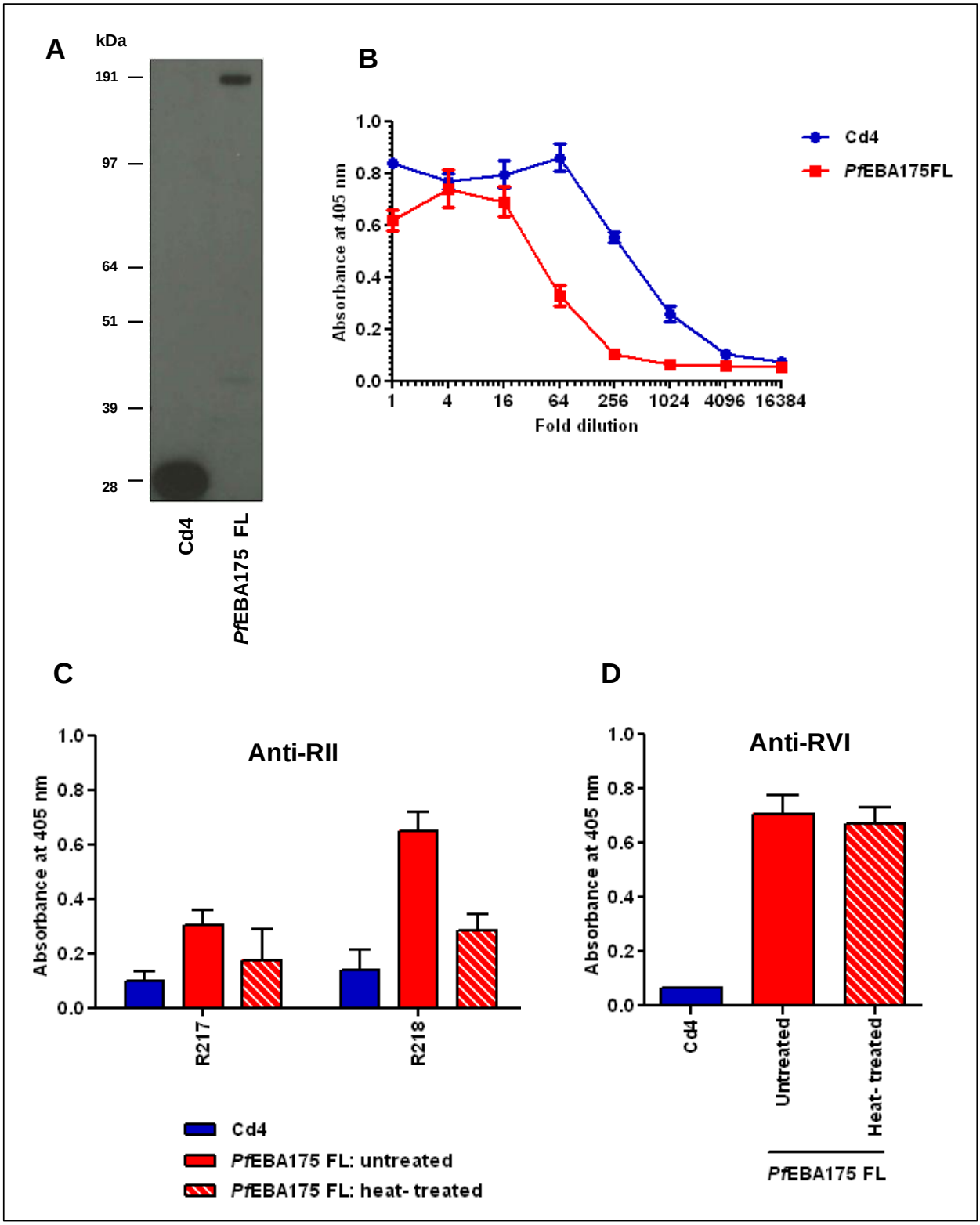
A
kDa
191
97
64
51
39
28
Cd4
PfEBA175 FL
B
Absorbance at 405 nm
Fold dilution
Cd4
PfEBA175FL
C
Anti-RII
Absorbance at 405 nm
R217
R218
Cd4
PfEBA175 FL: untreated
PfEBA175 FL: heat- treated
D
Anti-RVI
Absorbance at 405 nm
Cd4
Untreated
Heat- treated
PfEBA175 FL

Figure 9. Recombinant *Pf*EBA175 FL was expressed at the expected size and immunologically active. *Pf*EBA175 FL was expressed in the soluble form with C-terminal Cd4 and biotin tags using the HEK293E expression system. **A)** A western blot of *Pf*EBA175 FL (185.7 kDa) and monobiotinylated Cd4 (25 kDa), performed using HRP-conjugated extravidin as the probe. **B)** Quantitation of *Pf*EBA175 FL relative to Cd4 by ELISA. The anti-Cd4 mouse monoclonal OX68, was used as the primary antibody. **C)** and **D)** Recognition of untreated and heat-treated *Pf*EBA175 FL by two mouse monoclonals, R217 and R218, raised against a baculovirus-derived *Pf*EBA175 RII antigen **(C)** and a mouse monoclonal, raised against a yeast-expressed *Pf*EBA175 RVI antigen **(D)**. Binding of these monoclonals was also detected by ELISA. Cd4 was used as the negative control in the assays. All ELISAs were performed on streptavidin-coated plates, using an alkaline phosphatase-conjugated anti-mouse antibody as the secondary. Alkaline phosphatase activity was quantified by the turnover of the colorimetric substrate, *p*-nitrophenyl phosphate, measured as an increase in absorbance at 405 nm. The graphically presented data indicate mean ± standard deviation; n=3.

3.2.2 Recombinant *Pf*EBA175 FL showed Glycophorin A-dependent binding to human erythrocytes.

To determine whether the mammalian-expressed *Pf*EBA175 FL is functionally active, a flow cytometry-based, quantitative assay was developed to investigate its binding to Glycophorin A on human erythrocytes.

Interactions between cell surface proteins are generally of very low affinity. Therefore, to enable detection of its interaction with Glycophorin A, highly-avid, multimeric arrays of *Pf*EBA175 FL were first generated by direct immobilisation of the biotinylated protein on streptavidin-coated Nile red beads. To monitor the process of immobilising *Pf*EBA175 FL on beads and to determine the least amount of protein necessary for full saturation of a set number of beads, ELISA assays were performed on 2-fold serially-diluted samples of *Pf*EBA175 FL with and without prior incubation with beads (Figure 10 A). This assessment was deemed necessary, because non-saturation of beads with *Pf*EBA175 FL could decrease the avidity of the resulting arrays, whereas the presence of excess amounts of free (non-bead bound) *Pf*EBA175 FL could potentially act in an inhibitory manner against the binding of the arrays to erythrocytes. Similar bead arrays were also constructed with Cd4, to use as negative controls in the erythrocyte binding assays.

The protein-coated bead arrays generated were then incubated with human erythrocytes and analysed by flow cytometry. Erythrocytes incubated with *Pf*EBA175 FL-coated beads were observed to have higher forward scatter (FSC) and side scatter (SSC) values on average than those incubated with Cd4-coated beads (FSC and SSC values are directly proportional to the size and granularity of the cells sampled, respectively) (Figure 10 B). Incubation with *Pf*EBA175 FL-coated beads also caused a large upwards shift in the fluorescence intensity (~ 10^3 difference in

median fluorescence) of the erythrocyte population at the Nile red emission wavelength relative to Cd4-coated beads (Figures 10 C and D). These observations together suggest that *Pf*EBA175 FL-coated beads were binding to human erythrocytes. The specificity of the detected association was then probed using treatments known to interfere with the *Pf*EBA175-Glycophorin A interaction, either enzymatic (pre-treatment of erythrocytes with trypsin, chymotrypsin and neuraminidase) or immunological (pre-incubation of erythrocytes with an anti-Glycophorin A monoclonal antibody), prior to being presented with *Pf*EBA175 FL-coated beads.

Glycophorin A has previously been demonstrated to be sensitive to treatment with the protease trypsin but not chymotrypsin (Camus & Hadley, 1985). Human erythrocytes were therefore pre-treated with 0.25, 0.5 and 1 mg/ml of trypsin and chymotrypsin prior to incubation with the protein-coated bead arrays. Pre-treatment of erythrocytes with trypsin reduced the binding of *Pf*EBA175 FL-coated beads in a concentration-dependent manner (Figure 11 A). By contrast, the binding of *Pf*EBA175-coated beads to erythrocytes was not significantly affected by pre-treatment with chymotrypsin (Figure 11 B).

The binding of *Pf*EBA175 FL-coated beads was completely inhibited by pre-treatment of erythrocytes with the *Vibrio cholerae* neuraminidase, which preferentially cleaves α (2→ 3) linked sialic acids of O-glycans that are necessary for the *Pf*EBA175-Glycophorin A interaction (Figure 11 C, Section 3.1.1). The enzymatic susceptibility profile of the *Pf*EBA175 FL-human erythrocyte interaction therefore matches the profile of the *Pf*EBA175-Glycophorin A interaction.

To gain more direct confirmation of specificity, the possibility of inhibiting the association of *Pf*EBA175 FL with human erythrocytes using anti-Glycophorin A monoclonals was tested. As a preliminary step two anti-Glycophorin A monoclonal antibodies, 11E4B7 and BRIC256, were

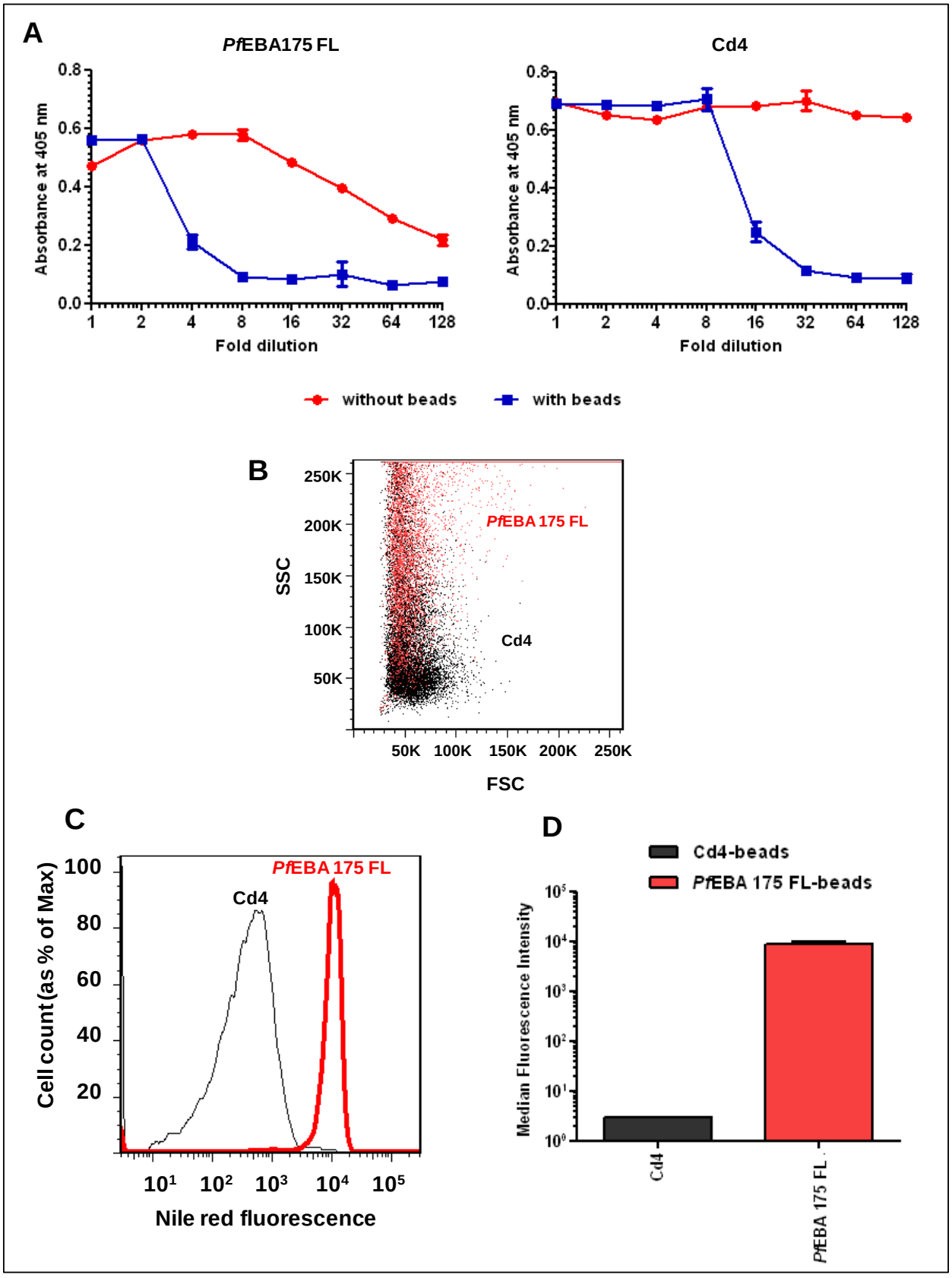
A
PfEBA175 FL
Cd4
Absorbance at 405 nm
Fold dilution
without beads
with beads
B
PfEBA 175 FL
Cd4
SSC
FSC
C
PfEBA 175 FL
Cd4
Cell count (as % of Max)
Nile red fluorescence
D
Cd4-beads
PfEBA 175 FL-beads
Median Fluorescence Intensity
Cd4
PfEBA 175 FL

0

Figure 10. Recombinant *Pf*EBA175 FL showed binding to human erythrocytes. To monitor the binding of *Pf*EBA175 FL to human erythrocytes, multimeric arrays of the protein were generated by immobilising on streptavidin-coated Nile red beads. Erythrocytes were incubated with these arrays for 1 h at 4°C before analysis by flow cytometry. Cd4-coated beads were used as the negative control in these erythrocyte binding assays. **A)** To determine the minimum amount of *Pf*EBA175 FL and Cd4 necessary for complete saturation of a set number of streptavidin-coated Nile red beads, ELISAs were performed on 2-fold serial dilutions of the proteins, with and without pre-incubation with beads. The ELISAs were carried out on a streptavidin-coated plate, using OX68 as the primary antibody and an alkaline phosphatase-conjugated anti-mouse antibody as the secondary. Data is shown as mean ± standard deviation; *n*=3. Based on the ELISA results, *Pf*EBA175 FL and Cd4 were used at dilutions of 4-fold and 16-fold respectively, for coating the fluorescent beads, which were then incubated with erythrocytes. **B)** A dot-plot of the FSC (α size) and SSC (α granularity) parameters of the erythrocyte populations as estimated by flow cytometry. **C)** A histogram of the fluorescence intensity of the erythrocyte populations at the Nile red emission wavelength, as a function of cell count. **D)** Representation of the median fluorescence intensity of erythrocyte populations at the Nile red emission wavelength. Each bar indicates mean ± standard deviation; *n*=3. In **B**, **C** and **D**, erythrocytes incubated with *Pf*EBA175 FL-coated beads are indicated in red and those incubated with Cd4-coated beads in black.

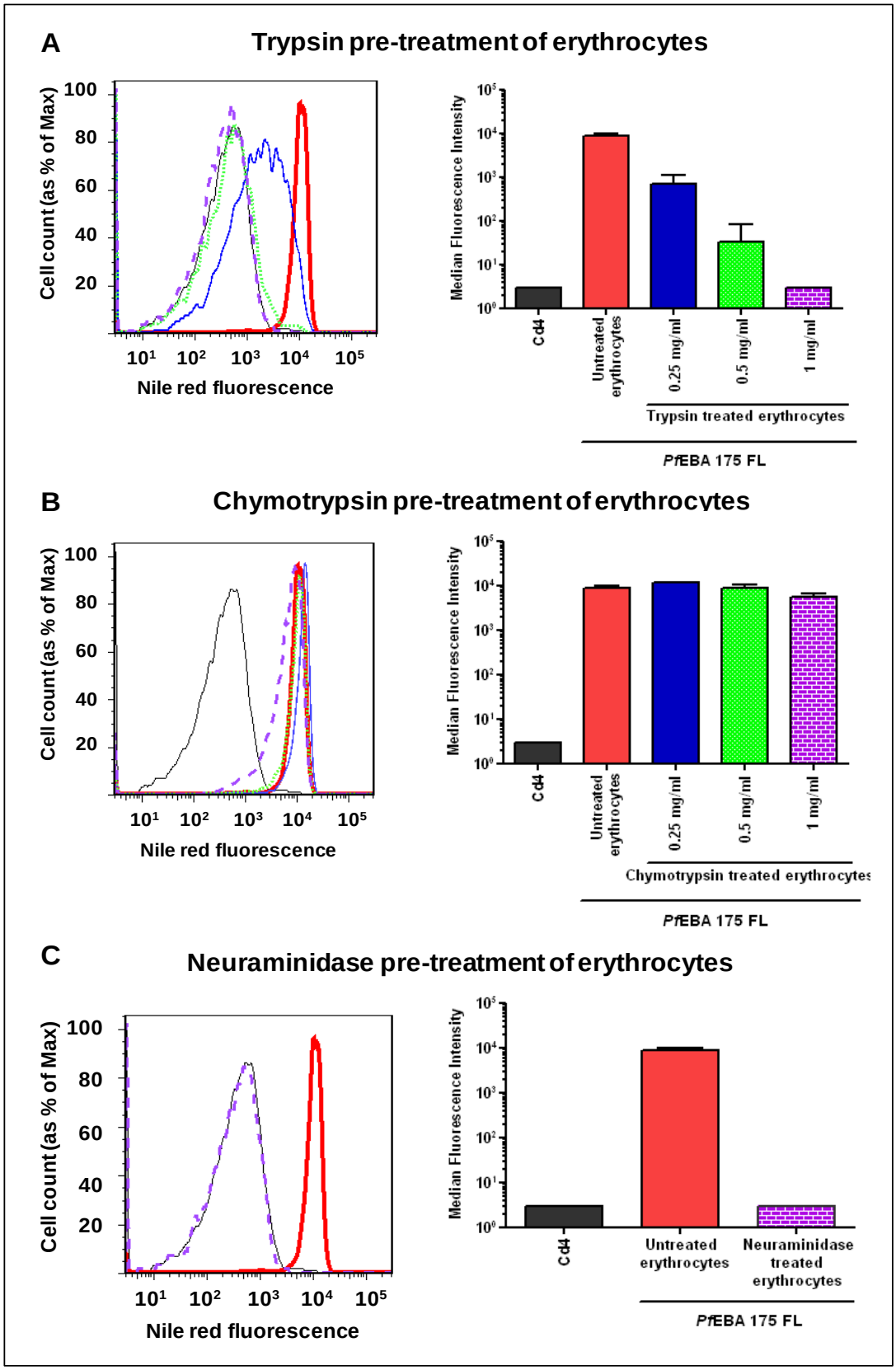
A
Trypsin pre-treatment of erythrocytes
Cell count (as % of Max)
Nile red fluorescence
Median Fluorescence Intensity
Cd4
Untreated erythrocytes
0.25 mg/ml
0.5 mg/ml
1 mg/ml
Trypsin treated erythrocytes
PfEBA 175 FL
B
Chymotrypsin pre-treatment of erythrocytes
Cell count (as % of Max)
Nile red fluorescence
Median Fluorescence Intensity
Cd4
Untreated erythrocytes
0.25 mg/ml
0.5 mg/ml
1 mg/ml
Chymotrypsin treated erythrocytes
PfEBA 175 FL
C
Neuraminidase pre-treatment of erythrocytes
Cell count (as % of Max)
Nile red fluorescence
Median Fluorescence Intensity
Cd4
Untreated erythrocytes
Neuraminidase treated erythrocytes
PfEBA 175 FL

Figure 11. The binding of *Pf*EBA175 FL to human erythrocytes was sensitive to treatment with trypsin and neuraminidase, but not chymotrypsin. Human erythrocytes were pre-treated with the enzymes, trypsin **(A)**, chymotrypsin **(B)** and neuraminidase **(C)** prior to incubation with *Pf*EBA175 FL-coated beads and analysis by flow cytometry. The histograms and the bar charts represent the fluorescence intensity of the erythrocyte populations at the Nile red emission wavelength. Untreated erythrocytes incubated with *Pf*EBA175 FL-coated beads (positive control) and Cd4-coated beads (negative control), are indicated in red and black respectively. **A)** Erythrocytes pre-treated with 0.25, 0.5 and 1 mg/ml of trypsin are represented in blue, green and purple respectively. **B)** Erythrocytes pre-treated with 0.25, 0.5 and 1 mg/ml of chymotrypsin are indicated in blue, green and purple respectively. **C)** Erythrocytes pre-treated with 100 mU/ml of neuraminidase are represented in purple. All enzymatic pre-treatments were carried out for 1 h at 37°C. The bar charts show mean ± standard deviation; n=3.

first tested for binding to human erythrocytes. 11E4B7 and BRIC256 have been raised using human erythrocytes and full-length native human Glycophorin A as immunogens, respectively. At the concentration used (0.5 µg of antibody/10^6 cells), 11E4B7 caused erythrocytes to aggregate, BRIC256 however showed clear binding to erythrocytes without causing cell aggregation (Figure 12 A). Pre-incubation of erythrocytes with BRIC256, significantly decreased the binding of *Pf*EBA175 FL-coated beads, confirming the Glycophorin A-dependency of the association of *Pf*EBA175 FL-coated beads with human erythrocytes (Figure 12 B).

3.2.3 Recombinant *Pf*EBA175 FL showed binding to native human Glycophorin A in a sialic acid-dependent manner.

As a second independent assay for validating the activity of *Pf*EBA175 FL, its binding to native Glycophorin A extracted from human erythrocyte membranes was tested using an ELISA-based method adapted from AVEXIS (Section 2.5.2). Glycophorin A from both MM and MN blood types were included as well as an asialylated form Glycophorin A from the MN blood type.

As the 'Neu5Ac (α-2,3) Gal' sequence of the O-linked tetrasaccharides of Glycophorin A is known to be essential for its interaction with *Pf*EBA175 (Section 3.1.1) , the glycan composition of the commercially available native Glycophorin A preparations was first tested by analysing its binding to three lectins with known glycan-binding preferences, *Arachis hypogaea* lectin (recognising non-sialylated Gal (β-1,3) GalNAc), *Sambucus nigra* lectin (recognising terminal Neu5Ac (α-2,6)) and *Maackia amurensis* lectin (recognising terminal Neu5Ac (α-2,3)). The biotinylated lectins were immobilised on streptavidin-coated plates and probed with the native Glycophorin A preparations using an ELISA-based method as described in Section 2.6.1. Native Glycophorin A (both MM and MN forms) seemed to predominantly carry glycans with terminal

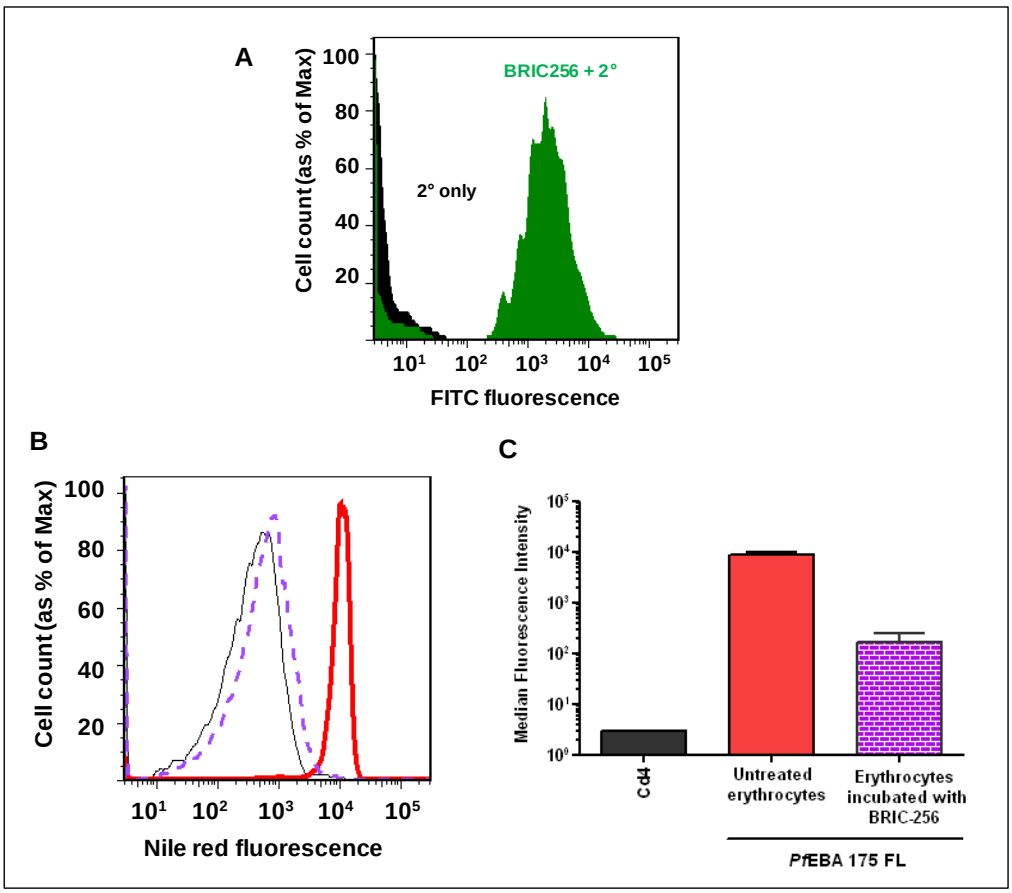

Figure 12. The binding of *Pf*EBA175 FL to human erythrocytes was significantly reduced by pre-incubation of cells with an anti-Glycophorin A monoclonal (BRIC256). Human erythrocytes were pre-treated with BRIC256 prior to incubation with *Pf*EBA175 FL-coated beads and analysis by flow cytometry. **A)** A histogram showing the staining of human erythrocytes by BRIC256, detected using a FITC-conjugated anti-mouse secondary (green). Erythrocytes incubated with only the secondary antibody (negative control) are represented in black. **B)** and **C)** Histogram and bar chart of the fluorescence intensity of the erythrocyte populations at the Nile red emission wavelength. Untreated erythrocytes incubated with *Pf*EBA175 FL-coated beads (positive control) and Cd4-coated beads (negative control), are indicated in red and black respectively. Erythrocytes pre-treated with BRIC256 (0.5 µg /10^6 cells) for 1 h at room temperature prior to incubation with *Pf*EBA175 FL-coated beads, are represented in purple. The bar chart shows mean ± standard deviation; *n*=3.

Neu5Ac (α-2,3), whereas the asialylated Glycophorin A preparation mainly contained non-sialylated Gal (β-1,3) GalNAc (Figure 13 A).

The native Glycophorin A preparations were then biotinylated *in vitro* to enable immobilisation on streptavidin-coated plates, for testing their binding to *Pf*EBA175 FL. The amount of biotinylated protein in each of the three Glycophorin A preparations was quantified relative to each other by ELISA using BRIC256 as the primary antibody (Figure 13 B).

For probing against native Glycophorin A, *Pf*EBA175 FL was expressed as a soluble β-lactamase tagged pentamer, by in-frame fusion with the pentamerisation domain of the rat COMP protein and a β-lactamase enzyme, in addition to the Cd4 tag, as described in Section 2.1.1 (Figure 5). The level of expression of *Pf*EBA175 FL was compared to that of pentameric, β-lactamase tagged Cd4 by monitoring the turnover of the β-lactamase substrate, nitrocefin in a time-course assay (Section 2.2.4). Neat, 2-fold and 4-fold dilutions of the proteins were tested in this manner. The level of expression of *Pf*EBA175 FL was lower than the threshold specified for the AVEXIS assay (i.e. sufficient protein in 20 µl of filtered culture supernatant for complete turnover of 7.5 µg of nitrocefin within 10 min), and so had to be concentrated 5-fold, the results shown for *Pf*EBA175 FL are from the β-lactamase activity assay done after this step (Figure 14 A).

Biotinylated native Glycophorin A preparations, immobilised on a streptavidin-coated plate, were finally probed with normalised *Pf*EBA175 FL and Cd4 'prey' proteins in a 2-fold dilution series. Both MM and MN forms of Glycophorin A showed similar levels of clear, saturable binding to *Pf*EBA175 FL, but not to Cd4 (Figure 14 B). Some slight binding to *Pf*EBA175 FL was also observed with asialylated Glycophorin A, which might have been due to the presence of some sialylated Glycophorin A in the initial protein preparation (Figure 14 B).

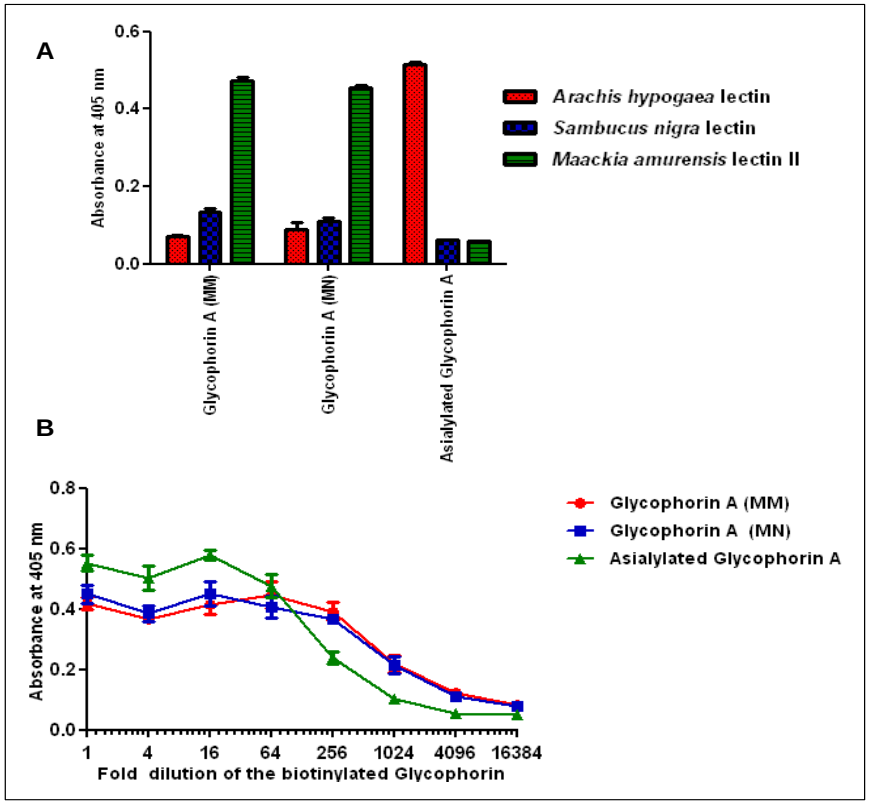

Figure 13. Commercially-available native human Glycophorin A preparations were biochemically characterised. A) Analysis of the glycan composition of the native Glycophorin A preparations, performed by the testing binding to three lectins using an ELISA-based method. The biotinylated lectins were immobilised on a streptavidin coated-plate and incubated with the Glycophorin A preparations (used at 0.02 mg/ml) for 2 h at room temperature. The glycan-binding specificities of the three lectins are as follows: *Arachis hypogaea* lectin (red)- non-sialylated Gal (β-1,3) GalNAc, *Sambucus nigra* lectin (blue)- terminal Neu5Ac (α-2,6) and *Maackia amurensis* lectin (green)- terminal Neu5Ac (α-2,3). **B)** The native Glycophorin A preparations were subsequently biotinylated *in vitro* for use in downstream assays. The amount of biotinylated protein in each of the preparations was normalised against each other by ELISA on a streptavidin-coated plate. In both assays, **A** and **B**, the binding of Glycophorin A was detected by sequential incubation with BRIC256 as the primary antibody and an alkaline phosphatase-conjugated anti-mouse secondary. All data is shown as mean ± standard deviation; *n*=3.

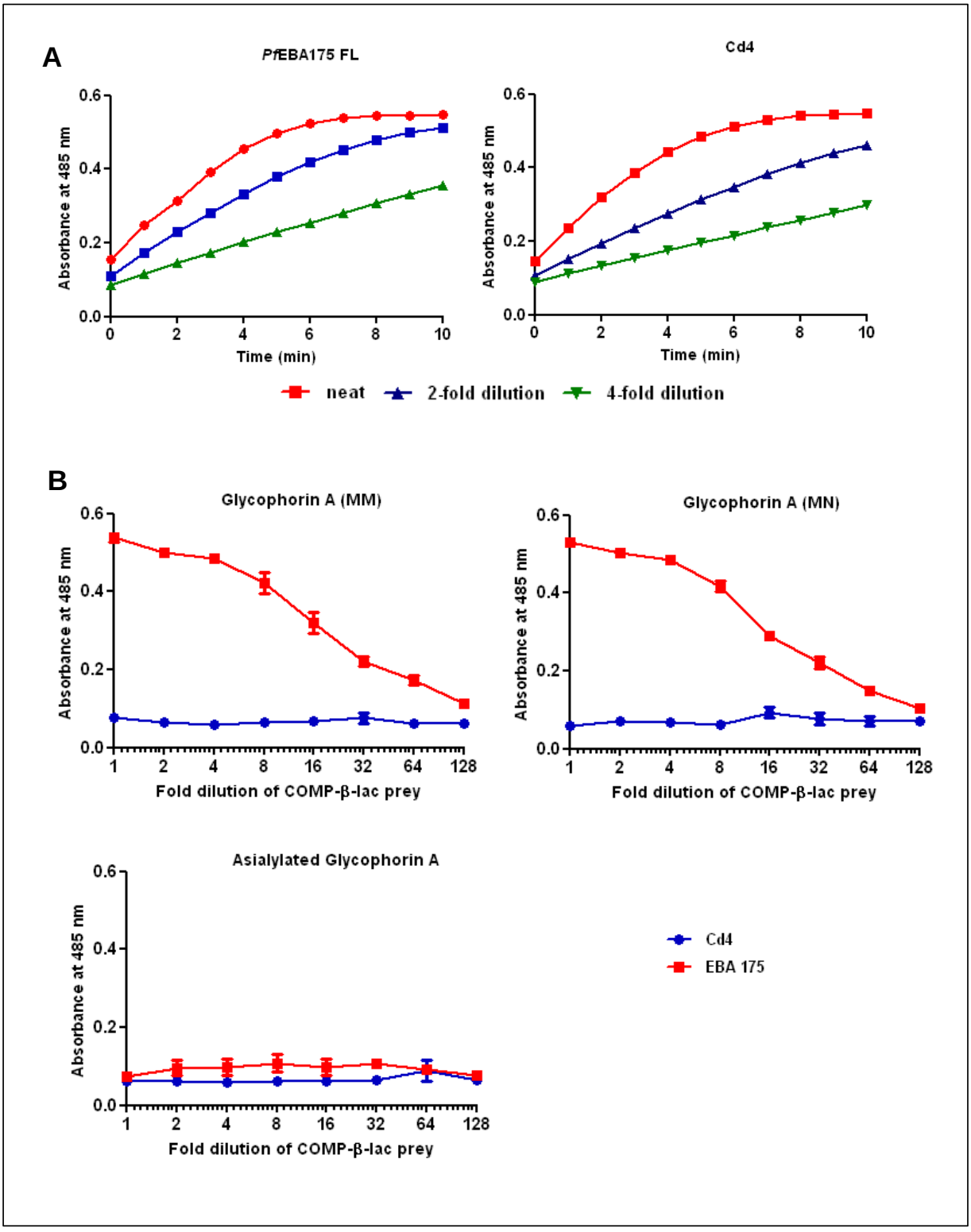
A
PfEBA175 FL
Cd4
Absorbance at 485 nm
Time (min)
neat
2-fold dilution
4-fold dilution
B
Glycophorin A (MM)
Glycophorin A (MN)
Asialylated Glycophorin A
Fold dilution of COMP-β-lac prey
Cd4
EBA 175

Figure 14. Recombinant *Pf*EBA175 FL showed sialic acid-dependent binding to native human Glycophorin A. *Pf*EBA175 FL, expressed as a soluble β-lactamase tagged pentamer was tested against the three biotinylated Glycophorin A preparations; sialylated native Glycophorin A of the MM and MN blood types and asialylated Glycophorin A, all immobilised on a streptavidin-coated plate. **A)** Prior to testing against Glycophorin A, *Pf*EBA175 FL and Cd4, both expressed in the pentameric form with a β-lactamase tag, were normalised against each other using a time-course assay, monitoring the turnover of the colorimetric β-lactamase substrate, nitrocefin, at an absorbance of 485 nm. **B)** A 2-fold dilution series of *Pf*EBA175 FL was probed against Glycophorin A and binding was detected using nitrocefin. Cd4 was used as the negative control in the assay. The pentameric proteins were incubated with the immobilised Glycophorin A for 2 h at room temperature and the absorbance at 485 nm was measured 1 h after the addition of nitrocefin. COMP- the pentamerisation tag. The data are shown as mean ± standard deviation; *n*=3.

3.2.4 The full-length ectodomain of human Glycophorin A was expressed in soluble recombinant form.

While commercially-available native human Glycophorin A can be used to confirm functionality of *Pf*EBA175 FL, a more detailed biochemical characterisation of the interaction requires recombinantly-expressed Glycophorin A, both because it would be amenable to site-directed mutagenesis and because it could potentially be isolated in much larger quantities with higher levels of purity than the native protein. The full-length ectodomain of human Glycophorin A (NP_002090.4) was therefore expressed in soluble, recombinant form using the HEK293E expression system.

For use in reciprocal AVEXIS assays with *Pf*EBA175 FL, the full-length ectodomain of Glycophorin A was expressed as both a mono-biotinylated 'bait' and as a pentameric β-lactamase tagged 'prey' protein as described above for *Pf*EBA175 FL. Human Glycophorin B (NP_002091.3) was also expressed with the same fusion partners, for use as a negative control in the AVEXIS assays. The proteins were normalised by ELISA (biotinylated proteins) (Figure 15 B) and β-lactamase activity assays (Figure 15 D). To confirm expression at the correct size, biotinylated recombinant Glycophorin A and B were analysed by western blotting using a streptavidin-HRP probe (Figure 15 A). The expected molecular weights of un-glycosylated monomers of recombinant Glycophorin A and B were 32.2 and 28.8 kDa respectively. The migration of these recombinant proteins as broad smears was probably due to the structural heterogeneity of the carbohydrate moieties added on to the protein backbone during glycosylation in the secretory pathway.

To confirm expression of recombinant Glycophorin A in the native conformation, the biotinylated proteins were probed with two anti-Glycophorin A mouse monoclonal antibodies,

11E4B7 and BRIC256, by ELISA (Figure 15 C). Both 11E4B7 and BRIC256 showed higher binding to untreated Glycophorin A than to its heat-treated derivative, suggesting the presence of correctly folded, heat-labile epitopes in the recombinant antigen. No binding of either was observed to the negative control, Glycophorin B. Interestingly 11E4B7 showed significantly greater binding to Glycophorin A than BRIC256 and as both antibodies were used at equivalent amounts, the former likely binds Glycophorin A with much higher affinity, potentially explaining the aggregation-inducing behaviour of 11E4B7 in the erythrocyte-staining experiment described previously in Section 3.2.1.

The glycan composition of the recombinant Glycophorins was analysed by incubation of their pentameric, β-lactamase tagged 'prey' forms with the biotinylated lectins from *Arachis hypogaea, Sambucus nigra* and *Maackia amurensis* as described in Section 2.6.1 (Figure 15 E). Both recombinant Glycophorin A and B, were observed to contain some glycans with terminal Neu5Ac (α-2,3) and Neu5Ac (α-2,6) but seemed to predominantly carry non-sialylated Gal (β-1,3) GalNAc moieties. Cd4, which doesn't contain any O-linked glycosylation sites, was used as the control 'prey' in this assay.

3.2.5 No binding was detected between recombinant human Glycophorin A and *Pf*EBA175 FL using AVEXIS.

The binding of recombinant Glycophorin A to *Pf*EBA175 FL was analysed in reciprocal AVEXIS assays.

When the pentameric, β-lactamase tagged *Pf*EBA175 FL 'prey' was tested against the biotinylated 'bait' form of recombinant Glycophorin A, Cd4 and recombinant Glycophorin B were included as negative control 'baits' and native Glycophorin A (MM) as a positive control

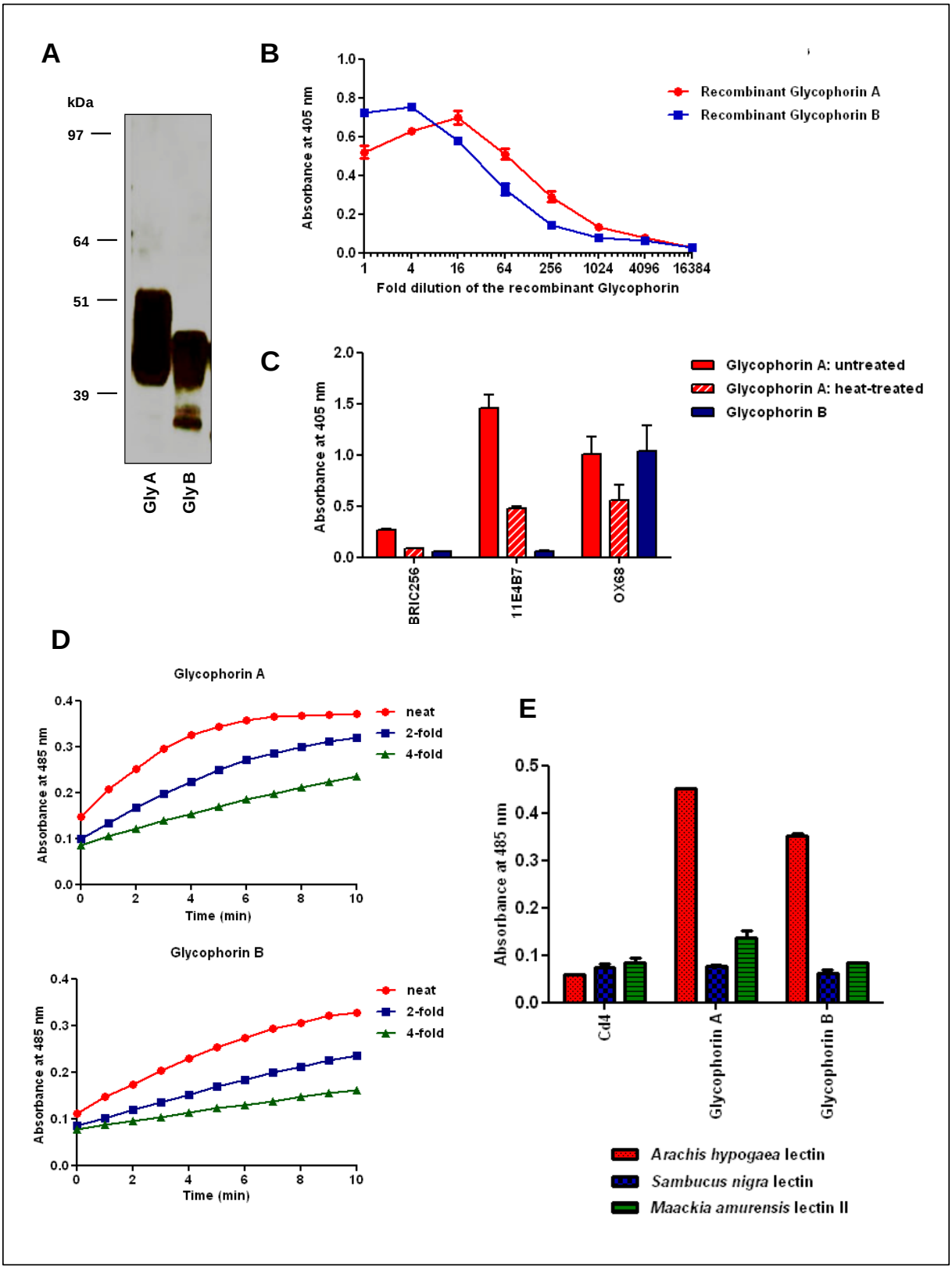
A
kDa
97
64
51
39
Gly A
Gly B
B
Absorbance at 405 nm
Fold dilution of the recombinant Glycophorin
Recombinant Glycophorin A
Recombinant Glycophorin B
C
Absorbance at 405 nm
Glycophorin A: untreated
Glycophorin A: heat-treated
Glycophorin B
BRIC256
11E4B7
OX68
D
Glycophorin A
Absorbance at 485 nm
Time (min)
neat
2-fold
4-fold
Glycophorin B
E
Absorbance at 485 nm
Cd4
Glycophorin A
Glycophorin B
Arachis hypogaea lectin
Sambucus nigra lectin
Maackia amurensis lectin II

Figure 15. The full-length ectodomain of human Glycophorin A was expressed in soluble form and characterised biochemically. Glycophorin A was expressed recombinantly using the HEK293E expression system, both as a monobiotinylated 'bait' and as a pentameric β-lactamase tagged 'prey'. The full-length ectodomain of Glycophorin B was similarly expressed for use as a control in downstream assays with Glycophorin A. **A)** Western blot of biotinylated Glycophorins A and B performed using HRP-conjugated extravidin as the probe. The expected molecular weight of an un-glycosylated monomer of Glycophorin A is 32.2 kDa. **B)** Quantitation of biotinylated Glycophorins A and B relative to each other by ELISA. The anti-Cd4 mouse monoclonal OX68, was used as the primary antibody. **C)** Recognition of untreated and heat-treated Glycophorin A by two mouse monoclonals, 11E4B7 and BRIC256, raised using human erythrocytes and native full-length Glycophorin A as immunogens respectively. Binding of these monoclonals was also detected by ELISA. Glycophorin B was used as a negative control 'bait' in the assays and OX68 as a positive control antibody. All ELISAs were performed on streptavidin-coated plates, using an alkaline phosphatase-conjugated anti-mouse antibody as the secondary. The data from ELISA assays are shown as mean ± standard deviation; *n*=3. **D)** Normalisation of pentameric β-lactamase tagged forms of Glycophorin A and B against each other by monitoring the turnover of nitrocefin at 485 nm over a period of 10 min. **E)** Analysis of the glycan composition of recombinant Glycophorin A, performed by testing its binding to three lectins. The biotinylated lectins were immobilised on a streptavidin coated-plate and incubated with β-lactamase tagged pentamers of Glycophorin A for 2 h at room temperature. Binding was subsequently detected by monitoring the turnover of nitrocefin at 485 nm. The glycan-binding specificities of the three lectins are as follows: *Arachis hypogaea* lectin (red)- non-sialylated Gal (β-1,3) GalNAc, *Sambucus nigra* lectin (blue)- terminal Neu5Ac (α-2,6) and *Maackia amurensis* lectin (green)- terminal Neu5Ac (α-2,3). Cd4 and Glycophorin B were used as controls in the assay. The bar chart shows mean ± standard deviation; *n*=3.

'bait' (Figure 16 A). Biotinylated OX68 was used as the positive control 'bait', when probing the 'prey' form of recombinant Glycophorin A against the *Pf*EBA175 FL 'bait' (Figure 16 B). Biotinylated Cd4 and pentameric Glycophorin B were used as the negative control 'bait' and 'prey' respectively in this experiment.

No interaction between recombinant human Glycophorin A and *Pf*EBA175 FL was observed in the AVEXIS assays.

3.2.6 No binding of recombinant Glycophorin A to *Pf*EBA175 FL was detected by SPR.

The ability of recombinant Glycophorin A to recognise *Pf*EBA175 FL was also tested using surface plasmon resonance, a method of very high sensitivity that allows protein-protein interactions to be monitored in real-time (van der Merwe, 2011).

To this purpose, the ectodomain of Glycophorin A was expressed with C-terminal Cd4 and hexa-His tags (Section 2.1.1 and Figure 4) and purified from the cell culture supernatant by affinity chromatography on a nickel-charged Sepharose column (Section 2.2.5) (Figure 17 A). The purified protein was analysed by SDS-PAGE under reducing conditions to confirm its expression at the correct size (Figure 17 B). The presence of carbohydrate moieties on recombinant Glycophorin A was verified by staining the polyacrylamide gel using a periodic acid-Schiff reagent method (Figure 17 C). The purified protein was then subjected to gel filtration to separate any aggregates that can confound SPR measurements and to exchange the protein into the SPR buffer. The protein eluted from the gel filtration column mainly as a monodisperse peak (Figure 17 D). The elution volume of the peak fraction, 34.9 ml, corresponds to an estimated size of approximately 60 kDa, suggesting that Glycophorin A was possibly eluting as a dimer.

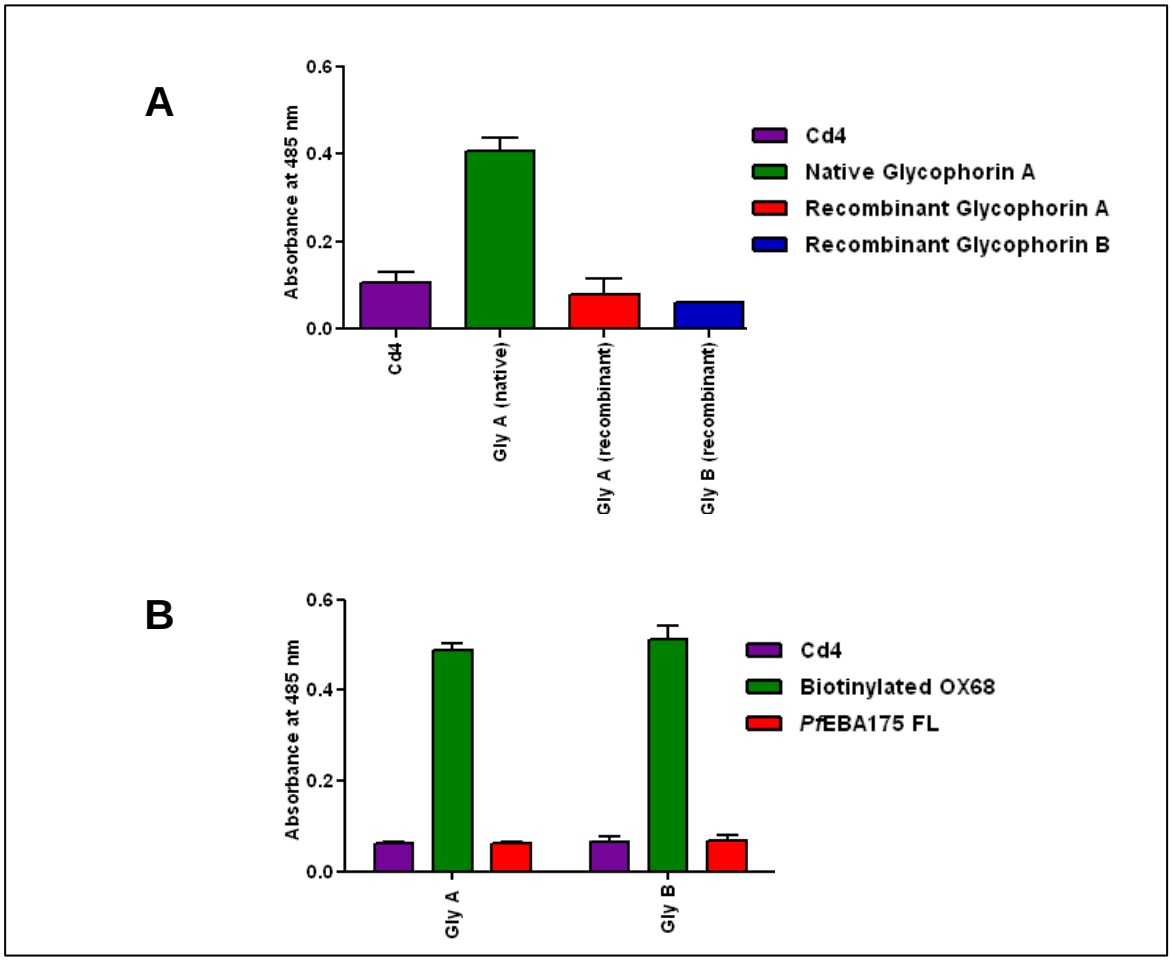

Figure 16. Recombinant human Glycophorin A was not recognized by *Pf*EBA175 FL. The AVEXIS assays were performed in two orientations. **A)** *Pf*EBA175 FL, in the pentameric, β-lactamase tagged 'prey' form, was tested against biotinylated recombinant Glycophorin A. Biotinylated native Glycophorin A was used as the positive control 'bait' in the assay and biotinylated Cd4 and Glycophorin B, the negative control 'baits'. **B)** Recombinant Glycophorin A, in the pentameric, β-lactamase tagged 'prey' form, was tested against biotinylated *Pf*EBA175 FL. Biotinylated OX68 and Cd4 were used as the positive and negative control 'baits' and recombinant Glycophorin B as the negative control 'prey'. The assays were performed on streptavidin-coated plates and the binding of the soluble 'preys' to the immobilised 'baits' was detected by monitoring the turnover of nitrocefin at 485 nm. The results are shown as mean ± standard deviation; *n*=3.

In the SPR experiment, the purified recombinant Glycophorin A was injected across biotinylated *Pf*EBA175 FL immobilised on a streptavidin-coated sensor chip. However, no interaction between the recombinant proteins could be detected (Figure 17 E). The activity of the immobilised *Pf*EBA175 FL was subsequently confirmed by injecting purified native Glycophorin A across the sensor surfaces (Figure 17 E).

3.2.7 The level of sialylation of recombinant Glycophorin A was increased by co-expression with sialyltransferases and a sialic acid transporter.

The inability of recombinant Glycophorin A to interact with *Pf*EBA175 FL could potentially be due to its lower levels of sialylation in comparison with native Glycophorin A (sections 3.2.3 and 3.2.4). Sialylation of recombinant proteins in mammalian systems has previously been shown to be increased by several strategies including supplementing the culture medium with sialic acid precursors (Gu & Wang, 1998) and co-expression of the glycoproteins-of-interest with Golgi-targeted sialyltransferases (Chitlaru *et al.*, 1998; Weikert *et al.*, 1999; Hossler et *al.*, 2009) or the CMP-sialic acid transporter (Wong *et al.*, 2006). Whereas sialyltransferases catalyse the addition of sialic acid moieties to the termini of N- and O-linked oligosaccharides, the CMP-sialic acid transporter mediates the trafficking of CMP-sialic acid from the cytosol into the Golgi lumen.

To try and increase its level of sialylation, recombinant Glycophorin A was co-expressed with the Golgi apparatus-targeted human α-2,3-sialyltransferase 1 (NP_003024.1), which catalyses the synthesis of the 'Neu5Ac (α-2,3) Gal' sequence on O-linked glycans, either singly or in combination with the rat α-2,6-sialyltransferase 1 (NP_001106815.1) or the human CMP-sialic acid transporter (NP_006407.1). The plasmids encoding the sialyltransferases and the CMP-sialic acid transporter were co-transfected with the Glycophorin A expression construct in either

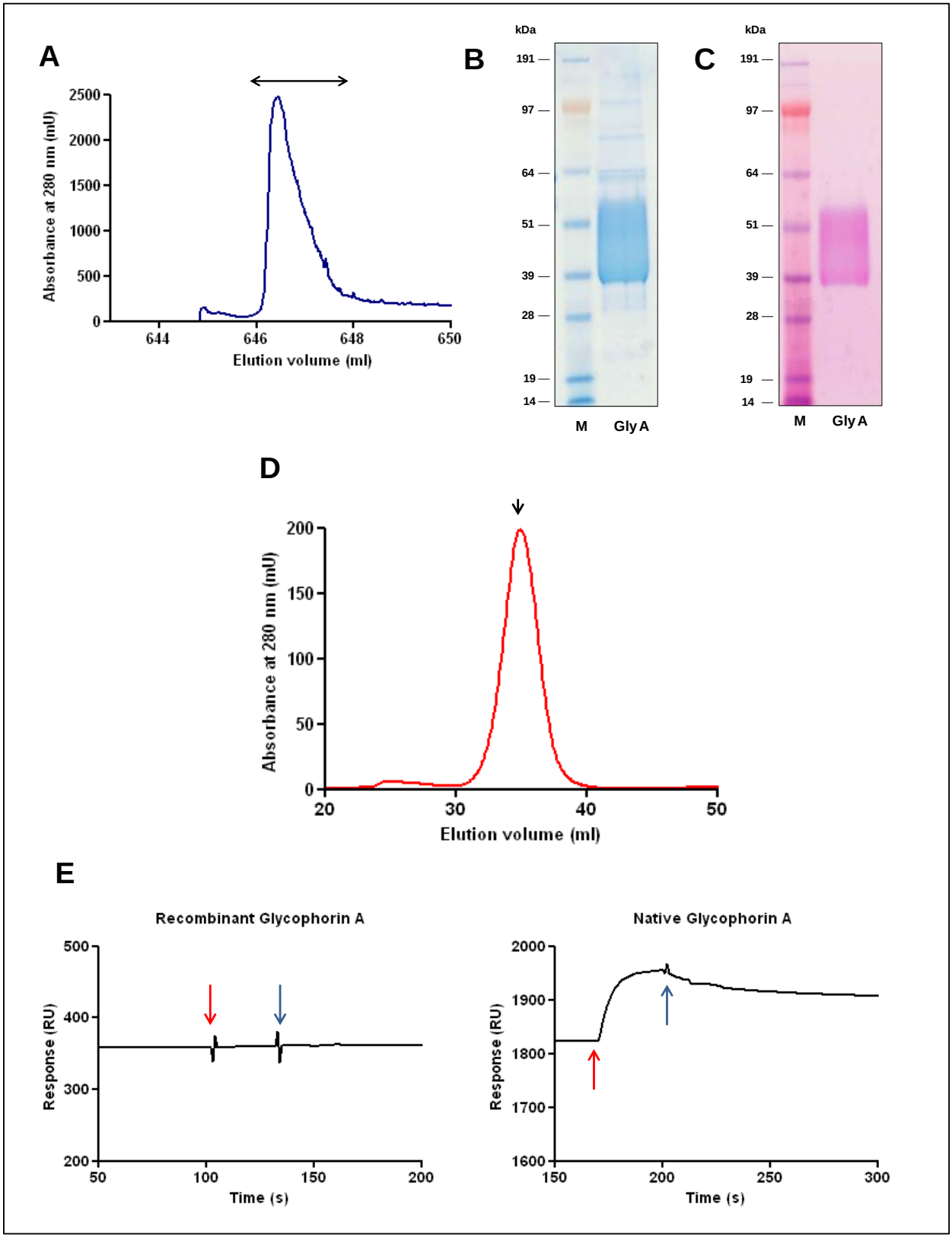
A
Absorbance at 280 nm (mU)
2500
2000
1500
1000
500
0
644
646
648
650
Elution volume (ml)
B
kDa
191
97
64
51
39
28
19
14
M
Gly A
C
kDa
191
97
64
51
39
28
19
14
M
Gly A
D
Absorbance at 280 nm (mU)
200
150
100
50
0
20
30
40
50
Elution volume (ml)
E
Recombinant Glycophorin A
Response (RU)
500
400
300
200
50
100
150
200
Time (s)
Native Glycophorin A
Response (RU)
2000
1900
1800
1700
1600
150
200
250
300
Time (s)

Figure 17. No interaction between recombinant human Glycophorin A and *Pf*EBA175 FL was detected by SPR. A) Hexa-His tagged Glycophorin A was purified from the culture supernatant by affinity chromatography on a nickel-charged sepharose column. The eluant from the column was monitored at 280 nm in real-time and the peak fractions containing protein (indicated by ⟷) were pooled. The affinity purified protein was analysed by SDS-PAGE and visualised using Coomassie brilliant blue **(B)** and a glycoprotein-specific staining method **(C)**. **D)** The elution profile of Glycophorin A from gel filtration. The peak fraction at ~35 ml is indicated by ↓. **E)** Reference subtracted sensorgrams from SPR analysis. Gel filtered-recombinant Glycophorin A (at 10 µM) and subsequently sialylated native Glycophorin A (at an approximately equivalent concentration) were injected at a flow rate of 30 µl/min, for 30 s across biotinylated *Pf*EBA175 and Cd4 (reference) immobilised on a streptavidin-coated sensor chip. The red and blue arrows indicate the start and the end of the 'prey' injections, respectively. The baits, *Pf*EBA175 FL and Cd4 (reference) were immobilised at molar equivalent amounts, *Pf*EBA175 FL- 2084 RU and Cd4- 261 RU respectively.

a 1:10 or a 1:5 ratio. The culture medium was additionally supplemented with the sialic acid precursor, N-acetyl-D-mannosamine, when the CMP-sialic acid transporter was co-transfected. The effects of these strategies on the glycan composition of recombinant Glycophorin A was analysed by testing β-lactamase tagged pentamers of Glycophorin A, expressed under the different conditions, against the lectins from *Arachis hypogaea*, *Sambucus nigra* and *Maackia amurensis* as described before (Section 3.2.4) (Figure 18). Co-transfection of Glycophorin A with the α-2,3-sialyltransferase 1 resulted in a clear increase in the level of glycans with terminal Neu5Ac (α-2,3), and this was further improved by co-transfection with the CMP-sialic acid transporter and supplementation with N-acetyl-D-mannosamine. Co-transfection with both α-2,3-sialyltransferase 1 and α-2,6-sialyltransferase 1, increased the level of terminal Neu5Ac (α-2,6) but had no noticeable effect on the Neu5Ac (α-2,3) level. Overall however the strategies were not effective enough to improve the sialylation of recombinant Glycophorin A to the levels observed in the native protein (Figure 18 B).

The sialylation-enhanced forms of recombinant Glycophorin A were tested against *Pf*EBA175 FL by AVEXIS and SPR as described previously. No binding of recombinant Glycophorin A to *Pf*EBA175 FL was observed (data not shown).

3.2.8 Kinetic parameters for the interaction between native Glycophorin A and *Pf*EBA175 FL were estimated by SPR.

Although recombinant Glycophorin A could not be produced in a form that bound to *Pf*EBA175, mechanistic insights can still be gleaned by investigating the binding of *Pf*EBA175 FL to native Glycophorin A, using SPR.

To perform this experiment, it was first necessary to identify a suitable method for immobilising the native Glycophorin A preparations (MM, MN and asialylated) on a SPR sensor chip. Direct

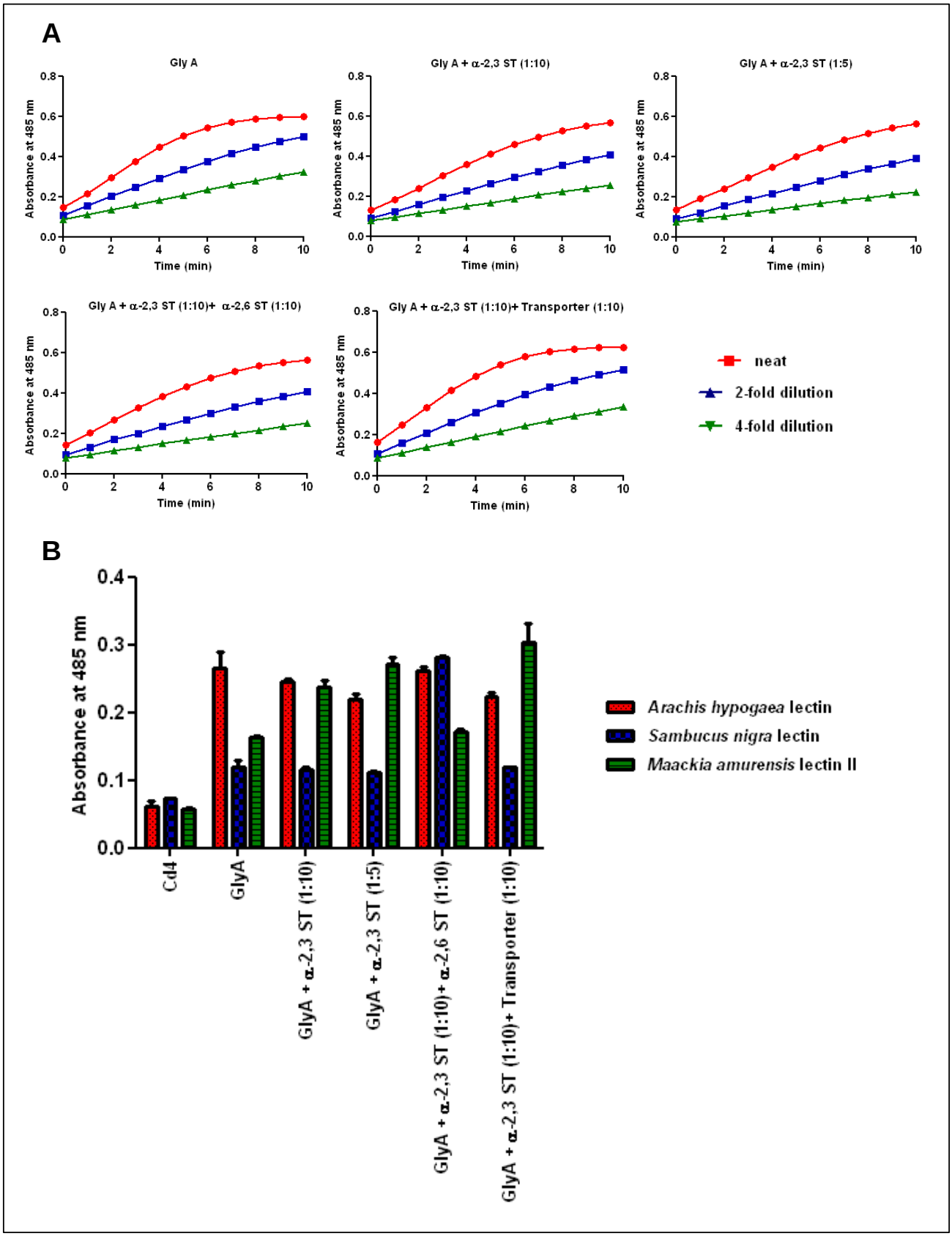
A
Gly A
Gly A + α-2,3 ST (1:10)
Gly A + α-2,3 ST (1:5)
Gly A + α-2,3 ST (1:10)+ α-2,6 ST (1:10)
Gly A + α-2,3 ST (1:10)+ Transporter (1:10)
Absorbance at 485 nm
Time (min)
neat
2-fold dilution
4-fold dilution
B
Absorbance at 485 nm
Cd4
GlyA
GlyA + α-2,3 ST (1:10)
GlyA + α-2,3 ST (1:5)
GlyA + α-2,3 ST (1:10)+ α-2,6 ST (1:10)
GlyA + α-2,3 ST (1:10)+ Transporter (1:10)
Arachis hypogaea lectin
Sambucus nigra lectin
Maackia amurensis lectin II

Figure 18. The sialylation of recombinant Glycophorin A was improved by co-expression with sialyltransferases and a sialic acid transporter. To potentially enhance its sialylation, recombinant Glycophorin A was co-expressed with the human α-2,3-sialyltransferase 1 (α-2,3 ST) either singly or in combination with the rat α-2,6-sialyltransferase 1 (α-2,6 ST) or the human CMP-sialic acid transporter. The expression plasmids encoding the transferases and the transporter were co-transfected with the Glycophorin A expression constructs either in a 1:5 or a 1:10 ratio. When the transporter was co-transfected, the culture medium was supplemented with 20 mM N-acetyl-D-mannosamine, a sialic-acid precursor. **A)** β-lactamase tagged pentamers of Glycophorin A expressed under the different conditions were normalised by monitoring the turnover of nitrocefin at 485 nm in a time-course assay. **B)** Analysis of the glycan composition of recombinant Glycophorin A pentamers, performed by testing their binding to three lectins. The biotinylated lectins were immobilised on a streptavidin coated-plate and incubated with β-lactamase tagged pentamers of Glycophorin A for 2 h at room temperature. Binding was subsequently detected by monitoring the turnover of nitrocefin at 485 nm. The glycan-binding specificities of the three lectins are as follows: *Arachis hypogaea* lectin (red)- non-sialylated Gal (β-1,3) GalNAc, *Sambucus nigra* lectin (blue)- terminal Neu5Ac (α-2,6) and *Maackia amurensis* lectin (green)- terminal Neu5Ac (α-2,3). Cd4 was used as a negative control in the assay. The bar chart shows mean ± standard deviation; *n*=3.

covalent attachment to a carboxymethylated dextran sensor surface via primary amine groups was tested as the first strategy. Covalent immobilisation is dependent on electrostatic pre-concentration of the ligand on the sensor surface, therefore to determine suitable coupling conditions, pre-concentration of Glycophorin A on the sensor chip surface was tested at a range of different pHs, by injecting the protein preparations across a non-activated sensor chip surface in short pulses, as recommended in the Biacore sensor surface handbook (*GE Healthcare*) (Figure 19 A). Electrostatic pre-concentration is dependent on the sensor surface and the injected ligand carrying opposite net charges, therefore the range of pHs tested was based on the predicted isoelectric point of unglycosyalted Glycophorin A (5.15) and the pK_a of the sensor chip surface (3.5). Whereas asialylated Glycophorin A showed increasingly efficient pre-concentration (observed as an increase in the response) at pHs 5.5 to 4.5, no electrostatic binding of Glycophorin A (MN) could be observed even at pH 4.0, suggesting that sialylated Glycophorin A might be too acidic to bind efficiently to carboxymethylated dextran. Both Glycophorin A (MN) and asialylated Glycophorin A were subsequently injected across a NHS/EDC-activated carboxymethyl dextran sensor surface, at a pH of 4.5, to check for covalent immobilisation (Figure 19 B). As expected, only asialylated Glycophorin A showed binding to the sensor surface. It was therefore necessary to find an alternative immobilisation strategy for Glycophorin A that was not dependent on electrostatic pre-concentration. To this purpose, native Glycophorin A preparations were tested for binding to a streptavidin-coated sensor chip, after biotinylation *in vitro*. This approach was observed to be suitable for immobilising both sialylated and asialylated forms of Glycophorin A (Figure 19 C).

For testing against native Glycophorin A by SPR, *Pf*EBA175 FL was expressed with C-terminal Cd4 and hexa-His tags and purified from harvested culture supernatant by affinity

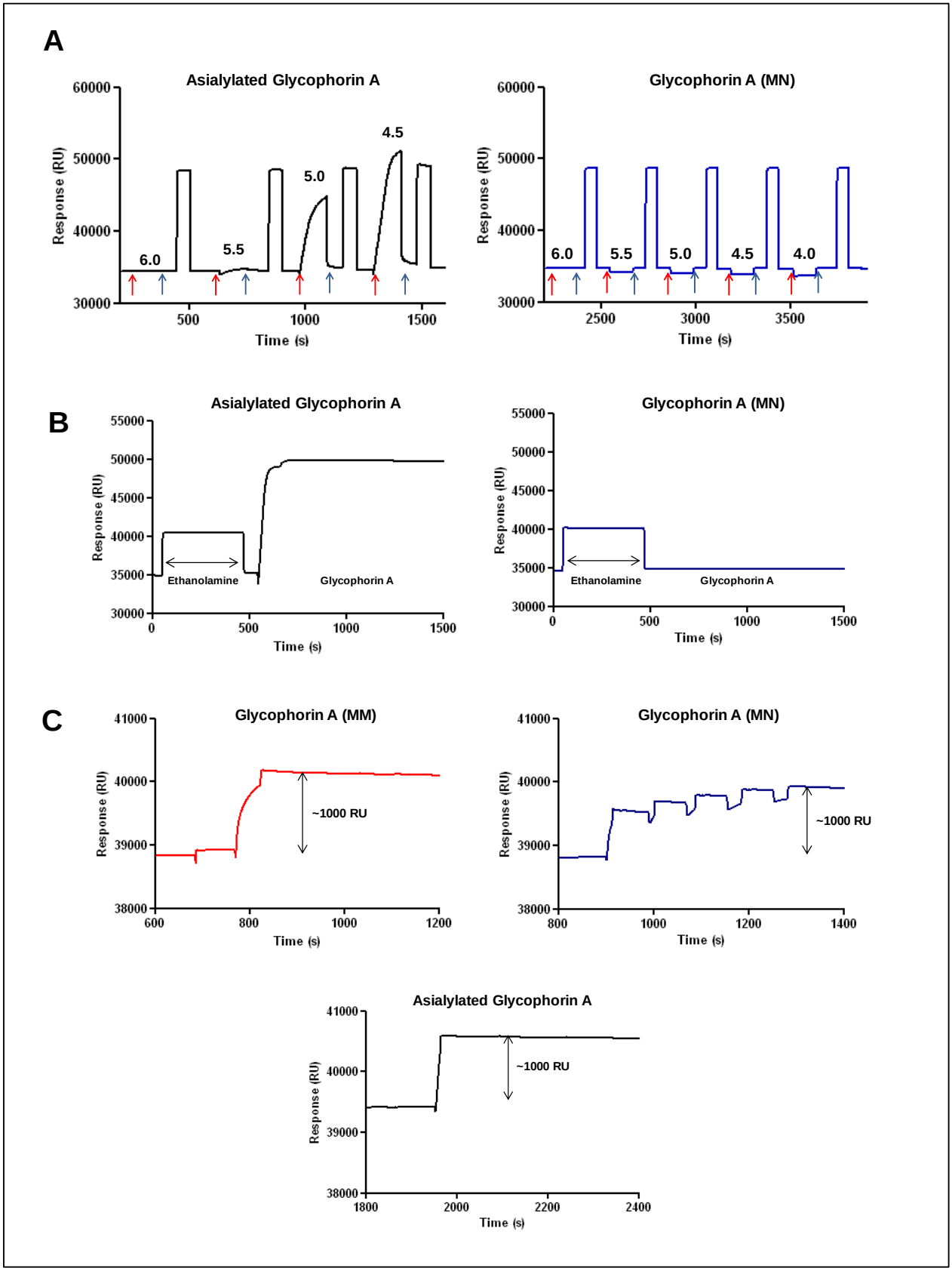
A
Asialylated Glycophorin A
Response (RU)
Time (s)
6.0
5.5
5.0
4.5
Glycophorin A (MN)
6.0
5.5
5.0
4.5
4.0
B
Asialylated Glycophorin A
Ethanolamine
Glycophorin A
Glycophorin A (MN)
Ethanolamine
Glycophorin A
C
Glycophorin A (MM)
~1000 RU
Glycophorin A (MN)
~1000 RU
Asialylated Glycophorin A
~1000 RU

Figure 19. Immobilisation of native Glycophorin A on SPR sensor chips. The native Glycophorin A preparations were tested for immobilisation on both carboxymethylated dextran-coated (CM5) and streptavidin-coated sensor chips. **A)** Testing the Glycophorin A preparations for electrostatic pre-concentration on a non-activated CM5 sensor chip, at different pHs. The protein preparations were injected at 50 µg/ml in 10 mM sodium acetate buffer of varying pH, using a flow rate of 10 µl/min for 120 s. The red and blue arrows indicate the start and the end respectively of these 'bait' injections. Each injection of Glycophorin A was followed by a 60 s injection of 1 M ethanolamine-HCl (pH 8.5) to remove any electrostatically-bound protein. **B)** Testing the Glycophorin A preparations for covalent immobilisation on the CM5 sensor chip at a pH of 4.5. Prior to injecting the protein the sensor surface was activated with a pulse of 0.2 M EDC and 0.05 M NHS. **C)** Immobilisation of the Glycophorin A preparations on a streptavidin-coated sensor chip after *in vitro* biotinylation. The proteins were injected in HBS buffer at a flow rate of 10 µl/min.

chromatography on nickel-charged Sepharose (Figure 20 A). Analysis of the purified protein by SDS-PAGE under reducing conditions, confirmed its expression at the expected size of 184.2 kDa (Figure 20 B). Some of the protein however appeared to be N-terminally processed, generating shorter fragments. Separation of the full-length form of the protein from the processed fragments was attempted with gel filtration (Figure 20 C). The expected elution volumes of monomeric (184.2 kDa) and dimeric (368.4 kDa) forms of *Pf*EBA175 FL were 29.38 and 26.42 ml respectively. The observed elution profile of *Pf*EBA175 FL consisted of four peaks at 25.14, 28.65, 33.46 and 39.08 ml. The elution volumes suggest that peaks 1 and 2 contained dimers and monomers of *Pf*EBA175 FL respectively, whereas peaks 3 and 4 carried shorter processed fragments. This was confirmed to some extent by analysing the peak fractions using denaturing SDS-PAGE and silver staining (Figure 20 D). Peaks 1 and 2 were observed to be enriched in the full-length form of the protein, whereas peaks 3 and 4 predominantly contained processed fragments at ~60 kDa and ~40 kDa respectively. Although 1 µg of protein from each of peaks 1 and 2 were loaded onto the gel, only some of the protein from peak 1 appeared to have entered the gel. This could be due to some dimers (or higher-order aggregates) persisting after heat-denaturation and not passing through the polyacrylamide matrix.

When the four peak fractions of *Pf*EBA175 FL were injected across native Glycophorin A immobilised on the streptavidin-coated SPR sensor chip, the highest binding to both MM and MN types of sialylated Glycophorin A was observed with peak fraction 2, containing monomeric *Pf*EBA175 FL (Figure 21 A). No binding of the peak fractions to asialylated Glycophorin A was observed.

To derive equilibrium and kinetic parameters for its interaction with native Glycophorin A, a 2-fold dilution series of monomeric *Pf*EBA175 FL was injected across the SPR sensor chip

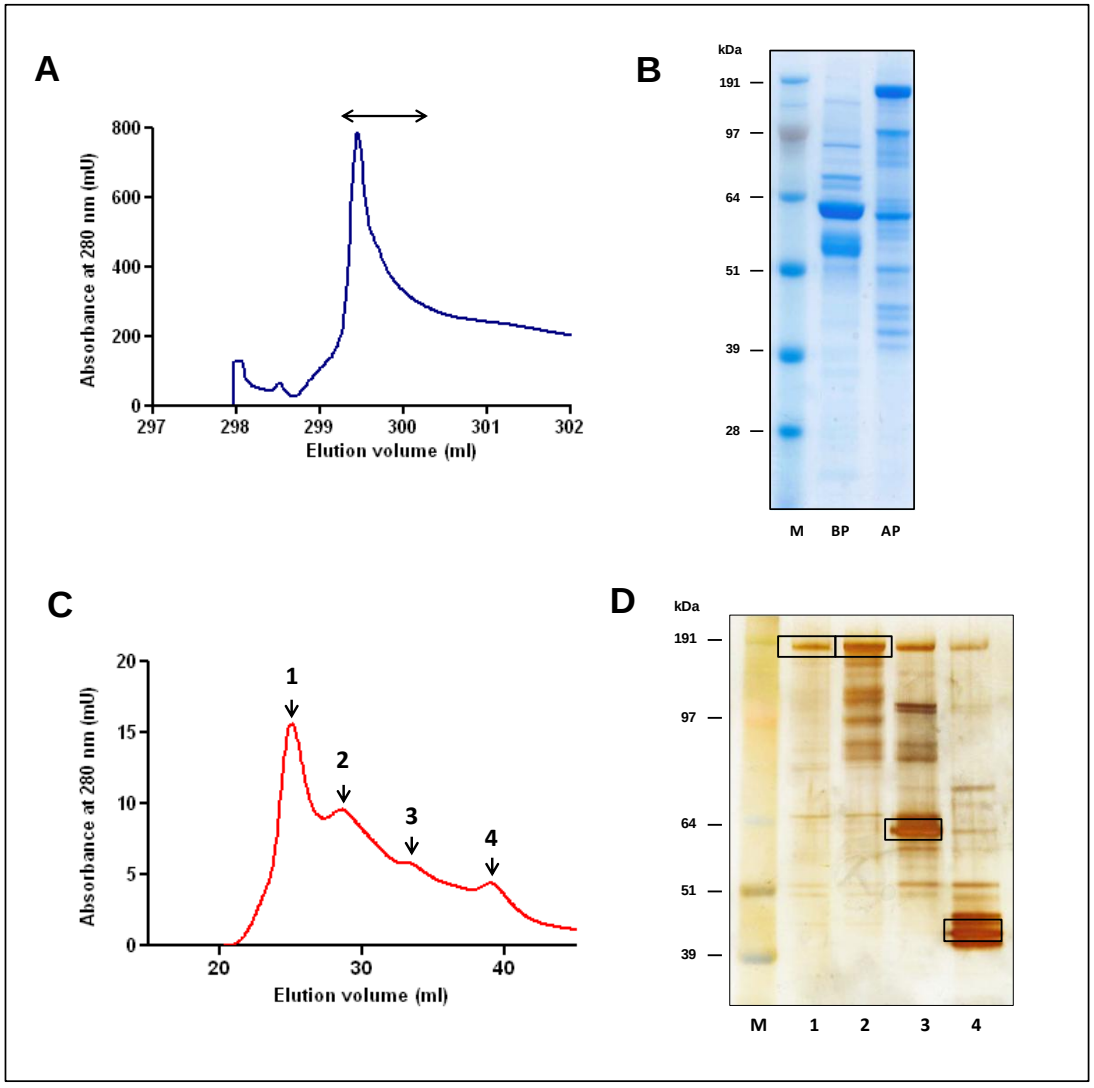

Figure 20. *Pf*EBA175 FL was expressed in soluble, hexa-His tagged form and purified from the culture supernatant. A) *Pf*EAB175 FL was purified from the culture supernatant by affinity chromatography on a nickel-charged Sepharose column. The eluant from the column was monitored at 280 nm in real-time and the peak fractions containing protein (indicated by ↓) were pooled. **B)** The affinity purified protein was analysed by SDS-PAGE and visualised using Coomassie brilliant blue. BP- before purification, AP- after purification. **C)** The elution profile of *Pf*EBA175 FL from gel filtration. The four peak fractions at 25.14 (1), 28.65 (2), 33.46 (3) and 39.08 ml (4) are indicated by ↔ . **D)** The peak fractions of *Pf*EBA175 FL from gel filtration were analysed by SDS-PAGE and visualised by silver staining. 1 µg of peak fractions 1 and 2 were loaded onto the gel and 0.5 µg of fractions 3 and 4. The most prominent band on each lane of the gel is boxed-in.

surfaces as described in Section 2.5.3 (Figure 21 B). Each set of binding curves (sensorgrams) obtained after reference subtraction (i.e. binding to Glycophorin A- binding to Cd4 immobilised in flow cell 1) was first evaluated for affinity, by plotting response at equilibrium (when association= dissociation, so that there is no net binding) against *Pf*EBA175 FL concentration (Figure 22 A). The data sets were fitted globally to a steady-state 1:1 binding model to derive the equilibrium dissociation constant, K_D. The Chi^2 (R^2) value, a measure of the difference between the experimental data and the fitted curve, was taken into account as an indication of the fidelity of the fit. The K_D values computed for MM and MN types of Glycophorin A were (2.8 ± 0.7) x 10^{-7} M and (2.1 ± 0.5) x 10^{-7} M respectively. The fitting of the model to the data sets were acceptable with corresponding R^2 values of 5.70 and 14.6. The difference in K_D values suggests that *Pf*EBA175 FL was binding to MN Glycophorin with a slightly higher affinity than to MM Glycophorin.

For kinetic evaluation, the data sets were globally fitted to a simple 1:1 binding model and to a more complicated two state reaction model (Figure 22 B). The latter assumes a 1:1 binding of the analyte to the immobilised ligand followed by a conformational change that stabilises the complex and was selected based on the 'ligand-induced dimerisation model' for the EBA175-Glycophorin A interaction proposed by Tolia *et al*. (2005). The two sets of binding curves obtained from the interaction of *Pf*EBA175 FL with MM and MN Glycophorin A were observed to show a much better fit (lower R^2) to the two state reaction model than to the 1:1 binding model (Figure 22 C). The K_D values calculated from the k_d/k_a parameters deduced using the two state reaction model, were also closer to the K_D values estimated from the equilibrium analysis.

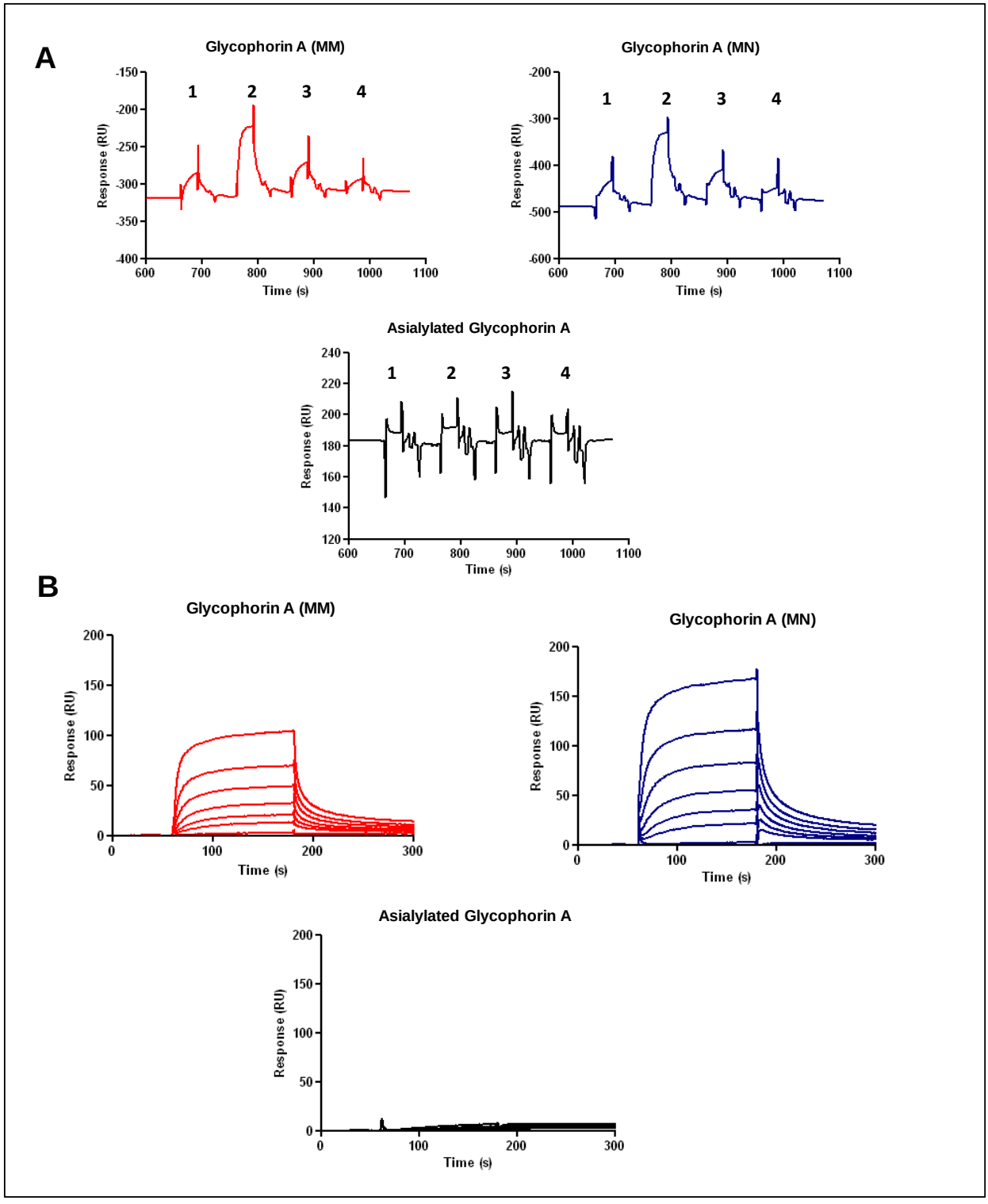
A
Glycophorin A (MM)
Response (RU)
Time (s)
1
2
3
4
Glycophorin A (MN)
Response (RU)
Time (s)
1
2
3
4
Asialylated Glycophorin A
Response (RU)
Time (s)
1
2
3
4
B
Glycophorin A (MM)
Response (RU)
Time (s)
Glycophorin A (MN)
Response (RU)
Time (s)
Asialylated Glycophorin A
Response (RU)
Time (s)

Figure 21. The binding of *Pf*EBA175 FL to native Glycophorin A was analysed by SPR. Reference subtracted sensorgrams from the injection of the four peak fractions of *Pf*EBA175 FL from gel filtration **(A)** or a 2-fold dilution series of peak fraction 2 **(B)**, across biotinylated native Glycophorin A immobilised on a streptavidin-coated sensor chip. The binding to Glycophorin A (MM), Glycophorin A (MN) and asialylated Glycophorin A are shown in red, blue and black respectively. The biotinylated baits were immobilised at Cd4 (reference)-1000 RU , Glycophorin A (MM)-1267 RU, Glycophorin A (MN)-1070 RU and asialylated Glycophorin A-1170 RU. **A)** The peak fractions with estimated concentrations of 380 nM (peak 1), 300 nM (peak 2), 180 nM (peak 3) and 150 nM (peak 4) were injected across the sensor chip surfaces at a flow rate of 30 µl/min, for 60 s each. **B)** The concentration series of *Pf*EBA175 FL, ranging from 93-300 nM, was injected at a flow rate of 20 µl/min, with a contact time of 120 s and a dissociation time of 200 s. At the end of each injection the sensor surface was regenerated with a pulse of 5 M NaCl.

A

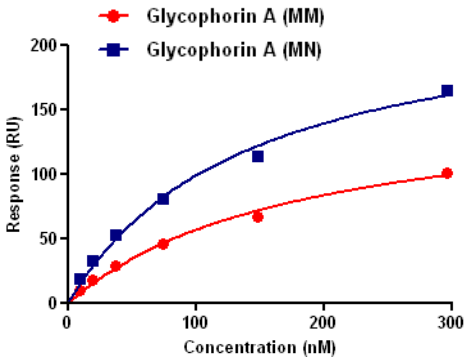

B

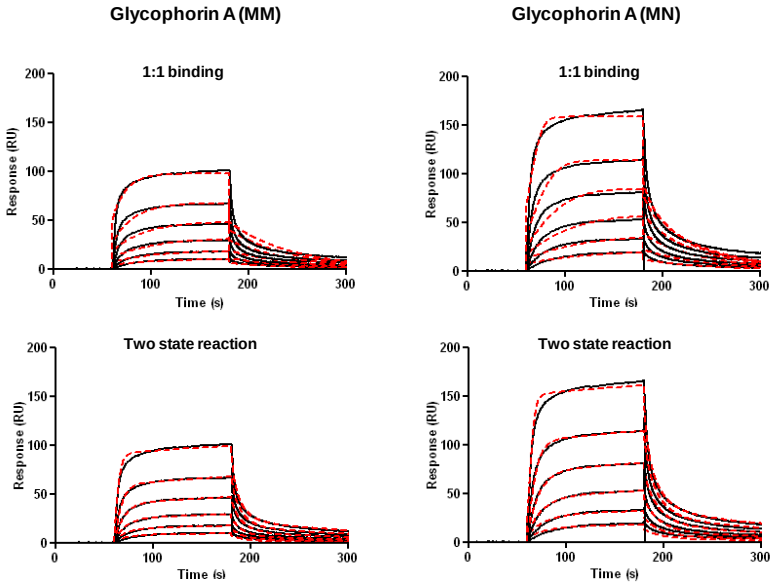

C

Glycophorin A (MM)				
Model	**Chi² (R^2)**	**k_a ($M^{-1}s^{-1}$)**	**k_d (s^{-1})**	**K_D (M)**
Steady-state affinity	5.70			$(2.8 \pm 0.7) \times 10^{-7}$
1:1 binding (kinetic)	12.9	$(2.10 \pm 0.04) \times 10^{5}$	$(1.57 \pm 0.03) \times 10^{-2}$	0.75×10^{-7}
Two state reaction (kinetic)	1.72	I $(1.40 \pm 0.02) \times 10^{9}$ II $(5.1 \pm 0.1) \times 10^{-3}$	I 302.0 ± 3.7 II $(2.83 \pm 0.06) \times 10^{-3}$	1.38×10^{-7}

Glycophorin A (MN)				
Model	**Chi² (R^2)**	**k_a ($M^{-1}s^{-1}$)**	**k_d (s^{-1})**	**K_D (M)**
Steady-state affinity	14.6			$(2.1 \pm 0.5) \times 10^{-7}$
1:1 binding (kinetic)	24.4	$(2.5 \pm 0.2) \times 10^{6}$	0.17 ± 0.01	0.70×10^{-7}
Two state reaction (kinetic)	4.36	I $(1.14 \pm 0.01) \times 10^{9}$ II $(2.58 \pm 0.06) \times 10^{-3}$	I 178.7 ± 1.2 II $(5.0 \pm 0.2) \times 10^{-3}$	1.03×10^{-7}

Figure 22. Equilibrium and kinetic parameters for the interaction of *Pf*EBA175 FL with native Glycophorin A were derived from the SPR data. The reference subtracted SPR sensorgrams from the binding of *Pf*EBA175 FL to MM and MN types of native Glycophorin A were subjected to equilibrium **(A)** and kinetic **(B)** analysis. **A)** For each set of sensorgrams the response at equilibrium was plotted as a function of *Pf*EBA175 FL concentration and globally fitted to a steady-state 1:1 binding model to obtain an estimate of the K_D. **B)** To obtain estimates of kinetic parameters, the sensorgrams were globally fitted to two models, simple 1:1 binding and a more complex two-state reaction. The black lines represent experimental data and the red dotted lines, the fitted curves. **C)** Tables with equilibrium and kinetic parameters estimated for the *Pf*EBA175 FL- Glycophorin A interaction using the different models. For each model, the fit to the experimental data is indicated as the Chi^2 value (i.e. average squared residuals). The estimated values for the k_a, k_d and K_D are indicated with the standard error.

3.2.9 *Pf*EBA175 RII was produced in soluble form and its interaction with native Glycophorin A was probed.

The vast majority of the previous studies on the *Pf*EBA175-Glycophorin A interaction have been carried out using *Pf*EBA175 RII. In order to determine whether *Pf*EBA175 RII binds to native Glycophorin A with the same affinity as *Pf*EBA175 FL, the SPR experiment described in the previous section was repeated with *Pf*EBA175 RII.

In order to express *Pf*EBA175 RII, the segment of the coding sequence for this region of the extracellular domain was PCR-amplified from an expression construct of *Pf*EBA175 FL (Figure 23 A), digested with the restriction endonucleases NotI and AscI and then cloned into a NotI/AscI- digested expression vector that would enable it to be expressed with C-terminal Cd4 and hexa-His tags, as described in Section 2.1.1 (Figure 23 B).

After expression, *Pf*EBA175 RII was purified from the culture supernatant as described before for *Pf*EBA175 FL (Figure 23 C), analysed by SDS-PAGE (Figure 23 D) and subjected to gel filtration immediately prior to SPR (Figure 23 E). The expected elution volume of a monomer of *Pf*EBA175 RII (97.52 kDa) from the gel filtration column was 32 ml. The observed elution profile of the protein consisted of a single peak with the highest absorbance at 34.6 ml. A sample of the protein was subsequently sent for analysis by size exclusion chromatography-multi angle light scattering (SEC-MALS) and found to be present predominantly in the monomeric form with a small degree of self-association (data not shown, the analysis was performed by Dr. Steven Johnson, University of Oxford).

In the SPR experiment, a 2-fold dilution series of gel filtered-*Pf*EBA175 RII was injected across native Glycophorin A preparations (MM, MN and asialylated) immobilised on a streptavidin-coated sensor chip (Figure 23 F). The sets of binding curves obtained after reference subtraction

were first fitted globally to a steady-state 1:1 binding model to estimate the K_D, as described previously for *Pf*EBA175 FL (Figure 24 A). The values obtained for MM and MN types of Glycophorin A, (26.1 ± 1.6) x 10^{-7} M and (20.2 ± 1.6) x 10^{-7} M respectively, suggest not only that *Pf*EBA175 RII was binding to MN Glycophorin A with a higher affinity than to MM Glycophorin A, but also that the interaction of native Glycophorin A with *Pf*EBA175 RII is about 10-fold weaker than its binding to *Pf*EBA175 FL. As before the data sets were also fitted to two kinetic models, 1:1 binding and two-state reaction (Figure 24 B). The experimental data sets fitted more closely to the two-state reaction model than to the 1:1 binding model and the K_D values calculated from the k_a/k_d parameters deduced using the two state reaction model, were also closer to the K_D values estimated from the steady-state affinity analysis (Figure 24 C).

3.3 DISCUSSION

Since its first identification almost three decades ago (Camus and Hadley, 1985), the *P. falciparum* antigen, *Pf*EBA175 FL, has remained a subject of rigorous scientific investigation. Although not essential for the invasion of erythrocytes by *P. falciparum*, *Pf*EBA175 is postulated to play an important functional role in both sialic acid-dependent and -independent strains of *P. falciparum* (Duraisingh *et al*., 2003). Antibodies raised against *Pf*EBA175 inhibit erythrocyte entry by both types of strains (Narum *et al*., 2000) and deletion of *Pf*EBA175 leads to a change in the expression of other invasion ligands in sialic acid-dependent strains like W2mef as well as in those such as 3D7 which do not require sialic acid for invasion (Duraisingh *et al*., 2003; Lopaticki *et al*., 2011). The sialic acid-dependent interaction of native *Pf*EBA175 with Glycophorin A on the erythrocyte surface was identified from studies using enzymatically pre-treated erythrocytes as well as polymorphic erythrocytes lacking sialic acid on O-linked

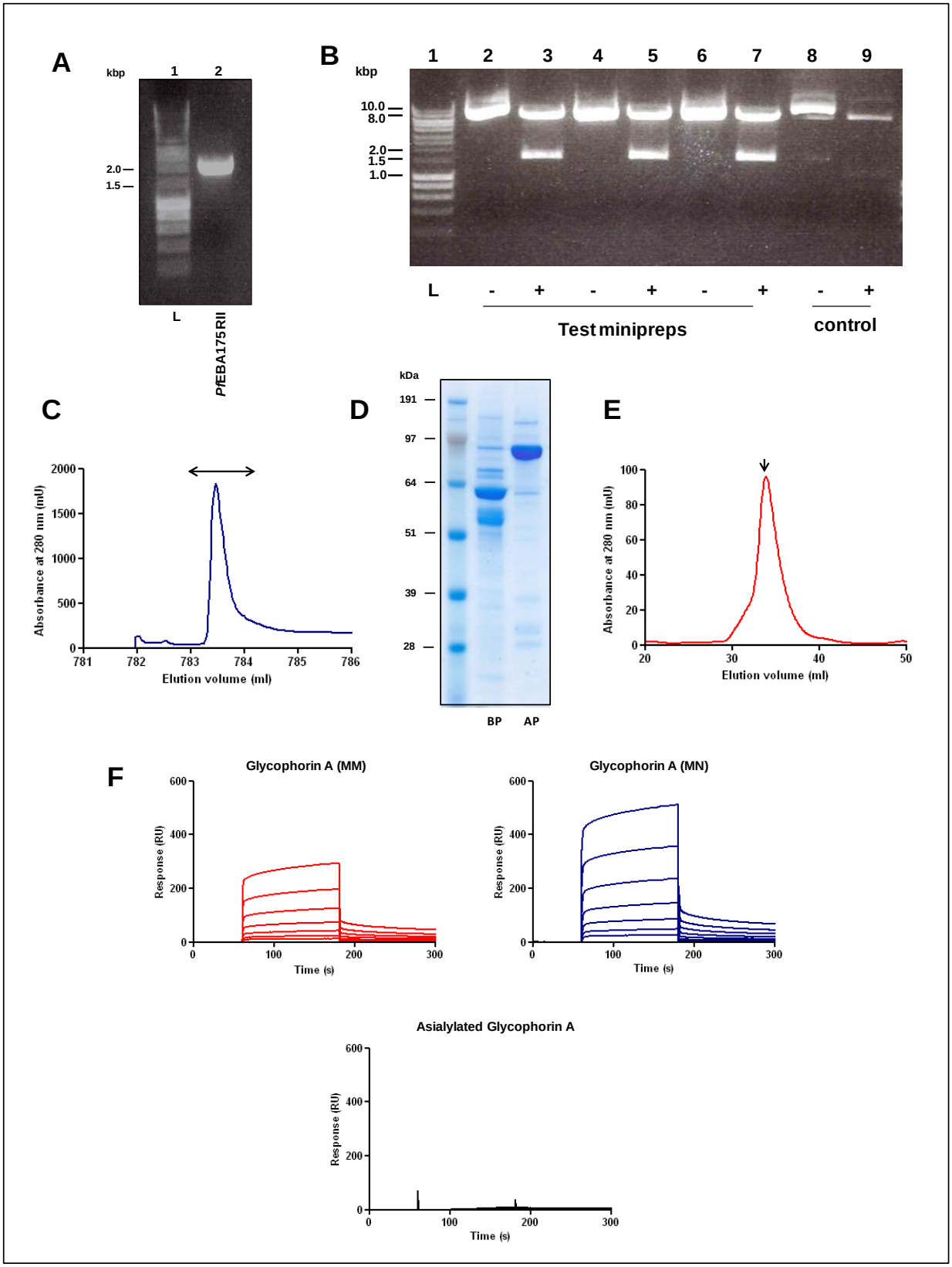
A
kbp
1
2
2.0
1.5
L
PfEBA175RII
B
kbp
1 2 3 4 5 6 7 8 9
10.0
8.0
2.0
1.5
1.0
L
- + - + - + - +
Test minipreps
control
C
Absorbance at 280 nm (mU)
2000
1500
1000
500
0
781 782 783 784 785 786
Elution volume (ml)
D
kDa
191
97
64
51
39
28
BP
AP
E
Absorbance at 280 nm (mU)
100
80
60
40
20
0
20 30 40 50
Elution volume (ml)
F
Glycophorin A (MM)
Response (RU)
600
400
200
0
0 100 200 300
Time (s)
Glycophorin A (MN)
Response (RU)
600
400
200
0
0 100 200 300
Time (s)
Asialylated Glycophorin A
Response (RU)
600
400
200
0
0 100 200 300
Time (s)

0

Figure 23. *Pf*EBA175 RII was expressed in soluble form and its binding to native human Glycophorin A was analysed by SPR. A) The region of the coding sequence for *Pf*EBA175 RII was amplified from an expression plasmid of *Pf*EBA175 FL by PCR. The expected length of the PCR product was 1.9 kbp. The PCR-amplified sequence was ligated into a vector (for expression with C-terminal Cd4 and hexa-His tags) using NotI and AscI restriction sites. **B)** After propagation in *E. coli*, the purified recombinant plasmids were tested for the presence of an insert of the expected size by digestion with NotI and AscI (+). Control reactions were set up with no enzymes (-). **C)** His-tagged *Pf*EAB175 RII was purified from the culture supernatant by affinity chromatography on a nickel-charged Sepharose column. The eluant from the column was monitored at 280 nm in real-time and the peak fractions containing protein (indicated by ⟷) were pooled. **D)** The affinity purified protein was analysed by SDS-PAGE and visualised using Coomassie brilliant blue. BP- before purification, AP- after purification. **E)** The elution profile of *Pf*EBA175 FL from gel filtration. The peak fraction at 34.6 ml is indicated by ↓. **F)** Reference subtracted sensorgrams from the injection of a 2-fold dilution series, ranging from 2.9-0.045 µM, of the main peak fraction of gel filtered-*Pf*EBA175 RII across biotinylated native Glycophorin A immobilised on a streptavidin-coated sensor chip. The binding to Glycophorin A (MM), Glycophorin A (MN) and asialylated Glycophorin A are shown in red, blue and black respectively. The biotinylated baits were immobilised at Cd4 (reference)-1000 RU , Glycophorin A (MM)-1267 RU, Glycophorin A (MN)-1070 RU and asialylated Glycophorin A-1170 RU. *Pf*EBA175 RII was injected at a flow rate of 20 µl/min, with a contact time of 120 s and a dissociation time of 200 s. At the end of each injection the sensor surface was regenerated with a pulse of 5 M NaCl.

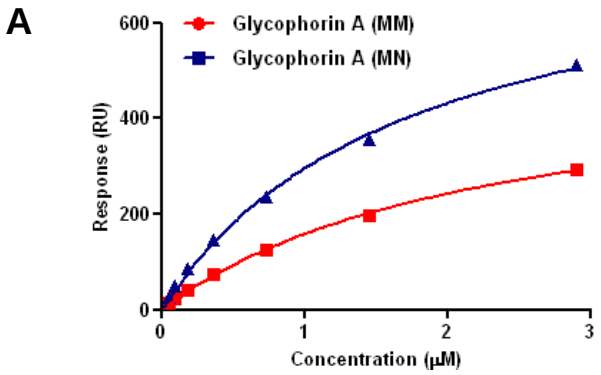

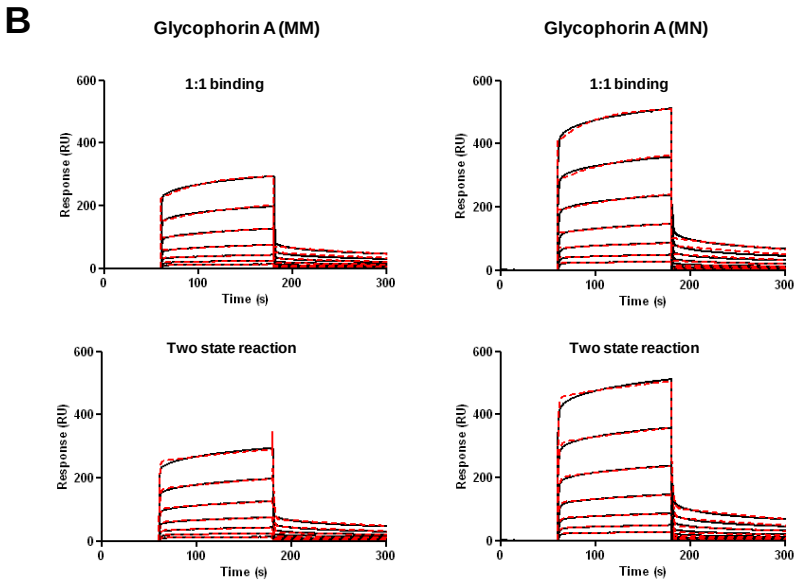

C

Glycophorin A (MM)				
Model	**Chi² (R^2)**	**k_a ($M^{-1}s^{-1}$)**	**k_d (s^{-1})**	**K_D (M)**
Steady-state affinity	5.9			$(26.1 \pm 1.6) \times 10^{-7}$
1:1 binding (kinetic)	25.2	6251 ± 170	$(3.58 \pm 0.09) \times 10^{-3}$	5.79×10^{-7}
Two state reaction (kinetic)	6.8	I $(7.7 \pm 0.6) \times 10^{5}$ II $(2.208 \pm 0.008) \times 10^{-3}$	I 2.7 ± 0.2 II $(3.10 \pm 0.02) \times 10^{-3}$	21.34×10^{-7}

Glycophorin A (MN)				
Model	**Chi² (R^2)**	**k_a ($M^{-1}s^{-1}$)**	**k_d (s^{-1})**	**K_D (M)**
Steady-state affinity	28.3			$(20.2 \pm 1.6) \times 10^{-7}$
1:1 binding (kinetic)	40.3	6203 ± 160	$(3.53 \pm 0.09) \times 10^{-3}$	5.49×10^{-7}
Two state reaction (kinetic)	17.5	I $(2.52 \pm 0.02)\ 10^{5}$ II $(2.216 \pm 0.009) \times 10^{-3}$	I 0.884 ± 0.005 II $(3.09 \pm 0.02) \times 10^{-3}$	10.81×10^{-7}

Figure 24. Equilibrium and kinetic parameters for the interaction of *Pf*EBA175 RII with native Glycophorin A were derived from the SPR data. The reference subtracted SPR sensorgrams from the binding of *Pf*EBA175 RII to MM and MN types of native Glycophorin A were subjected to equilibrium **(A)** and kinetic **(B)** analysis. **A)** For each set of sensorgrams the response at equilibrium was plotted as a function of *Pf*EBA175 RII concentration and globally fitted to a steady-state 1:1 binding model to obtain an estimate of the K_D. **B)** To obtain estimates of kinetic parameters, the sensorgrams were globally fitted to two models, simple 1:1 binding and a more complex two-state reaction. The black lines represent experimental data and the red dotted lines, the fitted curves. **C)** Tables with equilibrium and kinetic parameters estimated for the *Pf*EBA175 RII-Glycophorin A interaction using the different models. For each model, the fit to the experimental data is indicated as the Chi^2 value (i.e. average squared residuals). The estimated values for the k_a, k_d and K_D are indicated with the standard errors.

tetrasaccharides (T_n) or deficient in Glycophorin A expression (Ena^- , M^kM^k) (Camus and Hadley, 1985; Orlandi *et al*., 1992). Primarily due to the inability to express the large (175 kDa) full-length ectodomain of *Pf*EBA175 in soluble recombinant form using traditional methods, much of the detailed biochemical characterisation of the *Pf*EBA175-Glycophorin A interaction, has been performed using a truncated fragment of the *Pf*EBA175 extracellular domain, RII, which contains the tandem DBL domains essential for erythrocyte binding (Sim *et al*., 1994). The possible involvement of the extracellular regions of *Pf*EBA175 outside of RII in Glycophorin A binding and/or erythrocyte invasion has therefore not been investigated. To enable such a role/s to be identified, the expression of the full-length ectodomain of *Pf*EBA175 (*Pf*EBA175 FL) in a biochemically-amenable manner, is a pre-requisite. In this study, a soluble recombinant *Pf*EBA175 FL antigen, produced in mammalian HEK293E cells, was extensively characterised using biochemical methods, both to confirm its similarity to native *Pf*EBA175 in terms of function and to gain mechanistic insight into its interaction with Glycophorin A.

3.3.1 Recombinant *Pf*EBA175 FL is functionally similar to native *Pf*EBA175 isolated from parasite cultures.

The production of *Pf*EBA175 FL in recombinant form was facilitated by codon-optimisation of its coding sequence, for mammalian expression, by gene synthesis. *P. falciparum* proteins are not glycosylated in the parasite (Gowda & Davidson, 1999), therefore structural similarity of the recombinant protein to native *Pf*EBA175 was ensured by removal of the potential N-linked glycosylation sites during gene assembly. Secretion of the protein into the culture medium after transient expression was achieved by replacement of the endogenous signal peptide with a mammalian leader sequence. The recombinant *Pf*EBA175 FL protein was observed to be expressed in the full-length form (Figure 9 A). It was also recognised by three anti-*Pf*EBA175

monoclonals, two of which are known to bind heat-labile epitopes, suggesting that it was correctly-folded, at least in RII (Figures 9 C and D).

The binding of recombinant *Pf*EBA175 FL to human erythrocytes was then investigated using a quantitative, flow cytometry-based assay. Multimeric arrays of *Pf*EBA175 FL, generated by immobilisation on fluorescent beads, showed trypsin and neuraminidase-sensitive, but chymotrypsin-resistant association with human erythrocytes (Figures 10 and 11), suggesting a specific sialic-acid dependent interaction with Glycophorin A (a trypsin-sensitive but chymotrypsin-resistant erythrocyte receptor). In addition to the enzymatic pre-treatments of cells, the Glycophorin A-dependency of the interaction was further confirmed by pre-incubation of erythrocytes with an anti-Glycophorin A monoclonal (BRIC256), which significantly decreased the binding of *Pf*EBA175 FL (Figure 12). These results suggest that the recombinant *Pf*EBA175 FL is functionally similar to native *Pf*EBA175.

The binding of *Pf*EBA175 FL to commercially-available native Glycophorin A was then tested in an ELISA-based assay, to validate the biochemical activity of the recombinant protein independently. *Pf*EBA175 FL was observed to recognise native Glycophorin A but not an asialylated derivative, indicating specificity (Figure 14). The Glycophorin preparations used in this assay, were pre-characterised both for the presence of Glycophorin A (by staining with the anti-Glycophorin A monoclonal, BRIC256) and for the presence/absence of covalently-linked sialic acid (by testing the binding to three lectins of known glycan-binding specificity) (Figure 13). Glycans with terminal α-2,3 linked sialic acid (Neu5Ac) were predominant in the native Glycophorin A preparations, whereas the asialyalted protein mainly contained the T antigen, Gal (β-1,3) GalNAc (Figure 13 A).

3.3.2 The kinetic profile of the binding of *Pf*EBA175 FL to native Glycophorin A is consistent with the 'ligand-induced dimerisation model'.

The binding of *Pf*EBA175 FL to native Glycophorin A was then probed by SPR to gain insight into the mechanistic basis of the interaction. For this purpose, *Pf*EBA175 FL was expressed with a C-terminal hexa-His tag and purified from the cell culture supernatant by affinity chromatography. Analysis of the purified protein by denaturing SDS-PAGE confirmed the presence of the full-length form, but also revealed the presence of a number of shorter fragments (Figure 20 B). These fragments were present at a lower abundance than the full-length form and are likely to be products of proteolytic processing, as the cell culture medium was not supplemented with protease inhibitors during protein expression. Such additional fragments can also be seen on immunoblots of *P. falciparum* culture supernatants, performed using anti-*Pf*EBA175 monoclonals as probes, suggesting that some processing of the native *Pf*EBA175 also occurs, after release from the parasite surface (Orlandi *et al*., 1990).

Analysis of purified recombinant *Pf*EBA175 FL by gel filtration revealed the presence of both (potential) dimers/oligomers and monomers of the full-length protein (Figures 20 C and D). The monomeric fraction of *Pf*EBA175 FL showed higher binding to native Glycophorin A than the dimeric/oligomeric fraction when probed by SPR, and was thus used for the subsequent kinetic analysis (Figure 21). The reference subtracted SPR sensorgrams obtained from the binding of *Pf*EBA175 FL to native Glycophorin A were clearly biphasic, with both the association and dissociation of the soluble analyte consisting of a 'fast' stage followed by a 'slow' stage. Such behaviour is characteristic of an in interaction involving a conformational change in the binding partners and indeed the sensorgrams globally fitted to a 'two-state reaction' kinetic model far better than to a simple '1:1 binding' kinetic model (Figure 22 B and C). The K_D values calculated

from the 'two-state reaction' model were also in closer agreement with the K_D values estimated from the equilibrium analysis (Figure 22 C). This binding data is therefore, consistent with the proposed 'ligand-induced dimerisation' model for the binding of *Pf*EBA175 to Glycophorin A, which postulates that monomeric *Pf*EBA175 assembles into a dimer around the dimeric Glycophorin A receptor (Tolia *et al*., 2005, Section 3.1.2).

The 'biphasic' characteristic of the SPR sensorgrams could however also be a consequence of the presence of protein aggregates in the soluble analyte sample. Due care was taken to separate out the potentially monomeric fraction of full-length *Pf*EBA175 FL from the rest, prior to SPR. However, as gel filtration, the technique used for this purpose, has relatively low resolution, the presence of contaminant aggregates in the monomer fraction cannot be ruled out.

3.3.3 The affinity of *Pf*EBA175 FL for MN Glycophorin A is x 1.3-fold higher than that for MM Glycophorin A.

The binding of *Pf*EBA175 FL to native Glycophorin A isolated from both MM and MN types of human erythrocytes was analysed by SPR as described. The K_D values estimated (by equilibrium analysis) for the interactions with MM and MN Glycophorin A were ~ 0.28 µM and ~0.21 µM respectively, indicating a small (x 1.3-fold) but perhaps significant difference in the affinity of *Pf*EBA175 FL for the Glycophorin A variants (Figure 22). The M variant of Glycophorin A differs from the N variant at two amino acid residues. M is proposed to be ancestral to N in comparison with chimpanzee and orangutan sequences and has serine and glycine at positions 1 and 5 respectively (Ko *et al*., 2011). N on the other hand is characterised by leucine and glutamic acid at these positions. The non-synonomous single nucleotide polymorphisms (SNPs) that give rise to the M and N genotypes are located within the exon 2 of the Glycophorin A gene, GYPA. Interestingly, a recent comparative study of more than 200 GYPA sequences from

ethnically and geographically diverse African populations identified that polymorphisms in exon 2 are under significant balancing selection in individuals in malaria hyper-endemic regions (Ko *et al*., 2011). This finding suggests that the extracellular region of Glycophorin A encoded by exon 2, (containing amino acids 1-25), may play an important role in *P. falciparum* infection. From the observed difference in the affinity of *Pf*EBA175 FL for MM and MN Glycophorin A, it could be postulated that this region of Glycophorin A is directly involved in *Pf*EBA175 FL binding. It further suggests that even polymorphisms in residues that are not sialylated, in this Glycophorin A region, can influence its interaction with *Pf*EBA175 FL. This is consistent with the early observation that *Pf*EBA175 recognition of Glycophorin A is dependent on both the presence of sialic acid and also the sequence of the peptide backbone (Sim *et al*., 1994).

3.3.4 *Pf*EBA175 FL binds to native Glycophorin A with a ~10-fold higher affinity than *Pf*EBA175 RII.

To investigate the binding of *Pf*EBA175 RII to native Glycophorin A, this region of the *Pf*EBA175 extracellular domain was also expressed recombinantly in this study using the mammalian expression system. Denaturing SDS-PAGE analysis of recombinant *Pf*EBA175 RII, after purification of the protein from the culture supernatant by affinity chromatography, revealed that it was expressed at the expected size (Figure 23 D). The protein was found to be primarily monomeric by gel filtration (Figure 23 E). The reference-subtracted sensorgrams obtained by analysing the interaction between *Pf*EBA175 RII and native Glycophorin A, by SPR, were also ‘biphasic’ (Figure 23 F). These sensorgrams thus fitted more closely to a ‘two-state reaction’ kinetic model than to a ‘1:1 binding’ kinetic model, as seen with *Pf*EBA175 FL (Figure 24 B). The data for *Pf*EBA175 RII recognition of Glycophorin A is hence, also consistent with the ‘ligand-induced dimerisation’ model proposed for this interaction.

The K_D values estimated (by equilibrium analysis) for the binding of *Pf*EBA175 RII to MM and MN types of native Glycophorin A were ~2.6 µM and ~2.0 µM respectively, again indicating a x 1.3-fold difference in the affinity of *Pf*EBA175 for the Glycophorin A variants (Figure 24 C). These values also show that the affinity of *Pf*EBA175 RII for native Glycophorin A is ~x 10-fold lower than that of *Pf*EBA175 FL. This may be due to some role played by extracellular regions of *Pf*EBA175 outside of RII to facilitate binding to the erythrocyte receptor and suggests that *Pf*EBA175 FL may be a better vaccine antigen than RII alone.

3.3.5 Functional activity of the extracellular domain of Glycophorin A may be dependent on factors other than sialylation.

To potentially map the *Pf*EBA175 binding site on Glycophorin A, the full-length ectodomain of human Glycophorin A was recombinantly expressed in this study. The recombinant protein was observed to be soluble, glycosylated and immunologically active (Figure 15 A and C). Probing the glycan composition of recombinant Glycophorin A using lectins of known specificity, revealed that it was however under-sialylated in comparison to the native protein (Figure 15 E). Analysis by both AVEXIS and SPR, indicated no recognition of recombinant Glycophorin A by *Pf*EBA175 FL, indicating that the former is non-functional (Figures 16 and 17 E). Co-expression of Glycophorin A with sialyltransferases and a sialic acid transporter increased its level of sialylation (Figure 17 B), but did not confer binding to *Pf*EBA175 FL (data not shown). The lack of any detectable binding of recombinant Glycophorin A to *Pf*EBA175 FL, despite the presence of some α-2,3-linked sialic acid suggests that the activity of the former is perhaps dependent on one/more unknown factor/s in addition to sialylation. For instance, several lines of evidence point to a close association between native Glycophorin A and Band 3 during biosynthesis in erythrocytes (Hassoun *et al*., 1998; Auffray, 2001). Indeed, in Band 3-null mice erythrocytes,

Glycophorin A has been observed to be rapidly degraded in the cytoplasm (Hassoun *et al*., 1998). This has led to the suggestion that Band 3 may perform a chaperone-like role for Glycophorin A. Therefore, it is possible that when the extracellular domain of Glycophorin A is recombinantly-expressed in the absence of Band 3, its conformation deviates from that of the native protein, resulting in inactivity.

3.4 CONCLUSION

In this study, the full-length ectodomain of *P. falciparum* EBA175 (*Pf*EBA175 FL) was expressed in soluble recombinant form using a mammalian expression system and confirmed to be functionally similar to native *P. falciparum* EBA175 from parasite cultures. The recombinantly-expressed protein was shown to bind to native Glycophorin A from MN erythrocytes with a x 1.3-fold higher affinity than to that from MM erythrocytes. Whether this difference in the affinity for M and N Glycophorin A variants would directly influence the efficiency of erythrocyte invasion by *P. falciparum* is not known and should be investigated. Recombinant *Pf*EBA175 FL was also observed to bind native Glycophorin A with a ~10-fold higher affinity than *Pf*EBA175 RII, suggesting some role played by the extracellular regions outside of RII to facilitate binding. *Pf*EBA175 FL could also potentially be a better vaccine candidate than *Pf*EBA175 RII. *Pf*EBA175 FL may be more immunogenic than *Pf*EBA175 RII, due to its larger size and antibodies raised against the different regions of the *Pf*EBA175 FL extracellular domain may act in a synergistic manner to inhibit erythrocyte invasion. Polyclonal antibodies should therefore be raised against each of these antigens and directly compared for inhibition of erythrocyte entry by *P. falciparum*.

3.5 BIBLIOGRAPHY

Adams, J. H., Sim, B. K., Dolan, S. A., Fang, X., Kaslow, D. C. & Miller, L. H. (1992). A family of erythrocyte binding proteins of malaria parasites. *Proceedings of the National Academy of Sciences of the United States of America*, *89*(15), 7085-9.

Auffray, I. (2001). Glycophorin A dimerization and band 3 interaction during erythroid membrane biogenesis: *in vivo* studies in human glycophorin A transgenic mice. *Blood*, *97*(9), 2872-2878.

Batchelor, J. D., Zahm, J. A. & Tolia, N. H. (2012). Dimerisation of *Plasmodium vivax* DBP is induced upon receptor binding and drives recognition of DARC. *Nature Structural Molecular Biology*, *18*(3), 908-914.

Bharara, R., Singh, S., Pattnaik, P., Chitnis, C. E., & Sharma, A. (2004). Structural analogs of sialic acid interfere with the binding of erythrocyte binding antigen-175 to glycophorin A, an interaction crucial for erythrocyte invasion by *Plasmodium falciparum*. *Molecular and Biochemical Parasitology*, *138*(1), 123-9.

Camus, D., & Hadley, T. J. (1985). A *Plasmodium falciparum* antigen that binds to host erythrocytes and merozoites. *Science*, *230*(4725), 553-556.

Chasis JA and Mohandas N. (1992). Red blood cell glycophorins. *Blood*, *80*, 1869-1879.

Chitlaru, T., Kronman, C., Zeevi, M., Kam, M., Harel, A., Ordentlich, A., Velan, B., *et al*. (1998). Modulation of circulatory residence of recombinant acetylcholinesterase through biochemical or genetic manipulation of sialylation levels. *The Biochemical Journal*, *336*, 647-58.

Duraisingh, M. T., Maier, A. G., Triglia, T., & Cowman, A. F. (2003). Erythrocyte-binding antigen 175 mediates invasion in *Plasmodium falciparum* utilizing sialic acid-dependent and -independent pathways. *Proceedings of the National Academy of Sciences of the United States of America*, *100*(8), 4796-801.

El Sahly, H. M., Patel, S. M., Atmar, R. L., Lanford, T. a, Dube, T., Thompson, D., Sim, B. K. L., *et al*. (2010). Safety and immunogenicity of a recombinant nonglycosylated erythrocyte binding antigen 175 Region II malaria vaccine in healthy adults living in an area where malaria is not endemic. *Clinical and Vaccine Immunology*, *17*(10), 1552-9.

Gowda, D. C., & Davidson, E. A. (1999). Protein glycosylation in the malaria parasite. *Parasitology Today (Personal ed.)*, *15*(4), 147-52.

Gu, X., & Wang, D. I. (1998). Improvement of interferon-gamma sialylation in Chinese hamster ovary cell culture by feeding of N-acetylmannosamine. *Biotechnology and Bioengineering, 58*(6), 642-8.

Hassoun, H., Hanada, T., Lutchman, M., Sahr, K. E., Palek, J., Hanspal, M., & Chishti, A. H. (1998). Complete deficiency of glycophorin A in red blood cells from mice with targeted inactivation of the band 3 (AE1) gene. *Blood, 91*(6), 2146-51.

Hossler, P., Khattak, S. F., & Li, Z. J. (2009). Optimal and consistent protein glycosylation in mammalian cell culture. *Glycobiology, 19*(9), 936-49.

Jiang, L., Gaur, D., Mu, J., Zhou, H., Long, C. A., & Miller, L. H. (2011). Evidence for erythrocyte-binding antigen 175 as a component of a ligand-blocking blood-stage malaria vaccine. *Proceedings of the National Academy of Sciences of the United States of America, 108*(18), 7553-8.

Ko, W.-Y., Kaercher, K. A., Giombini, E., Marcatili, P., Froment, A., Ibrahim, M., Lema, G., *et al*. (2011). Effects of natural selection and gene conversion on the evolution of human glycophorins coding for MNS blood polymorphisms in malaria-endemic African populations. *American Journal of Human Genetics, 88*(6), 741-54.

Lopaticki, S., Maier, A. G., Thompson, J., Wilson, D. W., Tham, W.-H., Triglia, T., Gout, A., *et al*. (2011). Reticulocyte and erythrocyte binding-like proteins function cooperatively in invasion of human erythrocytes by malaria parasites. *Infection and Immunity, 79*(3), 1107-17.

Mackenzie, K. R., Prestegard, J. H., & Engelman, D. M. (1997). A Transmembrane Helix Dimer: Structure and Implications. *Science, 276*(5309), 131-133.

Narum, D. L., Haynes, J. D., Fuhrmann, S., Liang, H., Hoffman, S. L., Sim, B. K. L., Moch, K., *et al*. (2000). Antibodies against the *Plasmodium falciparum* receptor binding domain of EBA-175 block invasion pathways that do not involve sialic acids. *Infection and Immunity, 68*(4), 1964-6.

Ockenhouse, C. F., Barbosa, A., Blackall, D. P., Murphy, C. I., Kashala, O., Dutta, S., Lanar, D. E., *et al*. (2001). Sialic acid-dependent binding of baculovirus-expressed recombinant antigens from *Plasmodium falciparum* EBA-175 to Glycophorin A. *Molecular and Biochemical Parasitology, 113*(1), 9-21.

Orlandi, P. A., Klotz, F. W., Haynes, J. D., & Reed, W. (1992). A malaria invasion receptor, the 175-kilodalton erythrocyte binding antigen of *Plasmodium falciparum* recognizes the terminal Neu5Ac (alpha 2-3) Gal- sequences of glycophorin A. *The Journal of Cell Biology, 116*(4), 901-9.

Orlandi, P., Sim, B. K. L., & Chulay, J. (1990). Characterization of the 175-kilodalton erythrocyte binding antigen of *Plasmodium falciparum*. *Molecular and Biochemical Parasitology, 40*, 285-294.

O'Donnell, R. A., Hackett, F., Howell, S. A., Treeck, M., Struck, N., Krnajski, Z., Withers-Martinez, C., *et al*. (2006). Intramembrane proteolysis mediates shedding of a key adhesin during erythrocyte invasion by the malaria parasite. *The Journal of Cell Biology, 174*(7), 1023-33.

Pandey, K. C., Singh, S., Pattnaik, P., Pillai, C. R., Pillai, U., Lynn, A., Jain, S. K., *et al*. (2002). Bacterially expressed and refolded receptor binding domain of *Plasmodium falciparum* EBA-175 elicits invasion inhibitory antibodies. *Molecular and Biochemical Parasitology, 123*(1), 23-33.

Sim, A. B. K. L., Chitnis, C. E., Wasniowska, K., Hadley, T. J., & Miller, L. H. (1994). Receptor and ligand domains for invasion of erythrocytes by *Plasmodium falciparum*. *Science, 264*(5167), 1941-1944.

Sim, B. K. L., Narum, D. L., Chattopadhyay, R., Ahumada, A., Haynes, J. D., Fuhrmann, S. R., Wingard, J. N., *et al*. (2011). Delineation of stage specific expression of *Plasmodium falciparum* EBA-175 by biologically functional region II monoclonal antibodies. *PloS One, 6*(4), e18393.

Tolia, N. H., Enemark, E. J., Sim, B. K. L., & Joshua-Tor, L. (2005). Structural basis for the EBA-175 erythrocyte invasion pathway of the malaria parasite *Plasmodium falciparum*. *Cell, 122*(2), 183-93.

Tomita, M., & Marchesi, V. T. (1975). Amino-acid sequence and oligosaccharide attachment sites of human erythrocyte glycophorin. *Proceedings of the National Academy of Sciences, 72*(8), 2964-68.

van der Merwe, A.P. (2011) Surface Plasmon Resonance in Protein-Ligand interactions: hydrodynamics and calorimetry, edited by S Harding and P Z Chowdhry. *Practical Approach Series, Oxford University Press*, 137-170.

Weikert, S., Papac, D., Briggs, J., Cowfer, D., Tom, S., Gawlitzek, M., Lofgren, J., *et al*. (1999). Engineering Chinese hamster ovary cells to maximize sialic acid content of recombinant glycoproteins. *Nature Biotechnology, 17*(11), 1116-21.

Withers-Martinez, C., Haire, L. F., Hackett, F., Walker, P. A, Howell, S. A, Smerdon, S. J., Dodson, G. G., *et al*. (2008). Malarial EBA-175 region VI crystallographic structure reveals a KIX-like binding interface. *Journal of Molecular Biology, 375*(3), 773-81.

Wong, N. S. C., Yap, M. G. S., & Wang, D. I. C. (2006). Enhancing Recombinant Glycoprotein Sialylation Through CMP-Sialic Acid Transporter Over Expression in Chinese Hamster Ovary Cells. *Biotechnology and Bioengineering*, *93*(5), 1005-16.

Zhang, D., & Pan, W. (2005). Evaluation of three *Pichia pastoris*-expressed *Plasmodium falciparum* merozoite proteins as a combination vaccine against infection with blood-stage parasites. *Infection and Immunity*, *73*(10), 6530-36.

Chapter 4

Investigating the host-specificity of *Plasmodium* merozoite: primate erythrocyte interactions in the *Laverania* family

4.1 INTRODUCTION

4.1.1 The *Laverania* family of great ape parasites are host-specific.

P. falciparum is relatively divergent from the other species of *Plasmodium* that routinely infect humans; *P. vivax, P. malariae* and *P. ovale* (Liu *et al*., 2010; Prugnolle *et al*., 2011; Sharp *et al*., 2011). As outlined in the General Introduction (Chapter 1, Section 1.3), its closest relatives are found amongst a family of great ape parasites called *Laverania* which consists of six well-defined and closely related clades that appear to be strictly host-specific (Liu *et al*., 2010; Rayner *et al*., 2011). The clades *P. reichenowi* (C1), *P. gaboni* (C2) and *P. billcollinsi* (C3) have been found only in chimpanzees, whereas the *P. praefalciparum* (G1), *P. adleri* (G2) and *P. blacklocki* (G3) lineages appear to be restricted to gorillas. Within the *Laverania* family, *P. falciparum* is genetically most similar to *P. praefalciparum*; in fact *P. falciparum* mitochondrial DNA sequences form a single narrow group within the much broader spectrum of the *P. praefalciparum* sequences in phylogenetic trees. *P. falciparum* is therefore currently believed to have been derived from *P. praefalciparum* by means of a single cross-species transmission event from gorilla to human, dated to have occurred approximately 1 million-112,000 years ago (Liu *et al.,* 2010; Rayner *et al.,* 2011). The postulated gorilla-origin of *P. falciparum* and the continued presence of *P. falciparum*-like parasites in great apes pose two important questions with serious implications for global malaria eradication;

1. Are great apes a potential reservoir for *P. falciparum*?

2. Are the current *Laverania* strains harboured by great apes a possible source for future human infections?

Whether *P. falciparum* can successfully infect great ape species other than humans is a matter of debate. Although it has not yet been detected in wild living chimpanzees or gorillas, *P.*

falciparum has been identified in chimpanzees held in captivity close to human populations, suggesting that they are susceptible to anthroponosis of human-derived *P. falciparum* (Duval *et al.*, 2010). However, it has been shown that under experimental conditions even splenectomised chimpanzees show only low to moderate parasitemia when transfused with *P. falciparum* infected human blood and do not develop severe 'malignant tertian malaria' observed in human patients (Martin *et al.*, 2005). Conversely, from the evidence to date, *P. falciparum* appears to be the only *Laverania* species capable of infecting humans. Attempts to infect humans with *P. reichenowi* using parasitized chimpanzee blood in the 1920s-30s were unsuccessful (Blacklock & Adler, 1922; Martin *et al.*, 2005). Exactly which *Plasmodium* species were used in these experiments is unclear, as species distinctions were based on morphological analyses at the time, so it is possible that other chimpanzee *Laverania* parasites, in addition to *P. reichenowi*, were also used. There are, however, no recorded attempts of gorilla-derived material being used for experimental human infection and due to their ethically dubious nature, such studies can never be repeated. Systematic molecular-based approaches will, therefore, be required, in order to understand whether *Laverania* parasites are restricted to a specific host in the natural environment and identify what would enable them to cross species barriers and adapt to a new host (Duval & Ariey, 2012).

4.1.2 The molecular basis of the *Laverania* host-specificity is poorly understood.

The molecular mechanisms that impose host-specificity must act at the vector-host and/or parasite-host interface of the *Plasmodium* life cycle (Rayner *et al.*, 2011). Chimpanzees and gorillas harbour different *Laverania* species even when occupying the same geographical location and as *Anopheles* mosquitoes are not known to discriminate between these great apes, the host specificity of the *Laverania* clades is likely to be due to incompatibility at the parasite-

host interface (Rayner *et al.*, 2011). Mosquito preferences, however, cannot be ruled out and remains an important line of inquiry.

As the blood-stage of these parasites is crucial for maintaining a sustained infection within the primate host and for host-to-vector transmission (via the formation of gametocytes), the invasion of erythrocytes by the parasites has gained particular attention as a possible point of host-selection.

Of the numerous interactions between parasite and host cell surface proteins that mediate erythrocyte invasion, the EBA175-Glycophorin A interaction has been hypothesised to be one responsible for differences in host-selectivity between *Laverania* parasites (Chapter 3). *P. falciparum* EBA175 (*Pf*EBA175) and *P. reichenowi* EBA175 (*Pr*EBA175) have been observed to discriminate between human and chimpanzee erythrocytes when expressed as RII fragments on the surface of COS cells (Martin *et al.*, 2005). This has been attributed to the difference in the sialic acid composition of human and chimpanzee erythrocytes due to the absence in expression of the CMAH gene in humans (Martin *et al.*, 2005). The CMAH gene encodes an enzyme required for conversion of the Neu5Ac form of sialic acid to Neu5Gc, therefore human erythrocytes carry only Neu5Ac, whereas chimpanzee erythrocytes contain a mixture of the two, with Neu5Gc being predominant (Muchmore *et al.,* 1998). However, this sialic acid hypothesis does not explain the host-specificities of the *Laverania* family in general as chimpanzees and gorillas both carry active CMAH genes (Muchmore *et al.,* 1998).

4.1.3 The RH5-Basigin interaction as a possible determinant of host-specificity

The interaction of RH5 with its host receptor, Basigin (BSG), is essential for the invasion of human erythrocytes by *P. falciparum*, unlike the EBA175-Glycophorin A interaction which is only essential in some strains (Chapter 1, Section 1.7, Crosnier *et al.,* 2011). The contribution of

the RH5-BSG interaction towards determining host species-selectivity in the *Laverania* family has not been addressed before, but a previous study investigating the ability of different *P. falciparum* strains to invade erythrocytes of the new world monkey, *Aotus nancymaae*, suggested that polymorphisms in RH5 can influence the establishment/crossing of host-species barriers, in at least this instance (Hayton *et al.*, 2008). The hypothesis that the RH5-BSG interaction plays a similar role in the context of the *Laverania* family is therefore worth investigating.

4.1.4 Work described in this chapter

The molecular basis for the observed host-specificity within the *Laverania* family has previously not been investigated in a systematic manner. In this study, the potential contribution of two important parasite ligand-host receptor interactions, EBA175-Glycophorin A and RH5-BSG, towards the determination of host-specificity in *Laverania* was investigated. EBA175 RII orthologues from three *Laverania* species, namely the human parasite *P. falciparum* and two chimpanzee parasites *P. reichenowi* and *P. billcollinsi*, were expressed recombinantly and tested for specific binding to both human erythrocytes and purified native human Glycophorin A. RH5 orthologues from *P. falciparum* and *P. reichenowi* were also expressed and their interactions with human erythrocytes and recombinant BSG orthologues from three primates; human, chimpanzee (*Pan troglodytes*) and gorilla (*Gorilla gorilla*), were analysed. Site-directed mutants of human and chimpanzee BSG proteins were then generated and tested against *P. falciparum* RH5 to identify residues that confer species-selectivity.

4.2 RESULTS

4.2.1 EBA175 RII orthologues from three *Laverania* species were expressed and immunologically characterised.

The *P. falciparum* (3D7 strain) and *P. reichenowi* EBA175 sequences are publicly available (Ozwara *et al*., 2001; Gardner *et al*., 2002). The coding sequences of EBA175 orthologues from other *Laverania* species have now been derived by PCR-based sequencing of parasite genetic material, recovered from the fecal samples of wild-living chimpanzees in sub-Saharan Africa, by collaborators at the University of Pennsylvania, USA. The complete coding sequence for RII of the EBA175 ectodomain was obtained only for the chimpanzee parasite, *P. billcollinsi* (Weimin Liu and Beatrice Hahn, unpublished data). The EBA175 RII orthologues of *P. falciparum* (*Pf*EBA175 RII), *P. reichenowi* (*Pr*EBA175 RII) and *P. billcollinsi* (*Pb*EBA175 RII) exhibit a high degree of similarity (~ 80%) at the amino acid level (Figure 25).

In this study, these EBA175 RII orthologues were produced in soluble recombinant form to investigate their ability to interact with human erythrocytes and purified native human Glycophorin A. The coding sequences for *Pf*EBA175 RII and *Pr*EBA175 RII were PCR-amplified from expression constructs of their respective full-length ectodomains, *Pf*EBA175 FL (protein accession number: Q8IBE8) and *Pr*EBA175 FL (Q9N9G9) as described in section 2.1.1.1. The coding sequence for *Pb*EBA175 RII was assembled by gene synthesis for this study. The proteins were expressed in the human HEK293E cell line, with a mammalian signal peptide to ensure secretion into the culture medium.

The EBA175 RII orthologues produced with C-terminal Cd4 and biotin tags, were confirmed to be expressed at the expected size of ~ 97 kDa, by Western blotting (Figure 26 A). To determine whether they were correctly folded, their recognition by the two mouse monoclonals, R217 and

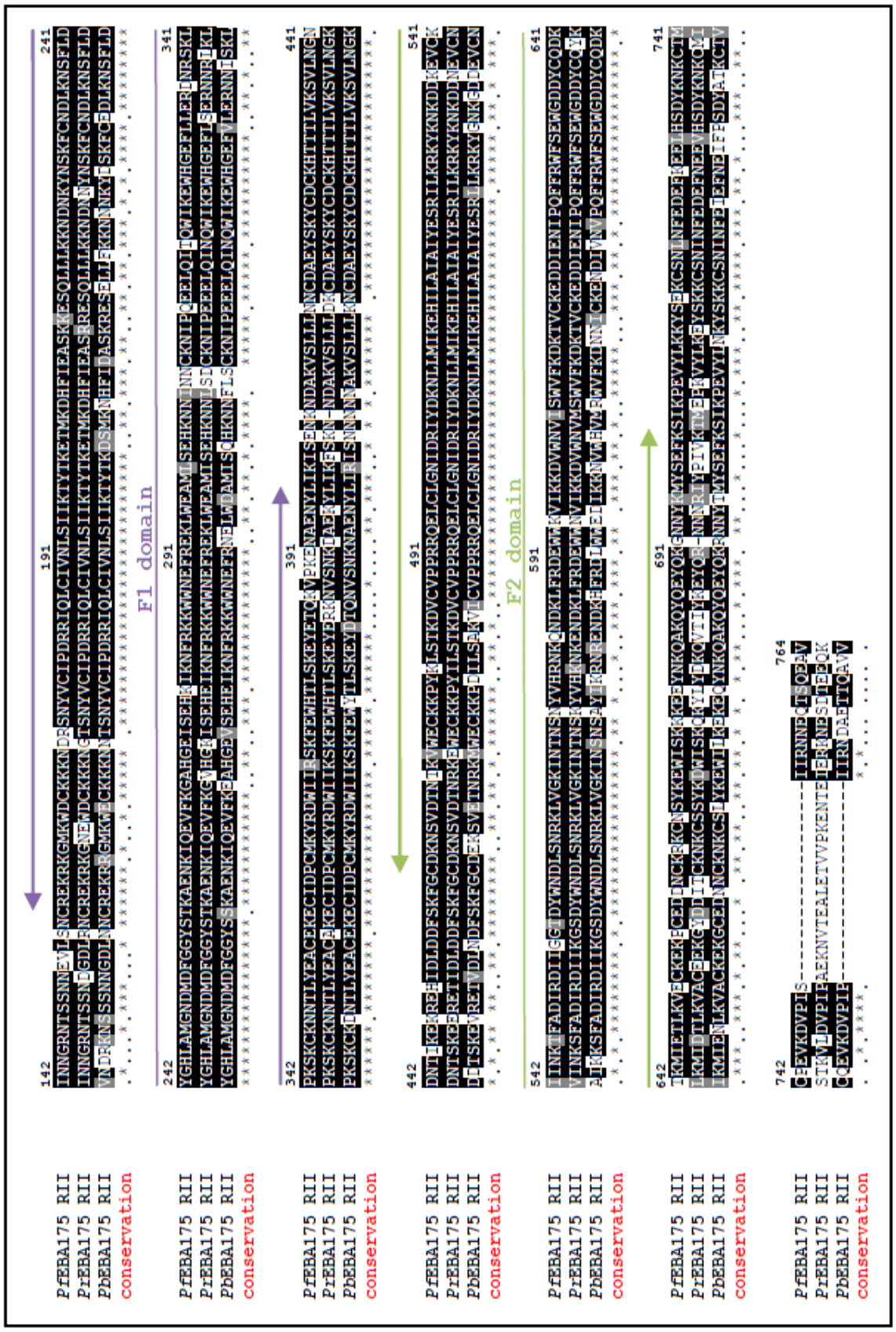
F1 domain
F2 domain
PfEBA175 RII
PrEBA175 RII
PbEBA175 RII
conservation

Figure 25. Sequence alignment of EBA175 RII orthologues from three species of *Laverania*. The amino acid sequences of RII of EBA175 from *P. falciparum* (*Pf*EBA175 RII), *P. reichenowi* (*Pr*EBA175 RII) and *P. billcollinsi* (*Pb*EBA175 RII) are shown. Conserved residues are shaded in black and semi-conserved residues in grey. The numbering indicated is for *Pf*EBA175 RII. The two DBL domains, F1 (aa 462-710) and F2 (aa 159-396) are marked in purple and green respectively. Sequences: *Pf*EBA175 RII (protein accession number Q8IBE8, aa 142-764), *Pr*EBA175 RII (Q9N9G9, aa 131-770). The *Pb*EBA175 RII sequence was obtained from Weimin Liu and Beatrice Hahn at the University of Washington, USA. The sequences were aligned using ClustalW software (Larkin *et al*., 2007).

R218, was tested by ELISA as performed before for *Pf*EBA175 FL (Section 3.2.1). R217 and R218, raised against a baculovirus-expressed *Pf*EBA175 RII antigen, have previously been characterised to bind non-linear, heat-labile epitopes within the F2 and F1 domains of RII respectively (Sim *et al*., 2011). All three EBA175 RII orthologues were recognised by R218, but R217 only appeared to bind to *Pf*EBA175 RII and *Pr*EBA175 RII (Figure 26 B), suggesting that it recognises a region that is divergent in *Pb*EBA175 RII.

4.2.2 All three EBA175 RII orthologues showed specific binding to human erythrocytes.

The binding of EBA175 RII orthologues to human erythrocytes was analysed using the fluorescent bead-based flow cytometry approach developed for the functional characterisation of *Pf*EBA175 FL (Chapter 3, Section 3.2.2).

Multivalent arrays of EBA175 RII orthologues were generated by direct immobilisation of the biotinylated proteins on streptavidin-coated Nile red beads. The minimum amount of each protein necessary for complete saturation of a set number of beads was determined by ELISA, as described before (Section 3.2.2, Figure 27 A). The protein-coated beads were then presented to human erythrocytes, which were either untreated or pre-treated with one of three enzymes: trypsin, chymotrypsin or neuraminidase. Binding of the fluorescently-labelled protein arrays to the erythrocytes was analysed by flow cytometry. Cd4-coated beads were used as a negative control in the assay. Enzymatic treatment of erythrocytes was used as a means of probing the specificity of any observed association of EBA175 RII-coated beads with erythrocytes. The EBA175-Glycophorin A interaction is known to be sensitive to treatment with trypsin and neuraminidase, but not chymotrypsin (Camus and Hadley, 1985).

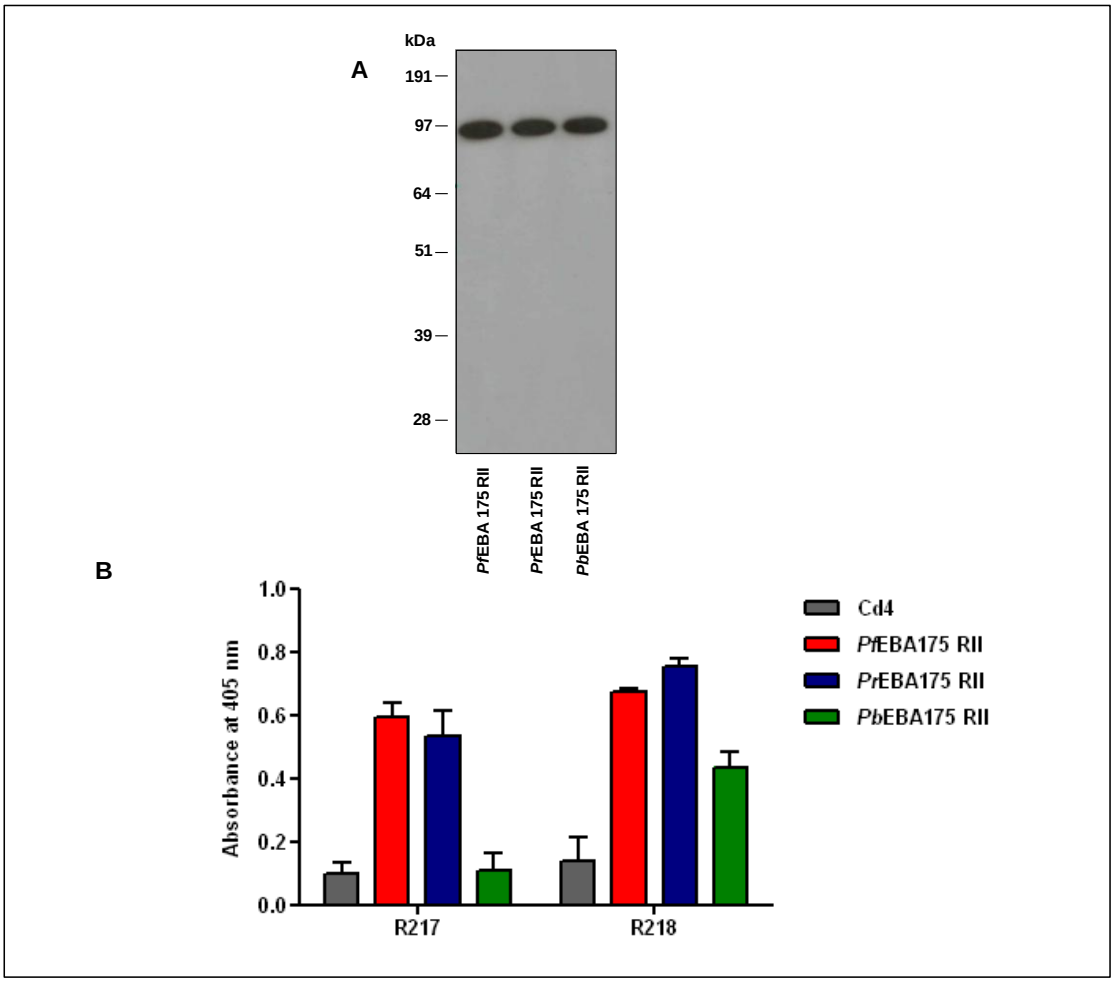

Figure 26. The EBA175 RII orthologues were expressed at the expected size of ~97 kDa and recognised by antibodies with conformation-specific epitopes. *Pf*EBA175 RII, *Pr*EBA175 RII and *Pb*EBA175 RII were expressed in the soluble form with C-terminal Cd4 and biotin tags using the HEK293E expression system. **A)** A Western blot of the EBA175 RII orthologues (~ 97 kDa) performed using HRP-conjugated extravidin as the probe. **B)** Recognition of the EBA175 RII orthologues by two mouse monoclonals, R217 and R218, which have been raised against a baculovirus-derived *Pf*EBA175 RII antigen and bind to non-linear epitopes. Binding of these monoclonals was detected by ELISA. Cd4 was used as the negative control in the assays. All ELISAs were performed on streptavidin-coated plates, using an alkaline phosphatase-conjugated anti-mouse antibody as the secondary. Alkaline phosphatase activity was quantified by the turnover of the colourimetric substrate, *p*-nitrophenyl phosphate, measured as an increase in absorbance at 405 nm. The graphically presented data indicate mean ± standard deviation; *n*=3.

A significant degree of self-association was observed with the EBA175 RII-coated beads and when evaluating the flow cytometry data, these aggregates were eliminated by gating on the erythrocyte population (Figure 27 B). The percentage of erythrocytes in each gated population that were binding to EBA175 RII-coated beads was calculated based on a fluorescence intensity threshold, set for selecting cells with a higher fluorescence at the Nile red emission wavelength than those incubated with Cd4-coated beads (Figure 28 A).

All three of the EBA175 orthologues showed clear and comparable binding to untreated and chymotrypsin-treated erythrocytes. Between 80-90% of erythrocytes in each of these populations were observed to interact with the EBA175 RII-coated beads (Figure 28 B and C). In comparison, only 1-4% of trypsin and neuraminidase-treated erythrocytes showed any binding to EBA175 RII-coated beads, suggesting almost no interaction of EBA175 RII orthologues with such cells.

4.2.3 Purified native human Glycophorin A was recognised by all three EBA175 RII orthologues in a sialic acid-dependent manner.

The binding of the EBA175 RII orthologues to commercially-available native Glycophorin A, (purified from human erythrocytes), was also directly compared using the ELISA-based approach developed for the characterisation of *Pf*EBA175 FL (Chapter 3, Section 3.2.3). An asialylated derivative of Glycophorin A was included in this assay as a negative control.

The Glycophorin A preparations were biotinylated *in vitro* (for immobilisation on streptavidin-coated plates) and quantified relative to each other by ELISA, prior to being tested against EBA175 RII (Figure 29 A). The EBA175 RII orthologues, expressed as β lactamase-tagged pentamers, were also normalised against each other by monitoring their enzymatic activity in a

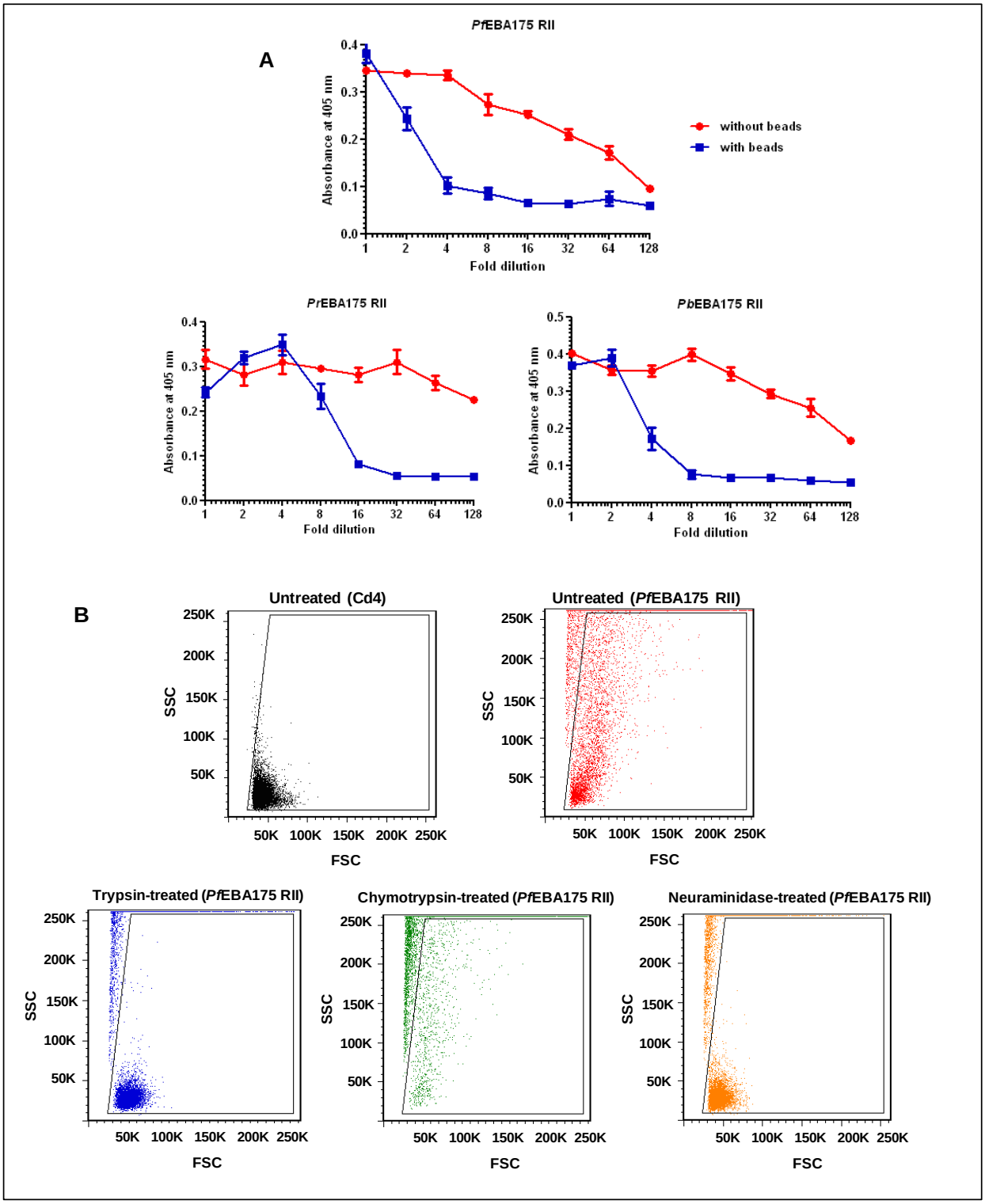
A
PfEBA175 RII
Absorbance at 405 nm
Fold dilution
without beads
with beads
PrEBA175 RII
PbEBA175 RII
B
Untreated (Cd4)
Untreated (PfEBA175 RII)
Trypsin-treated (PfEBA175 RII)
Chymotrypsin-treated (PfEBA175 RII)
Neuraminidase-treated (PfEBA175 RII)
SSC
FSC
50K
100K
150K
200K
250K

Figure 27. The EBA175 RII orthologues, multimerised on fluorescent beads, were presented to erythrocytes and analysed by flow cytometry. To monitor the binding of EBA175 RII orthologues to human erythrocytes, multimeric arrays of the proteins were generated by immobilising on streptavidin-coated Nile red beads. Erythrocytes were incubated with these arrays for 1 h at 4°C before analysis by flow cytometry. **A)** To determine the minimum amount of each EBA175 RII orthologue necessary for complete saturation of a set number of streptavidin-coated Nile red beads, ELISAs were performed on 2-fold serial dilutions of the proteins, with and without pre-incubation with beads. The ELISAs were carried out on a streptavidin-coated plate, using OX68 as the primary antibody and an alkaline phosphatase-conjugated anti-mouse antibody as the secondary. Data is shown as mean ± standard deviation; *n*=3. **B)** Dot-plots of the FSC (α size) and SSC (α granularity) parameters of the untreated and enzymatically-treated erythrocyte populations incubated with *Pf*EBA175 RII-coated beads, estimated by flow cytometry. Red: untreated erythrocytes. Erythrocytes pre-treated with trypsin, chymotrypsin and neuraminidase are shown in blue, green and orange respectively. The polygonal gate marked was used for separating the cells from bead aggregates. Erythrocytes incubated with Cd4-coated beads (negative control) are shown in black for comparison.

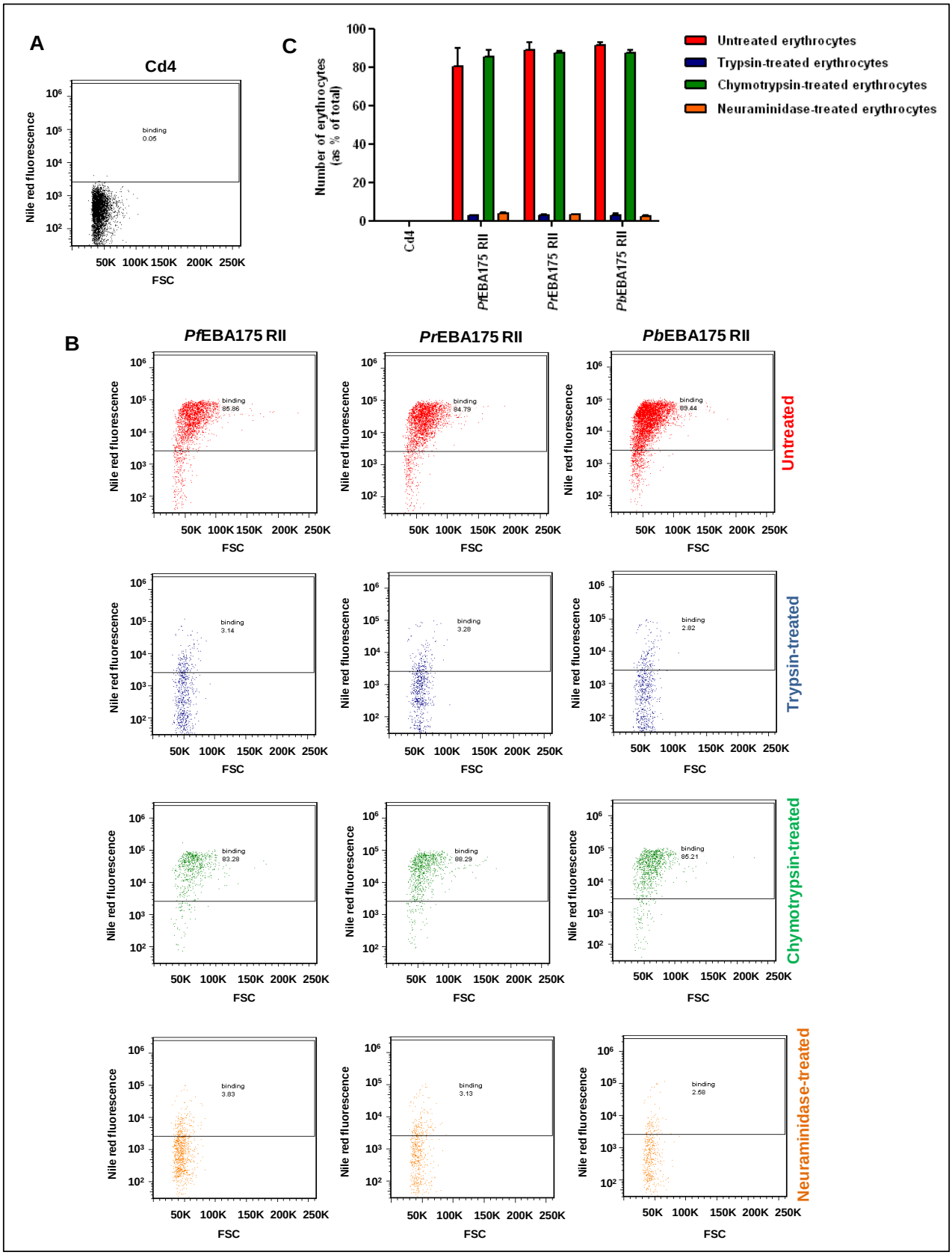
A
Cd4
Nile red fluorescence
FSC
binding
0.05
C
Number of erythrocytes (as % of total)
Untreated erythrocytes
Trypsin-treated erythrocytes
Chymotrypsin-treated erythrocytes
Neuraminidase-treated erythrocytes
Cd4
PfEBA175 RII
PrEBA175 RII
PbEBA175 RII
B
PfEBA175 RII
PrEBA175 RII
PbEBA175 RII
Untreated
Trypsin-treated
Chymotrypsin-treated
Neuraminidase-treated

Figure 28. All three EBA175 RII orthologues showed significantly more binding to untreated and chymotrypsin-treated erythrocytes, than to trypsin and neuraminidase-treated cells. A and **B** show dot plots of Nile red fluorescence intensity *versus* FSC for erythrocyte populations incubated either with Cd4-coated beads (**A**) or with EBA175RII-coated beads (**B**). The rectangular gate marked was used to estimate the fraction of Nile red 'positive' cells. The range of fluorescence intensities exhibited by cells incubated with Cd4-coated beads (the negative control) was used to determine the lower threshold of this gate. **C** is a bar chart representing the numbers of erythrocytes (as a percentage of total) binding to EBA175 RII-coated beads. In **B** and **C**, untreated cells are shown in red. Erythrocytes pre-treated with the enzymes trypsin, chymotrypsin and neuraminidase are indicated in blue, green and orange respectively.

time course assay (Figure 29 B).

All three of the EBA175 RII orthologues showed significantly more binding to sialylated Glycophorin A than to its asialylated derivative (Figure 29 C). The variation in the binding responses of the EBA175 RII orthologues with Glycophorin A could be indicative of the differential affinities of the interactions. However, this could also be due to discrepancies in the amount of functional EBA175 between the samples. Filtered culture supernatants containing EBA175 were used in this assay, rather than purified proteins and although care was taken to normalise the amount of recombinant protein in the supernatants by monitoring the activity of the β-lactamase fusion tag, this was only an approximate measure.

4.2.4 SPR studies revealed differences in the affinities of the EBA175 RII orthologues for human Glycophorin A.

In order to conclude whether the EBA175 RII orthologues bind human Glycophorin A with different affinities, it was therefore necessary to perform further analysis with SPR using purified EBA175. The K_D for the *Pf*EBA175 RII-Glycophorin A interaction was previously estimated to be ~2.5 μM (Chapter 3, section 3.2.9).

For this study, the three EBA175 RII orthologues, expressed with C-terminal Cd4 and hexa-His tags, were purified from the culture supernatant by affinity chromatography on nickel-charged Sepharose. The final yield of each purified protein was approximately 0.1 mg/100 ml culture. Analysis of the proteins by denaturing SDS-PAGE confirmed their expression at the expected size of ~97 kDa (Figure 30 A). When subjected to gel filtration prior to SPR analysis, each protein was observed to elute as a single peak at ~34 ml (corresponding to a molecular weight of ~70 kDa), indicating a monomeric form (Figure 30 B).

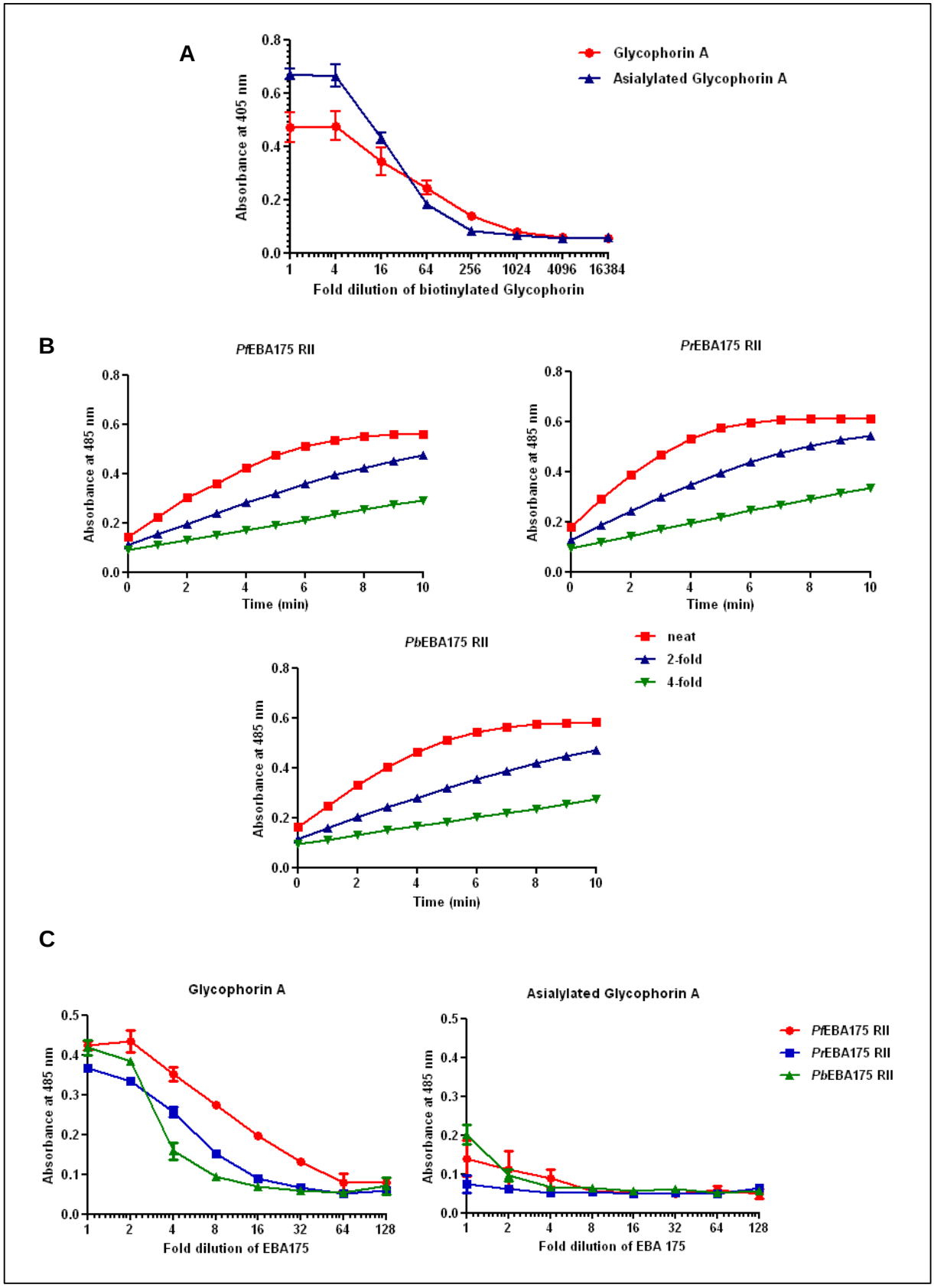
A
Glycophorin A
Asialylated Glycophorin A
Absorbance at 405 nm
Fold dilution of biotinylated Glycophorin
B
PfEBA175 RII
PrEBA175 RII
PbEBA175 RII
Absorbance at 485 nm
Time (min)
neat
2-fold
4-fold
C
Glycophorin A
Asialylated Glycophorin A
Fold dilution of EBA175
Fold dilution of EBA 175
PfEBA175 RII
PrEBA175 RII
PbEBA175 RII

Figure 29. An ELISA-based assay was used to compare the binding of the EBA175 RII orthologues to sialylated and asialyalted forms of native human Glycophorin A. The EBA175 RII orthologues, expressed as soluble β-lactamase tagged pentamers, were tested against two biotinylated Glycophorin A preparations, sialylated native Glycophorin A extracted from human erythrocytes and an asialylated derivative, immobilised on streptavidin-coated plates. **A)** The amount of biotinylated protein in each of the Glycophorin A preparations was normalised against each other by ELISA on a streptavidin-coated plate using BRIC256 (an anti-Glycophorin A mouse monoclonal) as the primary antibody and an alkaline phosphatase-conjugated anti-mouse secondary. The data are shown as mean ± standard deviation; *n*=3. **B)** The EBA175 RII orthologues expressed in the pentameric form with a β-lactamase tag, were normalised against each other using a time-course assay, monitoring the turnover of the colorimetric β-lactamase substrate, nitrocefin, at an absorbance of 485 nm. **C)** A 2-fold dilution series of each EBA175 RII orthologue was probed against Glycophorin A and binding was detected using nitrocefin. The pentameric proteins were incubated with the immobilised Glycophorin A for 2 h at room temperature and the absorbance at 485 nm was measured after overnight incubation with nitrocefin at 4°C. The data are shown as mean ± standard deviation; *n*=3.

The three EBA175 RII orthologues were first injected across biotinylated Glycophorin A, immobilised on a streptavidin-coated sensor chip, at equimolar concentrations, in succession. The binding responses of *Pr*EBA175 RII and *Pb*EBA175 RII were similar to each other but markedly lower than that of *Pf*EBA175 RII (Figure 30 C). To obtain estimates for the affinities of their interactions with Glycophorin A, a 2-fold serial dilution each of *Pr*EBA175 RII and *Pb*EBA175 RII were injected across the SPR sensor surfaces. The reference-subtracted sensorgrams were globally fitted to a steady-state 1:1 binding model. The predicted K_D values were similar, $(5.0 \pm 0.1) \times 10^{-6}$ M and $(5.3 \pm 0.08) \times 10^{-6}$ M respectively for the *Pr*EBA175 RII-Glycophorin A and *Pb*EBA175 RII-Glycophorin A interactions.

The observed shape of the reference-subtracted sensorgrams was typical of a two-stage reaction, with both association and dissociation of the soluble analyte, consisting of a fast phase, followed by a slower phase. Whilst this could be indicative of an interaction involving a conformational change of the proteins, it could also be due to the presence of aggregates in the analyte samples. When the EBA175 orthologues were gel filtered before the SPR analysis no multimeric forms were detected; however, aggregates could have formed after this stage.

The reference-subtracted sensorgrams could not be fitted to a 1:1 binding kinetic model with confidence. The K_D values calculated by local fitting of the curves to a two-state reaction model (Figure 30 D) were consistent with the estimates from the equilibrium analysis and suggested only a ~2-fold difference in the affinity for human Glycophorin A between *Pr*/*Pb*EBA175 RII and *Pf*EBA175 RII.

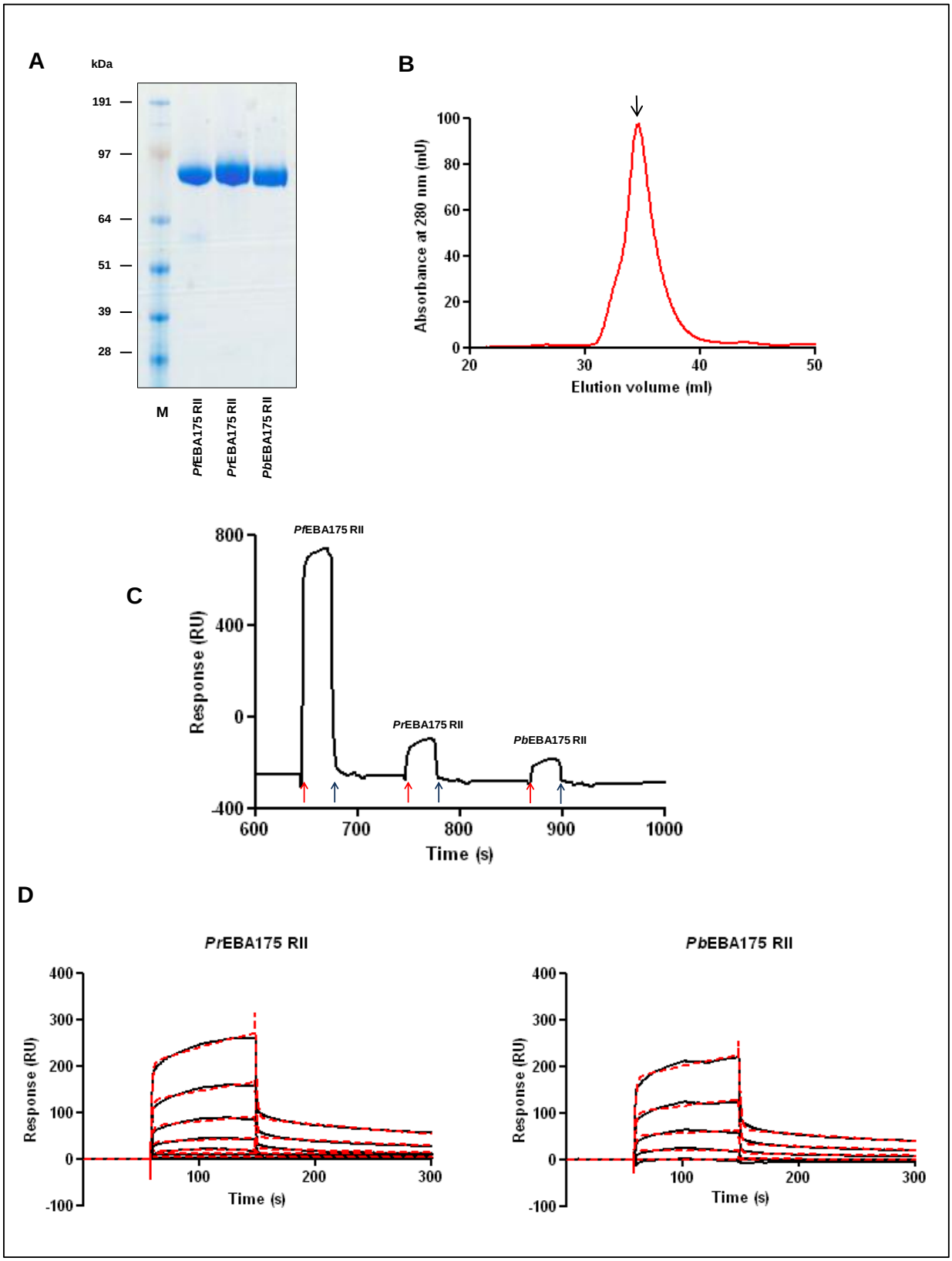
A
kDa
191
97
64
51
39
28
M
PfEBA175 RII
PrEBA175 RII
PbEBA175 RII
B
Absorbance at 280 nm (mU)
Elution volume (ml)
C
PfEBA175 RII
PrEBA175 RII
PbEBA175 RII
Response (RU)
Time (s)
D
PrEBA175 RII
PbEBA175 RII
Response (RU)
Time (s)

Figure 30. Hexa-His tagged EBA175 RII orthologues were purified from culture supernatants and tested against native Glycophorin A by SPR, to derive quantitative affinity estimates. A) Denaturing SDS-PAGE analysis of affinity-purified EBA175 RII orthologues. The proteins were visualised using Coomassie brilliant blue. **B)** The typical elution profile of an EBA175 RII orthologue from gel filtration. The peak fraction at ~34 ml is indicated by ↓. **C)** Reference subtracted sensorgram from the sequential injection of the three EBA175 RII orthologues, each at 3 µM, over biotinylated native Glycophorin A immobilised on a streptavidin-coated sensor chip. The red and blue arrows indicate the start and the end of each injection. The EBA175 proteins were injected at a flow rate of 10 µl/min for 30 s each. **D)** Reference subtracted sensorgrams from the injection of a 2-fold dilution series (0.2-3.0 µM) each of *Pr*EBA175 RII and *Pb*EBA175 RII over immobilised Glycophorin A. The EBA175 proteins were injected at a flow rate of 20 µl/min, with a contact time of 120 s and a dissociation time of 200 s. The black lines represent experimental data and the red dotted lines, the local fitting to a two-state reaction model. The biotinylated baits were immobilised at Cd4 (reference)- 820 RU and Glycophorin A-980 RU.

4.2.5 RH5 orthologues from two *Laverania* species were expressed and biochemically characterised.

Whereas the EBA 175 orthologues of the *Laverania* parasites are relatively highly conserved, only approximately 68% sequence similarity is observed between the RH5 orthologues of *P. falciparum* (*Pf*RH5) and *P. reichenowi* (*Pr*RH5) (Figure 31), implying more scope for species-specific recognition.

In this study, *Pf*RH5 and *Pr*RH5 were expressed in soluble recombinant form in order to compare their ability to recognise human erythrocytes and recombinant BSG. The predicted full-length coding sequences of both proteins were codon optimised for expression in the HEK293E system and their endogenous signal peptides (residues 1-24) were replaced by a mammalian-derived sequence. The potential N-linked glycosylation sites on both proteins were also removed during gene synthesis to prevent the inappropriate addition of carbohydrate moieties in the human secretory pathway. *Pf*RH5 and *Pr*RH5, produced with C-terminal Cd4 and biotin tags, were expected to be approximately 88 kDa in size. Analysis of these proteins by Western blotting confirmed their expression in the full-length form (Figure 32 A). A certain proportion of both proteins, however, appeared to be N-terminally processed, generating fragments of ~68 kDa and ~28 kDa (Figure 32 A). The processing of both *Pf*RH5 and *Pr*RH5 in a similar manner, suggests conservation of these proteolytic cleavage sites. The size of the Cd4 tag is ~25 kDa, therefore the ~88 kDa and ~68 kDa forms correspond well to the 63 kDa and 45 kDa native forms of *Pf*RH5 that have been observed in parasite cultures (Baum *et al*., 2009).

After normalisation by ELISA (Figure 32 B), the RH5 orthologues were tested against a panel of 27 mouse monoclonal antibodies that had been raised against a partially-glycosylated

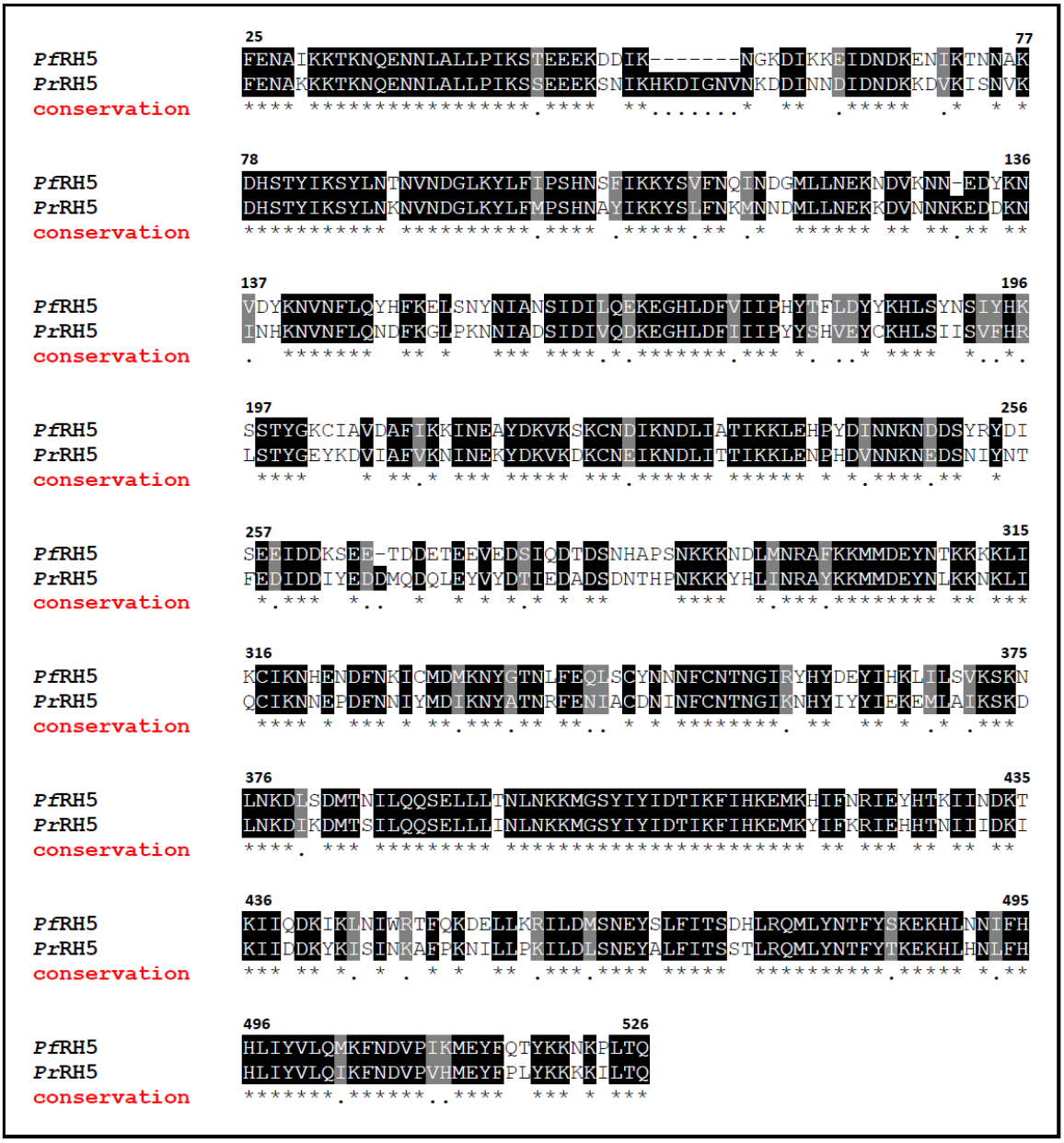

Figure 31. Sequence alignment of RH5 orthologues from *P. falciparum* and *P. reichenowi*. The amino acid sequences of RH5 from *P. falciparum* (*Pf*RH5) and *P. reichenowi* (*Pr*RH5) are shown. Conserved residues are shaded in black and semi-conserved residues in grey. The numbering indicated is for *Pf*RH5. Sequences: *Pf*RH5 (protein accession number Q8IFM5, aa 25-526), *Pr*EBA175 RII (B4X6H6, aa 25-535). The endoegnous signal peptides (aa 1-24) of *Pf*RH5 and *Pr*Rh5 were replaced by a mammalian leader sequence, prior to expression in HEK293E cells. The sequences were aligned using ClustalW software (Larkin *et al*., 2007).

mammalian-expressed *Pf*RH5 antigen, by collaborators at the University of Oxford (Sandy Douglas, unpublished data). All the monoclonal antibodies, with the exception of 3AG12, were observed to bind to *Pf*RH5. *Pr*RH5 was however not recognised by any of the monoclonals (Figure 32 C). The absence of binding of 3AG12 to *Pf*RH5 might be due to recognition of a glycosylated epitope by this antibody.

Untreated and heat-treated samples of *Pf*RH5 and *Pr*RH5 were then tested against polyclonal sera raised against *Pf*RH5 in rabbit. Prior to this analysis, antibodies binding to the Cd4 tag were removed from the sera by pre-adsorption on immobilised Cd4. The binding of the polyclonal to *Pf*RH5 was reduced upon heat-denaturation of the former, suggesting the recognition of heat-labile epitopes in the antigen (Figure 32 D). In comparison to the negative control, Cd4, some slight binding of the polyclonal to *Pr*RH5 was observed. Heat-treatment of *Pr*RH5 appeared to have little effect on this binding, indicating recognition of one or more linear epitopes (Figure 32 D).

4.2.6 Both RH5 orthologues showed sialic acid-independent binding to human erythrocytes.

Multivalent arrays of *Pf*RH5 and *Pr*RH5, generated by direct immobilisation of the biotinylated proteins on streptavidin-coated Nile red beads, as described before for the EBA175 RII orthologues, were presented to untreated and neuraminidase-treated human erythrocytes, to observe any putative interactions. *Pf*EBA175 RII and Cd4-coated beads were included as the positive and negative controls respectively (section 4.2.2 above). Compared to the negative control, only about 5-8% of the erythrocytes were observed to associate with the RH5-coated beads (Figure 33 A and B). Neuraminidase-treatment of erythrocytes had almost no effect on this binding, as expected given that recognition of BSG by *Pf*RH5 is not known to be sialic acid dependent.

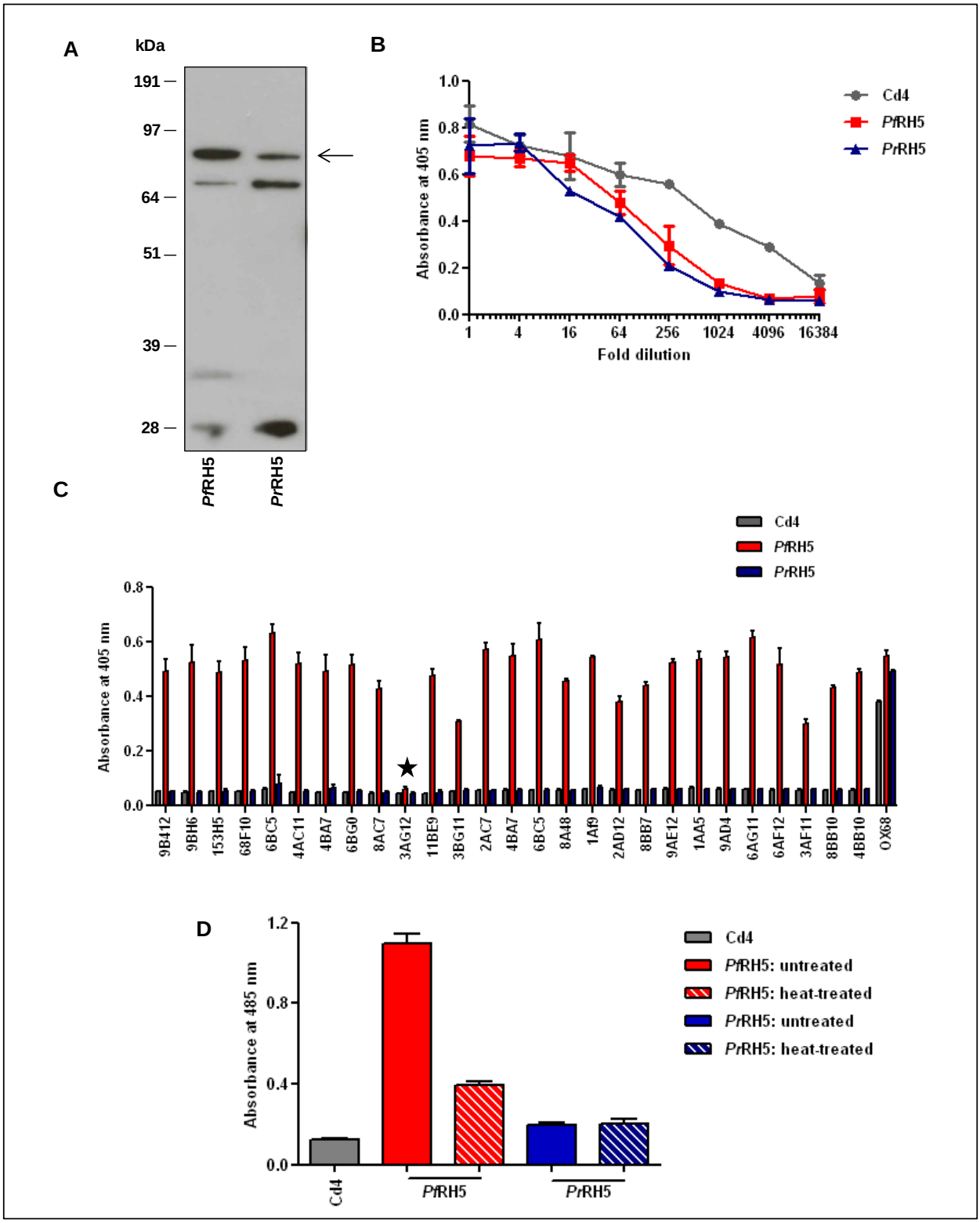
A
kDa
191
97
64
51
39
28
PfRH5
PrRH5
B
Absorbance at 405 nm
Fold dilution
Cd4
PfRH5
PrRH5
C
Absorbance at 405 nm
9B412
9BH6
153H5
68F10
6BC5
4AC11
4BA7
6BG0
8AC7
3AG12
11BE9
3BG11
2AC7
4BA7
6BC5
8A48
1Af9
2AD12
8BB7
9AE12
1AA5
9AD4
6AG11
6AF12
3AF11
8BB10
4BB10
OX68
D
Absorbance at 485 nm
Cd4
PfRH5: untreated
PfRH5: heat-treated
PrRH5: untreated
PrRH5: heat-treated

Figure 32. The RH5 orthologues of *P. falciparum* and *P. reichenowi* were recombinantly expressed. *Pf*RH5 and *Pr*RH5 were expressed in the soluble form with C-terminal Cd4 and biotin tags using the HEK293E expression system. **A)** A Western blot of *Pf*RH5 and *Pr*RH5 performed using HRP-conjugated extravidin as the probe. The full-length form of each of the fusion proteins (88 kDa) is indicated with the arrowhead. **B)** Relative quantitation of *Pf*RH5 and *Pr*RH5, against Cd4 by ELISA. The anti-Cd4 mouse monoclonal OX68, was used as the primary antibody. **C)** Recognition of *Pf*RH5 and *Pr*Rh5 by a panel of 26 mouse monoclonal antibodies that had been raised against a partially-glycosylated mammalian-derived *Pf*RH5. ★– No binding of *Pf*RH5 was observed to 3AG12. OX68 was used as a positive control. **D)** Binding of untreated and heat-treated samples of *Pf*RH5 and *Pr*Rh5 to a polyclonal raised against *Pf*RH5. Prior to the assay, anti-Cd4 antibodies were removed from the sera by pre-adsorption on immobilised Cd4. Binding of the anti-RH5 antibodies was also detected by ELISA. Cd4 was used as the negative control in the assays. All ELISAs were performed on streptavidin-coated plates, using an alkaline phosphatase-conjugated anti-mouse antibody as the secondary. The graphically presented data indicate mean ± standard deviation; n=3.

The difference in the binding of *Pf*EBA175 RII and *Pf*RH5 to human erythrocytes was hypothesised to reflect the availability of their respective receptors, Glycophorin A and BSG, at the cell surface. This was tested by comparing the staining of erythrocytes by the anti-Glycophorin A monoclonal, BRIC256, with that by two anti-BSG mouse monoclonals, MEM-M6/1 and MEM-M6/2. The binding of these monoclonals were detected with the same FITC-conjugated anti-mouse secondary. The erythrocytes incubated with BRIC256 were observed to have a 10^2-fold higher median fluorescence intensity than those incubated with MEM-M6/1 and MEM-M6/6 (Figure 33 C and D), confirming much higher levels of expression of Glycophorin A on the erythrocyte surface, in comparison to BSG.

4.2.7 BSG orthologues from three species of primates were expressed and characterised.

Although both *Pf*RH5 and *Pr*RH5 showed some binding to human erythrocytes in the previous assay, whether they were recognising the same receptor on the erythrocyte surface could not be concluded. Therefore, to investigate whether *Pr*RH5 binds BSG (the known erythrocytic receptor of *Pf*RH5) and whether *Pf*RH5 and *Pr*RH5 show a preference for BSG from their natural host-species, full-length ectodomains of the BSG orthologues from human (*Homo sapiens*), chimpanzee (*Pan troglodytes*) and gorilla (*Gorilla gorilla*) were expressed in soluble recombinant form and tested against the two RH5 orthologues directly.

The short splice isoform of Basigin (BSG) is thought to be the major variant of this protein present on human erythrocytes. It comprises two IgSF domains in the extracellular region and has been shown to interact directly with *Pf*RH5 (Crosnier *et al*., 2011). The sequences for three predicted isoforms of Basigin in *P. troglodytes* and two in *G. gorilla* were retrieved from the

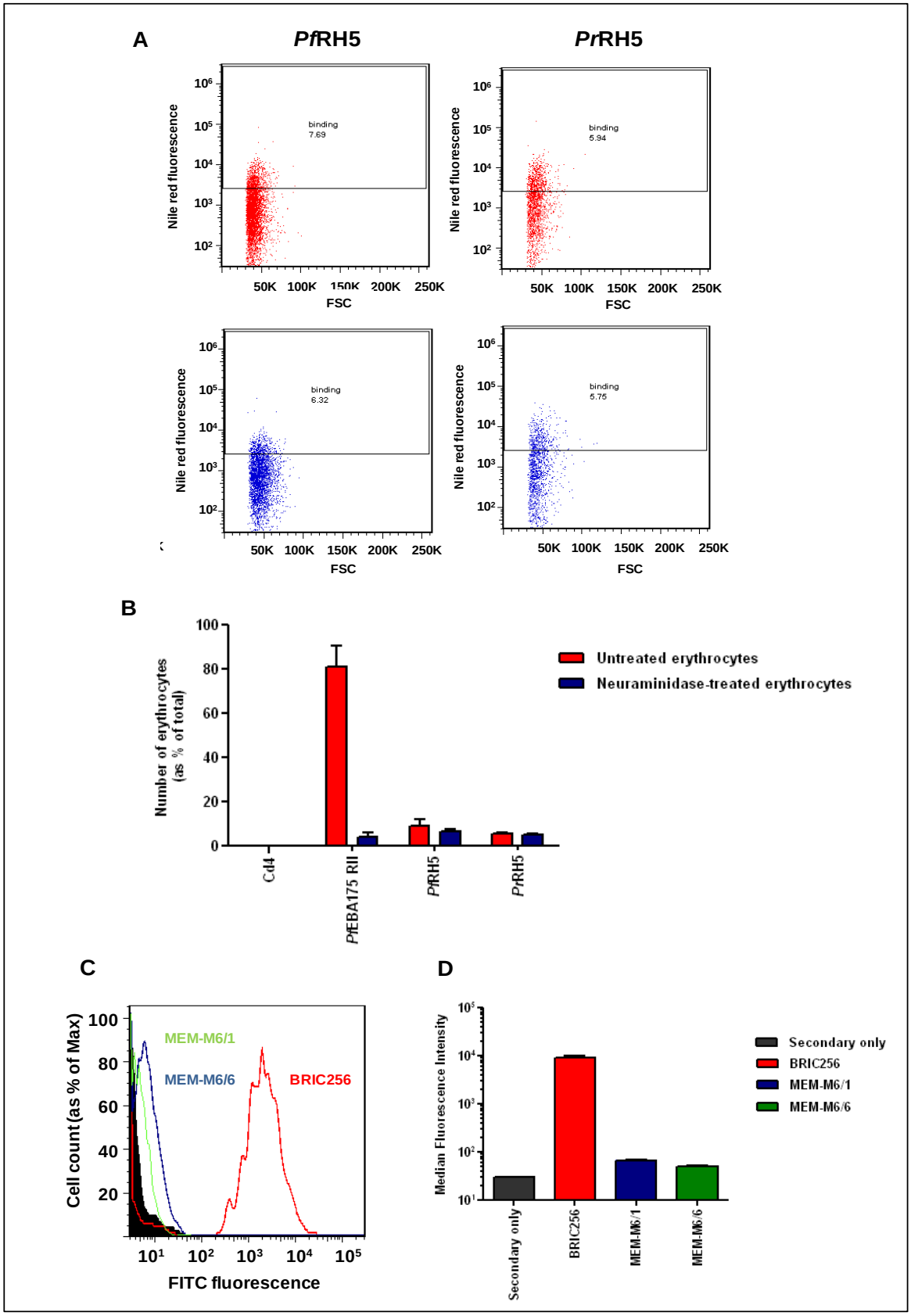
A
PfRH5
PrRH5
Nile red fluorescence
FSC
binding
7.69
5.94
6.32
5.75
B
Number of erythrocytes (as % of total)
Untreated erythrocytes
Neuraminidase-treated erythrocytes
Cd44
PfEBA175 RII
PfRH5
PrRH5
C
Cell count (as % of Max)
MEM-M6/1
MEM-M6/6
BRIC256
FITC fluorescence
D
Median Fluorescence Intensity
Secondary only
BRIC256
MEM-M6/1
MEM-M6/6

.

Figure 33. Both *P. falciparum* and *P. reichenowi* RH5 orthologues were observed to bind to human erythrocytes. Multimeric arrays of *Pf*RH5 and *Pr*Rh5, generated by immobilising the biotinylated proteins on streptavidin-coated Nile red beads, were incubated with untreated and neuraminidase-treated erythrocytes for 1 h at 4°C before analysis by flow cytometry. **A)** Dot plots of Nile red fluorescence intensity *versus* FSC for erythrocyte populations incubated with RH5-coated beads. The rectangular gate marked was used to estimate the fraction of Nile red 'positive' cells. The lower threshold of this gate was determined from the range of fluorescence intensities exhibited by erythrocytes incubated with Cd4-coated beads (the negative control) as previously (Figure 28 A). **B)** A bar chart representing the numbers of erythrocytes (as a percentage of total) binding to RH5-coated beads. The binding to beads coated with Cd4 (negative control) and *Pf*EBA175 RII (positive control) are also included for comparison. In **A** and **B**, untreated and neuraminidase pre-treated erythrocytes are shown in red and blue respectively. **C)** A histogram showing the staining of human erythrocytes by the mouse monoclonals BRIC256 (anti-Glycophorin A), MEM-M6/1 (anti-BSG) and MEM-M6/6 (anti-BSG), detected using a FITC-conjugated anti-mouse secondary. **D)** A bar chart of the median fluorescence intensity of the erythrocyte populations stained with BRIC256, MEM-M6/1 and MEM-M6/6 at the FITC emission wavelength. In **C** and **D**, the staining with BRIC256, MEM-M6/1 and MEM-M6/6 are shown in red, blue and green respectively. Erythrocytes incubated with only the secondary antibody (negative control) are represented in black. The bar charts show mean ± standard deviation; n=3.

Ensembl genome browser (Flicek *et al*., 2011). The InterPro Scan server (Zdobnov and Apweiler, 2001) was then used to analyse the possible domain architecture of these proteins. Only the isoforms with two IgSF domains, *P. troglodytes* ENSPTRP00000017252 (*Pt*BSG) and the *G. gorilla* ENSGGOP00000022655 (*Gg*BSG) were selected for expression (Figure 34 A).

When the sequences of the selected BSG orthologues were aligned, the leucine at position 174 of human BSG (*Hs*BSG) was observed to be deleted in *Pt*BSG, but present in *Gg*BSG (Figure 34 B). This leucine residue, located on a linker region between two β strands (Yu *et al*., 2008) was found to be conserved in predicted BSG orthologues from other primates, including the great apes bonobo and orang-utan, rhesus macaque (an old world monkey) and common marmoset (a new world monkey), by performing a blast search with the *Hs*BSG sequence. Inspection of the *Pt*BSG transcript sequence and its annotations on the Ensembl browser, revealed that the deletion of Leu-174 was probably an error arising from incorrect specification of intron-exon boundaries. Therefore, when assembling the *Pt*BSG coding sequence by gene synthesis, a codon for leucine was introduced at the corresponding position. Overall, the *Hs*BSG, *Pt*BSG and *Gg*BSG orthologues were observed to share a notably high degree (~95%) of primary sequence similarity (Figure 34 B).

The BSG orthologues, expressed with C-terminal Cd4 and biotin tags, were first analysed by Western blotting to confirm their expression at the correct size. An un-glycosylated monomer of recombinant BSG was expected to have a molecular weight of ~44 kDa. All three BSG orthologues were observed as smears on the Western blot ranging in size between ~51 kDa and ~64 kDa (Figure 35 A). Each of these proteins carry three putative N-linked glycosylation sites, hence the smearing is likely due to the presence of different glycoforms.

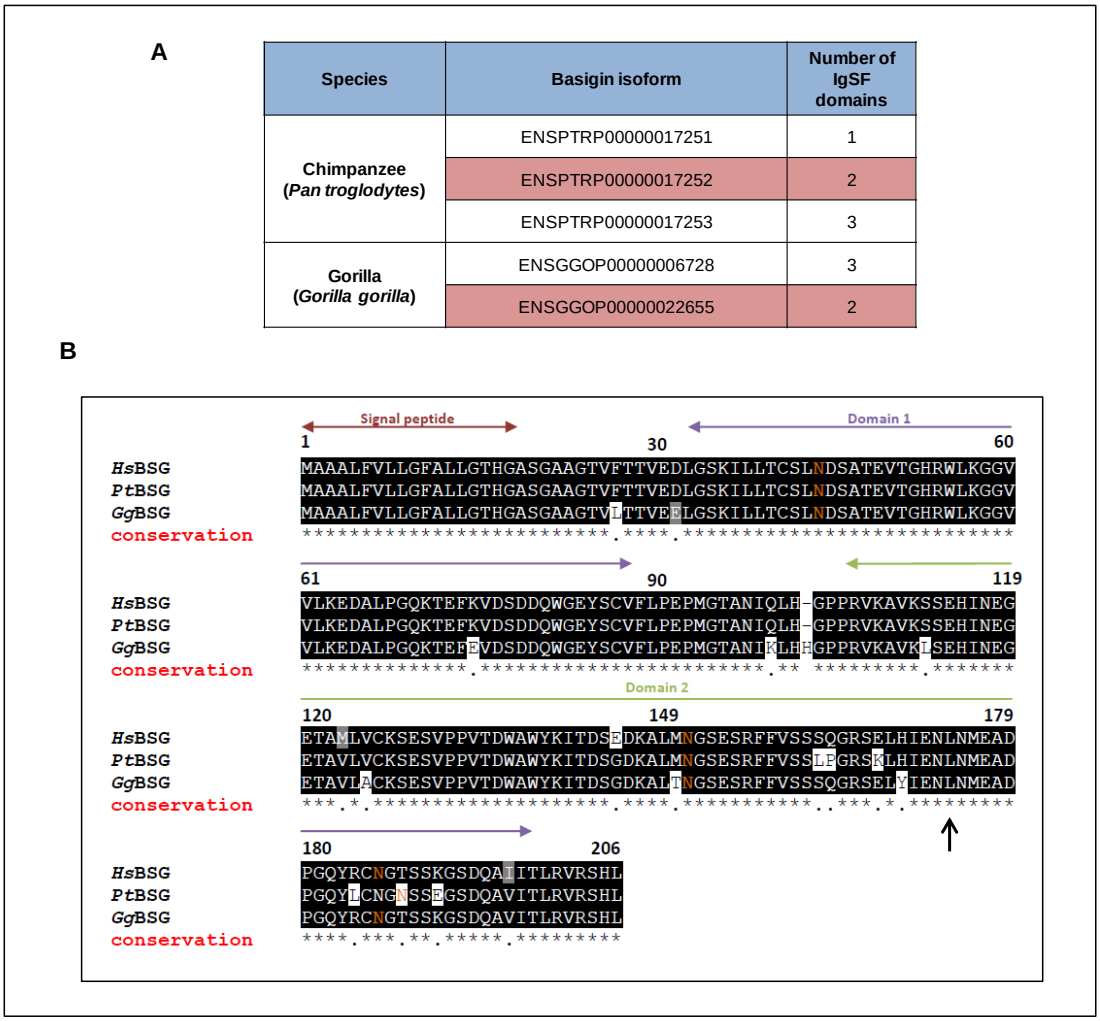

Figure 34. Basigin orthologues from human (*H. sapiens*), chimpanzee (*P. troglodytes*) and gorilla (*G. gorilla*): domain predictions and sequence alignments. A) The sequences of the predicted Basigin isoforms of *P. troglodytes* and *G. gorilla*, retrieved from the Ensembl genome browser (Flicek *et al*., 2011), were analysed for IgSF domains using InterPro Scan (Zdobnov and Apweiler, 2001). **B)** Alignment of the full-length ectodomains of BSG orthologues containing two IgSF domains from human (*Hs*BSG, protein accession number: NP_940991, aa 1-206), chimpanzee (*Pt*BSG, aa 1-206) and gorilla (*Gg*BSG, aa 1-207). Conserved residues are shaded in black and semi-conserved residues in grey. The numbering indicated is for *Hs*BSG. The signal peptide (aa 1-18), IgSF domain 1 (aa 20-88) and IgSF domain 2 (aa 100-204) are marked in maroon, purple and green respectively. The N-linked glycosylation sites on the proteins are shown in orange. The black arrow marks Leu-174, which is missing from the original *Pt*BSG sequence from Ensembl. The sequences were aligned using ClustalW software (Larkin *et al*., 2007).

The BSG orthologues were then tested against a panel of seven monoclonal antibodies that had been raised using a CHO cell-derived recombinant *Hs*BSG as the antigen (Koch *et al*., 1999). MEM-M6/6 is known to recognise an epitope on IgSF domain 2 of *Hs*BSG, and the others epitopes on domain 1 (Koch *et al*., 1999). The binding of these monoclonals to heat-treated *Hs*BSG was found to be significantly less than that to untreated *Hs*BSG, suggesting their epitopes are non-linear and heat-labile (Figure 35 B).

*Pt*BSG was recognised by all the monoclonals, apart from the anti-domain 2 antibody, MEM-M6/6 (Figure 35 C). *Gg*BSG showed clear binding to MEM-M6/6 and to the anti-domain 1 antibodies MEM-M6/1, MEM-M6/2 and MEM-M6/4. It did not appear to be recognised by MEM-M6/8 and MEM-M6/11 and showed reduced binding to MEM-M6/10. The recognition of *Pt*BSG and *Gg*BSG by monoclonals with non-linear epitopes, suggest that they are likely to have been expressed in their native conformation. The absence of binding of some of the monoclonals to *Pt*BSG and *Gg*BSG is probably due to non-conservation of their epitopes as a consequence of variations in the primary sequences of *Pt*BSG and *Gg*BSG relative to *Hs*BSG.

4.2.8 Differences in the binding of RH5 to the BSG orthologues were revealed by AVEXIS.

The BSG orthologues expressed as β-lactamase tagged pentameric 'preys' were tested against biotinylated *Pf*RH5 and *Pr*RH5 'baits' by AVEXIS to identify putative interactions (Figure 36). In addition to its known interaction with *Hs*BSG, *Pf*RH5 also showed some binding to *Pt*BSG (Figures 36 B and C). No interactions were observed between *Pf*RH5 and *Gg*BSG or between *Pr*RH5 and any BSG orthologue.

As a test for binding specificity, a 2-fold dilution series each of *Hs*BSG and *Pt*BSG, was subsequently tested against *Pf*RH5. A significant difference was observed in the binding

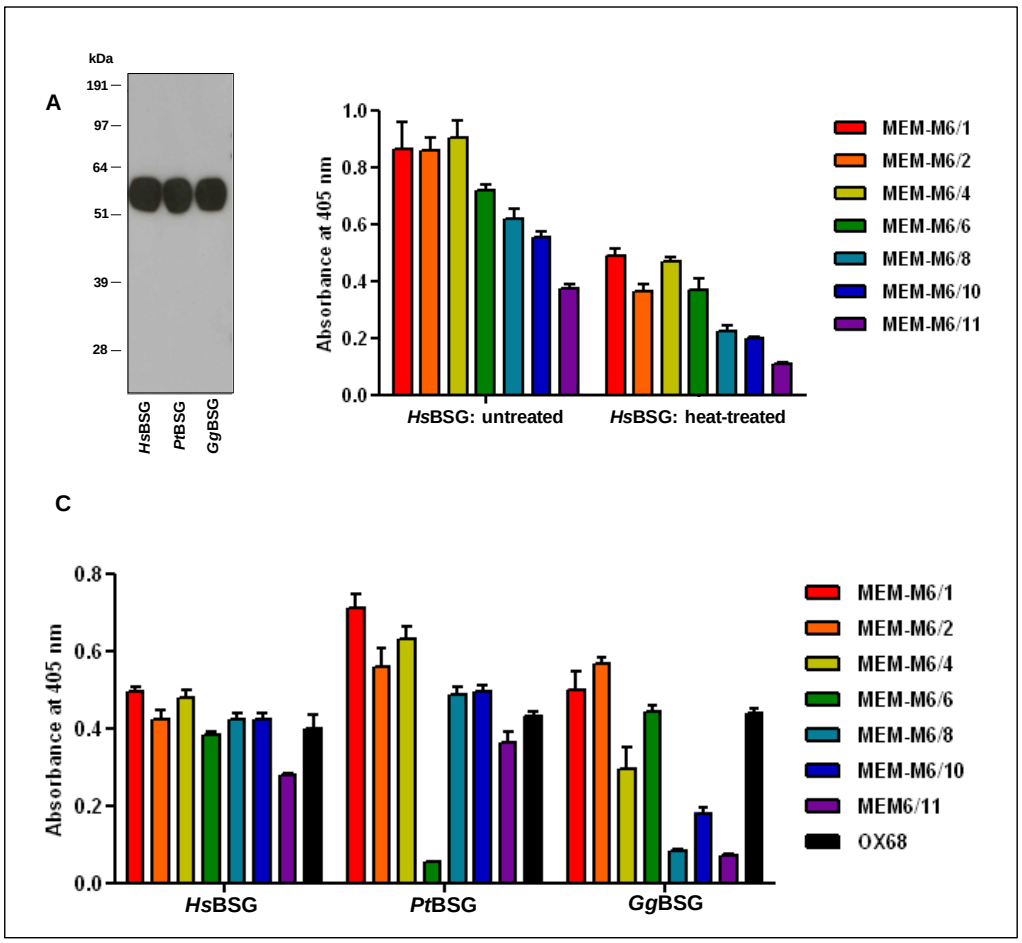

Figure 35. BSG orthologues from three primate species were recombinantly expressed and immunologically characterised. *Hs*BSG, *Pt*BSG and *Gg*BSG were expressed in the soluble form with C-terminal CD4 and biotin tags. These were then tested against a panel of seven mouse monoclonals raised against a *Hs*BSG antigen (Koch *et al*., 1999). **A)** A Western blot of the BSG orthologues performed using HRP-conjugated extravidin as the probe. The expected molecular weight of an un-glycosylated monomer of BSG is ~44 kDa. **B)** The panel of anti-BSG monoclonals were probed against untreated and heat-treated *Hs*BSG to identify the conformational properties of their epitopes (i.e. folded or linear). **C)** Recognition of the BSG orthologues by the anti-BSG monoclonals. OX68 was used as a positive control. Binding of the monoclonals to BSG was detected by ELISA. All ELISAs were performed on streptavidin-coated plates, using an alkaline phosphatase-conjugated anti-mouse antibody as the secondary. The graphically presented data indicate mean ± standard deviation; *n*=3.

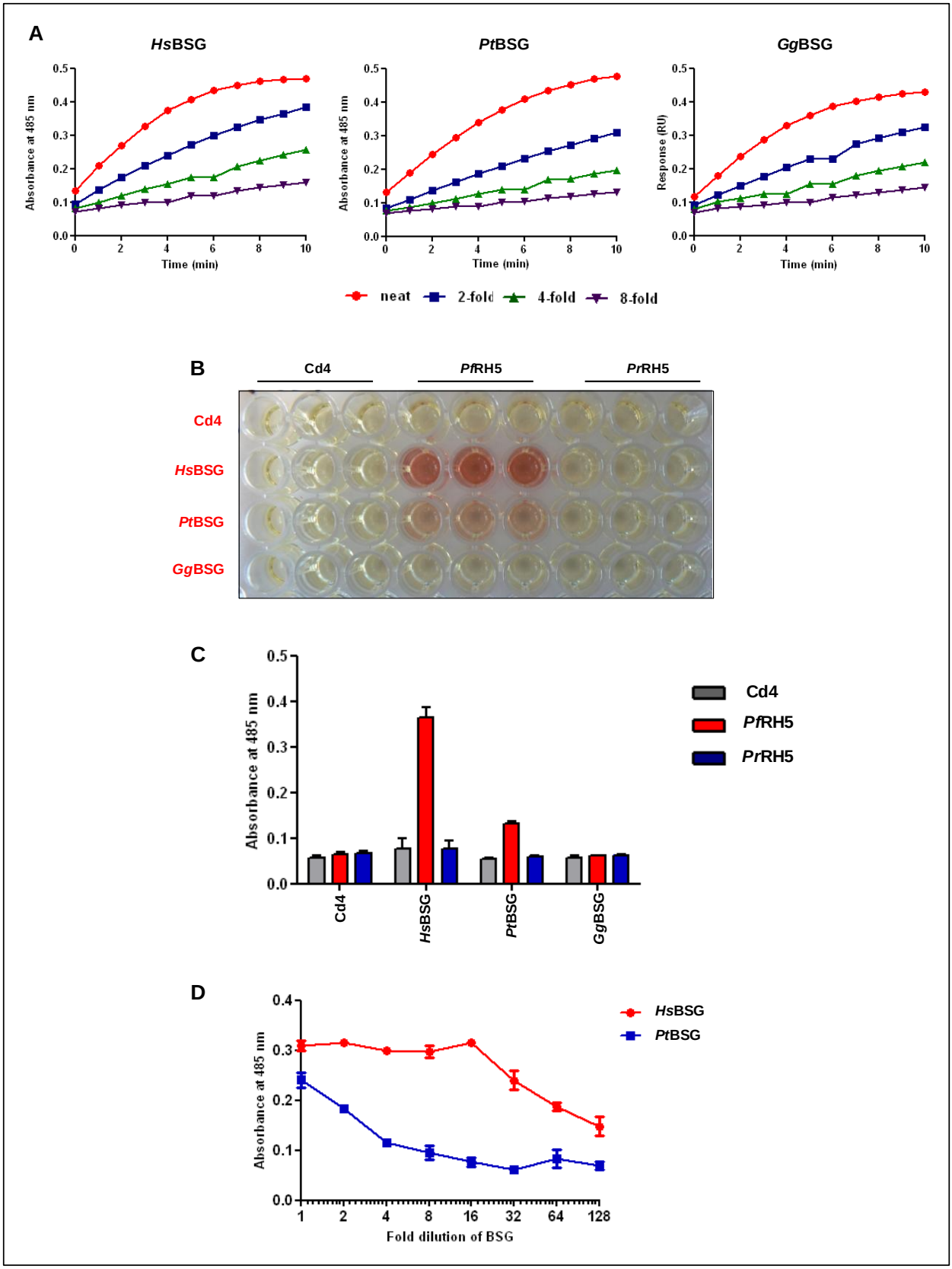
A
HsBSG
PtBSG
GgBSG
Absorbance at 485 nm
Response (RU)
Time (min)
neat
2-fold
4-fold
8-fold
B
Cd4
PfRH5
PrRH5
Cd4
HsBSG
PtBSG
GgBSG
C
Absorbance at 485 nm
Cd4
PfRH5
PrRH5
HsBSG
PtBSG
GgBSG
D
Absorbance at 485 nm
HsBSG
PtBSG
Fold dilution of BSG

Figure 36. The interactions between recombinantly-expressed RH5 and BSG orthologues were analysed by AVEXIS. The BSG orthologues, expressed as β-lactamase tagged pentameric 'preys' were probed against biotinylated RH5 'baits' immobilised on streptavidin-coated plates. **A)** The BSG orthologues were normalised against each other by monitoring the turnover of nitrocefin in a time-course assay. **B)** and **C)** Results from the AVEXIS screen, in which each BSG 'prey' was tested against both *Pf*RH5 and *Pr*RH5. Cd4 in both 'bait' and 'prey' forms was used as the negative control. **D)** Binding of a 2-fold dilution series each of only *Hs*BSG and *Pt*BSG to *Pf*RH5, as tested by AVEXIS. The pentameric preys were incubated with the baits for 2 h in the AVEXIS assays and binding was detected by measuring nitrocefin turnover, 3 h after addition of the substrate. All steps were carried out at room temperature. The data in **C** and **D** are shown as mean ± standard deviation; n=3.

responses of *Hs*BSG and *Pt*BSG with *Pf*RH5, which is indicative of the *Pt*BSG-*Pf*RH5 interaction being of a substantially lower affinity than the *Hs*BSG-*Pf*RH5 interaction (Figure 36 D).

4.2.9 Affinity measurements for the RH5-BSG interactions were obtained by SPR.

SPR is a method of very high sensitivity which could be expected to reveal even interactions that are of too low affinity to be detected by AVEXIS. Therefore, the binding of BSG orthologues to *Pf*RH5 and *Pr*RH5 was also tested in reciprocal orientations by SPR, to identify any putative interactions that may have been missed in the previous AVEXIS screen.

For testing against biotinylated RH5 immobilised on a streptavidin-coated SPR sensor chip, the BSG orthologues were expressed with C-terminal Cd4 and hexa-His tags. After purification from the culture supernatant by affinity chromatography, the proteins were identified to be expressed at the correct size by SDS-PAGE (Figure 37 A). Glycosylation of the proteins was confirmed by staining the gel using a carbohydrate-specific periodic acid-Schiff reagent method. The proteins were subjected to gel filtration immediately prior to use in the SPR assays. Each BSG orthologue eluted from the gel filtration column as a single prominent peak with an elution volume (of ~ 35 ml) corresponding to a size of ~50 kDa, indicating a monomeric form (Figure 37 B). When tested against the RH5 orthologues both *Hs*BSG and *Pt*BSG showed binding to *Pf*RH5 (Figure 3 6C). The binding response observed was much lower in magnitude for *Pt*BSG in comparison with *Hs*BSG. No binding was observed with either *Gg*BSG or *Pr*RH5.

The SPR experiment was then repeated in the reverse orientation, with biotinylated BSG immobilised on the SPR chip and soluble RH5 injected across the sensor surfaces. As RH5 is a larger protein than BSG, performing the SPR experiment in this orientation was expected to

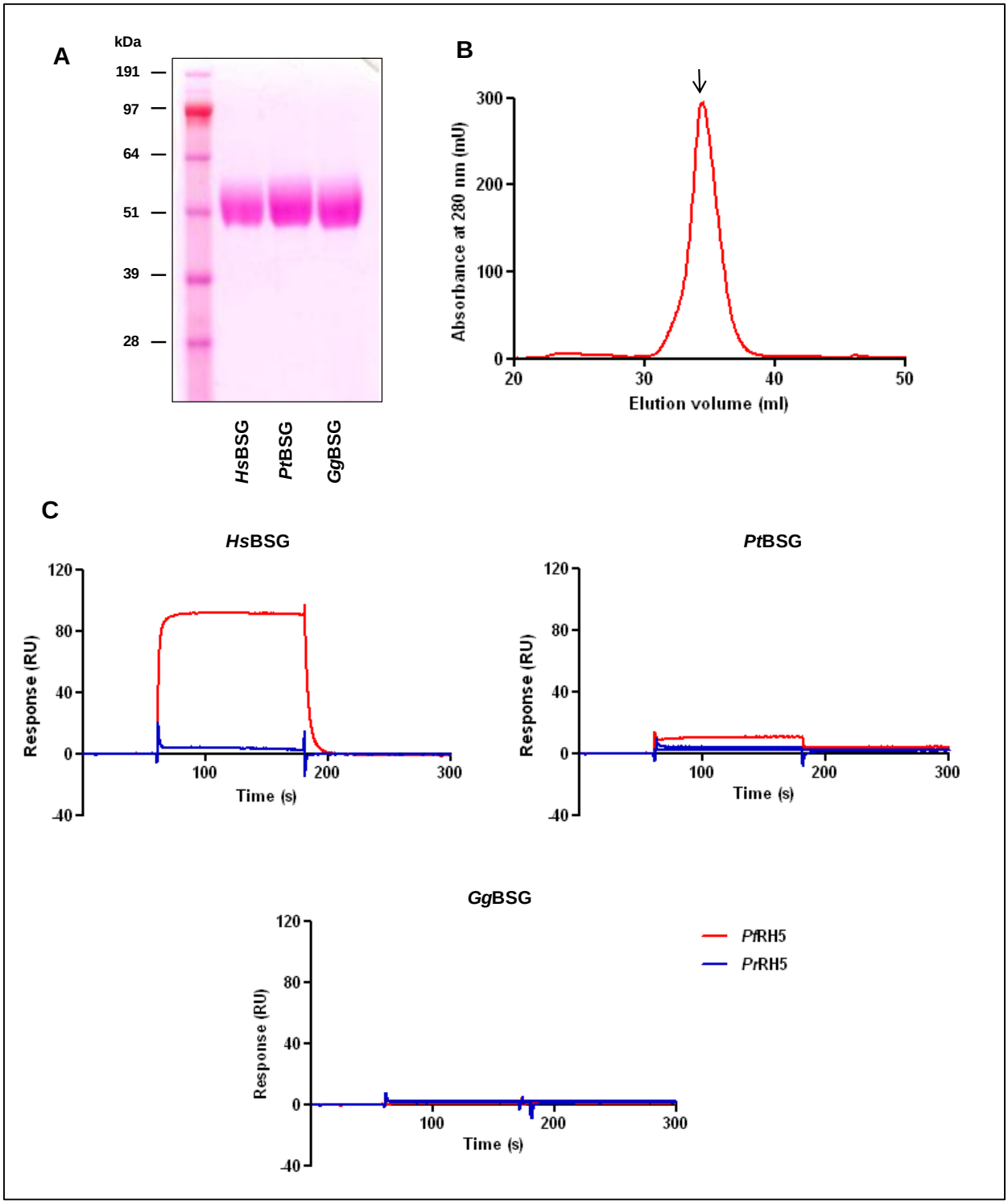
A
kDa
191
97
64
51
39
28
HsBSG
PtBSG
GgBSG
B
Absorbance at 280 nm (mU)
300
200
100
0
20
30
40
50
Elution volume (ml)
C
HsBSG
PtBSG
GgBSG
Response (RU)
120
80
40
0
-40
100
200
300
Time (s)
PfRH5
PrRH5

Figure 37. Recombinant hexa-His tagged BSG orthologues were purified from culture supernatants and tested against RH5 by SPR. A) Denaturing SDS-PAGE analysis of affinity-purified BSG orthologues. The proteins were visualised using a carbohydrate-specific dye to confirm glycosylation. **B)** The typical elution profile of a BSG orthologue from gel filtration. The peak fraction at ~35 ml is indicated by ↓. **C)** Reference subtracted sensorgrams from the injection of the BSG orthologues, each at 5 µM, over biotinylated *Pf*RH5 (red) and *Pr*RH5 (blue) immobilised on a streptavidin-coated sensor chip. The BSG proteins were injected at a flow rate of 20 µl/min, with a contact time of 120 s and a dissociation time of 200 s. The biotinylated baits were immobilised at Cd4 (reference)- 226 RU, *Pf*RH5-927 RU and *Pr*RH5-896 RU.

yield an improved signal to noise ratio with respect to the binding responses. For this experiment both *Pf*RH5 and *Pr*RH5 were expressed with C-terminal Cd4 and hexa-His tags. After purification from the culture supernatant by affinity chromatography on nickel-charged Sepharose, the proteins were analysed by SDS-PAGE under reducing conditions. Both proteins appeared to be expressed at the expected size of ~84 kDa (Figure 38 A). A significant proportion of each protein was however processed, generating fragments of ~64 kDa and ~28 kDa. When subjected to gel filtration, both *Pf*RH5 and *Pr*RH5 eluted in three peaks (Figure 38 B). The expected elution volume of the monomeric full-length forms of *Pf*RH5 (83.5 kDa) and *Pr*RH5 (84.4 kDa) was 32.8 ml. From the observed elution volumes of the peaks; 32.0 ml (peak 1), 35.3 ml (peak 2) and 38.0 ml (peak 3) in the case of *Pf*RH5 and 29.5 ml (peak 1), 34.2 ml (peak 2) and 38.9 ml (peak 3) for *Pr*RH5, the molecular weights of the species they contain were calculated to be ~100 kDa (peak 1), ~50 kDa (peak 2) and ~25 kDa (peak 3), indicating that they probably contain the ~84 kDa, ~64 kDa and ~28 kDa forms RH5 respectively. In the case of both *Pf*RH5 and *Pr*RH5 only the peak 2 fraction was used in the SPR binding studies with BSG.

In agreement with the observations from the previous AVEXIS and SPR experiments, no binding was observed with either *Pr*RH5 or *Gg*BSG (Figure 38 C). *Pf*RH5 showed much higher binding to *Hs*BSG than to *Pt*BSG.

To derive kinetic parameters for its interaction with *Hs*BSG and *Pt*BSG, a 2- fold dilution series of *Pf*RH5 was injected across the sensor surfaces (Figure 38 D). The k_a and k_d values estimated by globally fitting the reference subtracted sensorgrams to a 1:1 binding model (Figure 39 A) were consistent with previous data for the *Hs*BSG-*Pf*RH5 interaction (Crosnier *et al*., 2011) (Figure 39 B). The K_D values deduced from this analysis for the binding of *Pf*RH5 to *Hs*BSG and

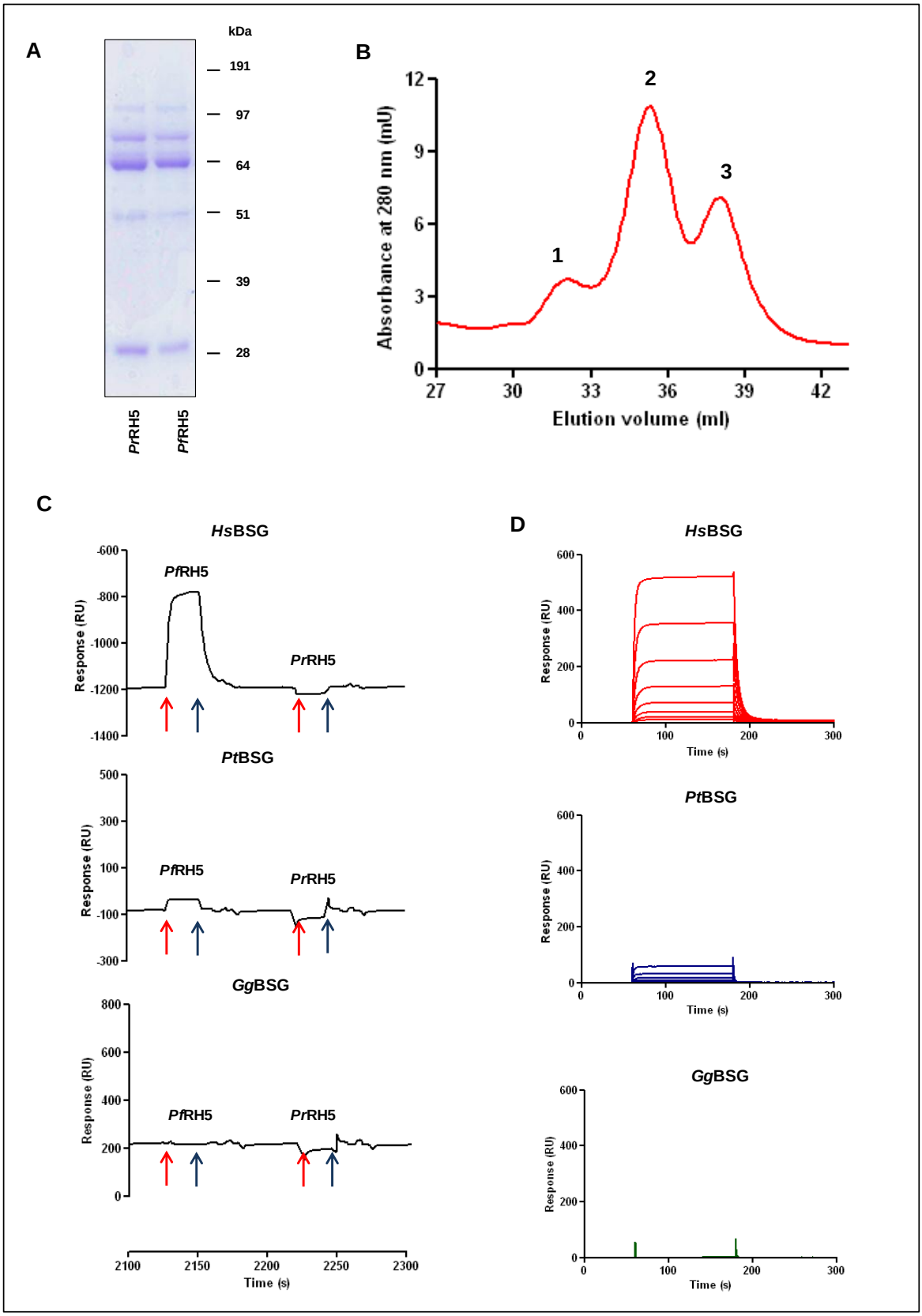
A
kDa
191
97
64
51
39
28
PrRH5
PfRH5
B
Absorbance at 280 nm (mU)
Elution volume (ml)
1
2
3
C
HsBSG
PfRH5
PrRH5
PtBSG
GgBSG
Response (RU)
Time (s)
D
HsBSG
PtBSG
GgBSG
Response (RU)
Time (s)

Figure 38. Hexa-His tagged RH5 orthologues were purified from culture supernatants and tested against BSG by SPR. A) Denaturing SDS-PAGE analysis of affinity-purified RH5 orthologues. The proteins were visualised using Coomassie brilliant blue. **B)** The typical elution profile of an RH5 orthologue from gel filtration. The three peak fractions, corresponding to the ~84 kDa (peak 1), ~64 kDa (peak 2) and ~28 kDa (peak 3) forms of RH5 are indicated. Only the peak 2 fractions of *Pf*RH5 and *Pr*RH5 were used in the SPR assays with BSG. **C)** Reference subtracted sensorgrams from the sequential injection of the RH5 orthologues, each at ~ 1 µM, over biotinylated *Hs*BSG, *Pt*BSG and *Gg*BSG immobilised on a streptavidin-coated sensor chip. The red and blue arrows represent the start and end of each injection. The RH5 proteins were injected at a flow rate of 30 µl/min for 30 s each. **D)** Reference subtracted sensorgrams from the injection of a 2-fold dilution series (0.02-1.1 µM) of *Pf*RH5, over the immobilised BSG orthologues. The RH5 proteins were injected at a flow rate of 20 µl/min, with a contact time of 120 s and a dissociation time of 200 s. The biotinylated baits were immobilised at Cd4 (reference) - 483 RU, *Hs*BSG, *Pt*BSG and *Gg*BSG- ~1050 RU.

A

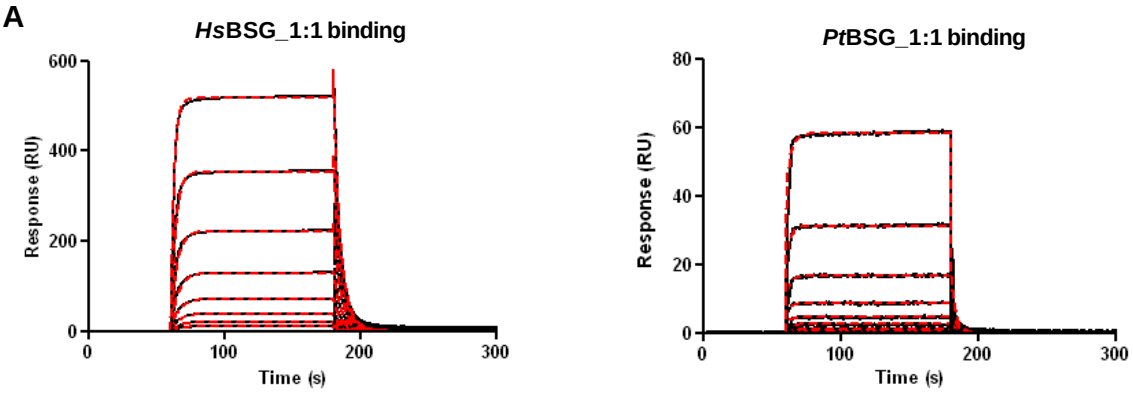

B

Kinetic parameter	*Hs*BSG	*Pt*BSG
k_a ($M^{-1}s^{-1}$)	(3.14 ± 0.04) x 10^5	(2.1 ± 0.3) x 10^4
k_d (s^{-1})	0.318 ± 0.005	0.312 ± 0.006
K_D (M)	1.02 x 10^{-6}	14.6 x 10^{-6}
Chi^2 (R^2)	11.2	7.43

Figure 39. Equilibrium and kinetic parameters for the interactions of *Pf*RH5 with *Hs*BSG and *Pt*BSG were derived from the SPR data. A) Global fitting of the reference subtracted SPR sensorgrams from the binding of *Pf*RH5 to *Hs*BSG and *Pt*BSG, to a simple 1:1 binding model to derive kinetic parameters. The black lines represent experimental data and the red dotted lines, the fitted curves. **B)** Table with kinetic parameters estimated for the *Hs*BSG-*Pf*RH5 and *Pt*BSG-*Pf*RH5 interactions using the 1:1 model. The estimated values for the k_a, k_d and K_D are indicated with the standard errors.

*Pt*BSG were ~1.1 µM and ~14.6 µM respectively, suggesting an approximate 15-fold difference in affinity between the two interactions.

4.2.10 Site-directed mutants of human and chimpanzee BSG proteins were generated and tested for correct folding.

To identify BSG residues important for the observed host-specificity of the *Pf*RH5-BSG interaction, site-directed mutants of *Hs*BSG and *Pt*BSG were generated.

*Pt*BSG and *Hs*BSG are identical in domain 1, therefore, the reduced affinity of *Pt*BSG for *Pf*RH5 was hypothesised to be due to differences in domain 2. The nine residues in domain 2 of *Pt*BSG which are different from *Hs*BSG were mutated to the corresponding *Hs*BSG residues (Table 5). Additionally five residues in *Hs*BSG were mutated to those found in *Gg*BSG at the equivalent positions. Four of these residues are located in domain 1 and the fifth in domain 2. A Histidine residue was also inserted into the *Hs*BSG sequence at position 103, as found in *Gg*BSG (Table 5). The 15 site-directed *Pt*BSG (C1-C9) and *Hs*BSG (H1-H6) mutants, expressed with C-terminal CD4 and biotin tags, were normalised against each other and characterised by testing against the panel of seven anti-BSG monoclonals (Figure 40 A). All *Pt*BSG mutants were recognised by the anti-domain 1 monoclonals, as expected given that *Hs*BSG and *Pt*BSG are identical in domain 1. The anti-domain 2 monoclonal, MEM-M6/6, which doesn't bind *Pt*BSG, was observed to recognise one of the *Pt*BSG mutants, C8, suggesting that the MEM-M6/6 epitope, which was absent in *Pt*BSG, has been restored by a single residue change in this mutant. C8 was mutated at residue 191 from the negatively charged glutamic acid (found in *Pt*BSG) to positively charged lysine (found in *Hs*BSG). This change is likely to be important as residue 191 lies in a surface-exposed β-turn region (Yu *et al*., 2008).

Site-directed mutant			Location
***Pt*BSG**	**C1**	V123 M	**Domain 2**
	C2	G145 E	
	C3	L163 S	
	C4	P164 Q	
	C5	E168 K	
	C6	L184 R	
	C7	N188 T	
	C8	E191 K	
	C9	V197 I	
***Hs*BSG**	**H1**	F27 L	**Domain 1**
	H2	D32 E	
	H3	K75 E	
	H4	Q100 K	
	H5	Insertion H at 103	
	H6	S112 L	**Domain 2**

Table 5. Site-directed mutants of *Pt*BSG and *Hs*BSG. Nine residues in the IgSF domain 2 of *Pt*BSG were substituted with the residues at the corresponding positions in *Hs*BSG. Five residues in *Hs*BSG were mutated to those in *Gg*BSG at the equivalent locations. A Histidine residue was also inserted in *Hs*BSG at position 103, as found in *Gg*BSG.

All the *Hs*BSG mutants, apart from H1, H2 and H3, showed binding to all anti-*Hs*BSG monoclonal antibodies. H2 showed no binding to two monoclonals, MEM-M6/8 and MEM-M6/10 and reduced binding to MEM-M6/4. These data are consistent with the conclusions from an epitope-mapping study performed by Koch *et al*. (1999) for the anti-*Hs*BSG monoclonals (Figure 40 B). In their study, Koch *et al*. identified that MEM-M6/8 and MEM-M6/10 bind the same epitope with MEM-M6/4 recognising a proximal/overlapping epitope. Therefore residue 32, which was mutated in H2, is probably located within the MEM-M6/8+ MEM-M6/10 epitope. Both H1 and H3 showed reduced binding to MEM-M6/11. In the epitope-mapping study mentioned above, the epitope recognised by MEM-M6/11 had been identified to be a central one close to/overlapping with MEM-M6/1, MEM-M6/4 and MEM-M6/8 epitopes (Koch *et al*., 1999).

4.2.11 The affinities of BSG mutants for *P. falciparum* RH5 were compared to those of human and chimpanzee BSG.

Based on these results, four of the BSG mutants, C8, H1, H2 and H3, were selected for testing against *Pf*RH5 by SPR.

C8 was selected on the basis of its 'gain' of MEM-M6/6 binding activity in comparison to *Pt*BSG. MEM-M6/6 has previously been shown to block the *Pf*RH5-*Hs*BSG interaction (Crosnier *et al*., 2011), suggesting that its epitope may be located either at or near the *Pf*RH5 interaction surface. The epitope recognised by MEM-M6/8 and MEM-M6/10 is thought to overlap with/be adjacent to the MEM-M6/6 epitope (Koch *et al.*, 1999), H2 was therefore chosen due to its observed 'loss-of-activity', relative to *Hs*BSG, in binding MEM-M6/8 and MEM-M6/10. The invasion of human erythrocytes by *P. falciparum* is inhibited at least partially by

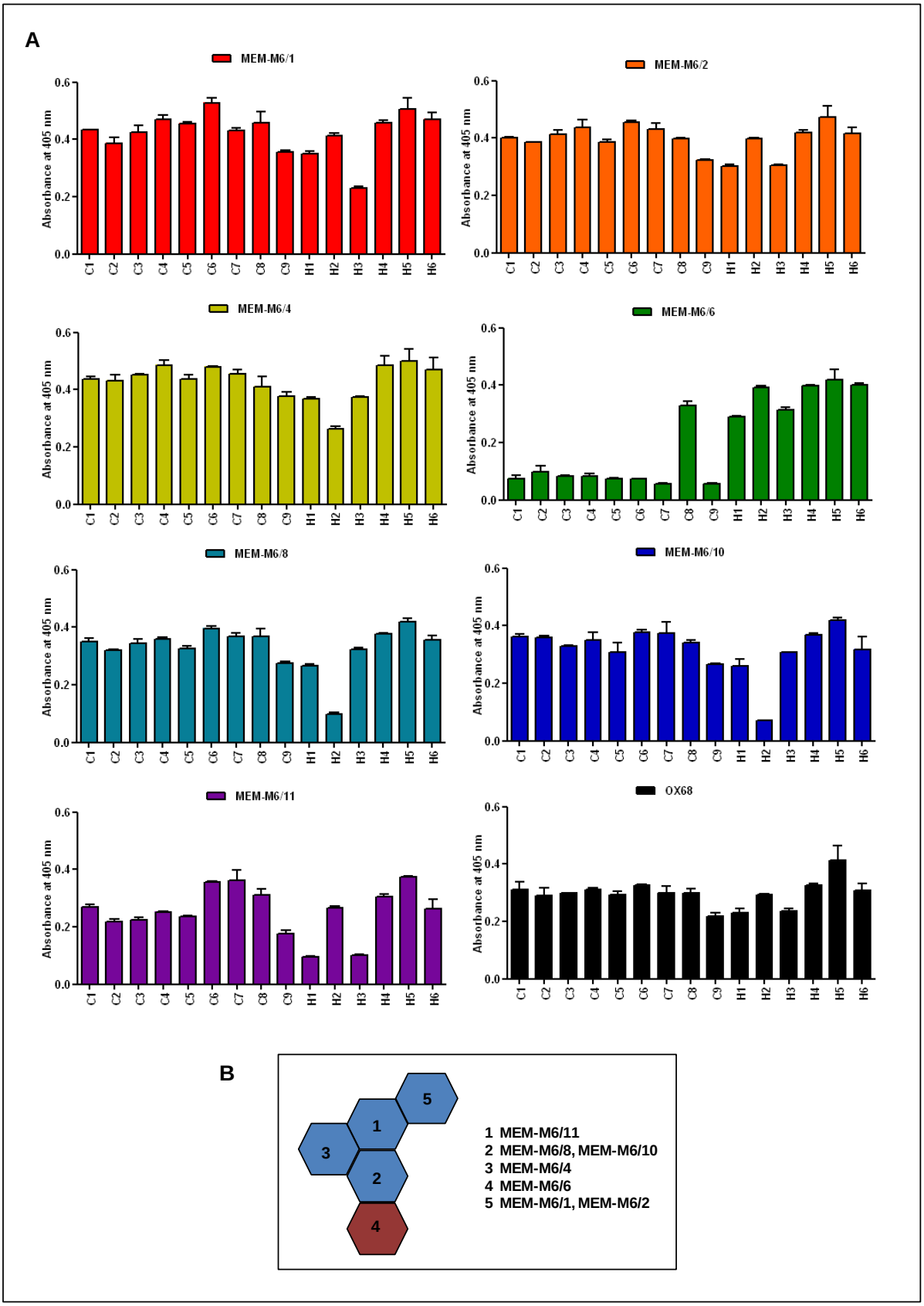
A
MEM-M6/1
MEM-M6/2
MEM-M6/4
MEM-M6/6
MEM-M6/8
MEM-M6/10
MEM-M6/11
OX68
Absorbance at 405 nm
0.0
0.2
0.4
0.6
C1 C2 C3 C4 C5 C6 C7 C8 C9 H1 H2 H3 H4 H5 H6
B
1
2
3
4
5
1 MEM-M6/11
2 MEM-M6/8, MEM-M6/10
3 MEM-M6/4
4 MEM-M6/6
5 MEM-M6/1, MEM-M6/2

Figure 40. The site-directed mutants of *Pt*BSG and *Hs*BSG were immunologically characterised. A) The 15 site-directed mutants of *Hs*BSG and *Pt*BSG, expressed with C-terminal Cd4 and biotin tags, were tested against the panel of seven anti-*Hs*BSG mouse monoclonals by ELISA. OX68 was used as a positive control. The assays were performed on streptavidin-coated plates, using an alkaline phosphatase-conjugated anti-mouse antibody as the secondary. The data are shown as mean ± standard deviation; *n*=2. **B)** A schematic diagram indicating the relation of the epitopes recognised by the seven anti-*Hs*BSG monoclonals, as determined by Koch *et al*. (1999). Each hexagon represents one epitope. The epitopes with adjacent sides are recognised by antibodies which mutually inhibit each other's binding. Epitopes in IgSF domain 1 are shown in blue and that in domain 2 in red.

MEM-M6/1 and MEM-M6/4 (Cecile Crosnier and Zenon Zenonos, unpublished data). The MEM-M6/11 epitope is proposed to be adjacent to both the MEM-M6/1 and MEM-M6/4 epitopes. H1 and H3, which show reduced binding to MEM-M6/11, were hence also included as potential 'loss-of-function' mutants.

In the SPR screen, a 2-fold dilution series of purified *Pf*RH5 was injected across the biotinylated BSG mutants immobilised at equivalent amounts on streptavidin-coated sensor chips. *Hs*BSG and *Pt*BSG were included in the screen as controls (Figure 41 A). The reference subtracted sensorgrams were globally fitted to a 1:1 binding kinetic model to estimate values for the K_D. The K_D estimates for H2 and H3 were similar to that of *Hs*BSG, indicating no significant effect of these mutations on *Pf*RH5 binding. H1 exhibited a 7-fold lower affinity for *Pf*RH5 in comparison with *Hs*BSG, indicating a partial 'loss-of-function', suggesting that the F27L mutation in *Gg*BSG may play a critical role in restricting *Pf*RH5 binding. C8 on the other hand showed a significant 'gain-of-function' with a 4-fold higher affinity for *Pf*RH5 than even *Hs*BSG (Figure 41 B), confirming that the MEM-M6/6 binding site plays a key role in the *Pf*RH5-BSG interaction and suggesting that the K191E mutation in *Pt*BSG may play a key role in reducing affinity for *Pf*RH5.

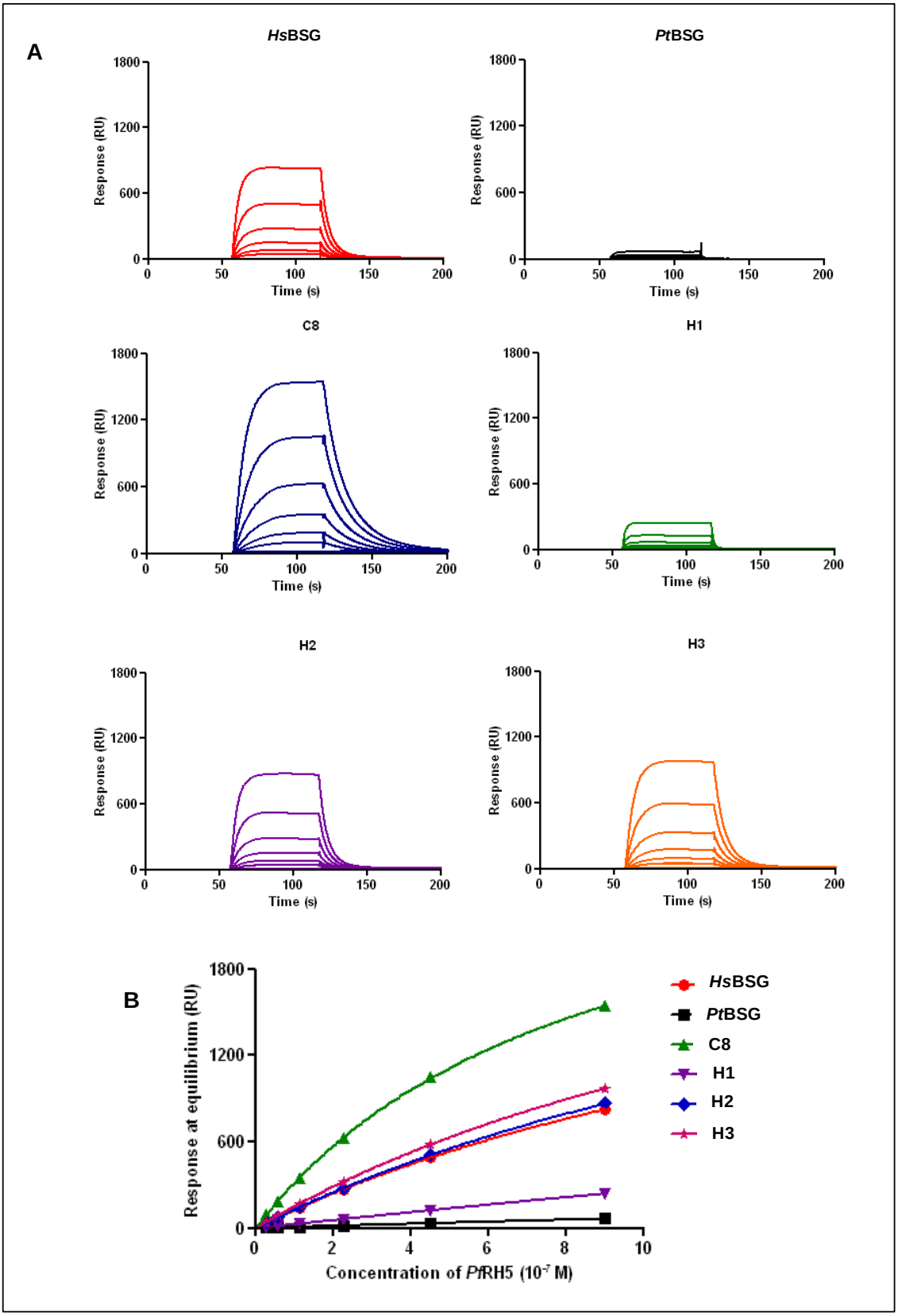
A
HsBSG
PtBSG
C8
H1
H2
H3
Response (RU)
Time (s)
B
Response at equilibrium (RU)
Concentration of PfRH5 (10⁻⁷ M)
HsBSG
PtBSG
C8
H1
H2
H3

Figure 41. Four selected site-directed mutants of cBSG and hBSG were screened against *Pf*RH5, by SPR. The cBSG mutant, C8 and the hBSG mutants, H1, H2 and H3, were tested for binding to *Pf*RH5. The biotinylated BSG mutants were immobilised on streptavidin-coated SPR sensor chips at equivalent amounts and a 2-fold dilution series of purified *Pf*RH5 (0.03-0.9 µM) was injected over the sensor surfaces. Biotinylated hBSG and cBSG were included in the screen as controls. **A)** Reference subtracted sensorgrams from the binding of *Pf*RH5 to the BSG mutants. **B)** A chart showing the binding response at equilibrium *versus Pf*RH5 concentration for each of the BSG mutants. *Pf*RH5 was injected at a flow rate of 20 µl/min, with a contact time of 120 s and a dissociation time of 200 s. The biotinylated baits were immobilised at CHIP 1: Cd4 (reference) - 1362 RU, hBSG- 2774 RU, cBSG-2651 RU and C8-2652 RU; CHIP 2: Cd4 (reference)-1250 RU, H1-2576 RU, H2-2625 RU and H3-2662 RU.

4.3 DISCUSSION

Modern humans share a close evolutionary kinship with chimpanzees and gorillas, with the human-chimpanzee and human-chimpanzee-gorilla speciation events predicted to have occurred only around six and ten million years ago, respectively (Scally *et al*., 2012). These three species of primates share many anatomical and physiological features and have been found to be more than 95% identical in most known protein sequences. The closest relatives of the human malaria parasite, *P. falciparum* are also found within a family of chimpanzee and gorilla parasites, called *Laverania* and *P. falciparum* is even hypothesised to have adapted to humans after a zoonotic transfer event of a predecessor, *P. praefalciparum*, from gorilla (Liu *et al*., 2010; Rayner *et al*., 2011). Despite the genetic similarities between the *Laverania* parasites and among their hosts, in their natural environment, the different *Laverania* species have been observed to be strictly host-specific, with *P. reichenowi*, *P. billcollinsi* and *P. gaboni* restricted to chimpanzees and *P. praefalciparum*, *P. blacklocki* and *P. adleri* found only in gorillas (Liu *et al.*, 2010). The molecular basis of the *Laverania* host-specificity is poorly understood and its investigation is necessarily restricted by the lack of availability of the great ape parasite strains for laboratory-based testing. Chimpanzees and gorillas are also endangered species, so their use as *in vivo* models for experimentation is not ethically acceptable (Rayner *et al*., 2011). In this study, these limitations were overcome by the expression of parasite and great ape proteins recombinantly, thus, enabling interactions between them to be studied directly using *in vitro* biochemical methods.

The potential factors that contribute to the determination of host-specificity in the *Laverania* family may act at the vector/host or parasite/host interfaces. The scope of this study was limited to investigating the possible determinants of host-restriction at the stage of erythrocyte invasion

by the parasite. The process of erythrocyte entry by *Plasmodium* is mediated by interactions between surface proteins on the host and parasite cells (Chapter 1, Section 1.5). *P. falciparum*, the best characterised member of the *Laverania* family, is known to invade erythrocytes using multiple, partially redundant interactions between a broad repertoire of parasite ligands and erythrocyte receptors (Chapter 1, Sections 1.5 and 1.7). The EBL and RH families of parasite invasion ligands are loosely conserved across primate *Plasmodium* species and are known to be important for erythrocyte entry (Miller *et al*., 2002). From the known EBL and RH ligands, two proteins in particular, EBA175 and RH5, have gained attention as central players in erythrocyte invasion by *P. falciparum*. The interaction of RH5 with its erythrocyte receptor, BSG, is essential for invasion (Crosnier *et al*., 2011). The binding of EBA175 to its receptor, Glycophorin A, whilst not essential, is the primary ligand-receptor pair of its type used by many *P. falciparum* strains and invasion in the absence of EBA175 has been shown to almost always occur with lower efficiency (Narum *et al.*, 2000; Duraisingh *et al*., 2003). Both the EBA175-Glycophorin A and RH5-BSG interactions were investigated in this study for their potential contribution towards determining the differential host-species selectivity observed between members of the *Laverania* family.

4.3.1 The EBA175-Glycophorin A interaction may not contribute significantly to the establishment of host-species selectivity in *Laverania*.

The ability of EBA175 RII orthologues from the human parasite, *P. falciparum* and two chimpanzee parasites, *P. reichenowi* and *P. billcollinsi*, to recognise human erythrocytes and purified native human Glycophorin A, was probed using a number of complementary biochemical methods in this study. Native human Glycophorin A rather than recombinant Glycophorin A was used in this study, as the latter had been observed to be non-functional

(Chapter 3, Sections 3.2.5 and 3.2.6). The three EBA175 RII orthologues, produced in soluble recombinant form and multimerised by direct immobilisation on fluorescent beads, showed trypsin and neuraminidase-sensitive, but chymotrypsin-resistant association with human erythrocytes (Section 4.2,2, Figure 28). These properties are in agreement with the sialic-acid dependent recognition of Glycophorin A (a trypsin-sensitive, but chymotrypsin-resistant receptor) on the erythrocyte surface, by these orthologues (Camus and Hadley, 1985). However, to confirm binding of these orthologues to human Glycophorin A, their recognition of native Glycophorin A, extracted from human erythrocytes, was tested directly using an ELISA-based approach (Section 4.2.3). This assay revealed preferential binding of the EBA175 RII orthologues to sialylated human Glycophorin A over its asialylated derivative (Figure 29 C). The magnitude of the binding responses observed with *Pr*EBA175 RII and *Pb*EBA175 RII were somewhat lower in comparison to *Pf*EBA175 RII. Whilst this was suggestive of a lower affinity of the chimpanzee parasite proteins for human Glycophorin A, it could also have been due to the unpurified culture supernatants used for this assay containing different levels of functional EBA175. To circumvent this confounding factor, SPR was used to probe these interactions further. Prior to the SPR experiment, the EBA175 RII orthologues, purified from the culture supernatant by affinity chromatography, were subjected to gel filtration. The elution profiles were suggestive of the proteins being primarily monomeric (Figure 30 B). When the EBA175 RII orthologues were tested against native sialylated Glycophorin A, immobilised on a SPR sensor chip, a difference in the magnitude of the binding response was yet again observed between *Pf*EBA175 RII and *Pr*/*Pb*EBA175 RII (Figure 30 C). Equilibrium analysis of the reference-subtracted sensorgrams revealed an approximately 2-fold lower affinity of *Pr*/*Pb*EBA175 RII for human Glycophorin A, relative to *Pf*EBA175 RII (Section 4.2.4). Based

on previous studies, this ~2-fold lower affinity of *Pr/Pb*EBA175 RII for human Glycophorin A, could be attributed to a lower preference for the Neu5Ac found on the human protein (Section 4.1.2). The scale of the difference in *Pr/Pf*EBA175RII binding to human Glycophorin A was found to be much greater in previous studies, but this is likely due to differences in the assays being used, with the SPR assay used here giving a much greater range and sensitivity than previous cell-based assays (Martin *et al.*, 2005).

By co-crystallisation of *Pf*EBA175 RII with the substrate analogue, α-2,3-sialyllactose (containing Neu5Ac (α-2,3) Gal, essential for the recognition of human Glycophorin A by *Pf*EBA175), Tolia *et al.* (1995) identified the amino acid residues that were in contact with glycans at six potential binding sites (Chapter 3, Section 3.1.1). Comparison of 17 such 'glycan-binding' residues between *P. falciparum*, *P. reichenowi* and *P. billcollinsi* EBA175 RII sequences, revealed that 10 are conserved in all three species (Table 6). From the remaining seven, three each were conserved only either between *Pf*EBA175 RII and *Pr*EBA175 RII or between *Pf*EBA175RII and *Pb*EBA175 RII. Only one residue, located at position 697, was observed to be divergent in both *Pr*EBA175 RII and *Pb*EBA175 RII from *Pf*EBA175 RII. Overall, ~76% of the 'glycan-binding' residues found in *Pf*EBA175 RII were conserved in *Pr*/*Pb*EBA175 RII. This relatively high conservation of 'glycan-binding' residues may account for the fairly low difference in affinity observed between *Pf*EBA175 RII and *Pr*/*Pb*EBA175 RII, for Neu5Ac-carrying human Glycophorin A.

Glycan	Residue number	*Pf*EBA175	*Pr*EBA175	*Pb*EBA175	DBL domain
1/2	583	K	K	R	F2
	586	D	D	D	F2
	172	K	K	K	F1
3/4	694	N	N	N	F2
	695	N	N	N	F2
	696	Y	N	Y	F2
	697	K	R	T	F2
	698	M	I	M	F2
	177	N	N	N	F1
5/6	484	T	T	T	F2
	485	K	K	K	F2
	486	D	D	V	F2
	487	V	V	I	F2
	559	Y	Y	Y	F2
	686	Q	I	Q	F2
	690	Y	Y	Y	F2
	173	N	N	N	F1

Table 6. The conservation of residues at six 'glycan-binding' sites between the EBA175 orthologues from *P. falciparum, P. reichenowi* and *P. billcollinsi*. 17 EBA175 residues identified by Tolia *et al.* (2005) as being in contact with glycans at six putative binding sites in the *Pf*EBA175RII+α-2,3-sialyllactose co-crystal structure were compared between the EBA 175 orthologues. Residues identical between all three orthologues are highlighted in dark pink. Residues identical only between *Pf*EBA175 and either *Pr*EBA175 or *Pb*EBA175 are highlighted in light pink.

4.3.2 The RH5-BSG interaction is likely to be a significant determinant of *Laverania* host-specificity.

The RH5 orthologues from *P. falciparum* and *P. reichenowi* were tested for species-specific interactions with human erythrocytes and with recombinantly-expressed BSG orthologues from human, chimpanzee and gorilla, in this study. The *Pf*RH5 and *Pr*RH5 orthologues share approximately 68% sequence identity (Figure 31), however, *Pr*RH5 was not recognised by any of 26 mouse monoclonal antibodies binding to *Pf*RH5 (Figure 32 C). Even a rabbit polyclonal raised against *Pf*RH5 exhibited only barely detectable binding to *Pr*RH5 (Figure 32 D). This data suggests that immunogenic, surface-exposed regions may not be well conserved between *Pf*RH5 and *Pr*RH5. Similar, neuraminidase-insensitive, low-level binding to human erythrocytes was observed with both *Pf*RH5 and *Pr*RH5 (Figures 33 A and B). The interaction of *Pf*RH5 with *Hs*BSG is known to be sialic-acid independent, moreover, the level of expression of BSG on the surface of human erythrocytes is relatively low (in comparison to Glycophorin A, Figures 33 C and D). Therefore, the properties of the observed interactions of *Pf*RH5 and *Pr*RH5 with human erythrocytes are consistent with the recognition of BSG on the erythrocyte surface. However, *Pr*RH5 showed no detectable binding to *Hs*BSG, *Pt*BSG or *Gg*BSG when tested directly against these recombinant proteins, both by AVEXIS and by SPR (Figures 36, 37 and 38). One possible explanation for the observed behaviour of *Pr*RH5 is its recognition of a receptor other than BSG on the chimpanzee erythrocyte surface. The observation by Hayton *et al*. (2008) of 28 kDa fragments of *Pf*RH5 proteins carrying different polymorphisms recognising different erythrocyte proteins, supports this theory of a possible 'receptor-switch', between hosts.

In this study, *Pf*RH5 was observed to bind to *Pt*BSG with an affinity 15-fold lower than that for *Hs*BSG and no interaction could be detected between *Pf*RH5 and *Gg*BSG (Figures 37, 37, 38

and 39), suggesting clear host-species selectivity in receptor recognition. To identify residues that confer this specificity, site-directed mutants of *Pt*BSG and *Hs*BSG were generated and a selection of these was tested against *Pf*RH5 in a preliminary screen (Table 6 and Figure 41). Both IgSF domains 1 and 2 of *Hs*BSG have been implicated in *Pf*RH5 binding (Crosnier *et al*., 2011). *Pt*BSG is different from *Hs*BSG only in nine residues, all located in domain 2 (Figure 34). Possible 'gain-of-function' *Pt*BSG mutants were made by replacing these divergent residues with the corresponding *Hs*BSG residues (Table 5). *Hs*BSG is different from *Gg*BSG in both domains 1 and 2 and potential 'loss-of-function' *Hs*BSG mutants were produced by replacing six variant residues (five located in domain 1 and one in domain 2) with those found in *Gg*BSG at the equivalent positions (Figure 34 and Table 5).

*Pt*BSG was not recognised by the anti-hBSG monoclonal MEM-M6/6 (Figure 35). This monoclonal has previously been shown to inhibit the interaction between *Hs*BSG and *Pf*RH5, suggesting that its epitope is likely to be located either at/near the *Pf*RH5 binding site on *Hs*BSG (Crosnier *et al*., 2011). The MEM-M6/6 epitope was however observed to have been 'recovered' in one of the *Pt*BSG mutants, C8 (E191K) and testing this mutant by SPR revealed complete restoration of *Pf*RH5 binding (Figures 40 and 41). Indeed, the affinity of this mutant for *Pf*RH5 was even 4-fold higher than that of *Hs*BSG. The data therefore suggest that the single residue difference between *Hs*BSG and *Pt*BSG at position 191 is responsible for the much weaker binding of *Pf*RH5 by *Pt*BSG relative to *Hs*BSG. Residue 191 is located in an accessible β-turn region proximal to the IgSF domain 1 and a change at this position from a positively-charged amino acid (found in *Hs*BSG) to a negatively-charged one (found in *Pt*BSG) seems likely to have a significant influence (Yu *et al*., 2008 and Figure 42).

*Gg*BSG was not recognised by the anti-*Hs*BSG monoclonals, MEM-M6/8 and MEM-M6/11, and also showed reduced binding to MEM-M6/10 (Figure 35). The epitope recognised by MEM-M6/8 and MEM-M6/10 is predicted to overlap with/be adjacent to the MEM-M6/6 epitope, whereas the MEM-M6/11 epitope is postulated to be proximal to both MEM-M6/1 and MEM-M6/4 epitopes (Koch *et al*., 1999). In addition to MEM-M6/6, both MEM-M6/1 and MEM-M6/4 have been observed to block the *Pf*RH5-*Hs*BSG interaction at least partially and their epitopes are therefore also likely to be close to the *Pf*RH5 binding site on *Hs*BSG (Cecile Crosnier and Zenon Zenonos, unpublished data).

From the *Hs*BSG mutants, H2 (D32E) showed no binding to both MEM-M6/8 and MEM-M6/10, suggesting that residue D32 is part of the MEM-M6/8+ MEM-M6/10 epitope (Figure 40). H1 (F27L) and H3 (K75E) mutants showed reduced binding to MEM-M6/11, indicating a change in these mutants close to the *Pf*RH5-*Hs*BSG interaction surface (Figure 40). Analysis of the H1, H2 and H3 mutants by SPR revealed that H2 and H3 bind to *Pf*RH5 with almost the same affinity as *Hs*BSG, indicating no significant 'loss-of-function' (Figure 41). H1 however showed a 7-fold lower affinity for *Pf*RH5 than *Hs*BSG, indicating that the change at position 27 of the primary sequence from the aromatic residue tryptophan (found in *Hs*BSG) to the non-aromatic residue leucine (found in *Gg*BSG), is one likely contributing factor to the inability of *Gg*BSG to bind *Pf*RH5. In *Hs*BSG, F27 is solvent-exposed and located on a β-strand constituting IgSF domain 1 (Yu *et al*., 2008, Figure 42).

Overall, the data from the screen of BSG mutants suggests that the residues K191 and F27 of *Hs*BSG are important for the interaction with *Pf*RH5 and that the non-conservation of these residues in *Pt*BSG and *Gg*BSG respectively may be responsible (at least partially in the case of *Gg*BSG) for the observed host-specificity of *Pf*RH5 binding.

Residue E92, located on a β-turn region of domain 1, has previously been identified to be important for the binding of *Hs*BSG to *Pf*RH5 (Crosnier *et al*., 2011). The mutation E92K, responsible for the Ok^{a-} blood type, has been shown to decrease the affinity of *Hs*BSG for *Pf*RH5 by 2-fold (Crosnier *et al*., 2011). In the X-ray crystal structure of *Hs*BSG, K191 is located ~27 Å and ~37 Å from F27 and E92 respectively, whereas F27 and E92 are located ~16 Å apart across domain 1 (Yu *et al*., 2008). Protein-protein interaction surfaces are in general fairly large, with standard sizes ranging from ~1200-~2000 $Å^2$, therefore the three residues, K191, F27 and E92 are all likely to be accommodated in the *Pf*RH5 binding site of BSG (Moreira *et al*., 2007).

4.4 CONCLUSION

In this study, only a 2-fold difference in the affinity for human Glycophorin A was observed between the EBA175 RII orthologues from *P. falciparum, P. reichenowi* and *P. billcollinsi*, suggesting that the EBA175RII-Glycophorin A interaction may not be a significant determinant of the observed host-selectivity within the *Laverania* family, unlike previous suggestions (Martin *et al.*, 2005). *P. falciparum* RH5 on the other hand showed clear host-species specificity in its binding of Basigin orthologues from human, chimpanzee and gorilla. No binding of *P. falciparum* RH5 to gorilla BSG was observed and its binding to chimpanzee BSG was approximately 15-fold weaker than its interaction with human BSG. The binding of *P. falciparum* RH5 to human BSG is essential for the invasion of human erythrocytes by the parasite, therefore the relative differences in the interactions of *P. falciparum* RH5 with chimpanzee and gorilla Basigin, may account for the observed lack of *P. falciparum* infection in their wild-living populations. This study only investigated the contributions of two known parasite ligand-erythrocyte receptor interactions towards host-species selection amongst *Laverania* parasites. In order to gain a more complete understanding of how host selectivity of

Laverania is imposed at the stage of erythrocyte entry, the systematic approach used in this study should necessarily be extended to other known parasite ligand-host receptor interactions, such as RH4-CR1.

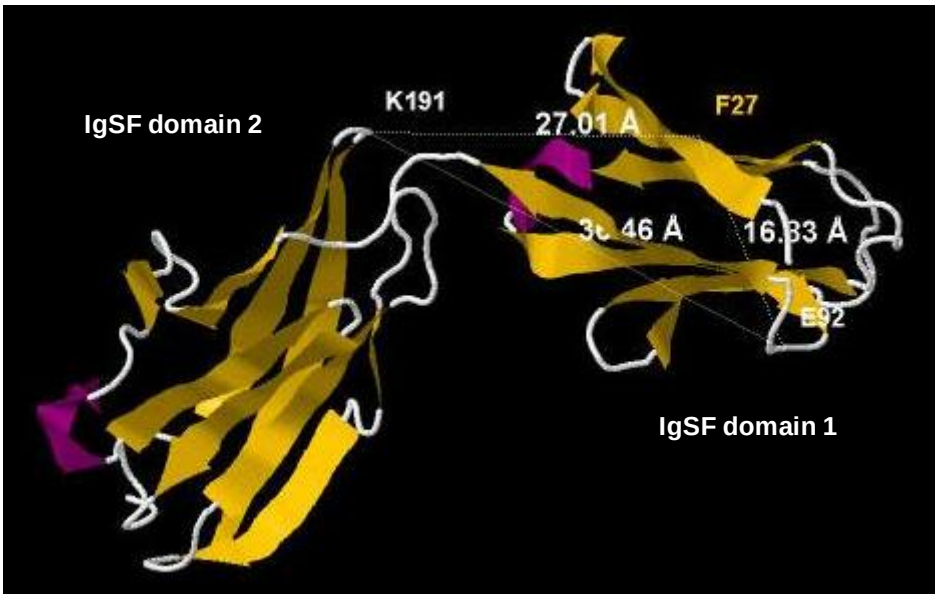

Figure 42. The structural organisation of the two IgSF domains of *Hs*BSG with the positions of the residues implicated in *Pf*RH5 binding, K191, F27 and E92 annotated. A schematic representation of the X-ray crystal structure of *Hs*BSG as determined by Yu *et al*. (2008) is shown (PDB ID: 3B5H). The residues predicted to be located at the *Pf*RH5 binding site are indicated with the approximate distances between them, K191-F27: 27.01 Å, K191-E92: 36.46 Å, F27-E92: 16.33 Å.

4.5 BIBLIOGRAPHY

Baum, J., Chen, L., Healer, J., Lopaticki, S., Boyle, M., Triglia, T., Ehlgen, F., *et al*. (2009). Reticulocyte-binding protein homologue 5 - an essential adhesin involved in invasion of human erythrocytes by *Plasmodium falciparum*. *International Journal for Parasitology, 39*(3), 371-80.

Blacklock, B. & Adler, S. (1922) A parasite resembling *Plasmodium falciparum* in a chimpanzee. *Annals of Tropical Medicine and Parasitology,16*, 99-106.

Camus, D., & Hadley, T. J. (1985). A *Plasmodium falciparum* antigen that binds to host erythrocytes and merozoites. *Science, 230*(4725), 553-556.

Crosnier, C., Bustamante, L. Y., Bartholdson, S. J., Bei, A. K., Theron, M., Uchikawa, M., Mboup, S., *et al*. (2011). Basigin is a receptor essential for erythrocyte invasion by *Plasmodium falciparum*. *Nature, 480*(7378), 534-7.

Duraisingh, M. T., Maier, A. G., Triglia, T., & Cowman, A. F. (2003). Erythrocyte-binding antigen 175 mediates invasion in *Plasmodium falciparum* utilizing sialic acid-dependent and -independent pathways. *Proceedings of the National Academy of Sciences of the United States of America, 100*(8), 4796-801.

Duval, L., Fourment, M., Nerrienet, E., Rousset, D., Sadeuh, S. A., Goodman, S. M., Andriaholinirina, N. V., *et al*. (2010). African apes as reservoirs of *Plasmodium falciparum* and the origin and diversification of the Laverania subgenus. *Proceedings of the National Academy of Sciences of the United States of America, 107*(23), 10561-6.

Duval, L., & Ariey, F. (2012). Ape *Plasmodium* parasites as a source of human outbreaks. *Clinical Microbiology and Infection, 18*(6), 528-32.

Flicek, P., Amode, M. R., Barrell, D., Bea,l K., Brent, S., Chen, Y., Clapham, P., *et al.* (2011). Ensembl 2011. *Nucleic Acid Research,39*, D800-6

Hayton, K., Gaur, D., Liu, A., Takahashi, J., Henschen, B., Singh, S., Lambert, L., *et al*. (2008). Erythrocyte binding protein PfRH5 polymorphisms determine species-specific pathways of *Plasmodium falciparum* invasion. *Cell Host & Microbe, 4*(1), 40-51.

Koch, C., Staffler, G., Hüttinger, R., Hilgert, I., Prager, E., Cerný, J., Steinlein, P., *et al*. (1999). T cell activation-associated epitopes of CD147 in regulation of the T cell response, and their definition by antibody affinity and antigen density. *International Immunology, 11*(5), 777-86.

Larkin, M. A., Blackshields, G., Brown, N. P., Chenna. R., McGettigan, P. A., McWilliam, H., *et al*. (2007) Clustal W and Clustal X version 2.0. *Bioinformatics, 23*(21), 2947-8.

Liu, W., Li, Y., Learn, G., Rudicell, R., & Robertson, J. (2010). Origin of the human malaria parasite *Plasmodium falciparum* in gorillas. *Nature*, *467*(7314), 420-425.

Martin, M. J., Rayner, J. C., Gagneux, P., Barnwell, J. W., & Varki, A. (2005). Evolution of human-chimpanzee differences in malaria susceptibility: relationship to human genetic loss of N-glycolylneuraminic acid. *Proceedings of the National Academy of Sciences of the United States of America*, *102*(36), 12819-24.

Miller, L. H., Baruch, D. I., Marsh, K., & Doumbo, O. K. (2002). The pathogenic basis of malaria. *Nature*, *415*(6872), 673-9.

Moreira, I. S., Fernandes, P. A., & Ramos, M. J. (2007). Hot spots—A review of the protein–protein interface determinant amino-acid residues. *Proteins*, *68*(4), 803-12.

Muchmore, E. A., Diaz, S., & Varki, A. (1998). A structural difference between the cell surfaces of humans and the great apes. *American Journal of Physical Anthropology*, *107*(2), 187-98.

Narum, D. L., Haynes, J. D., Fuhrmann, S., Liang, H., Hoffman, S. L., Sim, B. K. L., Moch, K., *et al*. (2000). Antibodies against the *Plasmodium falciparum* receptor binding domain of EBA-175 block invasion pathways that do not involve sialic acids. *Infection and Immunity*, *68*(4), 1964-6.

Ozwara, H., Kocken, C. H., Conway, D. J., Mwenda, J. M., & Thomas, A. W. (2001). Comparative analysis of *Plasmodium reichenowi* and *P. falciparum* erythrocyte-binding proteins reveals selection to maintain polymorphism in the erythrocyte-binding region of EBA-175. *Molecular and Biochemical Parasitology*, *116*(1), 81-4.

Prugnolle, F., Ayala, F., Ollomo, B., Arnathau, C., Durand, P., & Renaud, F. (2011). *Plasmodium falciparum* is not as lonely as previously considered. *Virulence*, *2*(1), 71-76.

Rayner, J. C., Liu, W., Peeters, M., Sharp, P. M., & Hahn, B. H. (2011, May). A plethora of Plasmodium species in wild apes: a source of human infection? *Trends in Parasitology*,*27*(5), 222-9.

Scally, A., Dutheil, J. Y., Hillier, L. W., Jordan, G. E., Goodhead, I., Herrero, J., Hobolth, A., *et al*. (2012). Insights into hominid evolution from the gorilla genome sequence. *Nature*, *483*(7388), 169-175.

Sharp, P. M., Liu, W., Learn, G. H., Rayner, J. C., Peeters, M., & Hahn, B. H. (2011). Source of the human malaria parasite *Plasmodium falciparum*. *Proceedings of the National Academy of Sciences of the United States of America*, *108*(38), E744-5.

Sim, B. K. L., Narum, D. L., Chattopadhyay, R., Ahumada, A., Haynes, J. D., Fuhrmann, S. R., Wingard, J. N., *et al*. (2011). Delineation of stage specific expression of *Plasmodium falciparum* EBA-175 by biologically functional region II monoclonal antibodies. *PloS One*, *6*(4), e18393.

Yu, X. L., Hu, T., Du, J. M., Ding, J. P., Yang, X. M., Zhang, J., Yang, B., *et al*. (2008). Crystal structure of HAb18G/CD147: implications for immunoglobulin superfamily homophilic adhesion. *The Journal of Biological Chemistry*, *283*(26), 18,056-65.

Zdobnov, E. M., Apweiler, R. (2001). InterProScan--an integration platform for the signature-recognition methods in InterPro. *Bioinformatics*, *17*(9), 847-8.

Chapter 5

Development of high-throughput assays for characterising a library of *P. falciparum* merozoite surface proteins

5.1 INTRODUCTION

5.1.1 Cell surface proteins of the human erythrocyte.

The cell surface protein repertoire of human erythrocytes has been studied extensively over the past five decades and more than 300 membrane-associated proteins have now been identified with the use of high-resolution mass-spectrometry based approaches (Kakhniashvili *et al*., 2004; Pasini *et a*l., 2006; Speicher, 2006; Pasini *et al*., 2010). Proteomic studies of erythrocyte membranes have revealed a very broad range of protein expression levels, with the highly abundant proteins such as Glycophorin A and Band 3 being present at ~10^6 copies/cell and others with very low abundance, including CR1, being available only at a few hundred copies/cell (Pasini *et al*., 2006). Lateral diffusion of membrane proteins along the plane of the lipid bilayer has been demonstrated to be restricted in certain cases by direct or indirect interactions with the spectrin-based cytoskeleton, which likely facilitates compartmentalisation of these proteins in specialised membrane domains such as the cholesterol-rich lipid rafts (Koppel *et al*., 1981; Tomishige *et al*., 1998). Proteins resident in lipid rafts have been observed to be recruited to the host-derived parasitophorous vacuolar membrane that surrounds the intra-erythrocytic stages of *Plasmodium* and are proposed to be important for parasite entry (Murphy *et al*., 2006).

5.1.2 The role of host-cell surface multi-pass membrane proteins in the invasion of erythrocytes by *Plasmodium* merozoites.

Multi-pass membrane proteins, comprising of two or more transmembrane domains, account for a major fraction of the total surface protein complement of the human erythrocyte. Many of these act as transporters and play important roles in nutrient import, regulation of cell volume and ionic balance (Pasini *et al*., 2006). A few of the multi-pass proteins, including the Duffy antigen

receptor for chemokines, Aquaporin 1 and Glucose transporter 1 are enriched in lipid rafts and trafficked to the parasitophorous vacuole of *Plasmodium* (Murphy *et al*., 2006).

A definitive role in erythrocyte invasion by *Plasmodium* has so far been identified only for one multi-pass protein, the Duffy antigen, a seven transmembrane G protein-coupled protein that also acts as a promiscuous receptor for several chemokines (Barnwell *et al*., 1989; de Brevern *et al*., 2005). The interaction of the Duffy antigen with the Duffy binding protein (DBP) from *P. vivax* and *P. knowlesi* is critical for invasion of human erythrocytes by these parasites. The Region II (RII) of the DBP ectodomain containing a single DBL (Duffy binding-like) domain is sufficient for binding to Duffy (Chitinis and Miller, 1994). Most of the biochemical characterisation of the Duffy-DBP interaction has been performed using recombinantly expressed DBP RII. Antibodies directed against *Pv*DBP RII inhibit erythrocyte invasion by the parasite *in vitro* and provide clinical protection against *P. vivax* infection in children, therefore *Pv*DBP RII is currently a leading vaccine candidate against *P. vivax* malaria (Grimberg *et al*., 2007; King *et al*., 2008). A single point mutation in the upstream promoter region of the Duffy gene (T→C, at position -33) that confers resistance from *P. vivax* and *P. knowlesi* infection by abolishing expression of the receptor, has been observed to be under strong positive selection in a number of human populations, reaching almost fixation in west and central Africa (Miller *et al*., 1975; Miller *et al*., 1976; Zimmerman *et al*., 1999). A 35-amino acid peptide comprising residues 8-42 of the N-terminal extracellular region of Duffy has been shown to inhibit the binding of *P. vivax* DBP (*Pv*DBP) to human erythrocytes, indicating the involvement of the corresponding region of the Duffy antigen in *Pv*DBP recognition (Chitnis *et al*., 1996). This region of Duffy also carries the antigenic determinant of the Fy^a and Fy^b blood groups. The Fy^a and Fy^b forms are characterised by Asp and Gly at position 42 respectively and a recent study has demonstrated ~50% lower

binding of *Pv*DBP to Fy^a in comparison to Fy^b (King *et al*., 2011). The Duffy antigen was previously thought to be essential for the invasion of human erythrocytes by *P. vivax*, but the recent identification of *P. vivax* infections in Duffy-negative individuals in Madagascar has called this universality into question (Ménard *et al*., 2010).

The Duffy antigen, while perhaps not essential, clearly plays a crucial function in *P. vivax* and *P. knowlesi* infections, however, a role for this multi-pass receptor has not yet been identified in erythrocyte invasion by *P. falciparum*.

Several independent lines of investigation have revealed a possible involvement of another multi-pass protein, Band 3, in *P. falciparum* infection. Band 3 consists of an N-terminal cytoplasmic domain linked to the spectrin-based cytoskeleton and a C-terminal transmembrane domain that functions as an anion transporter (Wang *et al*., 1993; Beckmann *et al*., 1998; Hassoun *et al*., 1998). The precise number of membrane-spanning helices in the C-terminal domain of Band 3 is not known, but predictions from topology modelling range from 11-14 (Tanner, 1997; Ota *et al*., 1998, Table 7). Invasion of human erythrocytes by *P. falciparum* has been observed to be inhibited by liposomes containing Band 3 and by a monoclonal antibody raised against Band 3 (Miller *et al*., 1983; Okoye and Bennett, 1985; Clough *et al*., 1995). Short peptides containing amino-acid stretches found in the extracellular regions of Band 3 have also been demonstrated to inhibit invasion of erythrocytes by *P. falciparum*, albeit at relatively high concentrations (Goel *et al*., 2003). These Band 3 peptides have been seen to bind to processed fragments of MSP1, $MSP1_{42}$ and $MSP1_{19}$ but interestingly not to full-length MSP1, suggesting that processing of MSP1 is perhaps necessary for the interaction with Band 3 (Goel *et al*., 2003).

Apart from the studies of Band 3 mentioned above, the role of multi-pass receptors in the invasion of erythrocytes by *P. falciparum* has not been investigated.

5.1.3 The recognition of glycan moieties on erythrocyte surface receptors by *Plasmodium* ligands.

Many of the proteins on the erythrocyte surface membrane are glycosylated and structural polymorphisms in glycans form the basis of several blood groups such as ABH, Lewis, T and Tn (King, 1994). Sialic acid moieties displayed on erythrocyte receptors are known to play an important role in the invasion of human erythrocytes by *P. falciparum* and indeed, the recognition of erythrocyte receptors by *P. falciparum* proteins has classically been categorised as being either sialic acid-dependent or independent. Of the known erythrocyte receptor-parasite protein interactions, the recognition of Glycophorins A, B and C by their respective *P. falciparum* ligands are all dependent on the presence of terminal sialic acid moieties (Camus & Hadley, 1985; Maier *et al*., 2002; Mayer *et al*., 2009). The interactions of *P. falciparum* surface proteins with glycans other than sialic acid are, however, relatively unknown.

5.1.4 Strategies for detecting and characterising interactions between erythrocyte and *Plasmodium* merozoite surface proteins.

The traditional biochemical assays used for investigating the interactions between erythrocyte receptors and *Plasmodium* ligands are relatively time consuming and laborious and are not suitable for use in high-throughput screening.

The original approach used by Camus and Hadley (1985) to identify EBA175, involved incubation of radio-labelled spent *P. falciparum* culture supernatant with erythrocytes, elution of specifically-bound supernatant proteins in a high salt solution and analysis of eluted proteins by SDS-PAGE and autoradiography. In these first reported studies, non-adherent proteins were removed by washing alone. The specificity of the assay was later improved by centrifugation of erythrocytes through silicone oil, after incubation with parasite supernatant, to remove non-

bound and weakly-bound supernatant proteins (Tran *et al*., 2005; Tham *et al*., 2009). The sensitivity of the detection step has also been enhanced by incorporation of Western blot procedures with protein-specific immuno-probes (Mayer *et al*., 2001; Narum *et al*., 2002).

Erythrocyte rosetting assays have also been used to map the specific binding sites of erythrocyte receptors on their known *Plasmodium* ligands. For example the sufficiency of the DBL domain-containing RII of *Pf*EBA175 and *Pv*DBP for erythrocyte binding was discovered by expressing fragments of the ectodomains of these proteins on the surface of COS cells and visually counting the aggregates (or rosettes) of erythrocytes around the transfected cells (Sim, 1995; Chitinis and Miller, 1994).

A simpler and less subjective approach for detecting binding of recombinant *Plasmodium* proteins to erythrocytes has recently been demonstrated using *Pv*DBP RII as an example (Tran *et al*., 2005). In this assay, a fluorescently-labelled anti-His antibody was used to detect the association of His tagged-*Pv*DBP RII with erythrocytes by flow cytometry. This assay is amenable for use in high-throughput screening, however, the requirement for purified *Plasmodium* proteins at relatively high (~50 µg/ml) concentrations to achieve clear binding, (probably due to the Duffy antigen-DBP interaction being of low affinity, a common property of cell surface protein-protein interactions), is a major drawback.

5.1.5 Work described in this chapter.

The work in this chapter was aimed at applying new approaches to investigate the roles of multi-pass transmembrane proteins and glycans in *P. falciparum* erythrocyte recognition, both of which are under-explored as potential receptors. The library of *P. falciparum* merozoite surface proteins introduced in Chapter 1 (Section 1.13) has previously been screened against a panel of single-pass erythrocyte surface proteins, expressed as full-length ectodomain fragments, by

AVEXIS (Cecile Wright-Crosnier, unpublished data). The AVEXIS platform however requires all proteins to be expressed in soluble form and is therefore not applicable to erythrocyte multi-pass membrane proteins, which are difficult to express as correctly folded amphiphilic fragments. In this study, 33 of the highest-expressing merozoite surface proteins from the library were screened against 41 erythrocyte multi-pass receptors (including two isoforms each of three proteins), using a flow cytometry-based approach derived from the assay developed previously for detecting the association of EBA175 and RH5 proteins to human erythrocytes (Chapters 3 and 4). The multi-pass proteins were each individually expressed on the surface of HEK293E cells by transient transfection and then used as 'baits' for *P. falciparum* proteins that had been multimerised by immobilisation on fluorescent beads. Putative interactions between the merozoite proteins and the multi-pass receptors were detected using flow cytometry (Figure 43). Prior to probing against the multi-pass receptors, the merozoite proteins were pre-screened against erythrocytes for specific interactions. A small subset of selected merozoite proteins were also subsequently tested against a panel of synthetic carbohydrate probes in a preliminary screen to identify potential glycan-binding activities.

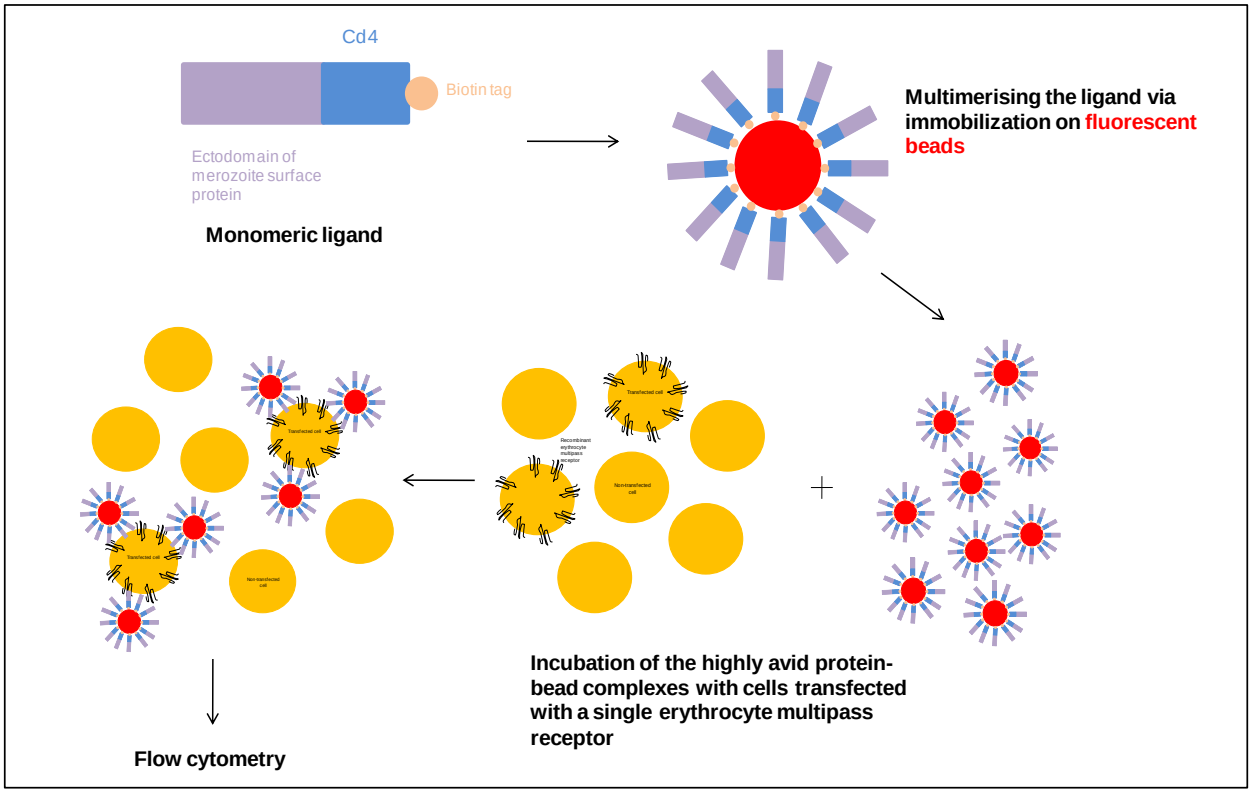

Figure 43. A schematic of the high-throughput screen used for identifying putative interactions between erythrocyte multi-pass receptors and *P. falciparum* merozoite surface proteins. In the screen, 33 merozoite surface proteins were tested individually against each of 41 erythrocyte multi-pass receptors**.** The ectodomain of each merozoite surface protein, produced recombinantly in fusion with rat Cd4 and a C-terminal biotin tag, was multimerised by clustering around streptavidin-coated Nile Red fluorescent beads. These multivalent ligand arrays were then be presented to HEK293E cells that had been transiently transfected with the expression construct for a single erythrocyte multi-pass receptor (in general only a certain fraction of the cell population displayed the recombinant multi-pass receptor , as transfection efficiency was < 100%) ; binding events were detected by flow cytometry.

5.2 RESULTS

5.2.1 40% of the *P. falciparum* merozoite surface proteins tested showed some association with human erythrocytes.

33 of the highest-expressing members of the *P. falciparum* merozoite surface protein library were selected for further characterisation in this study. Prior to testing against erythrocytes and recombinantly expressed erythrocytic multi-pass receptors, the merozoite proteins, produced in the monomeric form with C-terminal Cd4 and biotin tags, were immobilised on streptavidin-coated Nile red beads as described before (Chapter 3, Section 3.2.2). Multimerisation of the *Plasmodium* proteins on the bead-scaffolds was performed to potentially increase the avidity of their interactions with erythrocytic receptors, thereby prolonging them (increasing the half-lives) and facilitating their detection. The *Plasmodium* proteins were expressed using the HEK293E system and the cell culture supernatants containing the proteins were used in the assays with no pre-purification. The minimum amount of each protein necessary for saturating a uniform number of beads was assessed by ELISA individually (Figure 44). This assessment was deemed necessary, as non-saturation of beads with protein could decrease the avidity of the resulting arrays, whereas the presence of excess amounts of free (non-bead bound) protein could potentially act in an inhibitory manner against the binding of the arrays to erythrocytes.

The proteins arrayed on Nile red beads were presented to erythrocytes and binding was analysed by flow cytometry. The number of erythrocytes (as a percentage of total) binding to each protein was calculated based on a fluorescence intensity threshold, set with reference to the binding to Cd4-coated beads (negative control) and to EBA175-coated beads (positive control) (Figure 45 A). Although 13 out of the 33 proteins tested showed some association with erythrocytes, the

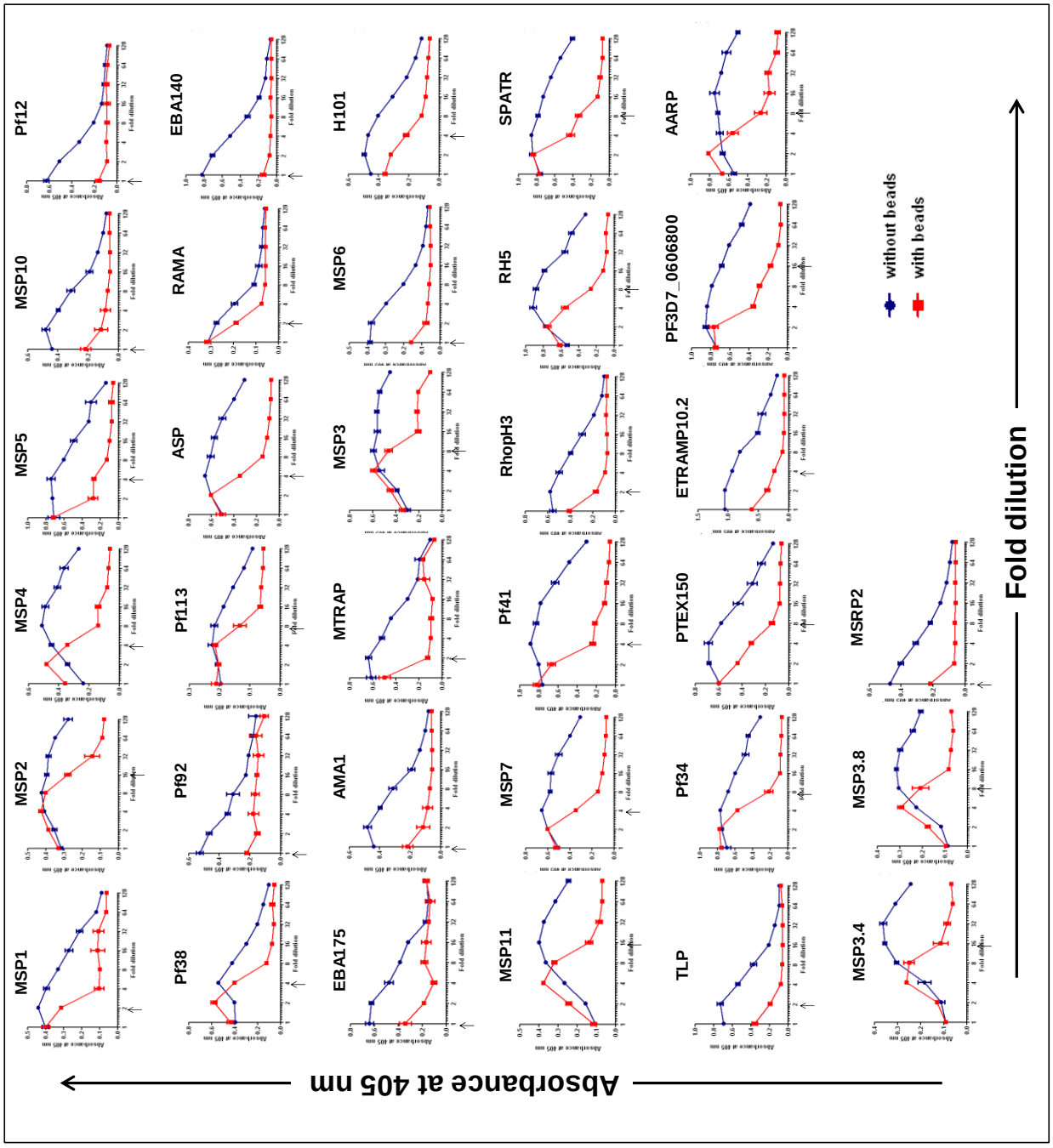
Absorbance at 405 nm
Fold dilution
without beads
with beads
Pf12
EBA140
H101
SPATR
AARP
MSP10
RAMA
MSP6
RH5
PF3D7_0606800
MSP5
ASP
MSP3
RhopH3
ETRAMP10.2
MSP4
Pf113
MTRAP
Pf41
PTEX150
MSRP2
MSP2
Pf92
AMA1
MSP7
Pf34
MSP3.8
MSP1
Pf38
EBA175
MSP11
TLP
MSP3.4

Figure 44. *P. falciparum* surface proteins were immobilised on streptavidin-coated beads to generate multivalent binding reagents for testing against surface receptors on erythrocytes and transiently-transfected HEK293E cells. 33 *P. falciparum* surface proteins, expressed with C-terminal Cd4 and biotin tags, were multimerised by direct attachment to streptavidin-coated Nile red beads. Cell culture supernatants containing the proteins were used for this purpose, with no prior purification step. The minimum amount of each protein necessary for complete saturation of a set number of beads was determined by performing ELISAs on 2-fold serially-diluted samples of the proteins, with and without pre-incubation with beads. The ELISAs were carried out on a streptavidin-coated plate, using OX68 as the primary antibody and an alkaline phosphatase-conjugated anti-mouse antibody as the secondary. Alkaline phosphatase activity was quantified by the turnover of the colorimetric substrate, *p*-nitrophenyl phosphate, measured as an increase in absorbance at 405 nm. Data is shown as mean ± standard deviation; n=3. In the case of the protein samples pre-incubated with beads, a signal was expected to be seen in the ELISA, only when there was biotinylated protein in excess of what was needed for saturating the beads. The dilutions of the proteins selected for coating the beads, prior to presenting them to cells, is indicated by ↑.

variation in the binding responses was quite large, ranging from binding to ~80% of the cells down to ~2% of the cells (Figure 45). This is likely to reflect the availability/copy number of the erythrocytic receptors of the different *Plasmodium* proteins, as the highest binding was observed with the two *Plasmodium* proteins, EBA175 and EBA140 known to bind to two of the most abundant erythrocytic receptors Glycophorin A and Glycophorin C (~ 10^6 and 10^5 copies/cell respectively), whereas only 4% of the cells were observed to interact with RH5-coated beads, whose putative receptor BSG is expressed at a much lower level (Chapter 4, section 4.2.6).

The specificity of the binding of EBA175-coated beads to erythrocytes was previously tested by enzymatic pre-treatment of the cells with trypsin, chymotrypsin and neuraminidase (Chapter 3, section 3.2.2). The interaction of EBA140 with Glycophorin C is also known to be sensitive to trypsin and neuraminidase treatment but not to chymotrypsin treatment, whereas, the binding of RH5 to BSG is not affected by treatment with any of the three enzymes. To test whether the binding of EBA140 and RH5-coated beads to erythrocytes in this assay was specific, the cells were pre-treated with trypsin, chymotrypsin and neuraminidase, prior to incubation with the bead arrays. The results were consistent with the expected properties of these interactions (Figure 46). The specificity of the putative binding of the *P. falciparum* proteins Pf34, MSP3.4 and MSP3.8 was also tested by pre-treatment of erythrocytes with trypsin, chymotrypsin and neuraminidase. No significant reduction in the binding of these proteins to erythrocytes in response to any of the enzyme treatments was observed (data not shown).

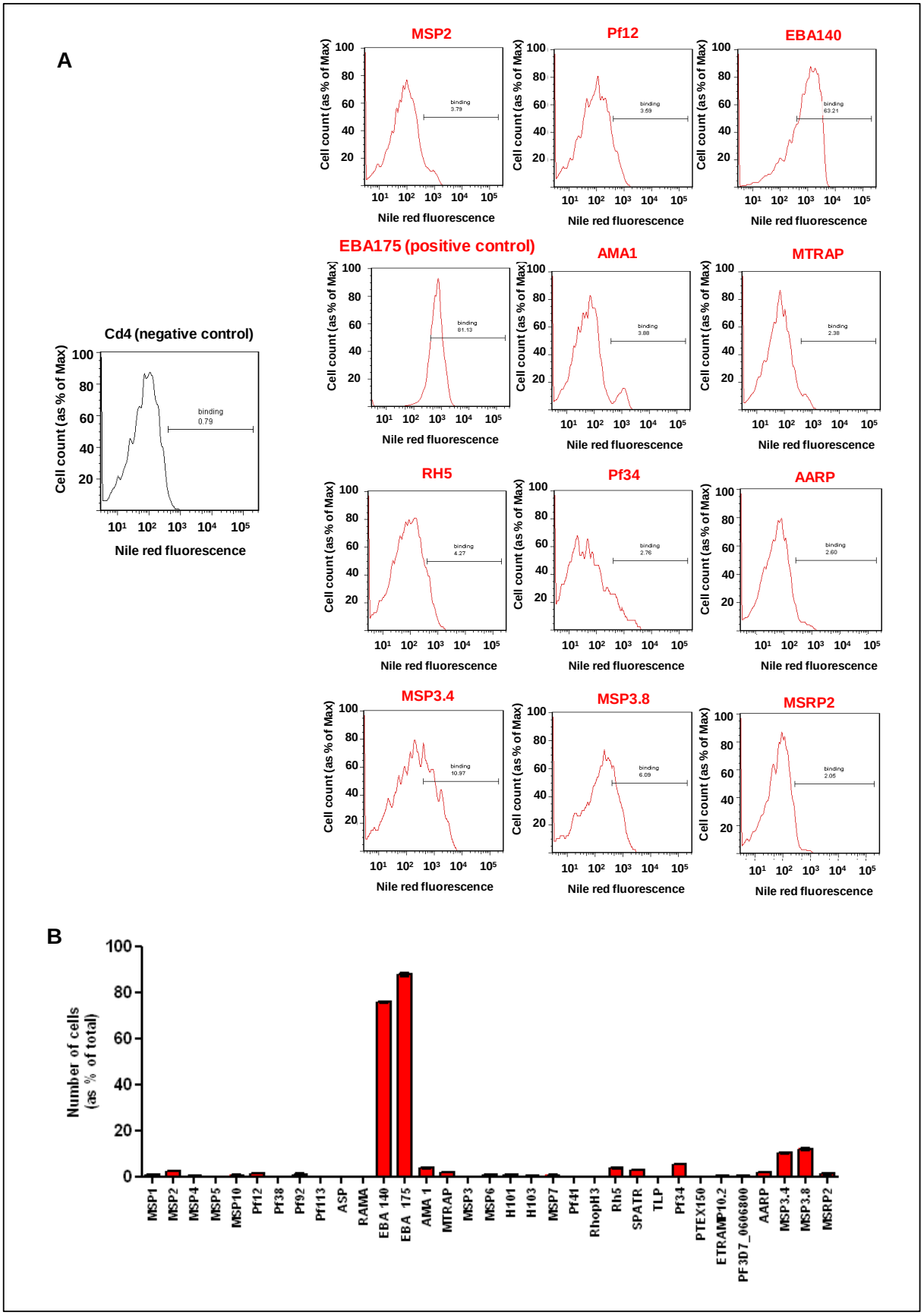
A
Cd4 (negative control)
MSP2
Pf12
EBA140
EBA175 (positive control)
AMA1
MTRAP
RH5
Pf34
AARP
MSP3.4
MSP3.8
MSRP2
Cell count (as % of Max)
Nile red fluorescence
B
Number of cells (as % of total)
MSP1
MSP2
MSP4
MSP5
MSP10
Pf12
Pf38
Pf92
Pf113
ASP
RAMA
EBA 140
EBA 175
AMA 1
MTRAP
MSP3
MSP6
H101
H103
MSP7
Pf41
RhopH3
Rh5
SPATR
TLP
Pf34
PTEX150
ETRAMP10.2
PF3D7_0606800
AARP
MSP3.4
MSP3.8
MSRP2

Figure 45. The *P. falciparum* surface proteins, multimerised on fluorescent beads, were presented to human erythrocytes to identify putative interactions. Multimeric arrays of the 33 *P. falciparum* proteins, generated by their immobilisation on streptavidin-coated Nile red beads, were incubated with untreated human erythrocytes for 1 h at 4°C before analysis by flow cytometry. The histograms **(A)** show the fluorescence intensities (at the Nile red emission wavelength) of selected erythrocyte populations each incubated with beads coated with a particular *Plasmodium* protein. The gate marked was used to estimate the number of erythrocytes (as a percentage of total) associated with beads in each case. The calculated values for the entire panel of *P. falciparum* proteins, after subtraction of the background binding (i.e. association with the negative control Cd4-coated beads), are shown in **B**. Each bar indicates mean ± standard deviation; *n*=2.

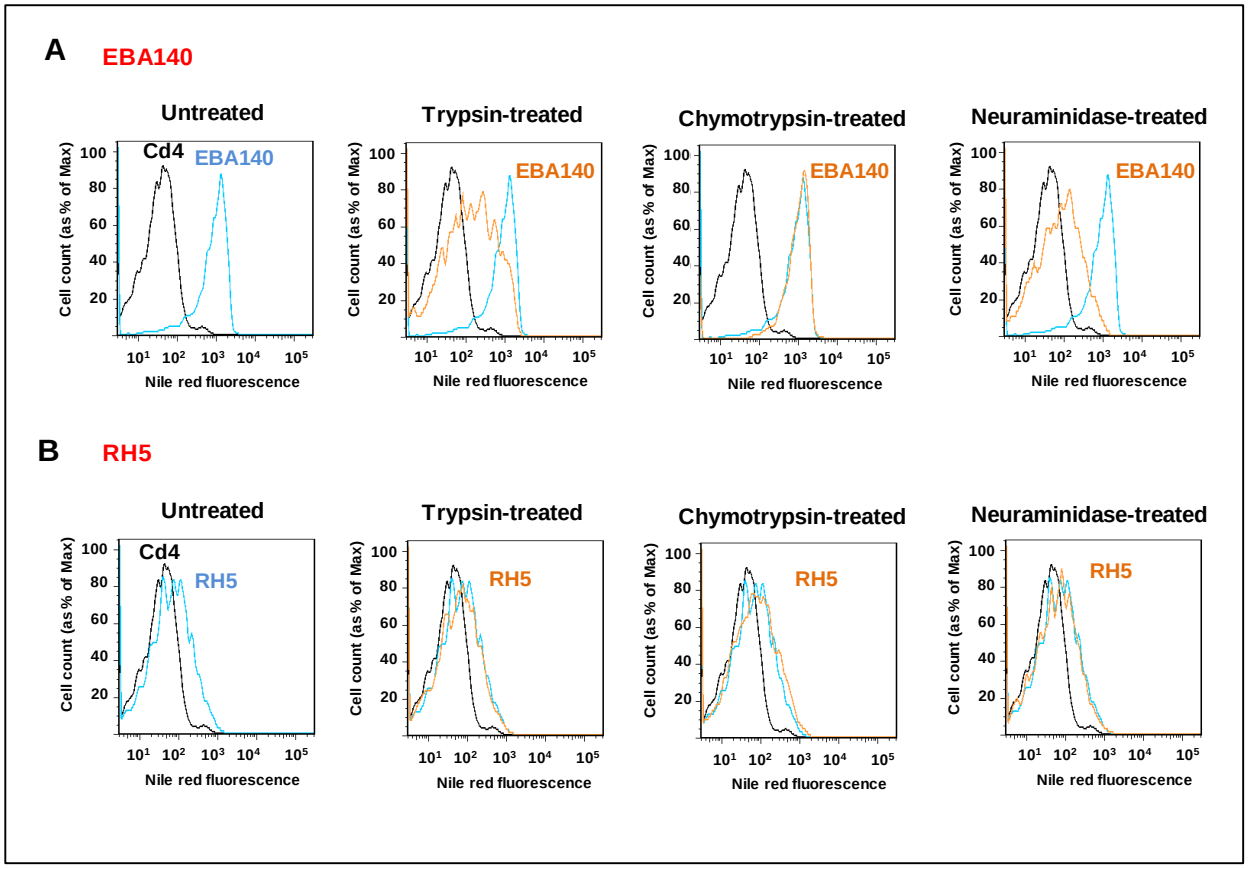

Figure 46. The specificity of the observed binding of EBA140 and RH5 to human erythrocytes was tested by probing these proteins against cells enzymatically pre-treated with trypsin, chymotrypsin and neuraminidase. Nile red beads coated with EBA140 or RH5 were incubated with erythrocytes, which were either untreated (positive control) or pre-treated with the enzymes trypsin (1 mg/ml), chymotrypsin (1 mg/ml) or neuraminidase (100 mU/ml). The histograms show the fluorescence intensities (at the Nile red emission wavelength) of the different erythrocyte populations as estimated by flow cytometry. Untreated erythrocytes incubated with Cd4-coated beads (negative control) are shown in black and those incubated with EBA140 (**A**) or RH5 (**B**) in blue. The enzymatically pre-treated erythrocytes are shown in orange. The results are representative of three independent experiments.

5.2.2 An expression library of erythrocyte multi-pass proteins was compiled based on published literature and protein topology modelling.

Thirty eight multi-pass proteins were chosen for probing against the *P. falciparum* merozoite surface protein library, all of which were identified in a recent mass-spectrometry based comprehensive study of the human erythrocyte proteome (Pasini *et al*., 2006; Table 7). Many of these receptors have multiple splice-isoforms. For 16 of these, it had not been possible to unequivocally discriminate between the different variants using only the mass-spectrometry data (Pasini *et al*., 2006; Table 7, Part 2). In these cases, the longest isoform of each receptor was obligatorily selected for inclusion in the screen. The amino acid sequence of each shorter isoform of each receptor was compared to that of its longest isoform by alignment using ClustalW software (Larkin *et al*., 2007), and if there were no differences in sequence with the exception of deletions, or if the differences lie in predicted intracellular regions, the shorter isoform was not selected for the screen. Selection of variants was based on the assumption that only sequence differences in the extracellular regions of the multi-pass receptors would influence the binding to any *Plasmodium* ligands. There was some difficulty in reaching a consensus regarding the membrane topology of certain proteins, as the predictions on UniProtKB significantly differed from literature sources and/or with the computational predictions from TMpred (Hofmann and Stofffel, 1993), TMHMM 2.0 (Krogh *et al*., 2003) and HMMTOP 2.0 (Tusnady and Simon, 2001). A total of 41 proteins (including two isoforms each of three receptors) were selected for the screen (Table 7). TrueORF clones (Figure 6) for these proteins were obtained from OriGene and DNA preparations at suitable concentrations for transfection of HEK293E were prepared.

TrueORF clones are designed to enable the expression of the encoded proteins with their endogenous signal sequences and C-terminal Myc and DDK tags, in mammalian expression systems (Figure 6). In principle, the recombinant erythrocyte multi-pass receptors should be

Table 7. Erythrocyte multi-pass receptors to be included in the screen.

Part 1: receptors for which a single isoform was unequivocally identified in the mass-spectrometry based study conducted by Pasini *et al*., 2006.

TMH: transmembrane helices, N-ext: N-terminus is extracellular, N-cyt: N-terminus is intracellular

Protein name (gene name)	NCBI reference sequence numbers		Predicted membrane topology of the protein			
	Protein	mRNA	TMpred	HMMTOP 2.0	TMHMM 2.0	UniProtKB entry
1. Potassium channel subfamily K member 5 (KCNK5)	NP_003731.1	NM_003740.3	7 TMH, N-ext	5 TMH, N-ext	6 TMH, N-ext	4 TMH, N-cyt
2. Secretory carrier-associated membrane protein 4 (SCAMP4)	NP_524558.1	NM_079834.2	3 TMH, N-ext	4 TMH, N-cyt	4 TMH, N-cyt	4 TMH, N-cyt
3. Intermediate conductance calcium-activated potassium channel protein 4 (KCNN4)	NP_002241.1	NM_002250.2	5 TMH, N-ext	7 TMH, N-ext	5 TMH, N-cyt	7 TMH
4. Solute carrier family 12 member 7 (SLC12A7)	NP_006589.2	NM_006598.2	12 TMH, N-cyt	11 TMH, N-cyt	11 TMH, N-cyt	12 TMH, N-cyt
5. Monocarboxylate transporter 1 (SLC16A1)	NP_003042.3	NM_003051.3	10 TMH, N-cyt	12 TMH, N-cyt	11 TMH, N-ext	12 TMH, N-cyt
6. Rhesus blood group-associated glycoprotein (RHAG)	NP_000315.2	NM_000324.2	10TMH, N-cyt	10 TMH, N-ext	11 TMH, N-ext	12 TMH, N-cyt
7. Solute carrier family 2, facilitated glucose transporter member 3 (SLC2A3)	NP_008862.1	NM_006931.2	12 TMH, N-cyt	12 TMH, N-cyt	10 TMH, N-cyt	12 TMH, N-cyt
8. Solute carrier family 2 facilitated glucose transporter member 1 (SLC2A1)	NP_006507.2	NM_006516.2	13 TMH, N-cyt	13 TMH, N-ext	12 TMH, N-cyt	12 TMH, N-cyt
9. Band 3 anion transport protein (SLC4A1)	NP_000333.1	NM_000342.3	11TMH, N-cyt	13 TMH, N-ext	11 TMH, N-ext	12 TMH, N-cyt
10. Fatty acid transporter 4 (SLC27A4)	NP_005085.2	NM_005094.2	5 TMH, N-ext	2 TMH, N-ext	2 TMH, N-ext	2 TMH, N-ext
11. ATP-binding cassette, sub-family G, member 2 (ABCG2)	NP_004818.2	NM_004827.2	6 TMH, N-ext	7 TMH, N-ext	6 TMH, N-ext	6 TMH, N-cyt
12. Vacuolar ATP synthase 16 kDa proteolipid subunit (ATP6V0C)	NP_001685.1	NM_001694.2	4 TMH, N-cyt	4 TMH, N-ext	4 TMH, N-ext	4 TMH, N-cyt
13. Transmembrane protein 222 (TMEM222)	NP_115501.2	NM_032125.2	3 TMH, N-ext	2 TMH, N-cyt	3 TMH, N-ext	3 TMH, N-ext
14. Large neutral amino acids transporter small subunit 4 (SLC43A2)	NP_689559.1	NM_152346.1	12 TMH, N-cyt	12 TMH, N-cyt	12 TMH, N-cyt	12 TMH
15. Glutamate receptor, metabotropic 4 precursor (GRM4)	NP_000832.1	NM_000841.1	9 TMH, N-ext	7 TMH, N-ext	6 TMH, N-ext	7 TMH, N-ext
16. Glutamate transporter (SLC1A7)	NP_006662.3	NM_006671.4	10 TMH, N-ext	11 TMH, N-cyt	7 TMH, N-cyt	10 TMH, N-cyt
17. RECS1 protein homolog (TMBIM1)	NP_071435.2	NM_022152.4	7 TMH, N-cyt	7 TMH, N-ext	7 TMH, N-cyt	7 TMH, N-cyt
18. Aquaporin 1 (Aquaporin-CHIP)(AQP1)	NP_932766.1	NM_198098.1	6 TMH, N-ext	6 TMH, N-cyt	6 TMH, N-cyt	6 TMH, N-cyt
19. Membrane transport protein XK (XK)	NP_066569.1	NM_021083.2	7 TMH, N-cyt	9 TMH, N-ext	9 TMH, N-cyt	10 TMH, N-cyt
20. Iron-regulated transporter, member 1 (SLC40A1)	NP_055400.1	NM_014585.5	9 TMH, N-cyt	11 TMH, N-ext	10 TMH, N-cyt	10 TMH, N-cyt
21. Folate transporter 1 (SLC19A1)	NP_919231.1	NM_194255.1	12 TMH, N-cyt	12 TMH, N-cyt	11 TMH, N-ext	12 TMH, N-cyt
22. Solute carrier family 43, member 1 (SLC43A1)	NP_003618.1	NM_003627.4	12 TMH, N-cyt	12 TMH, N-cyt	12 TMH, N-cyt	12 TMH, N-cyt
23. Sodium/potassium-transporting ATPase alpha-2 (ATP1A2)	NP_000693.1	NM_000702.3	9 TMH, N-cyt	10 TMH, N-cyt	8 TMH, N-cyt	10 TMH, N-cyt
24. Transmembrane protein 56 (TMEM56)	NP_689700.1	NM_152487.2	6 TMH, N-cyt	6 TMH, N-cyt	6 TMH, N-cyt	6 TMH

Table 7. Erythrocyte multi-pass receptors to be included in the screen.

Part 2: receptors for which a single isoform was not unequivocally identified in the mass-spectrometry based study conducted by Pasini *et al*., 2006.

TMH: transmembrane helices, N-ext: N-terminus is extracellular, N-cyt: N-terminus is intracellular

Protein name (gene name)	NCBI reference sequence numbers		Predicted membrane topology of the protein			
	Protein	mRNA	TMpred	HMMTOP 2.0	TMHMM 2.0	UniProtKB entry
25. Solute carrier family 43 member 3 (SLC43A3)	NP_054815.2	NM_014096.2	11 TMH, N-ext	11 TMH, N-ext	11 TMH, N-ext	12 TMH, N-cyt
26. Na/K-transporting ATPase alpha-1 (ATP1A1)	NP_001153705.1	NM_001160233.1	9 TMH, N-cyt	10 TMH, N-cyt	8 TMH, N-cyt	10 TMH, N-cyt
27. Plasma membrane calcium-transporting ATPase 4 (ATP2B4)	NP_001675.3	NM_001684.3	10 TMH, N-cyt	10 TMH, N-cyt	8 TMH, N-cyt	10 TMH, N-cyt
28. Ion transporter protein (SLC22A23)	NP_056297.1	NM_015482.1	13 TMH, N-ext	12 TMH, N-cyt	10 TMH, N-cyt	10 TMH, N-ext
29. Equilibrative nucleoside transporter 1 (SLC29A1)	NP_001071645.1	NM_001078177.1	11 TMH, N-ext	11 TMH, N-cyt	11 TMH, N-cyt	11 TMH, N-cyt
30. Leukocyte surface antigen CD47 precursor (CD47)	NP_001768.1	NM_001777.3	5 TMH, N-ext	5 TMH, N-ext	6 TMH, N-cyt	5 TMH, N-ext
31. Thyrotropin receptor precursor (TSHR)	NP_000360.2	NM_000369.2	7 TMH, N-ext	7 TMH, N-ext	7 TMH, N-cyt	7 TMH, N-ext
32. Urea transporter (SLC14A1)	NP_001122060.3	NM_001128588.3	8 TMH, N-cyt	10 TMH, N-cyt	8 TMH, N-cyt	9 TMH, N-cyt
33. Multidrug resistance-associated protein 1 (ABCC1)	NP_004987.2	NM_004996.3	17 TMH, N-ext	16 TMH, N-ext	16 TMH, N-ext	17 TMH, N-ext
34. Multidrug resistance-associated protein 4 (ABCC4)	NP_005836.2	NM_005845.3	10 TMH, N-cyt	10 TMH, N-ext	11 TMH, N-cyt	14 TMH, N-cyt
35. Tetraspanin-14 (TSPAN14)	NP_112189.2	NM_030927.2	4 TMH, N-cyt	4 TMH, N-cyt	4 TMH, N-cyt	4 TMH,N-cyt
36 and 37. Cytochrome b reductase 1 (CYBRD1)	NP_079119.3	NM_024843.3	6 TMH N-ext	6 TMH, N-cyt	6 TMH, N-cyt	6 TMH, N-cyt
	NP_001120855.1	NM_001127383.1	2 TMH, N-ext	2 TMH, N-ext	2 TMH, N-cyt	
38 and 39. Duffy antigen/chemokine receptor (DARC)	NP_001116423.1	NM_001122951.1	7 TMH, N-ext	7 TMH, N-ext	7 TMH, N-ext	7 TMH, N-ext
	NP_002027.2	NM_002036.2	7 TMH, N-ext	7 TMH, N-ext	7 TMH, N-cyt	
40 and 41. Rh blood CE group antigen polypeptide (RHCE)	NP_065231.2	NM_020485.3	10 TMH, N-cyt	12 TMH, N-cyt	12 TMH, N-cyt	11 TMH
	NP_619524.2	NM_138618.2	8 TMH, N-cyt	9 TMH, N-cyt	9 TMH, N-cyt	

successfully expressed and targeted to the cell surface in HEK293E; they are expressed in a human cell line (hence problems with codon usage and post-translational modifications should not be encountered), they carry their endogenous signal sequences (which would direct them to the surface membrane) and the C-terminal Myc and DDK tags are unlikely to interfere with the correct folding of the protein, due to their small size. To confirm this, the expression in HEK293E and trafficking to the surface membrane of a few of the proteins, were monitored over a period of 72 hours after transfection, by staining cells with appropriate antibodies and using flow cytometry. The longest isoform of the Duffy antigen (gene name DARC) was detected using a goat polyclonal antibody against its N-terminal ectodomain and a FITC-conjugated anti-goat antibody on non-permeabilised cells (Figure 47 A). The results suggest that this Duffy isoform was displayed on the surface of transfected cells in the correct orientation (i.e. with the N-terminus exposed at the extracellular face of the membrane). This was also confirmed by analysis of the antibody-stained cells using confocal microscopy (Figure 47 B). The flow cytometry data also suggests that the amount of recombinant Duffy at the cell surface was highest 48 hours after transfection (Figure 47 A). The RECS1 protein homolog (TMBIM1) and isoform 2 of cytochrome b reductase 1 (CYBRD1) were also detected on the surface of transfected non-permeabilised HEK293E cells using a mouse monoclonal antibody against the c-Myc fusion tag and a FITC-conjugated anti-mouse secondary (Figure 47 C and D). These proteins also showed the highest expression 48 h after transfection.

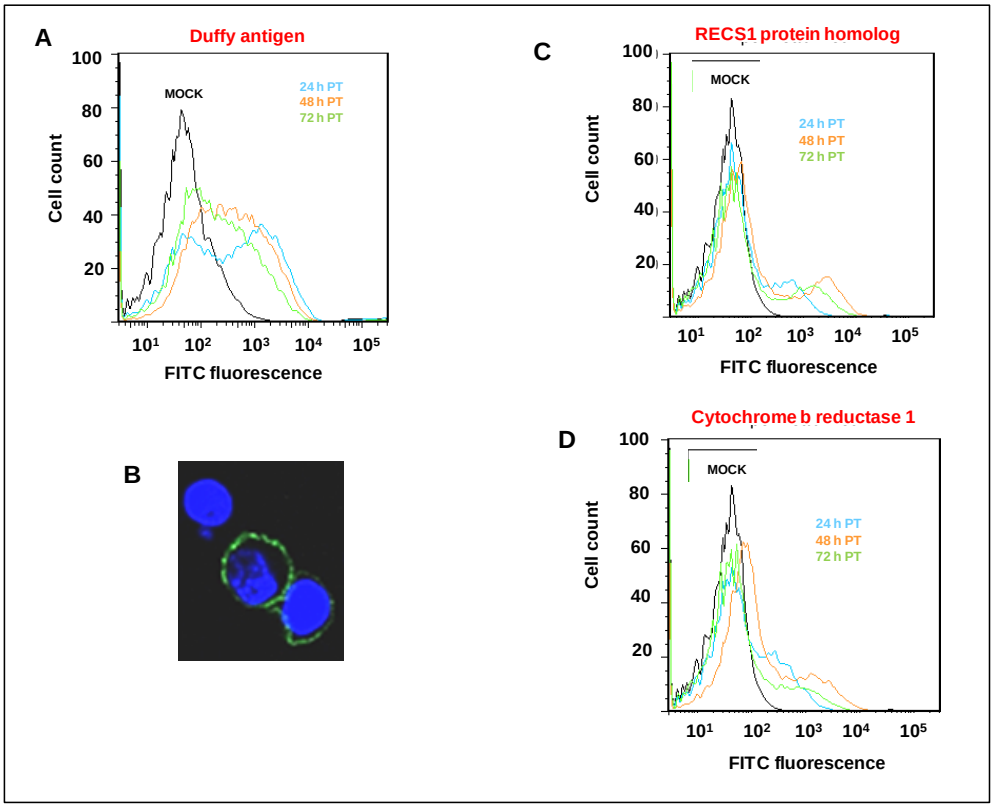

Figure 47. The expression of three recombinant multi-pass receptors on the surface of HEK293E cells was tracked after transient transfection of their expression constructs over a period of 72 h. The TrueORF clones of the long isoforms of the Duffy antigen and Cytochrome b reductase 1 as well as the RECS1 protein homolog were transiently transfected into HEK293E cells. The expression of the receptors and their display at the surface of transfected cells was monitored ~ every 24 h for 3 days. The Duffy antigen was detected using a goat polyclonal against its N-terminal extracellular domain and a FITC-conjugated donkey anti-goat secondary. The other two receptors are predicted to have C-terminal extracellular domains and hence were detected using a mouse monoclonal against their c-Myc tag and a FITC-conjugated rabbit anti-mouse secondary. Mock-transfected cells (treated only with the transfection reagent) stained with the same antibodies were used as a negative control in each case. The expression of the Duffy antigen was analysed both by flow cytometry (**A**) and confocal microscopy (**B**). In the confocal microscope image (taken 48 h after transfection), DAPI staining of the cell nuclei is shown in blue and FITC staining in green. The expression of the RECS1 protein homolog (**C**) and Cytochrome b reductase 1 (**D**) was analysed only by flow cytometry.

5.2.3 Proof-of-principle study: demonstration of the interaction between Cd200 and its receptor with one partner expressed transiently on the surface of HEK293E cells and the other immobilised on fluorescent beads.

A proof-of-principle study was performed to assess the technical feasibility and efficiency of detecting a low-affinity interaction between a protein expressed on the surface of HEK293E cells by transient transfection and another immobilised on fluorescent beads, using flow cytometry. The well characterised interaction (K_D= 2.5 μM) between the single-pass transmembrane proteins, rat Cd200 protein and its structurally related receptor (Cd200R) was selected for this purpose (Preston et al., 1997; Wright *et al*., 2000; Wright *et al*., 2003). In the first instance, Cd200 with a C-terminal EGFP tag was expressed on the surface of HEK293E cells by transient transfection and incubated with Nile red beads coated with biotinylated Cd4, Cd200 or Cd200R. Almost all of the transfected cells (EGFP+) were observed to bind to Cd200R-coated beads but not to beads coated with Cd4 or Cd200 (Figure 48 A). When the experiment was repeated in the reciprocal orientation with EGFP-tagged Cd200R expressed on the surface of HEK293E cells, the EGFP+ cells were also observed to bind only to Cd200-coated beads (Figure 48 A). The specificity of the observed interaction between Cd200 and Cd200R was probed further by pre-incubating the Cd200-expressing cells with an anti-Cd200 mouse monoclonal antibody, OX2 and an isotype-matched negative control antibody, W6/32. Pre-treatment of cells with OX2 but not W6/32, was observed to completely block the interaction with Cd200R-coated beads (Figure 48 B). Overall, the results from the proof-of-principle study suggest that this experimental method is of high efficiency and specificity.

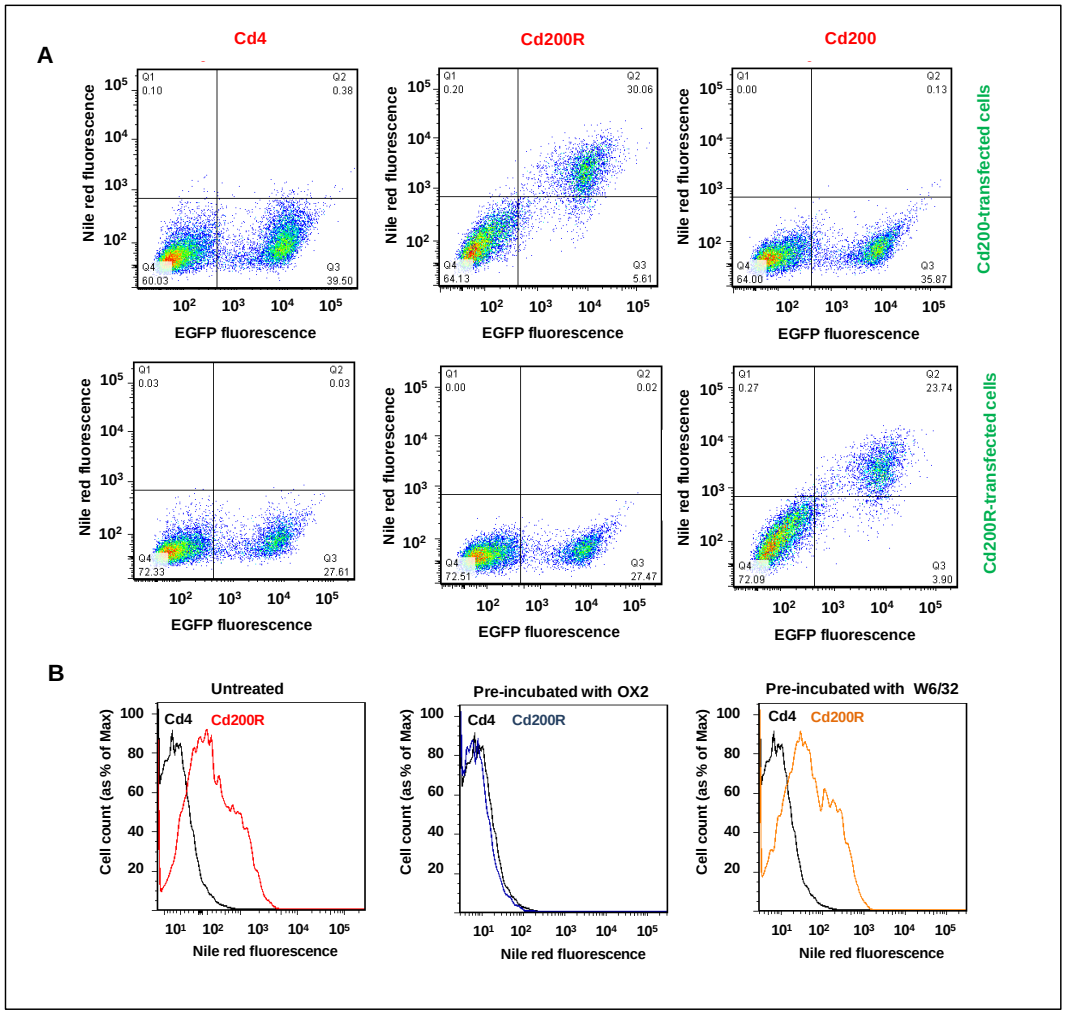

Figure 48. A 'proof-of-principle' study: The low-affinity interaction between the single-pass membrane proteins Cd200 and its structurally similar receptor (Cd200R) could be detected when one partner was expressed transiently on the surface of HEK293E cells and the ectodomain of the other immobilised on fluorescent beads. HEK293E cells were transiently transfected with the expression construct for cytosolic C-terminal EGFP-tagged Cd200 or Cd200R and then presented with Nile red beads coated with the biotinylated ectodomains of Cd200, Cd200R or Cd4. Binding events were detected by flow cytometry. **A**) Dot plots, of EGFP *versu*s Nile red fluorescence, of transfected HEK293E cells incubated with the protein-coated beads. **B**) Histograms of the fluorescence intensity, at the Nile red emission wavelength, of Cd200-expressing HEK293E cells that were either untreated or pre-treated with specific mouse monoclonals, prior to incubation with Cd200R- and Cd4-coated beads. OX2: anti-Cd200 antibody, W6/32: isotype-matched negative control antibody. Both antibodies were used at 0.5 µg/10^6 cells.

5.2.4 Positive control study: demonstration of the interaction between the Duffy antigen expressed recombinantly on the surface of HEK293E cells by transient transfection and *Pv*DBP immobilised on fluorescent beads.

The interaction between the Duffy antigen and *Pv*DBP was selected as a positive control to confirm the ability to detect low affinity binding of a multi-pass receptor transiently-expressed on the surface of HEK293E cells and a recombinant *Plasmodium* protein immobilised on fluorescent beads.

The full-length ectodomain of *Pv*DBP (*Pv*DBP FL) was produced in recombinant, soluble form with C-terminal Cd4 and biotin tags. The expression of the protein at the expected size of 136 kDa was confirmed by Western blotting and ELISA assays were used to monitor the process of immobilising this protein on streptavidin-coated Nile red beads (Figure 49 A and B). When presented to erythrocytes, *Pv*DBP FL-coated beads showed higher binding relative to the negative control (Cd4-coated beads) (Figure 49 C).

Two isoforms of the Duffy antigen have been identified, which differ only at the very beginning of the N-terminal extracellular domain. The major isoform is shorter than the minor by two residues and also differs in the identity of six residues. These differences reside outside of, but adjacent to, the putative *Pv*DBP binding region (Figure 49 D). The TrueORF clones of both Duffy isoforms were transiently-transfected in HEK293E cells and expression was monitored 48 h subsequently using the anti-DARC rabbit polyclonal raised against the N-terminal extracellular domain and a FITC-conjugated anti-rabbit secondary (Figure 49 E and F). In comparison to the secondary only control, some staining of mock-transfected cells (treated only with the transfection reagent) was observed, suggesting some basal-level of Duffy expression on HEK293E cells. Cells transfected with the expression constructs of the recombinant Duffy isoforms however, showed much higher binding to the anti-DARC antibody than mock-

transfected cells (the median fluorescence intensity of these cells was about 10-fold higher), suggesting that these recombinant proteins were present in the correct orientation at the cell surface. The expression levels of the two isoforms were fairly similar, with the shorter isoform being expressed slightly more.

Mock-transfected cells and those putatively expressing the two isoforms of Duffy were then tested against *Pv*DBP FL-coated beads (Figure 49 G, H and I). In comparison to Cd4-coated beads, binding of *Pv*DBP FL-coated beads was observed to mock-transfected cells as well as to those expressing recombinant Duffy (Figure 49 G). Direct comparison of *Pv*DBP binding to the different cell populations revealed significantly higher binding to cells over-expressing the short isoform of Duffy relative to mock-transfected cells (Figure 49 H and I). The binding of *Pv*DBP to cells expressing the long Duffy isoform was slightly less than the binding to mock-transfected cells. One possible explanation for these results is that only the short isoform of Duffy is capable of binding to *Pv*DBP and that HEK293E cells normally express a basal-level of this isoform endogenously. Therefore, only over-expression of the short isoform of Duffy and not the long would lead to higher binding to *Pv*DBP above the background binding observed with mock-transfected cells.

5.2.5 More than 40% of *P. falciparum* merozoite surface proteins tested showed binding to untreated and mock-transfected HEK293E cells.

Prior to screening the *P. falciparum* merozoite surface protein library against the panel of erythrocyte multi-pass receptors, the binding of the parasite proteins to untreated and mock-transfected HEK293E cells was tested (Figure 50). As HEK293E cells were to be used as the expression host for the recombinant multi-pass receptors, it was important to have an understanding of the background level of binding shown by each *P. falciparum* protein to

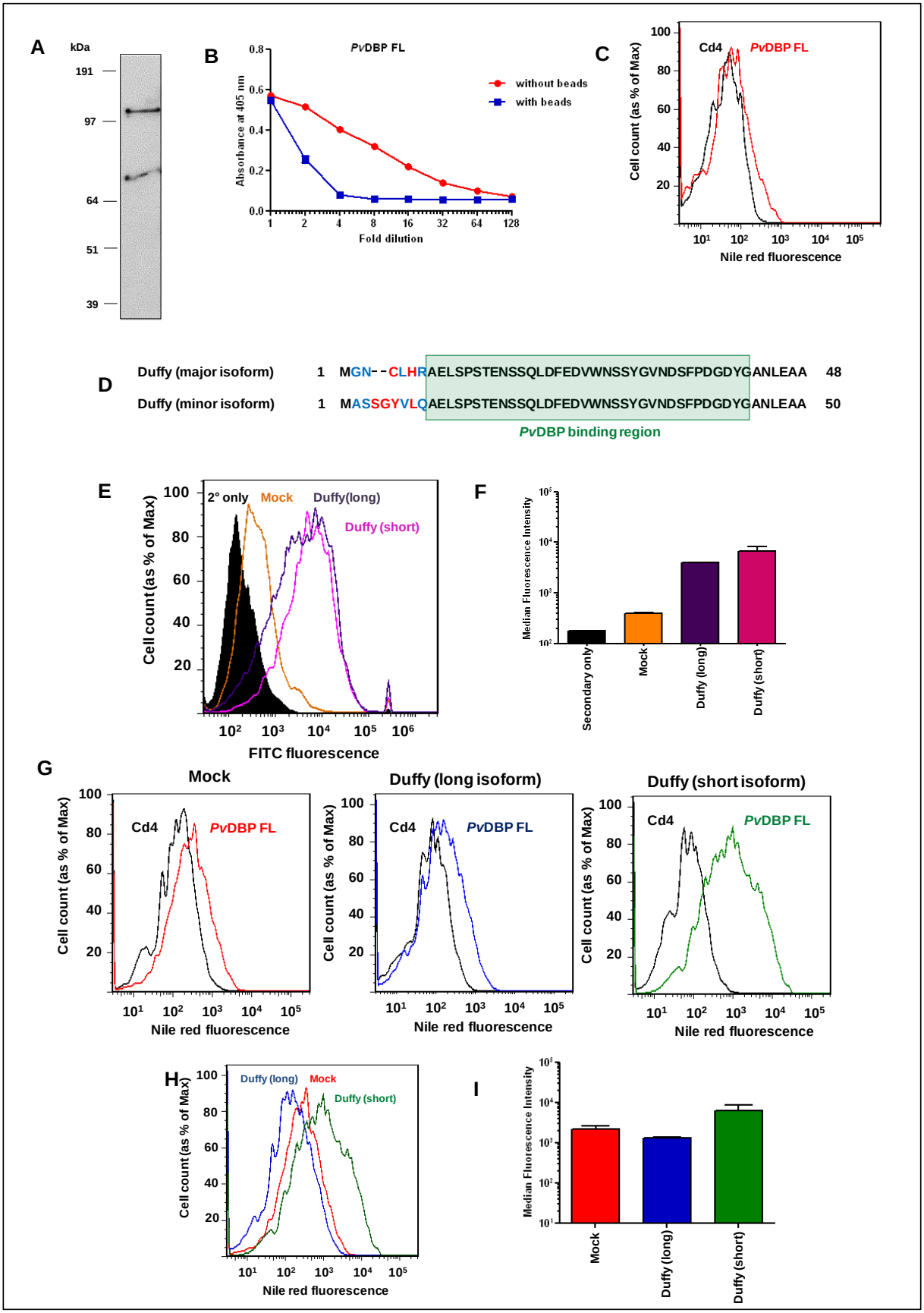
A
kDa
191
97
64
51
39
B
PvDBP FL
without beads
with beads
Absorbance at 405 nm
Fold dilution
C
Cd4
PvDBP FL
Cell count (as % of Max)
Nile red fluorescence
D
Duffy (major isoform) 1 MGN--CLHRAELSPSTENSSQLDFEDVWNSSYGVNDSFPDGDYGANLEAA 48
Duffy (minor isoform) 1 MASSGYVLQAELSPSTENSSQLDFEDVWNSSYGVNDSFPDGDYGANLEAA 50
PvDBP binding region
E
2° only
Mock
Duffy(long)
Duffy (short)
Cell count (as % of Max)
FITC fluorescence
F
Median Fluorescence Intensity
Secondary only
Mock
Duffy (long)
Duffy (short)
G
Mock
Duffy (long isoform)
Duffy (short isoform)
Cd4
PvDBP FL
Cell count (as % of Max)
Nile red fluorescence
H
Duffy (long)
Mock
Duffy (short)
Cell count (as % of Max)
Nile red fluorescence
I
Median Fluorescence Intensity
Mock
Duffy (long)
Duffy (short)

Figure 49. A "positive control" study: The Duffy antigen, a multi-pass receptor, expressed on the surface of HEK293E cells, showed binding to its known ligand, *P. vivax* DBP (*Pv*DBP) immobilised on fluorescent beads. The full-length ectodomain of *Pv*DBP (*Pv*DBP FL, protein accession number: P22290, residues 21-1070) was expressed with C-terminal Cd4 and biotin tags. Multimeric arrays of the protein were generated by direct attachment to streptavidin-coated Nile red beads. *Pv*DBP FL-coated beads were presented first to human erythrocytes to confirm functional activity and then to HEK293E cells transiently transfected with the TrueORF clones of the Duffy isoforms. The expression of the Duffy isoforms and the binding of *Pv*DBP FL-coated beads to cells were detected by flow cytometry. **A**) Western blot of *Pv*DBP FL (136 kDa), performed using extravidin-HRP as the probe. **B)** The minimum amount of *Pv*DBP FL necessary for complete saturation of a set number of streptavidin-coated Nile red beads was determined by ELISA, as described before. Data are shown as mean ± standard deviation; *n*=3. **C**) Histograms of Nile red fluorescence *versus* cell count, of erythrocyte populations incubated with *Pv*DBP FL-coated beads (red) or Cd4-coated beads (black, negative control). The data are representative of two independent experiments. **D)** The N-terminal sequences of the two isoforms of Duffy. Identical and similar residues are shown in black and blue respectively. The *Pv*DBP binding region (residues 8-42) is highlighted in green (Chitnis *et al*., 1996). **E)** Histograms of HEK293E cells, stained with an anti-Duffy goat polyclonal (directed against the N-terminal extracellular domain) and a FITC-conjugated anti-goat secondary. Mock-transfected cells are shown in orange. HEK293E cells transiently transfected with the Duffy isoforms are represented in purple (long isoform) and pink (short isoform) respectively. Cells stained with only the secondary antibody (negative control) are shown in black. **F)** A bar chart of the median fluorescence intensities (at the FITC emission wavelength) of the antibody-stained HEK293E cells. Data are shown as mean ± standard deviation; *n*=2. **G**) and **H**) Histograms showing the fluorescence intensities of HEK293E cells incubated with *Pv*DBP FL-coated Nile red beads. Red: mock-transfected cells, blue: cells transfected with the long isoform of Duffy, green: cells transfected with the short isoform of Duffy. The black histograms show the background fluorescence of the cells (i.e. when incubated with Cd4-coated beads). **I**) The bar chart shows the median fluorescence intensities of the different cell populations incubated with *Pv*DBP FL-coated beads. Each bar represents mean ± standard deviation; *n*=2.

endogenously expressed receptors on the HEK293E cell surface. The assays were performed with Nile red beads coated with the *Plasmodium* proteins and binding events were detected using flow cytometry. As before the number of cells (as a percentage of total) binding to each protein was calculated based on a fluorescence intensity threshold, set with reference to the binding to Cd4-coated beads (negative control) (Figure 50 A). Of the 33 *P. falciparum* proteins tested against untreated and mock-transfected HEK293E cells, 15 showed some degree of binding to both (Figures 50 B and C). Several of the proteins, including AARP, MSRP2 and RhopH3 showed higher binding to mock-transfected cells than to untreated cells suggesting some influence of the transfection reagent on the expression profile of their putative receptors. To confirm the specificity of the observed interactions, selected *Plasmodium* proteins were tested against HEK293E cells pre-treated with neuraminidase (Figure 51). Of the 11 proteins chosen for this analysis, nine had previously been observed to bind to human erythrocytes, the two exceptions were Pf113 and RhopH3. The binding of EBA175, EBA140, Pf113 and MSRP2 were observed to be susceptible to neuraminidase treatment, suggesting the involvement of sialic acid in their recognition of putative receptors on the surface of HEK293E cells (Figure 51). The binding of the other seven proteins, including RH5, was not inhibited by neuraminidase treatment. The gene expression profile of HEK cells, originally generated by adenoviral transformation of human embryonic kidney cells, is not generally considered to be representative of any particular human tissue type (Graham *et al*., 1977). Therefore, even proteins which are restricted to erythrocytic expression, could in theory be endogenously expressed in HEK293E cells. To test this hypothesis, HEK293E cells were stained with two mouse monoclonal antibodies, BRIC256 and MEM-M6/6, which recognise Glycophorin A and BSG respectively (Figure 52). The staining was detected using a FITC-conjugated anti-mouse secondary.

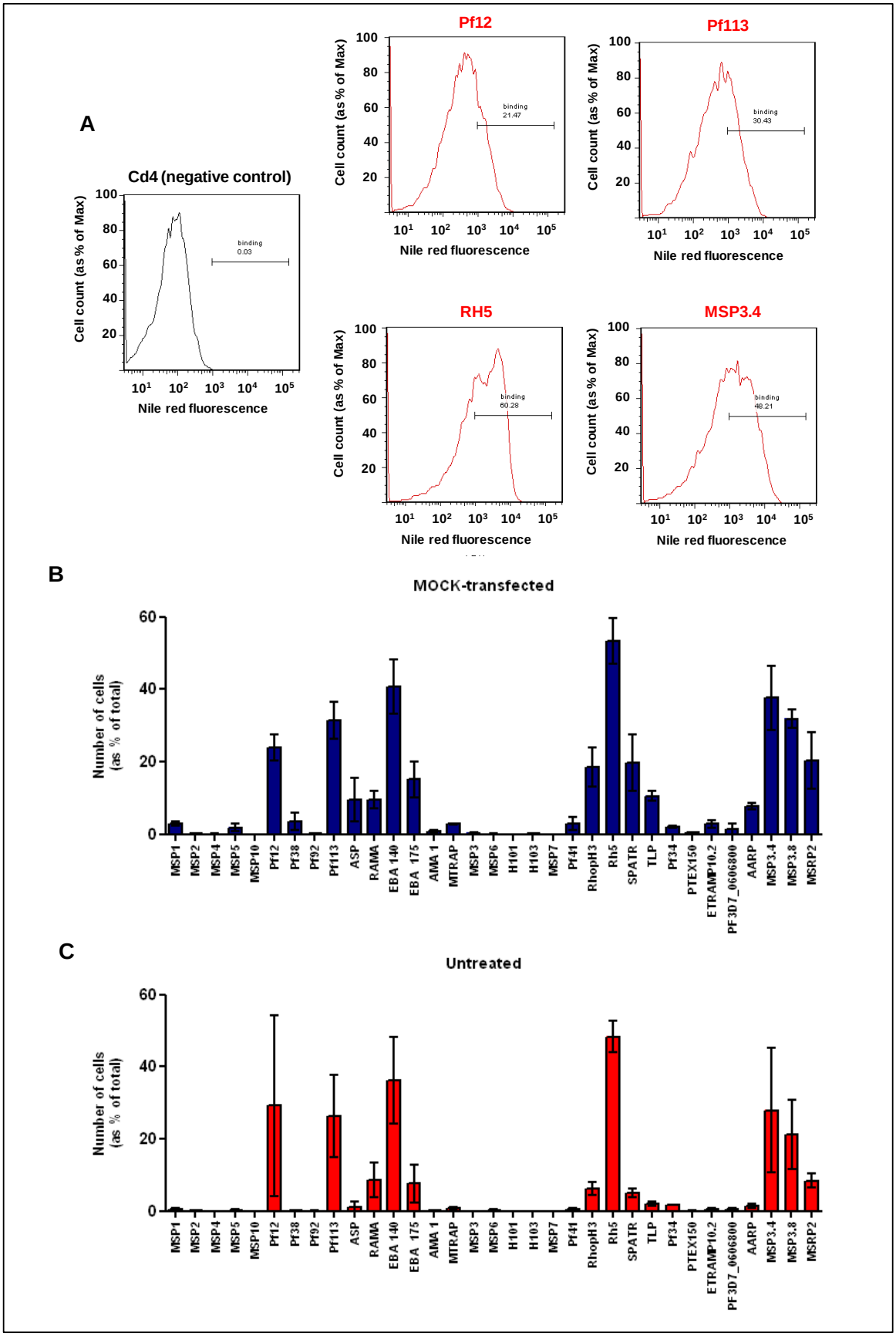
A
Cd4 (negative control)
Pf12
Pf113
RH5
MSP3.4
Cell count (as % of Max)
Nile red fluorescence
binding
0.03
21.47
30.43
60.28
48.21
B
MOCK-transfected
C
Untreated
Number of cells
(as % of total)
MSP1
MSP2
MSP4
MSP5
MSP10
Pf12
Pf38
Pf92
Pf113
ASP
RAMA
EBA 140
EBA 175
AMA 1
MTRAP
MSP3
MSP6
H101
H103
MSP7
Pf41
RhopH3
Rh5
SPATR
TLP
Pf34
PTEX150
ETRAMP10.2
PF3D7_0606800
AARP
MSP3.4
MSP3.8
MSRP2

Figure 50. A significant proportion of the *P. falciparum* surface proteins tested showed some binding to untreated and mock-transfected HEK293E cells. Multimeric arrays of the 33 *P. falciparum* proteins, generated by immobilising the proteins on streptavidin-coated Nile red beads, were incubated with untreated and mock-transfected HEK293E cells before analysis by flow cytometry. The histograms **(A)** show the fluorescence intensities (at the Nile red emission wavelength) of selected cell populations each incubated with beads coated with a specific *Plasmodium* protein. The gate marked was used to estimate the number of cells (as a percentage of total) associated with beads in each case. The calculated values for the entire panel of *P. falciparum* proteins, after subtraction of the background binding (i.e. association with the negative control Cd4-coated beads), are shown in **B** and **C**. Each bar indicates mean ± standard deviation; *n*=3.

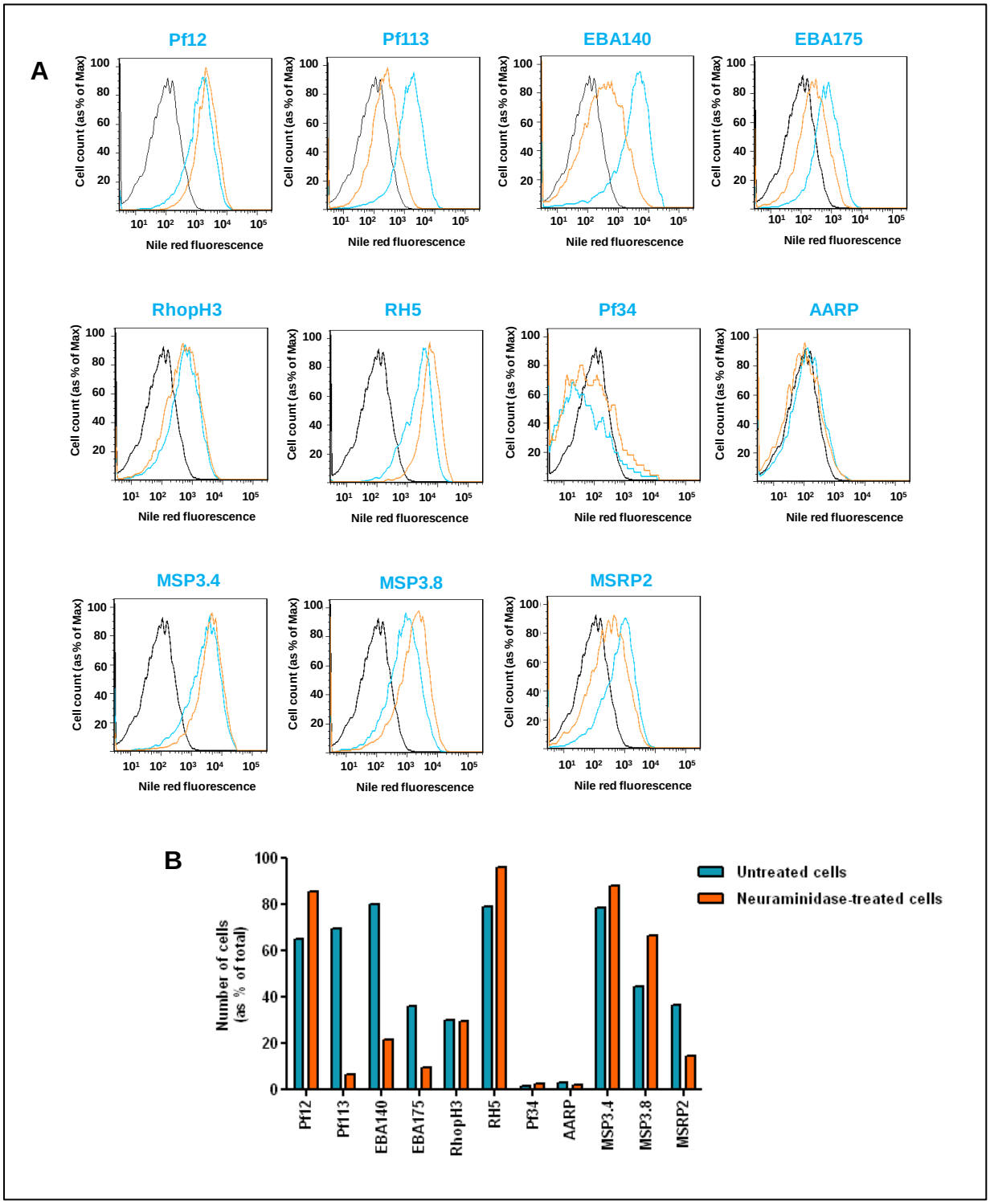
A
Pf12
Pf113
EBA140
EBA175
RhopH3
RH5
Pf34
AARP
MSP3.4
MSP3.8
MSRP2
Cell count (as % of Max)
Nile red fluorescence
B
Number of cells (as % of total)
Untreated cells
Neuraminidase-treated cells
Pf12
Pf113
EBA140
EBA175
RhopH3
RH5
Pf34
AARP
MSP3.4
MSP3.8
MSRP2

Figure 51. Four out of 11 *P. falciparum* proteins tested showed sialic-acid dependent binding to HEK293E cells. 11 of the *Plasmodium* proteins (immobilised on Nile red beads) were tested for binding to HEK293E cells pre-treated with neuraminidase (100 mU/ml). Untreated cells were included as a positive control. **A)** The histograms show the fluorescence intensities (at the Nile red emission wavelength) of cells incubated with each *Plasmodium* protein. Untreated cells are shown in blue and neuraminidase-treated cells in orange. The background fluorescence of the cells (i.e. the binding to Cd4-coated beads) is indicated in black. **B)** The bar chart represents the number of untreated and neuraminidase-treated cells (as a percentage of total) binding to each parasite protein, as calculated from the histograms above, using a fluorescence intensity threshold to select the Nile red 'positive' cells.

The average median fluorescence intensities (MFI) of the cells stained with BRIC256 and MEM-M6/6 were 102.2 and 5920.6 respectively, whereas those stained only with the secondary antibody had an average MFI of 75.03. Therefore BSG, the RH5 receptor, clearly appears to be expressed on HEK293E cells at possibly a higher level than observed on human erythrocytes. Some basal degree of Glycophorin A expression on HEK293E cells also seems probable and would account for the relatively low level EBA175 binding observed.

5.2.6 The *P. falciparum* merozoite surface proteins were screened against 41 erythrocytic multi-pass receptors, each expressed individually on the surface of HEK293E cells.

For screening against the *P. falciparum* merozoite surface proteins, the erythrocytic multi-pass receptors were expressed individually on the surface of HEK293E cells by transient transfection of their TrueORF clones. The expression of each receptor was tested by staining non-permeabilised cells with an anti-c-Myc mouse monoclonal and a FITC-conjugated secondary The multi-pass receptors exhibited a range of expression levels (Figure 53). In some cases (e.g. the Glutamate transporter (SLC1A7)) almost no expression of the protein was detected. However, this could be due to the proteins being oriented at the cell surface with the C-terminus on the cytosolic side. The c-Myc tag in such cases would not be accessible to the antibody.

In the screen, the multi-pass receptors were transfected and tested against the *Plasmodium* proteins in four batches of ten, for ease of handling. Mock-transfected cells were included as a negative control in each batch to account for batch-to-batch variation in the expression levels of cell surface proteins that arise independently of the exogenously-transfected DNA.

In the case of each *Plasmodium* protein, the observed (background) binding to mock-transfected cells was subtracted from the binding to cells transfected with each multi-pass receptor, during

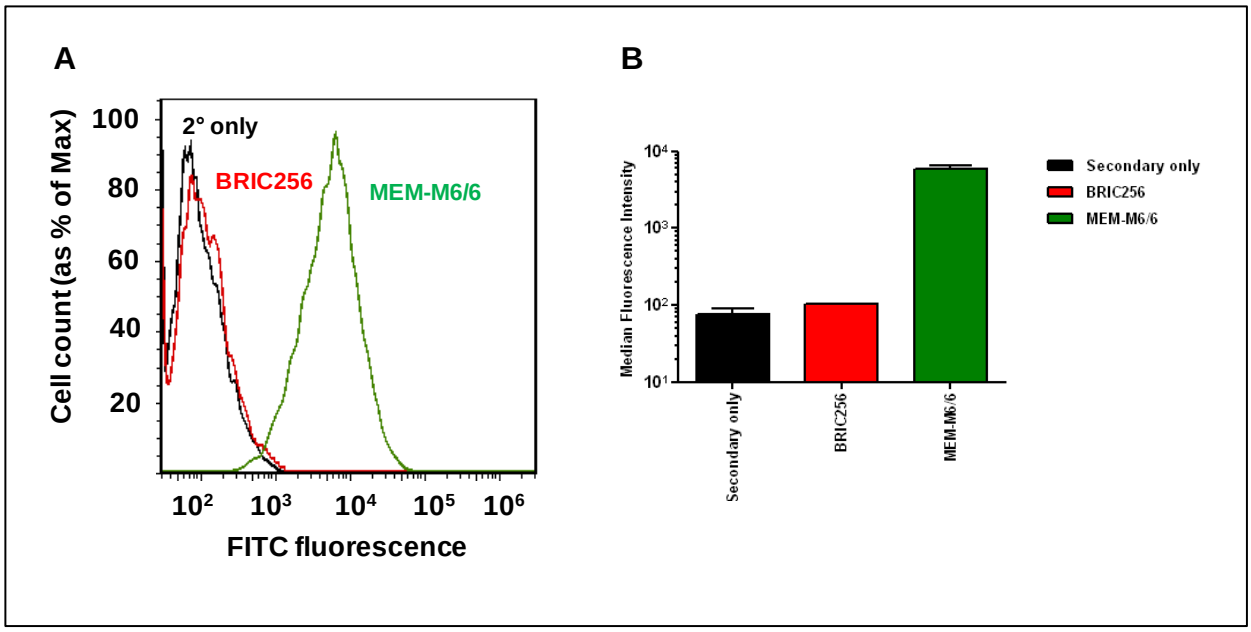

Figure 52. The expression of Glycophorin A and Basigin on the surface of HEK293E cells was tested by staining with specific antibodies. Untreated HEK293E cells were stained with the mouse monoclonals BRIC256 and MEM-M6/6, which recognise Glycophorin A and Basigin respectively. The binding of the monoclonals to the cells was detected with a FITC-conjugated anti-mouse secondary. The cells were also stained with only the secondary as a negative control. **A)** Histograms of fluorescence intensity *versus* cell count of the antibody-stained cells. **B)** A bar chart of the median fluorescence intensities (at the FITC emission wavelength) of the antibody-stained cells. Each bar represents mean ± standard deviation; *n*=2. Cells stained with BRIC256, MEM-M6/6 and only the secondary are shown in red, green and black respectively.

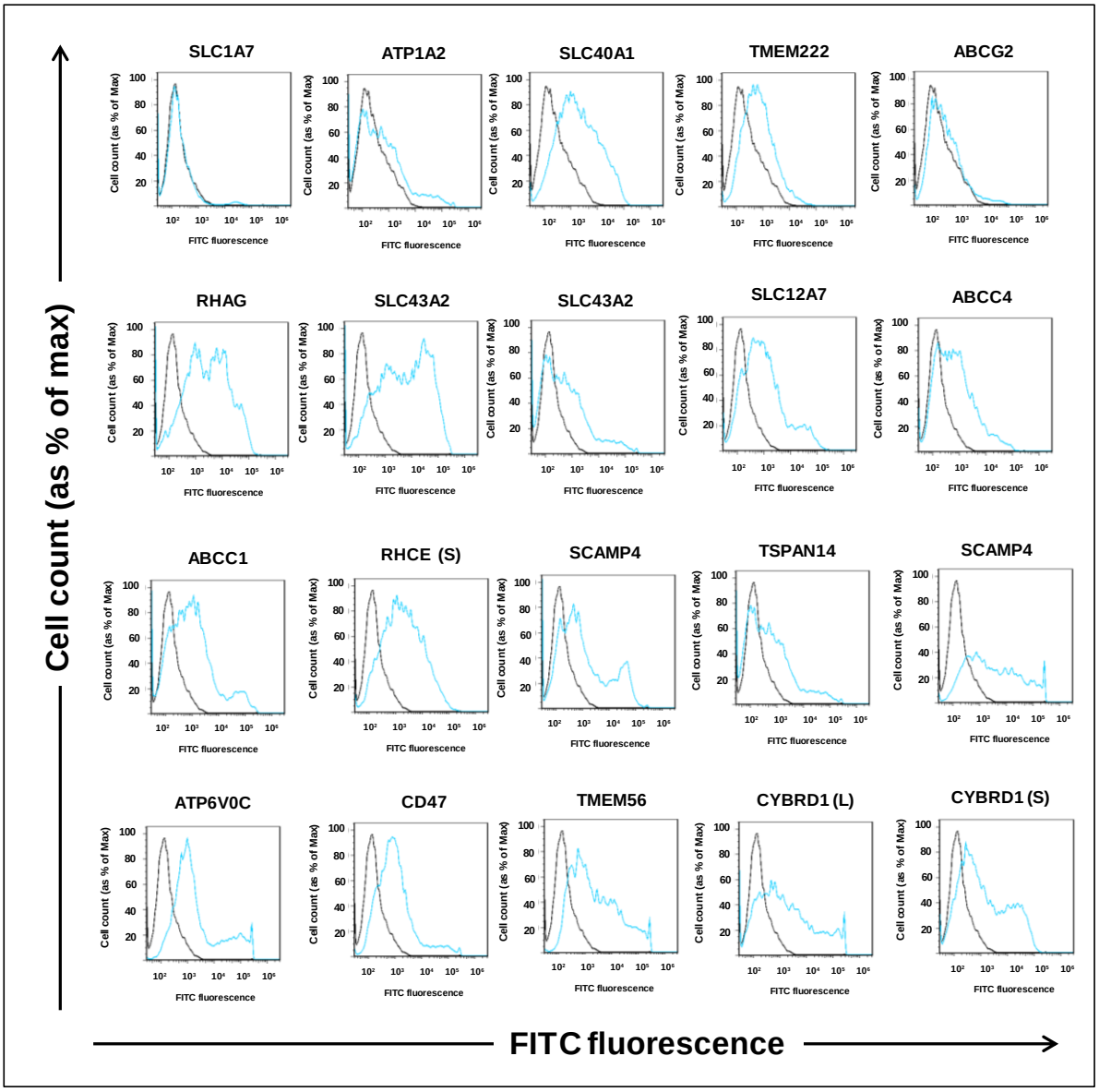

Figure 53. The expression of the recombinant multi-pass receptors on the surface of HEK293E cells was tested by staining with a mouse monoclonal antibody that recognises their C-terminal Myc tag. The cells were analysed 48h after transfection of the TrueORF clones coding for the multi-pass receptors. The binding of the anti-c-Myc monoclonal was detected with a FITC-conjugated anti-mouse secondary using flow cytometry. Mock-transfected cells stained with the same antibodies were used as a negative control. The histograms displayed show the fluorescence intensities (at the FITC emission wavelength) of cells transfected with each stated multi-pass receptor (blue) and mock-transfected cells (black). The multi-pass receptors are referred to by their gene names and the expression profiles of only 20 randomly selected receptors are shown.

data analysis, to estimate the 'actual' binding to the recombinant multi-pass receptor. The values obtained were then normalised (by calculating the z scores) across the whole panel of multi-pass receptors, to identify the most significant interactions more easily. This simple model used for evaluating the data, assumes that any increase seen in the binding of a parasite protein to cells transfected with a recombinant receptor, relative to mock-transfected cells, is the result only of the expression of the receptor and not due to indirect effects of the exogenous DNA.

All the interactions tested in the screen and their estimated z scores are shown (Figure 54). Overall, only two interactions had z scores of above 5, the binding of the *P. falciparum* protein AARP to the Fatty acid transporter 4 (gene name: SLC27A4) and the binding of MSP11 to the Plasma membrane calcium transporting ATPase 4 (ATP2B4) (Figure 55). A z score of 5 means that the binding of the parasite protein to the multi-pass receptor was five standard deviations above the average binding of that *Plasmodium* protein to the entire panel of multi-pass receptors and thus can be considered as an indication of a fairly robust interaction. 11 of the tested interactions had a z scores between 3 and 5 (Figures 56 and 57). These include the interaction of the *P. falciparum* protein H101 with the Plasma membrane calcium transporting ATPase 4 (ATP2B4). Both H101 and MSP11 are members of the MSP3 family of proteins, hence their putative binding to the same receptor seems promising (Figure 56 A). MSP6 was also observed to bind to the Fatty acid transporter 4 (SLC27A4) (Figure 56 B). MSP2 showed binding to two multi-pass receptors; the short isoform of the Rh blood CE group antigen polypeptide (RHCE) and the Monocarboxylate transporter 1 (SLC16A1) (Figure 56 C and D). The interactions of the *Plasmodium* proteins MSP3, MSP4, MSP7 and AMA 1 with the multi-pass receptors Na+/K+ transporting ATPase (ATP1A1), Multidrug resistance associated protein (ABCC4), Rhesus

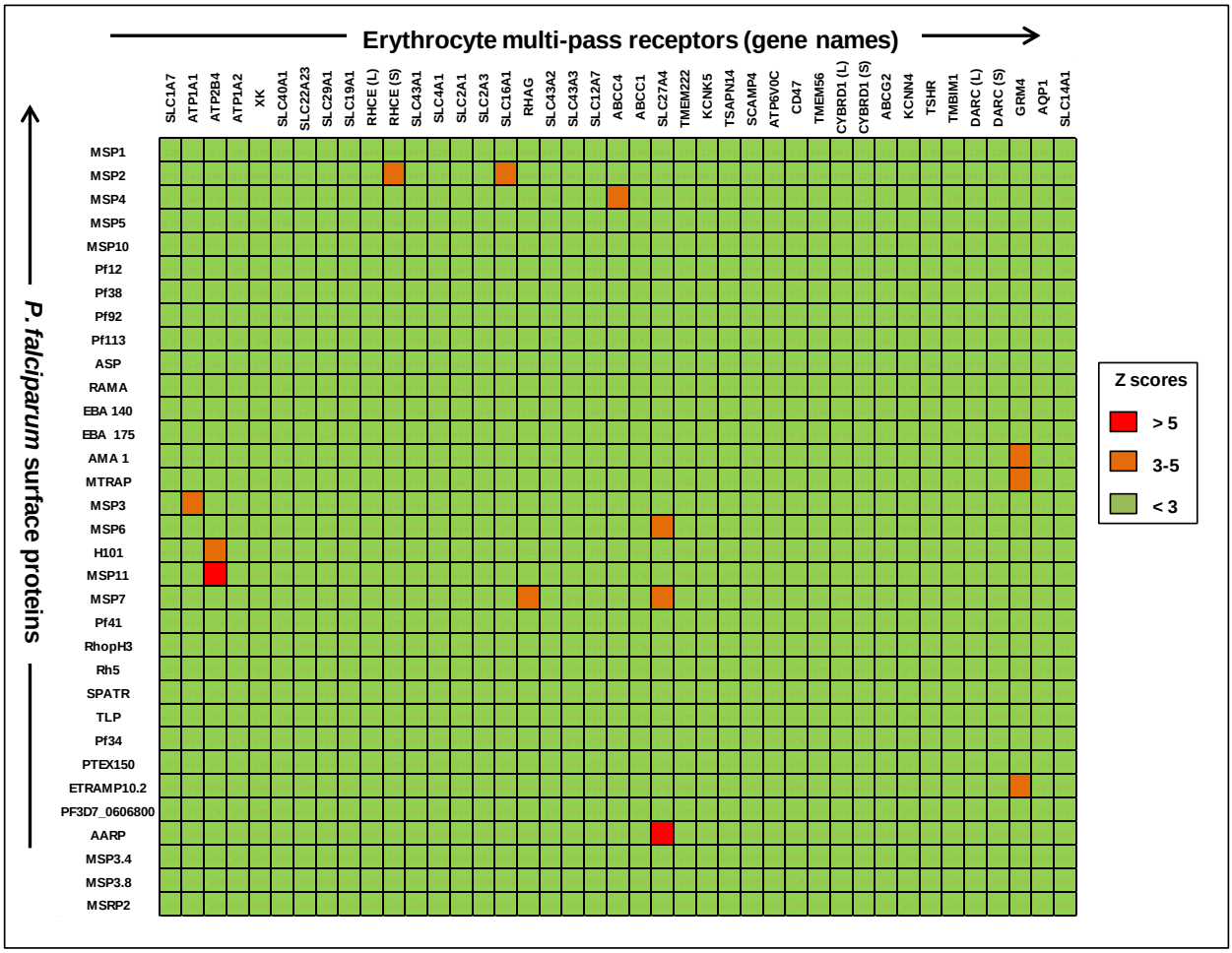

Figure 54. 33 *P. falciparum* proteins were tested against 41 erythrocyte multi-pass receptors (including two isoforms each of three proteins) expressed individually on the surface of HEK293E cells. Mock-transfected cells were used as a negative control in the screen. The binding of each *Plasmodium* protein, immobilised on Nile red beads, to cells transfected with the recombinant receptors was estimated using a fluorescence intensity threshold to select the Nile red 'positive' cells. The binding to mock-transfected cells was subtracted in each case to calculate the 'actual' binding to the recombinantly-expressed receptor. The values estimated for each *P. falciparum* protein were then normalised across the panel of erythrocyte multi-pass receptors to calculate a z score for each interaction (i.e. (actual binding to a specific multi-pass receptor - average binding to the panel of multi-pass receptors)/standard deviation of the binding to the panel of multi-pass receptors). The heat map shows the calculated z score of each *P. falciparum* protein: erythrocyte multi-pass receptor interaction. Two interactions had a z score of above 5 and another 11 had z scores between 3 and 5.

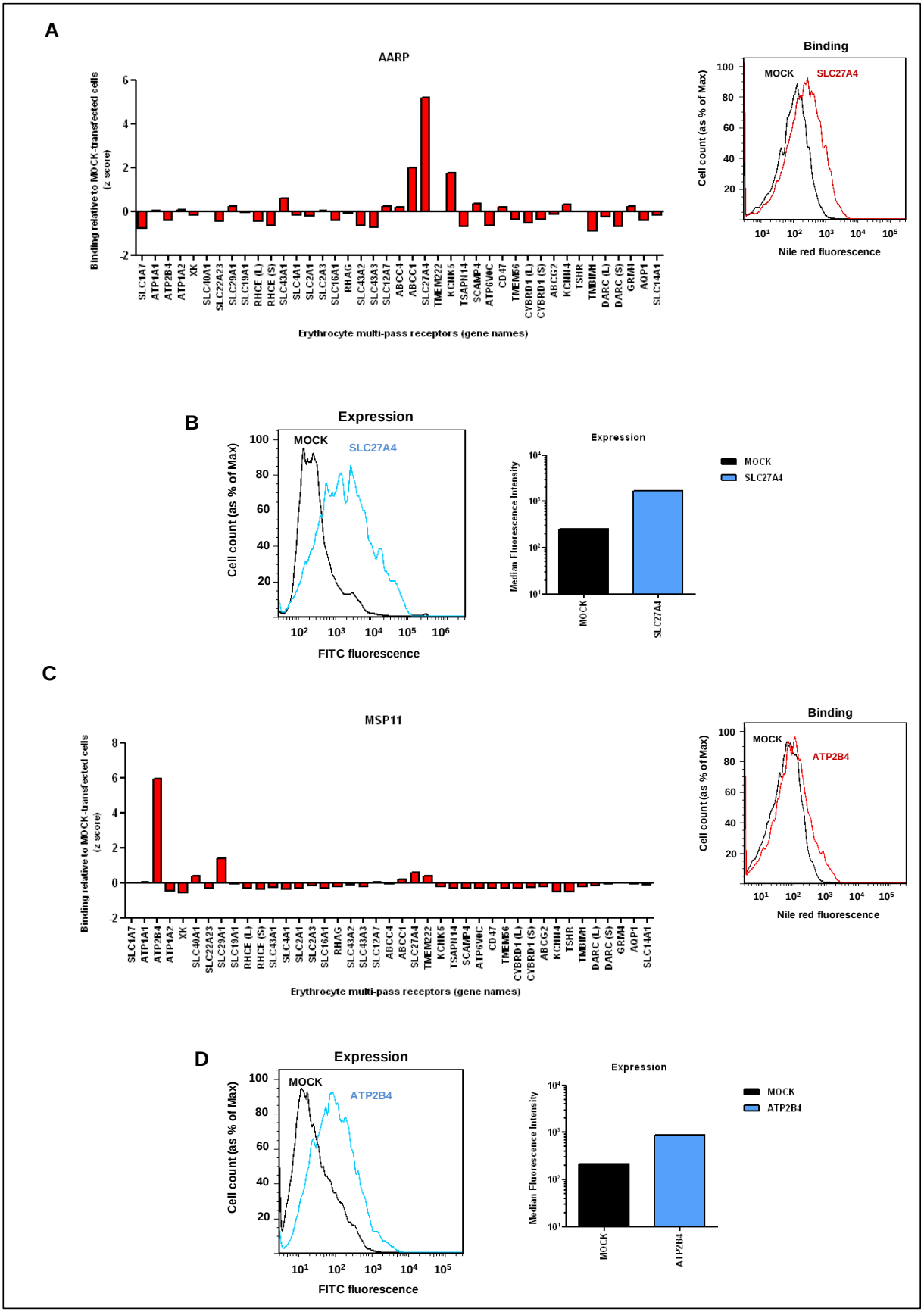
A
AARP
Binding relative to MOCK-transfected cells (z score)
Erythrocyte multi-pass receptors (gene names)
Binding
MOCK
SLC27A4
Cell count (as % of Max)
Nile red fluorescence
B
Expression
MOCK
SLC27A4
Cell count (as % of Max)
FITC fluorescence
Expression
Median Fluorescence Intensity
MOCK
SLC27A4
C
MSP11
Binding relative to MOCK-transfected cells (z score)
Erythrocyte multi-pass receptors (gene names)
Binding
MOCK
ATP2B4
Cell count (as % of Max)
Nile red fluorescence
D
Expression
MOCK
ATP2B4
Cell count (as % of Max)
FITC fluorescence
Expression
Median Fluorescence Intensity
MOCK
ATP2B4

Figure 55. The interactions between the *P. falciparum* proteins AARP and MSP11 with the multi-pass receptors encoded by SLC27A4 (the Fatty acid transporter) and ATP2B4 (Plasma membrane calcium transporting ATPase 4) respectively, were the most significant, with z scores of above 5. A) and **C)** The bar charts show the normalised binding (z scores) of AARP (**A**) and MSP11 (**C**) to the panel of erythrocyte multi-pass receptors. The histograms represent mock-transfected cells (black) and cells transfected with SLC27A4 (red) **(A)** or ATP2B4 (red) **(C)**, after incubation with AARP-coated Nile red beads. **B)** and **D)** The histograms are of mock-transfected cells (black) and cells transfected with SLC27A4 (blue) **(B)** or ATP2B4 (blue) **(D)**, stained with an anti-c-Myc mouse monoclonal and a FITC-conjugated anti-mouse secondary. The bar charts show the median fluorescence intensities (at the FITC emission wavelength) of the antibody stained cells.

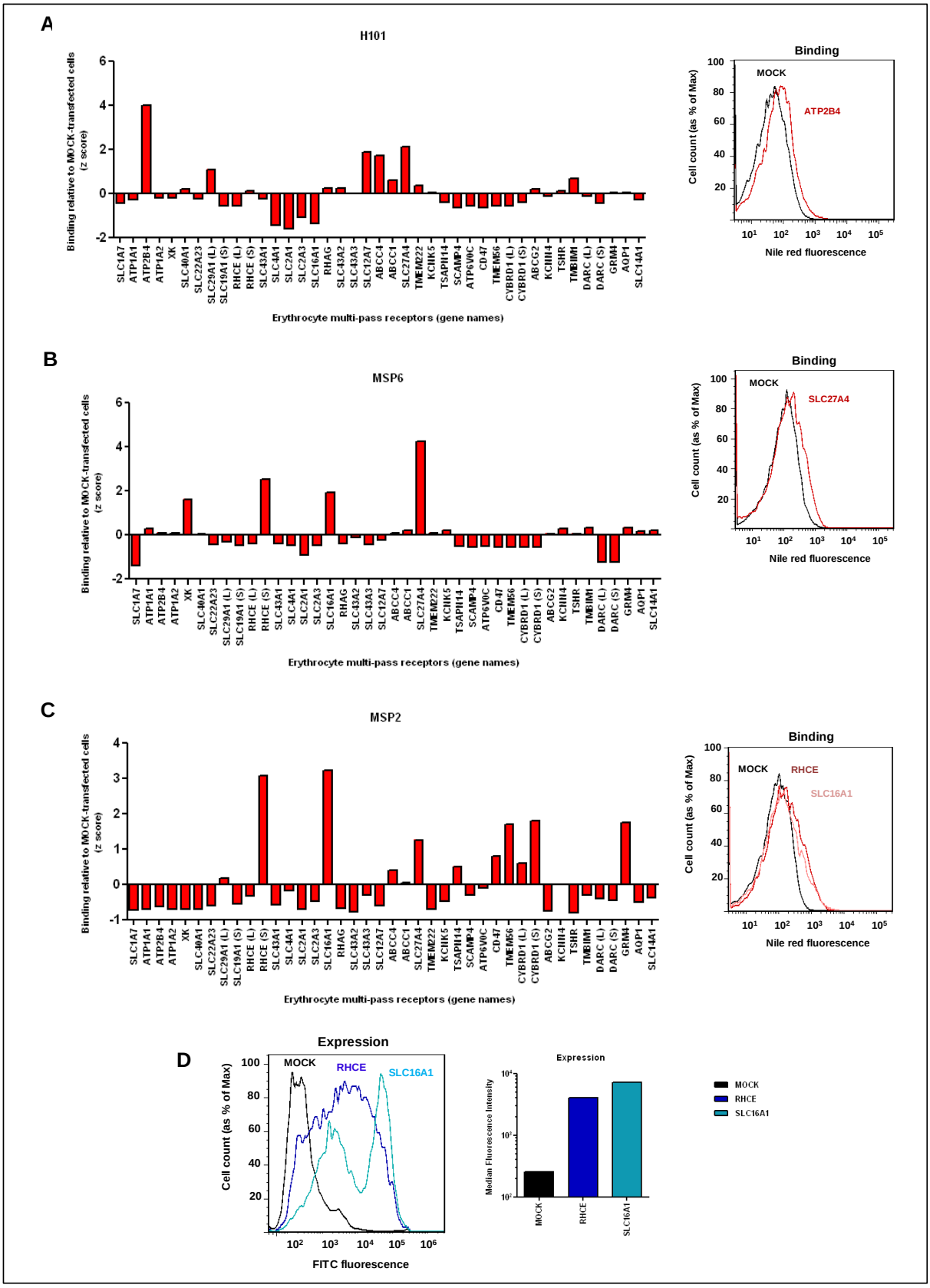
A
H101
Binding relative to MOCK-transfected cells (z score)
Erythrocyte multi-pass receptors (gene names)
Binding
MOCK
ATP2B4
Cell count (as % of Max)
Nile red fluorescence
B
MSP6
Binding relative to MOCK-transfected cells (z score)
Erythrocyte multi-pass receptors (gene names)
Binding
MOCK
SLC27A4
Cell count (as % of Max)
Nile red fluorescence
C
MSP2
Binding relative to MOCK-transfected cells (z score)
Erythrocyte multi-pass receptors (gene names)
Binding
MOCK
RHCE
SLC16A1
Cell count (as % of Max)
Nile red fluorescence
D
Expression
MOCK
RHCE
SLC16A1
Cell count (as % of Max)
FITC fluorescence
Expression
Median Fluorescence Intensity
MOCK
RHCE
SLC16A1

Figure 56. The *P. falciparum* proteins H101, MSP6 and MSP2 showed significant binding (z scores above 3) to specific recombinant multi-pass receptors. A), B) and C) The bar charts show the normalised binding (z scores) of H101 (**A**), MSP6 (**B**) and MSP2 (**C**) to the panel of erythrocyte multi-pass receptors. The histograms represent mock-transfected cells (black) and cells transfected with ATP2B4 (red) (**A**), SLC27A4 (red) (**B**), RHCE (red) (**C**) and SLC16A1 (pink) **(C)**, after incubation with AARP-coated Nile red beads. **D**) The histograms are of mock-transfected cells (black) and cells transfected with RHCE (dark blue) or SLC16A1 (light blue), stained with an anti-c-Myc mouse monoclonal and a FITC-conjugated anti-mouse secondary. The bar chart shows the median fluorescence intensities (at the FITC emission wavelength) of the antibody stained cells. ATP2B4, SLC27A4, RHCE and SLC16A1, code for the multi-pass receptors Plasma membrane calcium transporting ATPase 4, Fatty acid transporter 4, Rh blood CE group antigen polypeptide and Monocarboxylate transporter 1, respectively.

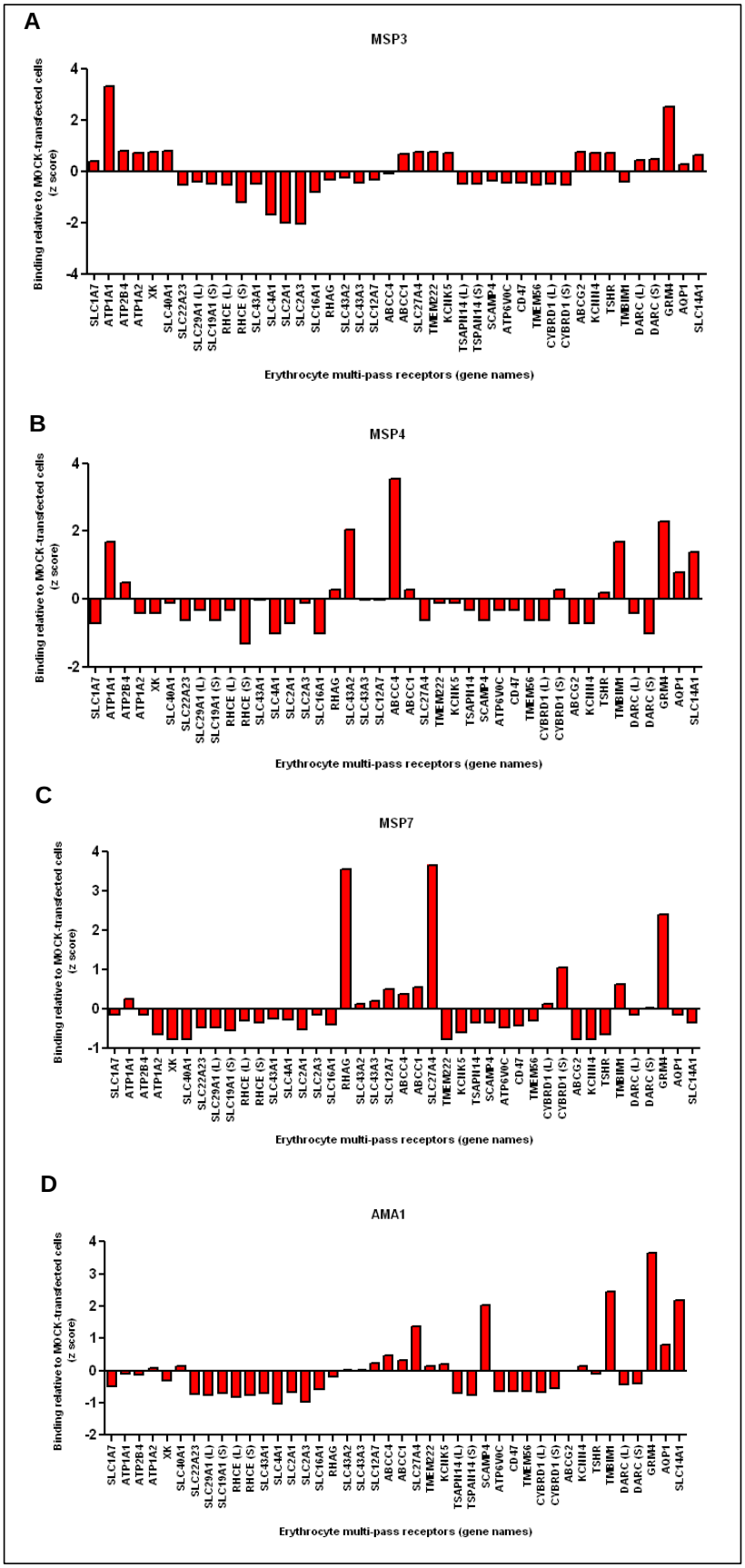
A
MSP3
Binding relative to MOCK-transfected cells (z score)
Erythrocyte multi-pass receptors (gene names)
B
MSP4
Binding relative to MOCK-transfected cells (z score)
Erythrocyte multi-pass receptors (gene names)
C
MSP7
Binding relative to MOCK-transfected cells (z score)
Erythrocyte multi-pass receptors (gene names)
D
AMA1
Binding relative to MOCK-transfected cells (z score)
Erythrocyte multi-pass receptors (gene names)

Figure 57. Significant (z scores above 3) binding to specific recombinant multi-pass receptors was also observed with the *P. falciparum* proteins MSP3, MSP4, MSP7 and AMA1. A), B), C) and D) The bar charts show the normalised binding (z scores) of MSP3 (**A**), MSP4 (**B**), MSP7 (**C**) and AMA1 (**D**) to the panel of erythrocyte multi-pass receptors.

blood group associated protein (RHAG) and Metabotropic glutamate receptor 4 (GRM4) respectively, also had relatively significant z scores of above 3 (Figure 57). No binding of the MSP1 protein to Band 3 was seen in the screen (Figure 58 A and B). Compared to mock-transfected cells, cells expressing Band 3 showed higher binding only to RH5 (Figure 58 C). The z score of this interaction was however less than 2, indicating that it wasn't very significant and probably a result of a slight up-regulation in the expression of Basigin (Figure 58 D).

5.2.7 Preliminary follow-up study: recapitulation of the interaction between AARP and the Fatty acid transporter 4.

The attempt to recapitulate the interaction between AARP and the Fatty acid transporter 4, using an independent preparation of AARP and a fresh batch of cells transfected with its putative erythrocytic receptor was successful (Figure 59). The level of expression of the recombinant receptor was less than what was observed in the original screen (Figure 59 A) and perhaps as a consequence the difference in the binding of AARP to mock-transfected cells and to those transfected with the Fatty acid transporter 4 was also lower (Figure 59 B).

5.2.8 Investigating the carbohydrate-binding properties of nine proteins selected from the *P. falciparum* merozoite surface protein library.

When tested against untreated HEK293E cells in a previous screen, 15 of the *P. falciparum* merozoite surface proteins showed some putative binding. It is likely that at least some of these proteins were recognising specific carbohydrate moieties at the cell surface and indeed the binding of four of the proteins, namely Pf113, EBA140, EBA175 and MSRP2, was observed to be dependent on sialic acid (Figure 51). To probe their glycan-binding properties further, these four proteins and five others (Pf12, RhopH3, AARP, MSP3.4 and MSP3.8) which had shown

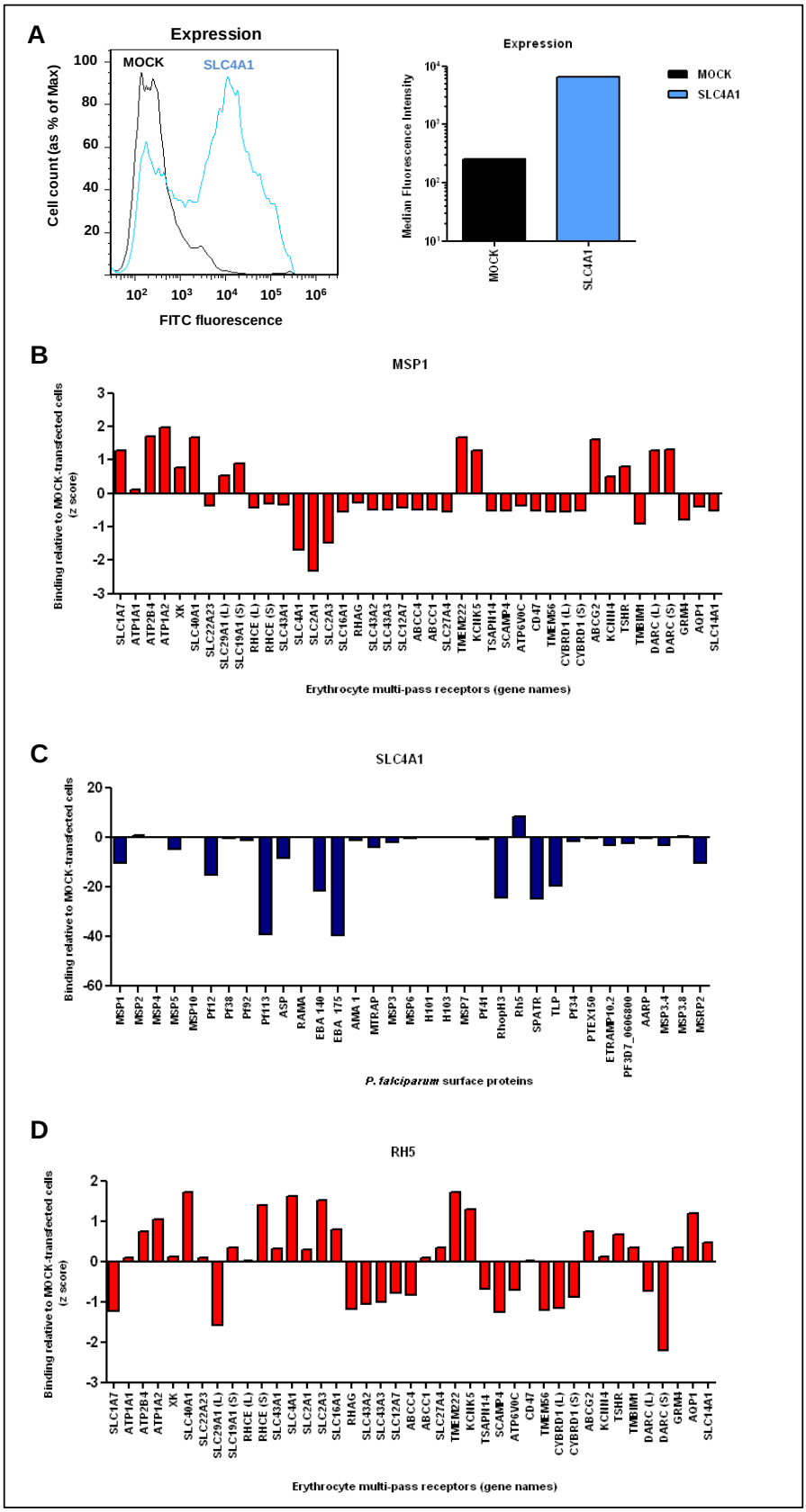
A
Expression
MOCK
SLC4A1
Cell count (as % of Max)
FITC fluorescence
Expression
Median Fluorescence Intensity
MOCK
SLC4A1
B
MSP1
Binding relative to MOCK-transfected cells (z score)
Erythrocyte multi-pass receptors (gene names)
C
SLC4A1
Binding relative to MOCK-transfected cells
P. falciparum surface proteins
D
RH5
Binding relative to MOCK-transfected cells (z score)
Erythrocyte multi-pass receptors (gene names)

Figure 58. No binding between the *P. falciparum* protein MSP1 and the erythrocyte multi-pass receptor Band3 (gene name: SLC4A1) was detected in the screen. A) The histograms are of mock-transfected cells (black) and cells transfected with SLC4A1(blue), stained with an anti-c-Myc mouse monoclonal and a FITC-conjugated anti-mouse secondary. The bar chart shows the median fluorescence intensities (at the FITC emission wavelength) of the antibody stained cells. **B**) and **D**) The bar charts represent the normalised binding (z scores) of MSP1 (**B**) and Rh5 (**D**) to the panel of erythrocyte multi-pass receptors. **C)** The non-normalised binding of the library of *P. falciparum* proteins to SLC4A1-transfected cells, relative to mock-transfected cells is shown.

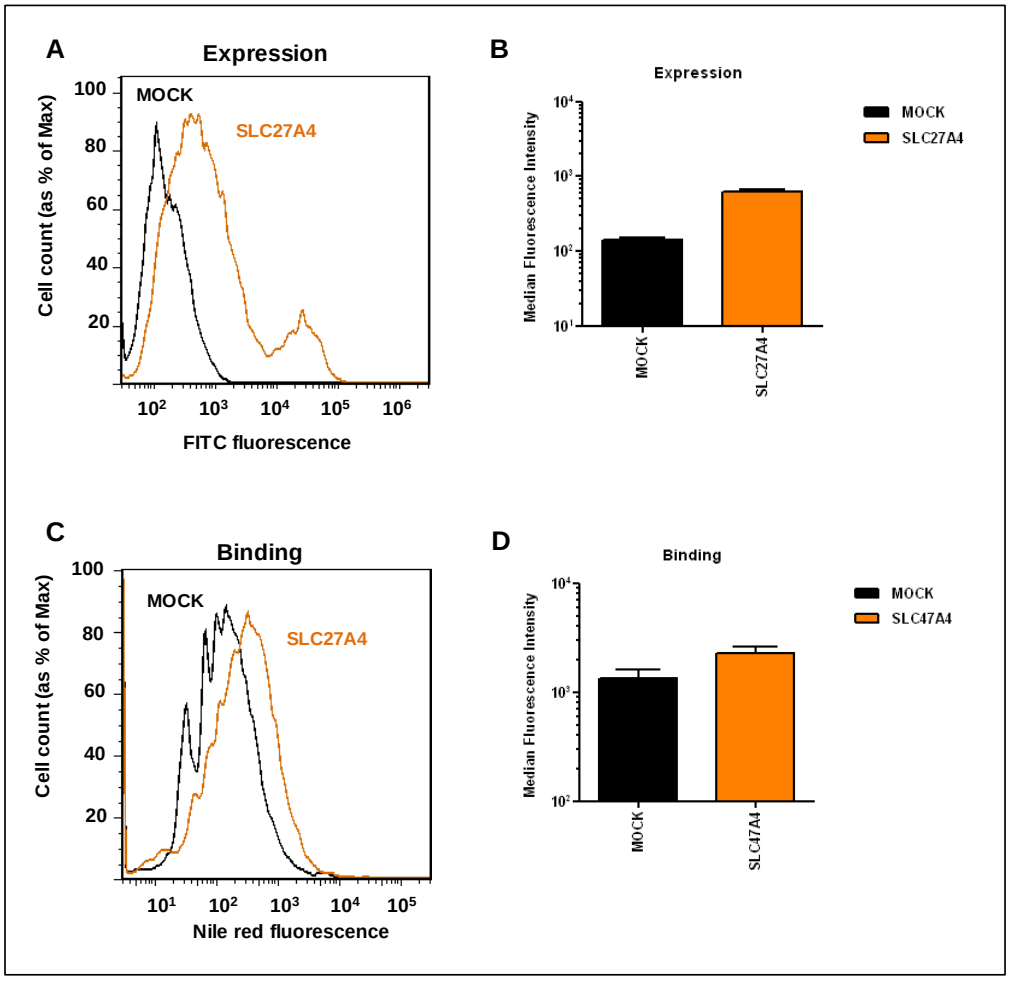

Figure 59. The interaction between the *P. falciparum* protein AARP and the recombinant multi-pass receptor, Fatty acid transporter 4 (gene name: SLC27A4) was recapitulated in an independent follow-up experiment, using the same assay as in the original screen. A) and **B)** The histograms are of mock-transfected cells (black) and cells transfected with SLC27A4 (yellow), stained with an anti-c-Myc mouse monoclonal and a FITC-conjugated anti-mouse secondary. The bar chart shows the median fluorescence intensities (at the FITC emission wavelength) of the antibody stained cells. **C**) and **D**) The histograms show mock-transfected cells (black) and cells transfected with SLC27A4 (yellow) **(A)**, after incubation with AARP-coated Nile red beads. The bar chart shows the median fluorescence intensities (at the Nile red emission wavelength) of the cells.

sialic-acid independent binding to HEK293E cells, were selected for testing against a panel of synthetic glycan probes in a pilot screen. The synthetic glycan probes used were purchased commercially from GlycoTech and included antigens of the ABH, Lewis, P_1, T, Tn blood types as well individual monosaccharides and the core glycan components of N-linked and O-linked oligosaccharides (Table 8 and Figure 60 A). In the screen, biotinylated forms of the glycans were immobilised on a streptavidin-coated plate and probed with the *P. falciparum* surface proteins expressed as β lactamase-tagged, pentameric preys. Binding events were detected using the β-lactamase substrate nitrocefin.

Prior to performing the screen, the well-characterised interaction between the human protein P-selectin and its carbohydrate ligand sialyl-Lewis X (sialyl-Le^x) was used in a proof-of-principle study to assess the technical feasibility and specificity of the assay (Polley *et al*., 1991). P-selectin, also expressed as a β-lactamase-tagged pentamer was observed to bind to the synthetic sialyl- Le^x probe and this Ca^{2+}-dependent interaction could be inhibited by the addition of EDTA in a concentration-dependent manner (Figure 60 C).

In the screen, any significant binding to the carbohydrate probes was seen only with Pf113, EBA140, EBA175 and MSRP2 (Figures 61, 62 and 63). These four proteins, which showed sialic-acid dependent binding to HEK293E cells, also recognised carbohydrate probes containing sialic-acid (Figures 62 and 63). The binding of each of these proteins to a number of sialic acid-containing but structurally different glycans needs to be investigated.

Table 8. The panel of 55 synthetic carbohydrate probes.

Number	Glycan	Structure
1	α-D-Glucose	**Monosaccharide**
2	β-D-Glucose	
3	α-D-Galactose	
4	β-D-Galactose	
5	α-D-Mannose	
6	α-D-Man-6-phosphate	
7	α-L-Fucose	
8	β-GlcNAc	
9	α-GalNAc (T_n antigen)	
10	β-GalNAc	
11	α-Neu5Ac	
12	GalNAcα1-3Galβ (A antigen)	**Disaccharide**
13	Galα1-3Galβ (B antigen)	
14	Fucα1-2Galβ (H antigen)	
15	Galβ1-3GlcNAcβ (Le^c antigen)	
16	Galβ1-4Glcβ (Lactose)	
17	Galβ1-4GlcNAcβ (N-acetyllactosamine, LacNAc)	
18	Galβ1-3GalNAcα (O-glycan core 1)	
19	Fucα1-3GlcNAcβ (Le antigen)	
20	Fucα1-4GlcNAcβ (Le antigen)	
21	GalNAcα1-3GalNAcβ	
22	Galα1-3GalNAcα ($T_{\alpha\alpha}$ antigen)	
23	Galβ1-3GalNAcβ ($T_{\beta\beta}$ antigen)	
24	Galα1-3GalNAcβ ($T_{\alpha\beta}$ antigen)	
25	Galβ1-3Galβ	
26	GalNAcα1-3(Fucα1-2)Galβ (A antigen)	**Trisaccharide**
27	Galα1-3(Fucα1-2)Galβ (B antigen)	
28	Le^a antigen	
29	Le^x antigen	
30	3'-Sialyllactose	
31	6'-Sialyllactose	
32	Le^b antigen	**Complex oligosaccharide**
33	Le^y antigen	
34	Sialyl Le^a	
35	Sialyl Le^x	
36	Neu5Gcα	**Monosaccharide**
37	GlcNAcβ1-3Galβ	**Disaccharide**
38	Galα1-4GlcNAcβ (α-N-acetyllactosamine)	
39	Glcα1-4Glcβ (Maltose)	
40	Galβ1-3GalNAcα (TF antigen)	
41	Neu5Acα2-6GalNAcα (6-$SiaT_n$)	
42	H antigen (type 3)	
43	Neu5Acα2-3Gal (Sialylated galactose)	
44	GlcNAcβ1-3GalNAcα (N-glycan core 3)	
45	GlcNAcβ1-6GalNAcα (N-glycan core 6)	
46	Neu5Acα2-3Galβ1-4GlcNAcβ (Sialyl-LacNAc)	**Trisaccharide**
47	Neu5Acα2-8Neu5Acα2-8Neu5Acα (Polysialic acid)	
48	Galβ1-3(GlcNAcβ1-6)GalNAcα (O-glycan core 2)	
49	Neu5Acα2-3Galβ1-3GalNAcα (O-glycan Sia-core1)	
50	GlcNAcβ1-3(GlcNacβ1-6)GalNAcα	
51	Galβ1-3GlcNAcβ1-3Galβ1-4Glcβ (LNT)	**Complex**
52	Galβ1-4GlcNAcβ1-3Galβ1-4Glcβ (LNnT)	
53	Neu5Gcα2-6GalNAcα	**Monosaccharide**
54	Neu5Acα2-3GalNAcα (3-$SiaT_n$)	
55	Galα1-4Galβ1-4GlcNAcβ (P_1 antigen)	**Trisaccharide**

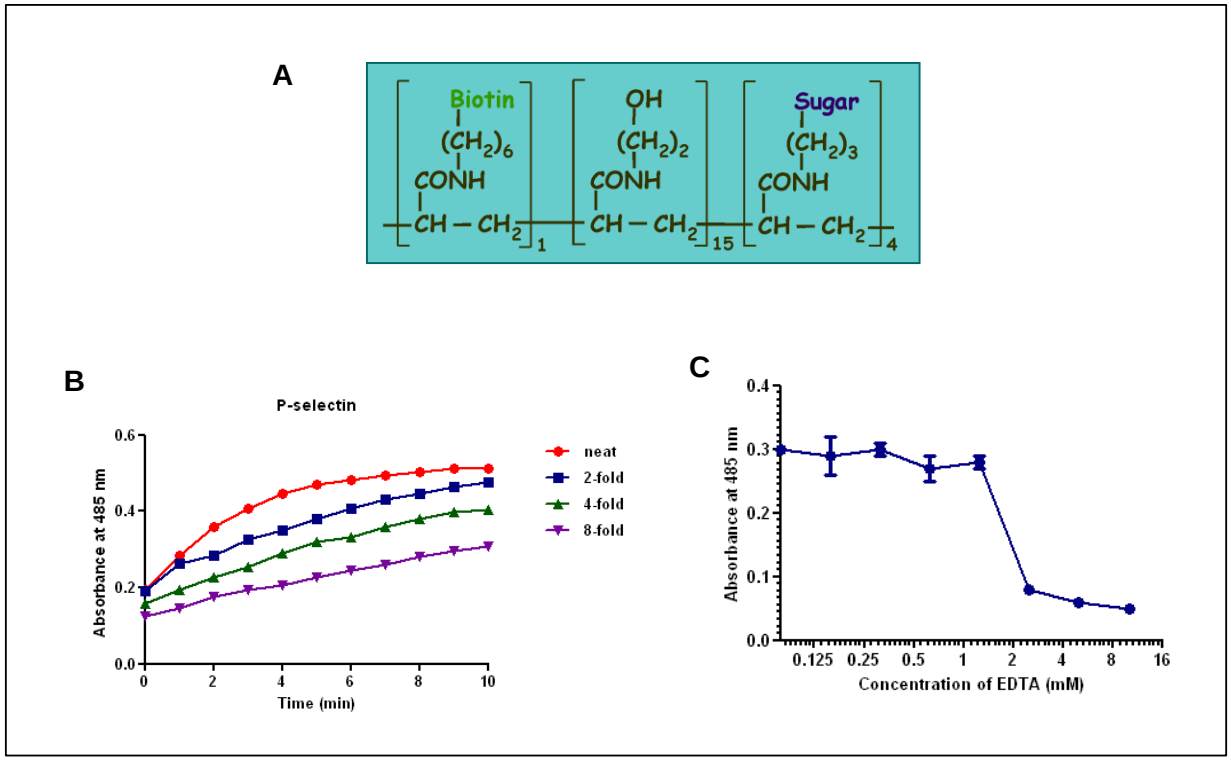

Figure 60. A 'proof-of-principle' study: the human protein P-selectin showed specific binding to synthetic sialyl-Le^x. P-selectin, expressed as a β-lactamase tagged pentamer (with C-terminal Cd4), was probed against biotinylated sialyl- Le^x immobilised on a streptavidin-coated plate. After incubation for 2 h at room temperature, putative protein-glycan binding was detected by the turnover of the β-lactamase substrate, nitrocefin at an absorbance of 485 nm. **A)** The synthetic sialyl-Le^x probe used was attached to a biotin tag via a flexible linker. The schematic was reproduced from the GlycoTech webpage http://www.glycotech.com/probes/multivalbio.html. **B)** The level of expression of the P-selectin protein was estimated by monitoring the turnover of nitrocefin in a time course assay. A 2-fold dilution series of the protein was used for this purpose. The protein was used neat for testing against the glycan probe. **C)** The graph shows the Ca^{2+}-dependent binding of P-selectin to synthetic sialyl- Le^x. The assay was performed in the presence of a range of different concentrations of EDTA, from 0.08- 10 mM. The data is shown as mean ± standard deviation, n=3.

A

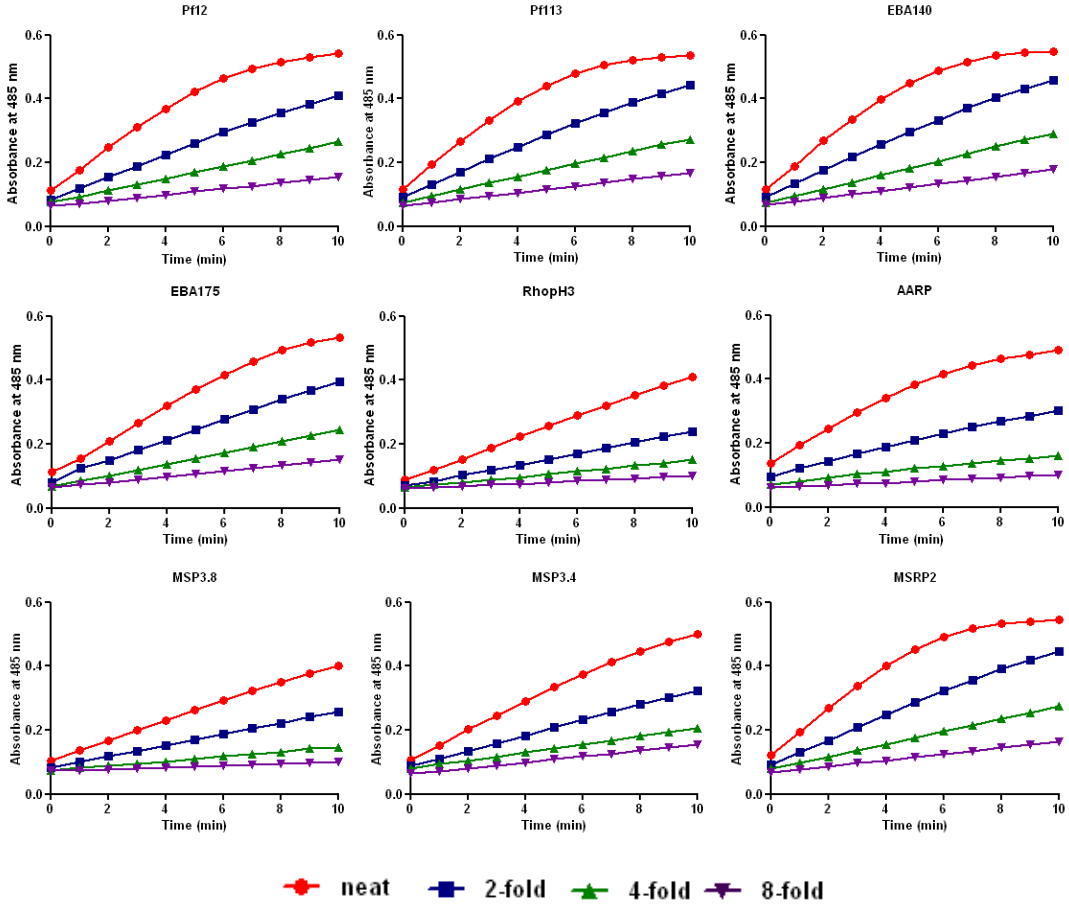

B

	Pf113	EBA140	EBA175	MSRP2
3'-Sialyllactose (30)	■	■	■	
Sialyl Le^a (34)		■		■
Sialyl Le^x (35)				■
Neu5Gcα (36)	■	■	■	
6-SiaT$_n$ (41)	■	■	■	
Sialyl galactose (43)			■	
Sialyl- LacNAc (46)	■	■	■	
Polysialic acid (47)			■	■
O-glycan Sia-core 1 (49)	■	■	■	■
Neu5Gcα2-6GalNAcα (53)	■	■	■	
3-SiaT$_n$ (54)	■	■	■	

Figure 61. Nine *P. falciparum* proteins were screened against a panel of 55 synthetic glycan probes. The *P. falciparum* proteins expressed as β lactamase-tagged pentamers (with C-terminal Cd4) were tested against the biotinylated glycans immobilised on streptavidin-coated plates. Protein-glycan binding was detected by the turnover of nitrocefin at 485 nm. **A)** The *Plasmodium* proteins were normalised against each other, by monitoring the turnover of nitrocefin in a time course assay. **B)** In the screen, four of the proteins showed binding to glycans containing sialic acid. Red indicates an interaction.

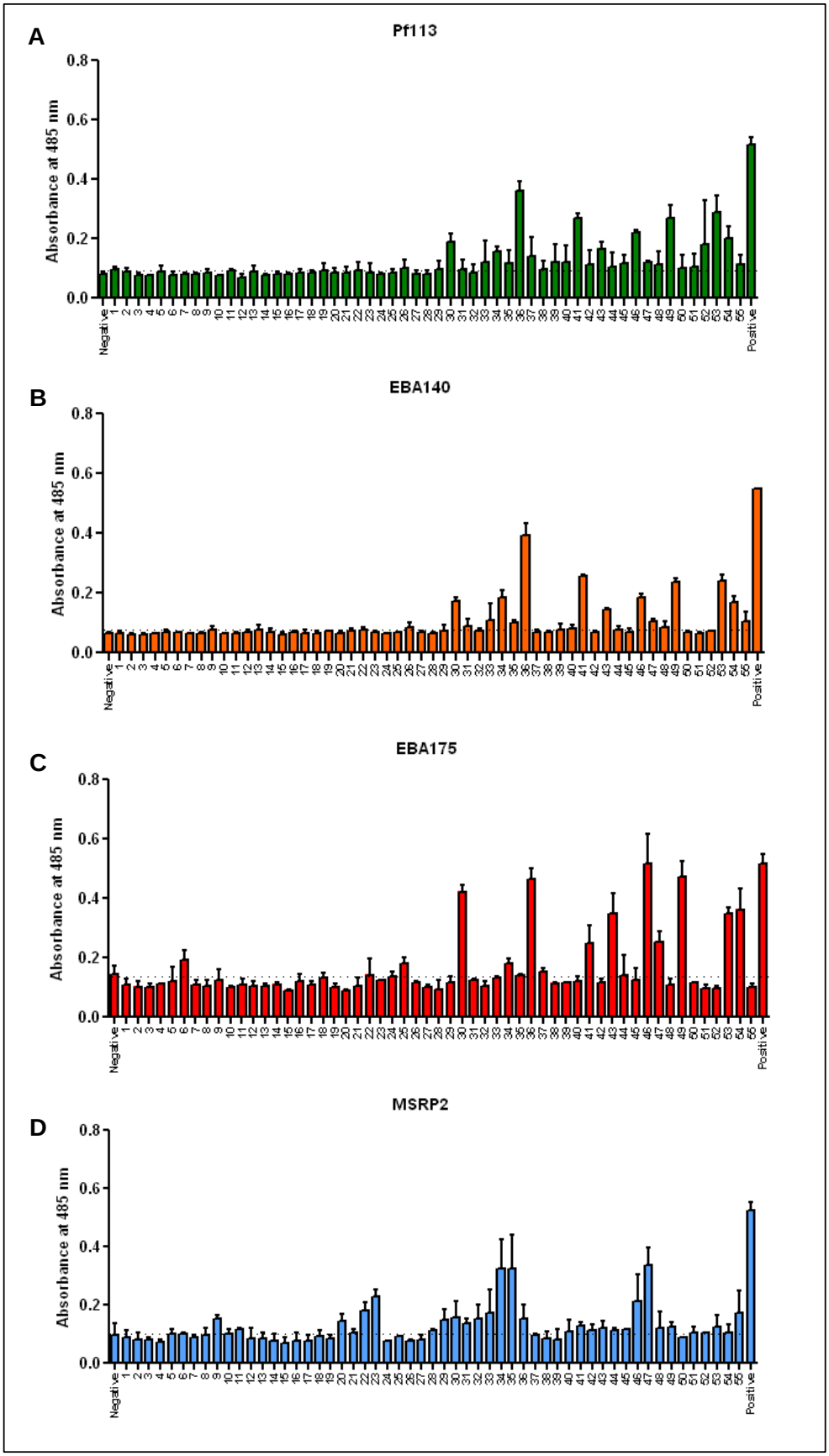
A
Pf113
Absorbance at 485 nm
0.0
0.2
0.4
0.6
0.8
Negative
Positive
B
EBA140
Absorbance at 485 nm
Negative
Positive
C
EBA175
Absorbance at 485 nm
Negative
Positive
D
MSRP2
Absorbance at 485 nm
Negative
Positive

Figure 62. Four *P. falciparum* proteins tested showed binding to sialic acid-containing glycans. The bar charts show the binding of Pf113, EBA140, EBA175 and MSRP2 to the panel of 55 synthetic glycan probes. Each bar shows mean ± standard deviation, n=2. Biotinylated OX68 (an anti-Cd4 monoclonal) was used as the positive control bait in the screen. The biotinylated bait used as the negative control contained the linker region carried by all the synthetic glycans.

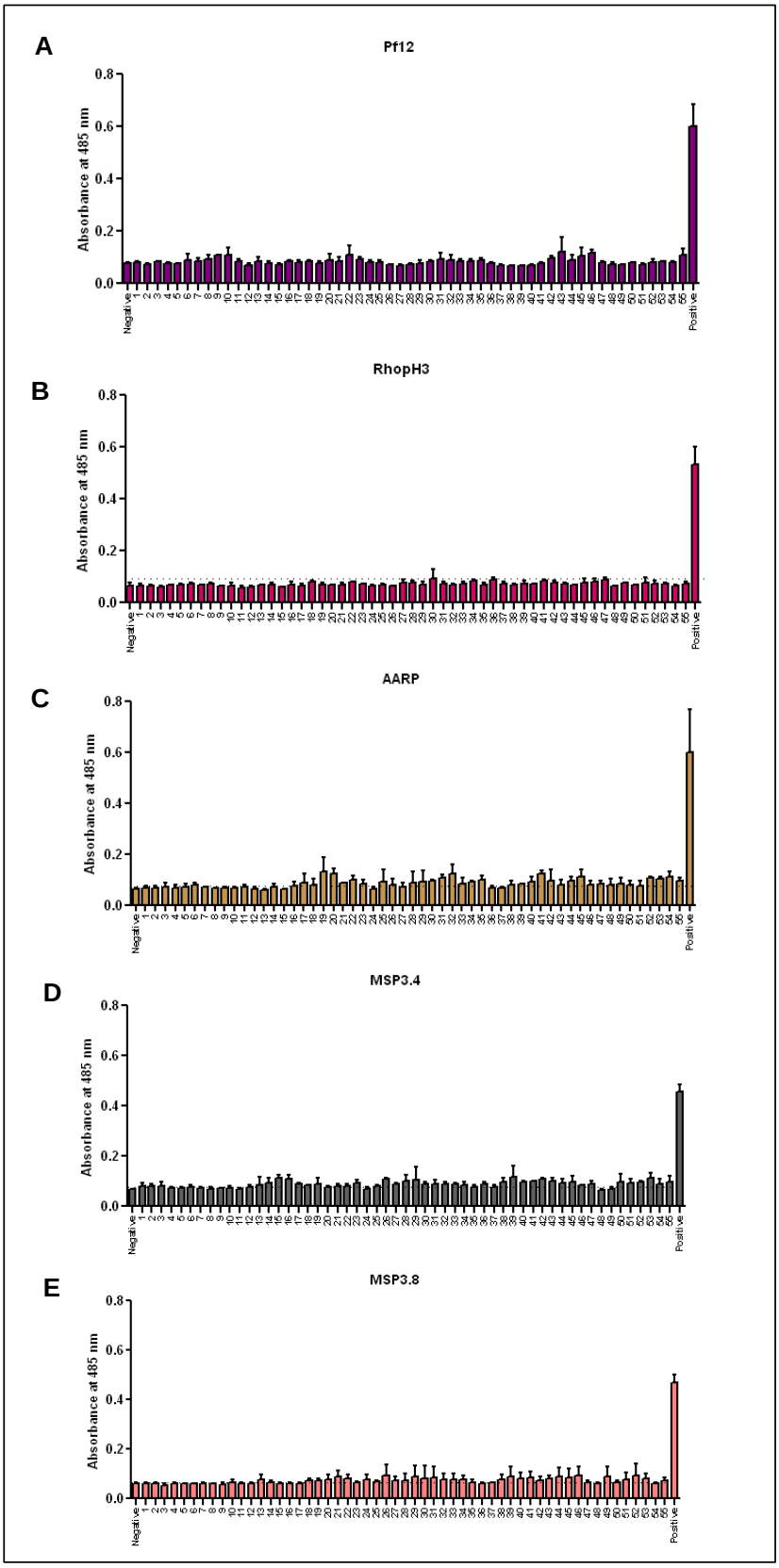
A
Pf12
Absorbance at 485 nm
0.0
0.2
0.4
0.6
0.8
Negative
Positive
B
RhopH3
Absorbance at 485 nm
Negative
Positive
C
AARP
Absorbance at 485 nm
Negative
Positive
D
MSP3.4
Absorbance at 485 nm
Negative
Positive
E
MSP3.8
Absorbance at 485 nm
Negative
Positive

Figure 63. Five *P. falciparum* proteins tested showed no significant binding to any glycan. The bar charts show the binding of Pf12, RhopH3, AARP, MSP3.4 and MSP3.8 to the panel of 55 synthetic glycan probes. Each bar shows mean ± standard deviation, n=2. Biotinylated OX68 (an anti-Cd4 monoclonal) was used as the positive control bait in the screen. The biotinylated bait used as the negative control contained the linker region carried by all the synthetic glycans.

5.3 DISCUSSION

An efficacious vaccine against malaria is vital for sustained control and eradication of this disease on a worldwide scale (Crompton *et al*., 2010). As the causative agent of the most clinically severe form of malaria, *P. falciparum* has been the primary focus of attempts to develop such a vaccine over the past three decades. Candidate vaccines that target only one particular stage of the *P. falciparum* life cycle have been observed to be incapable of conferring complete sterile protection against malaria, in clinical trials (Geels *et al*., 2011; Greenwood and Targett, 2011). A potentially more successful approach is to combine several antigens from different stages of the parasite life cycle in a multi-component vaccine. *P. falciparum* merozoite surface proteins that play an important role in erythrocyte invasion are ideal candidates for the blood stage component of such a next-generation vaccine (Tham *et al*., 2012). Transcriptomic and proteomic studies have identified around 260 proteins that are expressed at the merozoite stage in *P. falciparum*, however, more than 70% of these have no identified function (Bozdech *et al*., 2003; Florens *et al*., 2002). In order to determine which of the novel *P. falciparum* merozoite surface proteins should be prioritised as potential vaccine candidates, their functional characterisation with the use of large-scale, high-throughput techniques is therefore, a necessity (Tran *et al*., 2005).

Traditional methods used for identifying protein-protein interactions on a global scale, such as yeast-2-hybrid screening and tandem affinity purification-mass spectrometry cannot be used for detecting the low-affinity extracellular interactions between *P. falciparum* merozoite surface proteins and erythrocyte receptors (Bei and Duraisingh, 2012; Wright, 2009). Similarly the commonly used methods for identifying the binding of *P. falciparum* surface proteins to

erythrocytes (e.g. erythrocyte 'rosetting' assays) are not amenable for adaptation to high-throughput screening (Tran *et al*., 2005).

The AVEXIS platform developed in our laboratory is designed to facilitate the detection of low-affinity interactions between proteins in a high-throughput manner and has been used successfully to identify novel interactions between a library of *P. falciparum* merozoite surface proteins and a panel of erythrocyte receptors, expressed as full-length ectodomain fragments (Crosnier *et al*., 2011; Bartholdoson *et al*., unpublished data). The expression of proteins in soluble form is however a pre-requisite of this ELISA-based screening strategy and it is thus not applicable to multi-pass receptors.

In this study, a novel flow cytometry-based approach was used to screen the library of *P. falciparum* surface protein ectodomains against both human erythrocytes and recombinant erythrocyte multi-pass receptors expressed on HEK293E cells, in a high-throughput manner. An ELISA-based assay was also developed for identifying the glycan-binding properties of *P. falciparum* surface proteins, by screening against a panel of synthetic carbohydrate probes.

5.3.1 Investigating the binding of a library of *P. falciparum* merozoite surface proteins to human erythrocytes using a novel high-throughput, flow cytometry-based approach.

From the 33 *P. falciparum* proteins which were presented to human erythrocytes as multimeric arrays on Nile red beads, 13 showed some association with the erythrocyte surface (Figure 45). Of these, the interactions of EBA175, EBA140, RH5, Pf34, MSP3.4 and MSP3.8 were the most significant. In this assay, the binding of a bead-immobilised parasite protein to a receptor on the erythrocyte surface, was expected to cause an increase in the fluorescence intensity of the erythrocyte population (at the Nile red emission wavelength). The magnitude of this 'shift' in fluorescence would be proportional to the number of protein-coated beads associated with each

erythrocyte, which in turn would be dependent on the copy number/cell of the erythrocyte receptor recognised by the parasite protein. The largest shifts in the fluorescence intensity of the erythrocyte populations (i.e. the highest levels of binding) were seen with EBA175 and EBA140, the two parasite proteins known to recognise the highly abundant receptors, Glycophorins A and C, respectively (Figure 45). The other 11 parasite proteins, including RH5, seemed to interact with erythrocyte receptors which were present at much lower abundance. Probing the specificity of the observed interactions by enzymatic pre-treatment of erythrocytes revealed that EBA140 binds to erythrocytes in a trypsin and neuraminidase sensitive but chymotrypsin insensitive manner, which is consistent with its known sialic acid dependent binding to Glycophorin C (Figures 46). On the other hand, the binding of RH5 to erythrocytes was insensitive to treatment with trypsin, chymotrypsin and neuraminidase, which is in agreement with the enzymatic susceptibility profile of the interaction between RH5 and its known erythrocyte receptor, Basigin (Figure 46). The binding of the proteins, Pf34, MSP3.4 and MSP3.8, to erythrocytes was also not affected by treatment with any of the three enzymes (data not shown). These proteins may be interacting with multi-pass receptors, which are less susceptible to proteolytic digestion or with non-proteinaceous receptors such as glycolipids. Pf34 is a GPI-anchored protein, located in detergent-resistant membrane domains in the rhoptry neck of the parasite and synthetic peptides based on its sequence have been shown to inhibit erythrocyte invasion by *P. falciparum,* albeit at relatively high concentrations (Proellocks *et al*., 2007; Arévalo-Pinzón *et al*., 2010). MSP3.4 and MSP3.8, peripheral surface proteins of the MSP3-multigene family, are targets of naturally-acquired protective antibodies against *P. falciparum* infection (Singh *et al*., 2009). Pf34, MSP3.4 and MSP3.8 are therefore likely to be involved in interactions with erythrocyte surface receptors.

In comparison to traditional erythrocyte binding assays, the flow-cytometry based assay used in this study is fast, simple, quantitative and objective. It also incurs very little sample consumption. Immobilisation of parasite ligands on fluorescent beads was performed using small volumes (~100 µl per reaction on average) of cell culture supernatants containing the recombinantly-expressed proteins, with no prior purification. The biggest strength of this assay however is its amenability to high throughput screening, as demonstrated by testing with 33 *P. falciparum* surface proteins in parallel. Interactions with erythrocyte receptors of very low abundance are however likely to be missed with this approach, which is a major drawback. Based on the observations to date, this assay is probably most suitable for use in preliminary screens to narrow down large libraries of *Plasmodium* proteins to smaller selections of putative erythrocyte-binding ligands, which can then be characterised further using the traditional binding assays.

5.3.2 Screening *P. falciparum* merozoite surface proteins against a panel of erythrocyte multi-pass receptors expressed recombinantly on HEK293E cells, to identify novel interactions.

The major focus of the work described in this chapter, was the screening of the *P. falciparum* surface protein library against a panel of erythrocyte multi-pass receptors to identify novel interactions. The 41 erythrocyte receptors selected were expressed individually on the surface of HEK293E cells, in recombinant form, for this purpose and probed with multimeric bead-based arrays of the parasite proteins.

5.3.2.1 Endogenous receptors on HEK293E cells were recognised by some *P. falciparum* proteins.

Of the 33 *P. falciparum* proteins tested in the screen, 15 showed some ‘background’ binding to untreated and mock-transfected HEK293E cells, the expression host of the recombinant

erythrocyte multi-pass receptors (Figure 50). The highest binding was observed with the proteins RH5, EBA140, MSP3.4, MSP3.8, Pf12, MSRP2 and Pf113. Of these, some binding to human erythrocytes was previously observed with RH5, EBA140, MSP3.4, MSP3.8, Pf12 and MSRP2, suggesting that they are potentially binding to receptors present on both erythrocytes and HEK293E cells. Indeed, staining HEK293E cells with specific monoclonals revealed high endogenous expression of Basigin, accounting for the binding of RH5 to these cells (Figure 52).

Pf12 is a GPI-anchored protein located in detergent-resistant membrane domains at the merozoite surface (Sanders *et al*., 2005). It has been implicated in erythrocyte attachment, due to the presence of dual six-cysteine domains, a fold that is also found in some adhesive proteins expressed at other life cycle stages of the parasite (Carter *et al*., 1995; Sanders *et al*., 2005). MSRP2 is a member of the MSP7-multigene family, expressed at the asexual erythrocytic stage of the parasite. It has been identified as a potential substrate of the SUB1 protease which also cleaves MSP7 and MSP1 amongst others (Kadekoppala *et al*., 2010; Silmon de Monerri *et al*., 2011). Deletion of MSRP2 has however been found to have no effect on erythrocyte invasion and growth of *P. falciparum*, suggesting that it's likely to be functionally redundant (Kadekoppala *et al*., 2010).

Pf113 showed clear binding to HEK293E cells but not to erythrocytes (Figures 45 and 50), suggesting that it may be interacting with a surface receptor which is either absent on human erythrocytes or present only at very low levels. Pf113 is a putative GPI-anchored protein with cysteine-rich domains, located in lipid rafts and expressed both in the sporozoites and the merozoite stages of the *P. falciparum* life cycle (Sanders *et al*., 2005; Obando-Martinez *et al*., 2010).

Pre-treatment of HEK293E cells with neuraminidase significantly reduced the binding of EBA140, Pf113 and MSRP2 suggesting sialic-acid dependent recognition of surface receptors (Figure 51).

5.3.2.2 A number of potential erythrocyte multi-pass receptor: *P. falciparum* ligand pairs were identified in the screen.

A total of 13 putative interactions between erythrocyte multi-pass receptors and *P. falciparum* surface proteins were identified in the screen (Figures 54-57). The two most significant interactions were those between the *P. falciparum* protein AARP and the erythrocyte receptor Fatty acid transporter 4 (gene name: SLC27A4) and between the parasite protein MSP11 and the erythrocytic Plasma membrane calcium transporting ATPase 4 (ATP2B4) (Figure 55). AARP is a rhoptry protein, antibodies against which have been detected in malaria-immune individuals (Wickramarachchi *et al*., 2008). There is also some evidence to indicate binding of this protein to human erythrocytes (Wickramarachchi *et al*., 2008). MSP11, a member of the MSP3 family, is a peripheral protein associated with the merozoite surface (Pearce *et al*., 2005). Transfected parasite lines expressing truncated forms of MSP11 are viable, which suggests that this protein is not essential for blood-stage growth (Pearce *et al*., 2005).

Fatty acid transporter 4, belongs to a family of multi-pass receptors responsible for the cellular uptake and activation of long-chain fatty acids. This ~71 kDa protein is expressed in a relatively broad range of tissues (e.g. heart, liver, pancreas, adipose tissue) and mutations in its gene, SLC27A4, have so far been associated with the Ichthyosis prematurity (a keratinisation disorder which causes epidermal abnormalities) and insulin resistance syndromes, but not malaria (Gertow *et al*., 2004; Klar *et al*., 2009). On the other hand, single nucleotide polymorphisms in ATP2B4, the gene coding for the Plasma membrane calcium transporting ATPase 4, have been

found to correlate strongly with resistance against severe *P. falciparum* malaria in a West African population (Timmann *et al*., 2012). The intra-erythrocytic growth of *P. falciparum* is dependent on the presence of high levels of Ca^{2+} (Deasi *et al*., 1996). Therefore, mutations in ATP2B4 have been proposed to directly influence parasite growth by causing changes to the level of expression or structure of the erythrocytic Ca^{2+} pump (Timmann *et al*., 2012). However, the possibility of these mutations conferring protection against *P. falciparum* infection by preventing an interaction between the Ca^{2+} pump and a parasite ligand, which is important for erythrocyte invasion, cannot be excluded.

5.3.2.3 Further validation/characterisation of putative interactions between parasite proteins and recombinant multi-pass receptors.

On the surface of transiently-transfected HEK293E cells, the recombinant multi-pass receptors are displayed amongst a multitude of other surface proteins, lipids and glycans, any of which may be a target of particular *P. falciparum* merozoite proteins. In this screen, the binding of *P. falciparum* proteins to mock-transfected cells was subtracted from the binding to cells transiently-expressing each recombinant multi-pass receptor, in order to remove any such 'background' binding to endogenous HEK293E cell components. However, up- or down-regulation of particular endogenous surface receptors, as a direct or indirect consequence of the expression of exogenous DNA, could have led to confounding results in the binding assays. The up-regulation of unrelated endogenous receptors in particular could have resulted in the identification of 'false positives' in the screen.

When validating the potential interactions identified in the screen, the recombinant multi-pass receptors should ideally be incorporated into synthetic lipid bilayers, in order to eliminate any 'false positives' which resulted from the binding of the parasite proteins to endogenous

HEK293E cell components. The compositions of artificial membrane mimetics can be closely regulated, unlike those of native membranes. Erythrocytic multi-pass receptors reconstituted in such artificial bilayers can be tested for direct interaction with their putative parasite ligands using SPR, Backscattering Interferometry (BSI) or Isothermal Titration Calorimetry (ITC), all of which have been used with some success, to investigate the biomolecular interactions of integral membrane proteins, incorporated in to synthetic lipid bilayers (Baksh *et al*., 2011; Maynard *et al*., 2010; Sikora & Turner, 2005). These techniques allow the affinities of the interactions to be quantified, which is an advantage over flow-cytometry based approaches.

It is also necessary to investigate the importance of the identified receptor-ligand interactions for invasion of human erythrocytes by *P. falciparum*. For this purpose, antibodies raised against the multi-pass receptors should first be selected for blocking of the interaction with the parasite ligand *in vitro* and then tested for inhibition of erythrocyte entry by *P. falciparum* in functional assays (Crosnier *et al*., 2011).

5.3.3 The glycan-binding properties of a selected subset of merozoite surface proteins were tested by screening against a panel of synthetic carbohydrate probes.

In this study, a high-throughput ELISA-based method was used to identify the glycan-binding properties of a number of selected *P. falciparum* proteins. Each parasite protein, expressed as a soluble enzyme-tagged pentamer was tested against a panel of 55 synthetic biotinylated carbohydrate probes, immobilised on streptavidin-coated plates. The panel of glycans screened included a number of blood group antigens (Table 8). Five of the *P. falciparum* proteins tested, including Pf12, AARP, MSP3.4 and MSP3.8 showed no binding to any of the glycans (Figure 63). Recognition of sialic-acid containing glycans was observed with EBA175, EBA140, Pf113 and MSRP2, all of which had been observed to interact with erythrocytes and/or HEK293E cells

in a neuraminidase-sensitive manner (Figure 62). The binding of each of these latter four proteins to a number of sialic acid-containing but structurally-different glycans requires further investigation. Analysis of these protein-glycan interactions by SPR, for example, can reveal potential differences in the affinity of the parasite ligands for the variant glycan structures, indicating which is preferred. Glycans are also covalently-linked to proteins or lipids on the erythrocyte membrane, therefore specificity may come from the dual recognition of both the glycan and the protein/lipid backbone by the *P. falciparum* proteins.

5.4 CONCLUSION

In this study, new high-throughput screening strategies were developed for investigating the binding of *P. falciparum* merozoite surface proteins to human erythrocytes, recombinantly-expressed erythrocytic multi-pass receptors and glycans. A number of novel interactions were identified by the performed screens and are now awaiting further characterisation; including the binding of Pf34, MSP3.4 and MSP3.8 to human erythrocytes, the recognition of the multi-pass receptor Fatty acid transporter 4 by AARP and the binding of sialic acid by Pf113. Such screening platforms as those developed in this study have the potential to be useful tools for the large-scale functional characterisation of *P. falciparum* antigens, thereby facilitating the selection of new vaccine candidates.

5.5 BIBLIOGRAPHY

Arévalo-Pinzón, G., Curtidor, H., Vanegas, M., Vizcaíno, C., Patarroyo, M. A, & Patarroyo, M. E. (2010). Conserved high activity binding peptides from the *Plasmodium falciparum* Pf34 rhoptry protein inhibit merozoites in vitro invasion of red blood cells. *Peptides*, *31*(11), 1987-94.

Baksh, M. M., Kussrow, A. K., Mileni, M., Finn, M. G., & Bornhop, D. J. (2011). Label-free quantification of membrane-ligand interactions using backscattering interferometry. *Nature Biotechnology*, *29*(4), 357-60.

Beckmann, R., Smythe, J. S., Anstee, D. J., & Tanner, M. J. (1998). Functional cell surface expression of band 3, the human red blood cell anion exchange protein (AE1), in K562 erythroleukemia cells: band 3 enhances the cell surface reactivity of Rh antigens. *Blood*, *92*(11), 4428-38.

Bei, A. K., & Duraisingh, M. T. (2012). Functional analysis of erythrocyte determinants of *Plasmodium* infection. *International Journal for Parasitology*, *42*(6), 575-582.

Bozdech, Z., Llinás, M., Pulliam, B. L., Wong, E. D., Zhu, J., & DeRisi, J. L. (2003). The transcriptome of the intraerythrocytic developmental cycle of *Plasmodium falciparum*. *PLoS Biology*, *1*(1), E5.

de Brevern, A. G., Wong, H., Tournamille, C., Colin, Y., Le Van Kim, C., & Etchebest, C. (2005). A structural model of a seven-transmembrane helix receptor: the Duffy antigen/receptor for chemokine (DARC). *Biochimica et Biophysica Acta*, *1724*(3), 288-306.

Camus, D., & Hadley, T. J. (1985). A *Plasmodium falciparum* antigen that binds to host erythrocytes and merozoites. *Science*, *230*(4725), 553-556.

Chitinis, C. E. & Miller, H. M. (1994) Identification of the Erythrocyte Binding Domains of *Plasmodium vivax* and *Plasmodium knowlesi* Proteins Involved in Erythrocyte Invasion. *Journal of Experimental Medicine*, *180*(2), 497-506.

Chitinis, C. E., Chaudhuri, A., Horuk, R., Pogo, A. O. & Miller H. M. (1996) The domain on the Duffy blood group antigen for binding *Plasmodium vivax* and *P. knowlesi* malarial parasites to erythrocytes. J*ournal of Experimental Medicine*, *184*(4), 1531-6.

Carter, R., Coulson, a, Bhatti, S., Taylor, B. J., & Elliott, J. F. (1995). Predicted disulfide-bonded structures for three uniquely related proteins of *Plasmodium falciparum*, Pfs230, Pfs48/45 and Pf12. *Molecular and Biochemical Parasitology*, *71*(2), 203-10.

Clough, B., Paulitschke, M., Nash, G. B., Bayley, P. M., Anstee, D. J., Wilson, R. J. M., Pasvol, G., *et al*. (1995). Mechanism of regulation of malarial invasion by extraerythrocytic ligands. *Molecular and Biochemical Parasitology*, *69*(1), 19-27.

Crompton, P., & Pierce, S. (2010). Advances and challenges in malaria vaccine development. *The Journal of Clinical Investigation*, *120*(12), 4168-4178.

Crosnier, C., Bustamante, L. Y., Bartholdson, S. J., Bei, A. K., Theron, M., Uchikawa, M., Mboup, S., *et al*. (2011). Basigin is a receptor essential for erythrocyte invasion by *Plasmodium falciparum*. *Nature*, *480*(7378), 534-7.

Desai, S. J., McCleskey, E. W., Schlesinger, P. H. and Krogstad, D. J. (1996).A novel pathway for Ca^{++} entry into *Plasmodium falciparum*-infected blood cells. *American Journal of Tropical Medicine and Hygiene*, *54*(5), 464-470.

Florens, L., Washburn, M. P., Raine, J. D., Anthony, R. M., Grainger, M., Haynes, J. D., Moch, J. K., et al. (2002). A proteomic view of the *Plasmodium falciparum* life cycle. *Nature*, *419*(6906), 520-6.

Geels, M. J., Imoukhuede, E. B., Imbault, N., van Schooten, H., McWade, T., Troye-Blomberg, M., Dobbelaer, R., *et al*. (2011). European Vaccine Initiative: lessons from developing malaria vaccines. *Expert Review of Vaccines*, *10*(12), 1697-708.

Gertow, K., Bellanda, M., Eriksson, P., Boquist, S., Hamsten, A., Sunnerhagen, M. & Fisher, R. M. (2004). Genetic and Structural Evaluation of Fatty Acid Transport Protein-4 in Relation to Markers of the Insulin Resistance Syndrome. *Journal of Clinical Endocrinology & Metabolism*, *89*(1), 392-399.

Goel, V. K., Li, X., Chen, H., Liu, S.-chun, Chishti, A. H., & Oh, S. S. (2003). Band 3 is a host receptor binding merozoite surface protein 1 during the *Plasmodium falciparum* invasion of erythrocytes. *Proceedings of the National Academy of Sciences of the United States of America*, *100*(9),5164-69.

Graham, F. L., Smiley, J., Russell, W.C. & Nairn, N. (1977) Characteristics of a human cell line transformed by DNA from human adenovirus type 5. *The Journal of General Virology*, *36*(1), 59-74.

Greenwood, B. M., & Targett, G. A. T. (2011). Malaria vaccines and the new malaria agenda. *Clinical Microbiology and Infection,17*(11), 1600-7.

Hassoun, H., Hanada, T., Lutchman, M., Sahr, K. E., Palek, J., Hanspal, M., & Chishti, A. H. (1998). Complete deficiency of glycophorin A in red blood cells from mice with targeted inactivation of the band 3 (AE1) gene. *Blood*, *91*(6), 2146-51.

Hofmann, K. and Stoffel, W. (1993) TMbase- A database of membrane spanning protein segments. *Biological Chemistry Hoppe-Seyler*, *374*, 166–169.

Kadekoppala, M., Ogun, S. A., Howell, S., Gunaratne, R. S., & Holder, A. A. (2010). Systematic genetic analysis of the *Plasmodium falciparum* MSP7-like family reveals differences in

protein expression, location, and importance in asexual growth of the blood-stage parasite. *Eukaryotic Cell*, *9*(7), 1064-74.

Kakhniashvili, D. G., Bulla, L. A., & Goodman, S. R. (2004). The human erythrocyte proteome: analysis by ion trap mass spectrometry. *Molecular & Cellular Proteomics*, *3*(5), 501-9.

King, C. L., Adams, J. H., Xianli, J., Grimberg, B. T., McHenry, A. M., Greenberg, L. J., Siddiqui, A., *et al*. (2011). Fy(a)/Fy(b) antigen polymorphism in human erythrocyte Duffy antigen affects susceptibility to *Plasmodium vivax* malaria. *Proceedings of the National Academy of Sciences of the United States of America*, *108*(50), 20113-8.

Klar, J., Schweiger, M., Zimmerman, R., Zechner, R., Li, H., Törmä, H., Vahlquist, A., *et al*. (2009). Mutations in the fatty acid transport protein 4 gene cause the ichthyosis prematurity syndrome. *American Journal of Human Genetics*, *85*(2), 248-53.

Koppel, D. E., Sheetz, M. P., & Schindlert, M. (1981). Matrix control of protein diffusion in biological membranes. *Biophysics*, *78*(6), 3576-3580.

Krogh, A., Larsson,B., von Heijne, G. and Sonnhammer, E.L.L. (2001) Predicting transmembrane protein topology with a hidden Markov model: Application to complete genomes. *Journal of Molecular Biology*., 305, 567-580

Larkin, M. A., Blackshields, G., Brown, N. P., Chenna. R., McGettigan, P. A., McWilliam, H., *et al*. (2007) Clustal W and Clustal X version 2.0. *Bioinformatics*, *23*(21), 2947-8

Maier, A. G., Duraisingh, M. T., Reeder, J. C., Patel, S. S., Kazura, J. W., Zimmerman, P. A., & Cowman, A. F. (2002). *Plasmodium falciparum* erythrocyte invasion through glycophorin C and selection for Gerbich negativity in human populations. *Nature Medicine*, *9*(1), 87-92.

Mayer, D. C., Kaneko, O., Hudson-Taylor, D. E., Reid, M. E., & Miller, L. H. (2001). Characterization of a *Plasmodium falciparum* erythrocyte-binding protein paralogous to EBA-175. *Proceedings of the National Academy of Sciences of the United States of America*, *98*(9), 5222-7.

Maynard, J., Lindquist, N., Sutherland, N., Lesuffleur, A., Warrington, A., Rodriguez, M., & Oh, S.-H. (2009). Next generation SPR technology of membrane-bound proteins for ligand screening and biomarker discovery. *Biotechnology Journal*, *4*(11), 1542-1558.

Miller, L H, Hudson, D., Rener, J., Taylor, D., Hadley, T. J., & Zilberstein, D. (1983). A monoclonal antibody to rhesus erythrocyte band 3 inhibits invasion by malaria (*Plasmodium knowlesi*) merozoites. *The Journal of Clinical Investigation*, *72*(4), 1357-64.

Murphy, S. C., Hiller, N. L., Harrison, T., Lomasney, J. W., Mohandas, N., & Haldar, K. (2006). Lipid rafts and malaria parasite infection of erythrocytes. *Molecular Membrane Biology*, *23*(1), 81-8.

Ménard, D., Barnadas, C., Bouchier, C., Henry-Halldin, C., Gray, L. R., Ratsimbasoa, A., Thonier, V., et al. (2010). *Plasmodium vivax* clinical malaria is commonly observed in Duffy-negative Malagasy people. *Proceedings of the National Academy of Sciences of the United States of America*, *107*(13), 5967-71.

Narum, D. L., Fuhrmann, S. R., Luu, T., & Sim, B. K. L. (2002). A novel *Plasmodium falciparum* erythrocyte binding protein-2 (EBP2/BAEBL) involved in erythrocyte receptor binding. *Molecular and Biochemical Parasitology*, *119*(2), 159-68.

Obando-Martinez, A. Z., Curtidor, H., Arévalo-Pinzón, G., Vanegas, M., Vizcaino, C., Patarroyo, M. A., & Patarroyo, M. E. (2010). Conserved high activity binding peptides are involved in adhesion of two detergent-resistant membrane-associated merozoite proteins to red blood cells during invasion. *Journal of Medicinal Chemistry*, *53*(10), 3907-18.

Ota, K., Sakaguchi, M., Hamasaki, N., & Mihara, K. (1998). Assessment of topogenic functions of anticipated transmembrane segments of human band 3. *The Journal of Biological Chemistry*, *273*(43), 28286-91.

Barnwell, J.W., Nichols, M. E. & Rubinstein, P. (1989). *In vitro* evaluation of the role of the Duffy blood group in erythrocyte invasion by *Plasmodium vivax*. *Journal of Experimental Medicine*, *169* (5), 1795-802.

Pasini, E. M., Mann, M., & Thomas, A. W. (2010). Red blood cell proteomics, Protéomique du globule rouge. *Transfusion Clinique et Biologique*, *17*(3), 151-164.

Pasini, E. M., Kirkegaard, M., Mortensen, P., Lutz, H. U., Thomas, A. W., & Mann, M. (2006). In-depth analysis of the membrane and cytosolic proteome of red blood cells. *Blood*, *108*(3), 791-801.

Pearce, J. A., Mills, K., Triglia, T., Cowman, A. F., & Anders, R. F. (2005). Characterisation of two novel proteins from the asexual stage of *Plasmodium falciparum*, H101 and H103. *Molecular and Biochemical Parasitology*, *139*(2), 141-51.

Polley, M. J., Phillips, M. L., Wayner, E., Nudelman, E., Singhal, A. K., Hakomori, S., Paulson, J.C. (1991) CD62 and endothelial cell-leukocyte adhesion molecule 1 (ELAM-1) recognize the same carbohydrate ligand, sialyl-Lewis x. *Proceedings of the National Academy of Sciences of the United States of America*, *88*(14), 6224-8.

Proellocks, N. I., Kovacevic, S., Ferguson, D. J. P., Kats, L. M., Morahan, B. J., Black, C. G., Waller, K. L., *et al*. (2007). *Plasmodium falciparum* Pf34, a novel GPI-anchored rhoptry protein found in detergent-resistant microdomains. *International Journal for Parasitology*, *37*(11), 1233-41.

Sanders, P. R., Gilson, P. R., Cantin, G. T., Greenbaum, D. C., Nebl, T., Carucci, D. J., McConville, M. J., *et al*. (2005). Distinct protein classes including novel merozoite surface

antigens in Raft-like membranes of *Plasmodium falciparum*. *The Journal of Biological Chemistry*, *280*(48), 40169-76.

Sikora, C. W., & Turner, R. J. (2005). Investigation of ligand binding to the multidrug resistance protein EmrE by isothermal titration calorimetry. *Biophysical Journal*, *88*(1), 475-82.

Silmon de Monerri, N. C., Flynn, H. R., Campos, M. G., Hackett, F., Koussis, K., Withers-Martinez, C., Skehel, J. M., et al. (2011). Global identification of multiple substrates for *Plasmodium falciparum* SUB1, an essential malarial processing protease. *Infection and Immunity*, *79*(3), 1086-97.

Singh, S., Soe, S., Weisman, S., Barnwell, J. W., Pérignon, J. L., & Druilhe, P. (2009). A conserved multi-gene family induces cross-reactive antibodies effective in defense against *Plasmodium falciparum*. *PloS One*, *4*(4), e5410.

Speicher, D. W. (2006). Deep mining of the RBC proteome. *Blood*, *108*(3), 779-780.

Tham, W.-H., Healer, J., & Cowman, A. F. (2012). Erythrocyte and reticulocyte binding-like proteins of *Plasmodium falciparum*. *Trends in Parasitology*, *28*(1), 23-30.

Tham, W.-H., Wilson, D. W., Reiling, L., Chen, L., Beeson, J. G., & Cowman, A. F. (2009). Antibodies to reticulocyte binding protein-like homologue 4 inhibit invasion of *Plasmodium falciparum* into human erythrocytes. *Infection and Immunity*, *77*(6), 2427-35.

Timmann, C., Thye, T., Vens, M., Evans, J., May, J., Ehmen, C., Sievertsen, J., *et al*. (2012). Genome-wide association study indicates two novel resistance loci for severe malaria. *Nature*, 489(7416), 443-6

Tomishige, M., Sako, Y., & Kusumi, A. (1998). Regulation Mechanism of the Lateral Diffusion of Band 3 in Erythrocyte Membranes by the Membrane Skeleton. *Cell*, *142*(4), 989-1000.

Tran, T. M., Moreno, A., Yazdani, S. S., Chitnis, C. E., Barnwell, J. W., & Galinski, M. R. (2005). Detection of a *Plasmodium vivax* erythrocyte binding protein by flow cytometry. *Cytometry. Part A: the Journal of the International Society for Analytical Cytology*, *63*(1), 59-66.

Tsunady, G.E. and Simon, I. (2001) The HMMTOP transmembrane topology prediction server. B*ioinformatics*, 8, 849-850

Wang, D. N., Kühlbrandt, W., Sarabia, V. E., & Reithmeier, R. A. (1993). Two-dimensional structure of the membrane domain of human band 3, the anion transport protein of the erythrocyte membrane. *The EMBO Journal*, *12*(6), 2233-9.

Wickramarachchi, T., Devi, Y. S., Mohmmed, A., & Chauhan, V. S. (2008). Identification and characterization of a novel *Plasmodium falciparum* merozoite apical protein involved in erythrocyte binding and invasion. *PloS One*, *3*(3), e1732.

Wright, G. J. (2009). Signal initiation in biological systems: the properties and detection of transient extracellular protein interactions. *Molecular BioSystems*, *5*, 1405-1412.